Exploring the role of the microbiome in inflammatory arthritis disease pathogenesis

India Brough



University of Oxford

St Edmund Hall

Thesis submitted for the degree of

Doctor of Philosophy

Trinity 2023

“All disease begins in the gut”

Hippocrates, c. 400 BC

Abstract

Spondyloarthritis (SpA) is characterised by chronic, destructive joint inflammation and in many patients, intestinal inflammation. Microbiome profiling in SpA has identified increased abundances of inflammation-associated bacteria, and patients with reactive arthritis (ReA); a subset of SpA, develop joint inflammation following gastrointestinal (GI) infection. Despite the presence of these microbiome associations, the host-microbe interactions supporting disease remain largely unknown and may provide an avenue for microbiota-based therapies. The SKG mouse model of SpA develops microbiota-dependent joint and intestinal inflammation following dectin-1 activation with curdlan. Thus, in this thesis we aimed to study two forms of SpA; ReA and axial spondyloarthritis (AxSpA) in the SKG mouse model to delineate the host-microbe interactions driving joint disease. Firstly, we developed a microbiota-dependent model for ReA utilising GI infection with a murine enteropathogen in place of curdlan and characterised the microbiome and the T cell responses in this model. Secondly, we leveraged gnotobiotic SKG mice to delineate host-microbe interactions driving disease in the SKG-curdlan model. We found that although germ-free SKG mice did not develop disease, monocolonisation followed by depletion of the bacterium *Bifidobacterium animalis* did not prevent onset of disease. Furthermore, administration of heat-killed *B. animalis* to germ-free SKG mice enabled the induction of joint disease, suggesting that a component of *B. animalis* programs the host immune system to respond to curdlan and trigger disease. Finally, to determine the clinical relevance of studying the intestinal microbiome in SpA we completed immune phenotyping on AxSpA blood and stool, as well as stool metabolomic analysis. We identified a Th17 signature in the stool and blood of patients with AxSpA and identified several stool amino acids negatively associated with stool IL-23, suggesting an association between the host immune system and amino acid availability to microbes. Collectively, this work identifies several host-microbe associations in murine models of SpA as well as in patients with SpA and opens new avenues for the exploration of the host-microbe interactions supporting disease in SpA.

Acknowledgements

I would firstly like to thank my primary supervisor Professor Fiona Powrie for expert scientific guidance alongside her continued support to follow my experimental ideas. I am indebted to Dr Claire Pearson for her mentorship and friendship from when I first began working with the Powrie lab 6 years ago as she has provided me with endless hours of scientific and emotional support. I would also like to thank my co-supervisor Professor Kevin Foster, who has provided excellent ideas and a fresh view on each of my projects. Thank you to Dr Lilian Lam for bringing the gut-joint axis to the Powrie lab, and for providing inspiration to work in such a fascinating field. I am also incredibly grateful to Dr Alice Bertocchi for thorough and exceptional mentorship over the past year. I would also like to thank my thesis committee; Dr Jethro Johnson and Professor Andrew Macpherson, for excellent suggestions and viewpoints on studying the intestinal microbiome and the utilisation of gnotobiotics.

Working with Professor Paul Bowness and his infectious excitement for science fuelled my interest in continuing the study of the gut-joint axis and I am indebted to him for taking me on as a research assistant before my DPhil. I also want to thank past Bowness and Powrie lab members Dr Anna Ridley, Dr Frank Penkava, Dr Sam Bullers and Caroline Moussa for their wonderful mentorship and friendship from when I worked as a research assistant.

I would like to thank every member, past and present, from the Powrie lab for scientific and technical support, and for creating an exciting and collaborative work environment. In particular, I would like to thank my germ-free girls, Eli, Becky, Xinyue, and Ffion. Eli has given herself entirely to the running of the germ-free facility and I am grateful for her tireless hours of takedowns and a wonderful friendship. Becky, my DPhil sister, bench mate, and desk mate, a friendship that I would be lost without and has been there for me through my entire DPhil. Xinyue, for knowing myself better than I do and always putting 100% into every discussion, whether it be scientific or personal. Ffion, for support with experiments and incredible fun travelling to Canada for a Keystone

conference with me. Alina, as reading her thesis has helped me massively with writing my own, but also for always knowing exactly what to say or do in any situation.

I am grateful to the Kennedy Trust for their generous funding for my DPhil scholarship, as well as to Versus Arthritis and the inflammatory arthritis microbiome consortium (IAMC) for funding my research assistancy and the final results chapter of this thesis. I also would like to thank the BSU, histology, and all those who work in the core facilities. This project would not be possible without the patients and healthy controls that have volunteered to be a part of this research, as well as the research nurses at the BioBank and Nuffield Orthopaedic Centre for collecting these samples.

My friends have provided incredible support to me over the past 4 years. In particular, I am grateful to Libby for being such a fun thesis writing buddy, and to Vivian for wonderful friendship and invaluable advice. I am incredibly appreciative to St Edmund Hall Boat Club for giving me an outlet for DPhil-related stress and to all of the friends I have made there. In particular, I want to thank Jess, Felicity, Alicia, and Maddie for friendship that will last a lifetime. Jess, my dearest friend, thank you for providing me with an infinite supply of emotional support, amazing fun and for being with me through absolutely everything. Thank you, Felicity, for unwavering generosity and kindness, for our lovely chats, and for feeding me during my thesis write-up. Alicia, for being my first friend in the MCR, bringing wit alongside pragmatism to everything, and for holding our friendship group together with incredible organisation. Maddie, for injecting vibrancy and surprise into our friendship group, for bringing so much fun to travelling Malaysia and spending hours rowing with me.

I cannot thank my partner, Lydia, enough for the resolute love and support she provides me in every aspect of my life. She makes sure I face no challenge alone and provides a safe haven with our dog Kili from the stresses of life.

Lastly, I would like to thank my entire family, including my mum, dad, brother, and sister, for their unwavering support and encouragement, without which I would not have been able to do this DPhil.

Declaration of Authorship

Data presented in this thesis are from the authors' own experiments, aside from performance and analysis of NMR spectroscopy on stool from AxSpA patients (figure 5.10) which were completed by Professor Stephen Young (Birmingham, UK) and Dr Kelsey Thompson (Boston, US), respectively. Dr Nick Ilott (Oxford, UK) completed demultiplexing of 16S rRNA sequencing files which were subsequently processed and analysed by the author in figures 3.3 and 3.4.

Table of Contents

Abstract ..... *iii*

Acknowledgements ..... *iv*

Declaration of Authorship ..... *vi*

Table of Contents ..... *vii*

List of Figures ..... *xv*

List of Tables ..... *xix*

List of Abbreviations ..... *xx*

Chapter 1: Introduction *1*

1.1 Host immune mechanisms for microbiota control **1**

1.1.1 The intestinal barrier 2

1.1.2 The innate immune response 3

1.1.3 The adaptive immune response 4

1.2 Microbial calibration of the host immune system **6**

1.3 Spondyloarthritides **8**

1.3.1 Axial spondyloarthritis 8

1.3.2 Reactive arthritis 9

1.4 The genetic underpinnings of SpA **9**

1.4.1 Major histocompatibility complex genes 10

1.4.2 Common genetic variants in SpA and IBD 11

1.5 Animal models of SpA **11**

1.5.1 The SKG mouse model 12

1.6 Aberrant intestinal responses in SpA **14**

1.6.1 Impaired barrier integrity in SpA 14

1.6.2 Innate immune cells may bridge the gut-joint axis 15

1.6.3 Skewed T cell responses as a hallmark of SpA 16

1.7 Postulated mechanisms transposing intestinal disease to the joint 17

1.7.1 Lymphocyte egress 17

1.7.2 Translocation of bacterial components 18

1.7.3 Molecular mimicry 19

1.8 Intestinal microbiome implications in SpA 20

1.9 Demonstrating a causal role for the microbiome in SpA 23

1.9.1 Germ-free animals 24

1.9.2 Transient colonisation of microbiota 25

1.9.3 Curated communities 26

1.9.4 Modelling ReA using Citrobacter rodentium 27

1.10 Thesis aims 29

Chapter 2: Materials and methods *30*

2.1 Patient and control recruitment 30

2.1.1 Patient and control sample collection 31

2.2 Mice 32

2.2.1 Generation and maintenance of Oligo-MM^{12} SKG mice 32

2.2.2 Generation of monocolonised SKG mice 32

2.2.3 Antibiotic administration 33

2.2.4 Administration of heat-killed bacteria 33

2.3 Bacterial Culture 33

2.3.1 *Citrobacter rodentium* 33

2.3.2 *Parabacteroides distasonis* 34

2.3.3 *Leuconostoc citreum* 34

2.3.4 Oligo-Mouse-Microbiota members 34

2.4 Arthritis induction and animal models 35

2.4.1 Curdlan 35

2.4.2 *Citrobacter rodentium* 35

2.4.3 Paw swelling quantification 35

2.5 Histopathological scoring 36

2.5.1 Colon scoring 36

2.5.2 Small intestine scoring 37

2.5.3 Paw scoring 37

2.6 ELISA 38

2.6.1 Stool supernatant preparation 38

2.6.2 Human stool inflammatory marker quantification 38

2.6.3 Intestinal barrier marker quantification in human serum 38

2.6.4 Mouse Lipocalin-2 (LCN-2) ELISA 39

2.7 Bacterial CFUs from systemic organs 39

2.8 Assessment of immune cell populations by flow cytometry 40

2.8.1 PBMC isolation from human blood 40

2.8.2 Isolation of leukocytes from mouse tissue 40

2.8.3 Intracellular staining of human PBMCs 41

2.8.4 Staining of mouse leukocytes 42

2.8.5 Data acquisition 42

2.9 Bacterial flow cytometry 43

2.9.1 Immunoglobulin bacterial surface staining 43

2.10 Host RNA analysis 44

2.10.1 Host RNA Extraction 44

2.10.2 qRT-PCR 44

2.11 Bacterial DNA analysis 45

2.11.1 DNA extraction from stool or intestinal contents 45

2.11.2 DNA extraction from bacterial colonies 45

2.11.3 Quantification of Oligo-Mouse-Microbiota members 45

2.11.4 Sanger sequencing 47

2.11.5 16S sequencing 47

2.11.6 16S sequencing analysis 47

2.11.7 Shotgun metagenomic sequencing analysis 48

2.12 Bacterial fluorescent in-situ hybridisation 48

2.13 Metabolomics 49

2.13.1 NMR metabolomics on human stool samples 49

2.13.2 NMR downstream analysis 50

2.14 General data analysis 50

2.15 Diagrams 51

Chapter 3: *Citrobacter rodentium* infection serves as a murine model for ReA *52*

3.1 Introduction 52

3.2 Aim 54

3.3 Results 54

3.3.1 A novel model for ReA with enteric *Citrobacter rodentium* infection in SKG mice 54

3.3.2 *C. rodentium*-infected SKG mice display increased colonic and paw RORγt+ T cells 55

3.3.3 SKG mice infected with *C. rodentium* display no detectable changes to microbiome composition 57

3.3.4 Several bacteria are elevated in the stool of *C. rodentium* infected mice 57

3.3.5 Commensal intestinal bacteria translocate to the systemic organs in SKG mice 59

3.3.6 Intestinal commensal bacteria translocate to the systemic organs in Balb/C and SKG mice 62

3.3.7 *C. rodentium* requires intestinal commensals to drive arthritis and colitis in SKG mice 65

3.3.8 *C. rodentium* can drive local and systemic T cell responses in the absence of commensals despite not inducing inflammation 66

3.3.9 *C. rodentium* can translocate to systemic organs in germ-free SKG mice 68

3.3.10 The Oligo-MM^{12} community colonises SKG mice 70

3.3.11 The Oligo-MM^{12} community is a useful model for studying *C. rodentium* infection in SKG mice 71

3.3.12 *C. rodentium* elicits RORγt responses in the colon but not the paw of Oligo-MM^{12} SKG mice .. 73

3.3.13 SKG Oligo-MM^{12} mice infected with *C. rodentium* do not display altered intestinal microbiome composition 75

3.3.15 Numbers of specific Oligo-MM^{12} members are altered during *C. rodentium* infection in SKG mice 75

3.3.15 *E. faecalis* and *L. reuteri* translocate to the systemic organs in Oligo-MM^{12} SKG mice 77

3.4 Discussion 80

3.4.1 *Citrobacter rodentium* infection in SKG mice as a model for ReA 80

3.4.2 RORγt responses may be important in triggering but not maintaining arthritis 82

3.4.3 *Citrobacter rodentium* and commensal microbiota colonise the systemic organs 83

3.5 Conclusion 85

Chapter 4: *Bifidobacterium* programs the host immune system to support arthritis ... *86*

4.1 Introduction 86

4.2 Aim 88

4.3 Results 88

4.3.1 The SKG mutation in *Zap70* confers susceptibility to arthritis and small intestinal inflammation in mice 88

4.3.2 The Oligo-MM12 community is a useful model for studying curdlan-triggered disease in SKG mice 90

4.3.3 Paw RORγt responses are associated with disease in SKG mice 92

4.3.4 Curdlan induces shifts in the microbiome in both SPF and Oligo-MM^{12} SKG mice 92

4.3.5 *Weisella* blooms following curdlan injection in SKG mice 95

4.3.6 SKG disease is microbiota-dependent 97

4.3.7 Monocolonisation of bacteria permits arthritis in SKG mice 98

4.3.8 Monocolonisation of bacteria supports intestinal inflammation in SKG mice 102

4.3.9 *B. animalis* drives paw RORγt responses 103

4.3.10 *B. animalis* depletion by antibiotics to assess immune priming 103

4.3.11 Antibiotic treatment successfully clears *B animalis* from SKG mice 105

4.3.12 Germ-free SKG mice previously monocolonised with *B. animalis* develop arthritis following induction with curdlan 106

4.3.13 Germ-free SKG mice previously monocolonised with *B. animalis* develop intestinal inflammation following induction with curdlan 108

4.3.14 Administration of heat-killed *B. animalis* is sufficient to support arthritis in SKG mice 108

4.3.15 Administration of heat-killed *B. animalis* is sufficient to support intestinal inflammation in SKG mice 111

4.3.16 Heat-killed *B. animalis* drives paw RORγt responses in SKG mice 112

4.3.17 CD206- macrophages expand in the joint during inflammation 113

4.3.18 *B. animalis* colonisation does not upregulate the expression of PRRs in the small intestine of SKG mice 115

4.4 Discussion 117

4.4.1 The intestinal microbiome and genetic factors support arthritis 118

4.4.2 Induction of inflammation drives dysbiosis in the intestinal microbiome 119

4.4.3 RORγt responses are associated with inflammation but do not necessitate it 120

4.4.4 *Bifidobacterium animalis* developmentally programs the host immune system to drive arthritis 122

4.5 Conclusion 124

Chapter 5: A stool Th17 inflammatory signature exists in AxSpA..... *125*

5.1 Introduction 125

5.2 Aim 126

5.3 Results 127

5.3.1 Markers of intestinal inflammation are elevated in AxSpA 127

5.3.2 Serum barrier function proteins are unaltered in AxSpA 128

5.3.3 Patients with AxSpA display increased frequencies of circulating Th17 cells 129

5.3.3 Stool Th17 cytokines are elevated in AxSpA 130

5.3.4 Stool cytokines do not correlate with systemic cytokine production 131

5.3.5 Stool calprotectin positively correlates with stool IL-23 levels 132

5.3.6 HLA-B27 presence does not associate with stool and circulating Th17 immune phenotype 133

5.3.8 Markers of disease severity and medications are not associated with immune parameters 134

5.3.9 Extra-articular manifestations are associated with altered stool and circulating immune phenotype 135

5.3.10 Stool amino acid concentrations negatively correlate with stool IL-23 levels 136

5.4 Discussion 137

5.4.1 Th2 cytokine production is associated with HLA-B27 138

5.4.2 The intestinal barrier is not altered in our AxSpA cohort 138

5.4.3 The IL-23/Th17 axis in SpA may involve the intestinal microbiome 138

5.5 Conclusion 140

Chapter 6: General discussion *141*

6.1 Summary 141

6.2 SpA is driven by host-microbiota interplay 141

6.3 IL-23/Th17 immunity may connect the gut-joint axis in SpA 143

6.4 Microbiota-based therapies to treat established SpA 145

6.5 Lessons from utilising germ-free animals 147

6.6 Conclusion 147

References *148*

Appendix *186*

Chapter 3 Appendix: 186

Chapter 4 Appendix: 189

Chapter 5 Appendix: 193

List of Figures

Figure 1.1 Host-microbiota crosstalk in the intestine 7

Figure 1.2 The SKG-curdlan mouse model of SpA 13

Figure 1.3 Aberrant intestinal responses in SpA 19

Figure 1.4 Methods of gnotobiology to identify causality in host-microbiome studies 23

Figure 1.5 Mechanisms of host and microbial defence against *C. rodentium* infection 28

Figure 3.1 A novel model for ReA with enteric *Citrobacter rodentium* infection in SKG mice 56

Figure 3.2 *C. rodentium* infected SKG mice display increased colonic and paw RORγt+ T cells 58

Figure 3.3 SKG mice infected with C. rodentium display no detectable changes to microbiome composition 60

Figure 3.4 Several intestinal bacteria are elevated in the stool of *Citrobacter rodentium* infected mice 61

Figure 3.5 Intestinal commensal bacteria translocate to the systemic organs in SKG mice 63

Figure 3.6 Intestinal bacteria translocate to the systemic organs in Balb/C and SKG mice 65

Figure 3.7 *Citrobacter rodentium* requires intestinal commensals to drive arthritis and colitis in SKG mice 67

Figure 3.8 *Citrobacter rodentium* can drive local and systemic T cell responses in the absence of commensals despite not inducing inflammation 69

Figure 3.9 *Citrobacter rodentium* can translocate to systemic organs in germ-free SKG mice 70

Figure 3.10 The Oligo-MM^{12} community colonises SKG mice 71

Figure 3.11 The Oligo-MM^{12} community is a useful model for studying *C. rodentium* infection in SKG mice 72

Figure 3.12 *Citrobacter rodentium* elicits RORγt responses in the colon but not the paw of Oligo-MM^{12} SKG mice 74

Figure 3.13 SKG Oligo-MM^{12} mice infected with *Citrobacter rodentium* do not display altered intestinal microbiome composition 76

Figure 3.14 Numbers of specific Oligo-MM^{12} members are altered during *Citrobacter rodentium* infection in SKG mice 78

Figure 3.15 *Enterococcus faecalis* and *Limosilactobacillus reuteri* translocate to the systemic organs in Oligo-MM^{12} SKG mice 79

Figure 4.1 *Leuconostoc* is coated in host IgA 87

Figure 4.2 The SKG mutation in *Zap70* confers susceptibility to arthritis and small intestinal inflammation in mice 89

Figure 4.3 The Oligo-MM^{12} community is a useful model for studying curdlan-triggered disease in SKG mice 91

Figure 4.4 Paw RORγt responses are associated with disease in SKG mice 93

Figure 4.5 Curdlan induces shifts in the microbiome in SPF SKG mice 94

Figure 4.6 Curdlan induces shifts in the microbiome in Oligo-MM^{12} SKG mice 96

Figure 4.7 Weisella blooms following curdlan injection in SKG mice 97

Figure 4.8 SKG disease is microbiota-dependent 99

Figure 4.9 Monocolonisation of bacteria permits arthritis in SKG mice 100

Figure 4.10 Paw histopathology is supported in monocolonised SKG mice 101

Figure 4.11 Monocolonisation of intestinal microbiota supports intestinal inflammation in SKG mice 102

Figure 4.12 *Bifidobacterium animalis* drives paw RORγt responses when monocolonised in SKG mice 104

Figure 4.13 *Bifidobacterium animalis* depletion by antibiotics to assess immune priming 105

Figure 4.14 Antibiotic treatment successfully clears *Bifidobacterium animalis* from SKG mice 106

Figure 4.15 Germ-free SKG mice previously monocolonised with *B. animalis* develop arthritis following induction with curdlan 107

Figure 4.16 Germ-free SKG mice previously monocolonised with *B. animalis* develop intestinal inflammation following induction with curdlan 109

Figure 4.17 Administration of heat-killed *B. animalis* is sufficient to support arthritis in SKG mice 110

Figure 4.18 Administration of heat-killed *B. animalis* is sufficient to drive paw histopathology in SKG mice 111

Figure 4.19 Administration of heat-killed *B. animalis* is sufficient to support intestinal inflammation in SKG mice 113

Figure 4.20 Heat-killed *B. animalis* drives paw RORγt responses in SKG mice 114

Figure 4.21 CD206- macrophages expand in the joint during inflammation 116

Figure 4.22 *Bifidobacterium animalis* colonisation does not upregulate the expression of PRRs in the small intestine of SKG mice 117

Figure 4.23 Proposed mechanism for *Bifidobacterium animalis* in supporting the development of arthritis in SKG mice 118

Figure 5.1 Experimental outline to immune phenotype patients with AxSpA 127

Figure 5.2 Markers of intestinal inflammation are elevated in AxSpA 128

Figure 5.3 Serum barrier functions proteins are unaltered in AxSpA 129

Figure 5.4 Patients with AxSpA display increased frequencies of circulating Th17 cells 130

Figure 5.5 Stool Th17 cytokines are elevated in AxSpA 131

Figure 5.6 Stool cytokines do not correlate with systemic cytokine production 132

Figure 5.7 Stool calprotectin positively correlates with stool IL-23 levels 133

Figure 5.8 HLA-B27 presence does not associate with stool and circulating Th17 immune phenotype 134

Figure 5.9 Extra-articular manifestations are associated with altered stool and circulating immune phenotype 136

Figure 5.10 Stool amino acid concentrations negatively correlate with stool IL-23 levels 137

Figure 6.1 Proposed factors influencing SpA pathogenicity 142

Figure 6.2 Microbiome-based therapies for treating inflammatory disease 145

Appendix figure 3.1 Gating strategy for transcription factor flow cytometry 186

Appendix figure 3.2 Relative abundances of Oligo-MM12 members during *C. rodentium* infection in SKG mice 187

Appendix figure 3.3 Numbers of Oligo-MM12 members during *C. rodentium* infection in SKG mice 188

Appendix figure 4.1 Gating strategy for transcription factor flow cytometry 189

Appendix figure 4.2 Relative abundances of Oligo-MM^{12} members from strain-specific qPCR 190

Appendix figure 4.3 Absolute numbers of Oligo-MM^{12} members from strain-specific qPCR 191

Appendix figure 4.4 Gating strategy for flow cytometry 192

Appendix figure 5.1 Gating strategy for intracellular flow cytometry 193

Appendix figure 5.2 NSAID and biologic usage associations with stool or circulating immune parameters 195

Appendix figure 5.3 HLA-B27 associations with immune parameters 196

Appendix figure 5.4 Disease severity measures and disease duration associations with immune parameters in patients with AxSpA 197

Appendix figure 5.4 (continued from previous page) Disease severity measures and disease duration associations with immune parameters in patients with AxSpA 198

Appendix figure 5.5 Extra-articular manifestations and associations with immune parameters 199

Appendix figure 5.6 Stool calprotectin associations with immune parameters 200

List of Tables

Table 2.1 Assessment of Spondyloarthritis International Society (ASAS) classification criteria. 30

Table 2.2 Patient and control demographics. 31

Table 2.3 Scoring system used for histopathology of colon tissue. 36

Table 2.4 Scoring system used for histopathology of small intestine tissue 37

Table 2.5 Scoring system used for histopathology of arthritis. 38

Table 2.6 Proteins quantified by stool ELISA on patients with AxSpA and healthy controls. 39

Table 2.7 Antibodies used for intracellular staining of human PBMCs. 42

Table 2.8 Antibodies used for flow cytometric staining of murine leukocytes. 43

Table 2.9 Antibodies used for bacterial flow cytometric staining. 44

Table 2.10 TaqMan probes used for quantitative PCR. 45

Table 2.12 Primers and probes used to quantify Oligo-MM^{12} members by quantitative PCR. 46

Table 2.13 Primers used to quantify/amplify the 16S gene. 47

Table 2.14 DNA probe used for bacterial fluorescent in-situ hybridisation. 49

Appendix Table 5.1 Proteins quantified by stool ELISA. 194

List of Abbreviations

A. muciniphila	*Akkermansia muciniphila*
ABX	Antibiotics
ACK	Ammonium–chloride–potassium
AhR	Aryl hydrocarbon receptor
AJ	Adherens junction
AMP	Antimicrobial peptide
APC	Antigen presenting cell
ASAS	Assessment in Spondyloarthritis International Society
ASDAS	Ankylosing Spondylitis Disease Activity Score
ASF	Altered Schaedler flora
ASV	Amplicon sequence variant
AxSpA	Axial Spondyloarthritis
B. animalis	*Bifidobacterium animalis*
BASDAI	Bath Ankylosing Spondylitis Disease Activity Index
BLAST	Basic Local Alignment Search Tool
BSA	Bovine Serum Albumin
C. muridarum	*Chlamydia muridarum*
C. rodentium	*Citrobacter rodentium*
CARD	Caspase recruitment domain-containing protein
CFU	Colony forming units
CRP	C-reactive protein
DAMP	Damage-associated molecular patterns
DC	Dendritic cell
DMARD	Disease-modifying antirheumatic drug
DNA	Deoxyribonucleic acid
E. coli	*Escherichia coli*
E. faecalis	*Enterococcus faecalis*
ELISA	Enzyme-linked immunosorbent assay
ER	Endoplasmic reticulum
ERA	Enthesitis-related arthritis
FBS	Fetal bovine serum
FISH	Fluorescent in-situ hybridisation
FMT	Faecal microbiota transplant

FoxP3	Forkhead box P3
GF	Germ-free
GI	Gastrointestinal
GM-CSF	Granulocyte-macrophage colony-stimulating factor
GPI	Glucose-6-phosphate isomerase
GPR	G protein-coupled receptor
GVB	Gut vascular barrier
GWAS	Genome-wide association study
H&E	Hematoxylin and eosin
HK	Heat-killed
HLA	Human leukocyte antigen
I-FABP	Intestinal fatty-acid binding protein
I3Ald	Indole-3-acetaldehyde
IAA	Indole-3-acetic acid
IBD	Inflammatory bowel disease
IEC	Intestinal epithelial cell
IFN	Interferon
IgA	Immunoglobulin A
IL	Interleukin
IL-1Ra	Interleukin-1 receptor antagonist protein
IL-23R	Interleukin-23 receptor
Il12B	Interleukin-12 β subunit
ILC3	Type 3 innate lymphoid cell
JAM-A	Junctional adhesion molecule A
L. citreum	*Leuconostoc citreum*
L. murinus	*Ligilactobacillus murinus*
L. reuteri	*Limosilactobacillus reuteri*
LBP	LPS binding protein
LCN	Lipocalin
LP	Lamina propria
LPS	Lipopolysaccharide
LYPD8	LY6/PLAUR domain containing 8
MHC	Major histocompatibility complex
mLN	Mesenteric lymph node

MNP	Mononuclear phagocyte
MPO	Myeloperoxidase
MS	Multiple Sclerosis
NFκB	Nuclear factor kappa-light-chain-enhancer of activated B cells
NGS	Next-generation sequencing
NMR	nuclear magnetic resonance
NOD	Nucleotide-binding oligomerization domain-containing protein
Nramp1	Natural resistance-associated macrophage protein 1
NSAID	Non-steroidal anti-inflammatory drug
Oligo-MM^{12}	Oligo-mouse-microbiota-12
OMM	Oligo-mouse-microbiota
OSM	Oncostatin M
P. distasonis	*Parabacteroides distasonis*
PAMP	Pathogen-associated molecular patterns
PBMC	Peripheral blood mononuclear cells
PBS	Phosphate-buffered saline
PCR	Polymerase chain reaction
pLN	Popliteal lymph node
PRR	Pattern recognition receptor
PSA	Polysaccharide A
PsA	Psoriatic arthritis
PV-1	plasmalemma vesicle-associated protein-1
qPCR	Quantitative polymerase chain reaction
qRT-PCR	Quantitative real time polymerase chain reaction
ReA	Reactive arthritis
RNA	Ribonucleic acid
RORγt	RAR-related orphan receptor
ROS	Reactive oxygen species
RPM	Revolutions per minute
RPMI	Roswell Park Memorial Institute
rRNA	Ribosomal ribonucleic acid
S. saprophyticus	*Staphylococcus saprophyticus*
S-CD14	Soluble-CD14
S-IgA	Secretory Immunoglobulin A

SAA	Serum amyloid A
SBA	Secondary bile acid
SCFA	Short-chain fatty acid
SFB	Segmented filamentous bacteria
SpA	Spondyloarthritis
SPF	Specific pathogen free
SYK	Spleen tyrosine kinase
TCR	T cell receptor
Tfh	T follicular helper
TGF	Transforming growth factor
Th	T helper
TJ	Tight junction
TLR	Toll-like receptor
TNF	Tumor necrosis factor
TNFR	Tumor necrosis factor receptor
T_{reg}	T regulatory
UPR	Unfolded protein response
VE	Vascular endothelial
ZAP70	Zeta-chain-associated protein kinase 70
ZO	Zonula occluden

Chapter 1: Introduction

The intestinal microbiome is a collective term for the genomes of the varied bacteria, viruses, fungi, and archaea that colonise the mammalian gastrointestinal (GI) tract[1]. The intestinal "microbiota" refers to the collection of living microorganisms present in the GI tract[2]. Tightly controlled communication between the commensal microbiota and the host immune system facilitates intestinal homeostasis, promoting tolerance and preventing pathogen overgrowth through reinforcement of the intestinal barrier and the generation of defensive immune responses[3,4]. Breakdown of these homeostatic mechanisms including dysbiosis of the microbiome have been associated with inflammatory arthritides such as spondyloarthritis (SpA), but the host-microbiota interactions supporting the development of SpA have yet to be delineated[5,6]. Therefore, the role of the intestinal microbiota and its interactions with the host immune system provide an important area for further research to elucidate their impact on driving joint disease.

1.1 Host immune mechanisms for microbiota control

The host has evolved several strategies to protect itself from the threat of infection whilst simultaneously allowing for tolerance to the commensal microbiota (figure 1.1). These strategies comprise of the front-line structural compartmentalisation of the mucus and intestinal epithelial barriers that minimise the entrance of bacteria into the underlying lamina propria (LP), as well as a second line barrier called the gut vascular barrier (GVB) that prevents the dissemination of bacteria to systemic organs *via* the bloodstream[7]. In addition to physical barriers, the intestinal LP is patrolled by several immune cell populations such as IgA-secreting plasma cells, dendritic cells (DCs), T cells, and B cells[8]. When the tightly controlled crosstalk between the host immune system and the intestinal microbiota breaks down it can lead to overgrowth of pathogenic microbiota and the triggering of inflammatory diseases including SpA; chronic arthritides affecting the axial joints, and inflammatory bowel disease (IBD); a group of chronic inflammatory disorders of the GI tract.

1.1.1 The intestinal barrier

The first line of host defence comprises the intestinal mucus layer which is composed of mucin proteins produced by goblet cells, which, in the small intestine exist in a single, easily penetrable layer[9]. In the colon however, these proteins are organised into a dense inner layer and a loose outer layer[10]. The loosely adherent outer mucus layer acts as a lubricant for passing luminal contents and provides nutrients for commensal anaerobes such as *Akkermansia muciniphila*[11]. Underneath this outer layer is a firmly adherent inner mucus layer which is, under homeostatic conditions, void of bacteria to create a barrier between the intestinal epithelial layer and the microbiota[12].

Lying beneath the inner mucus layer is the intestinal epithelium which allows for homeostatic permeability to be maintained to allow for the transit of metabolites and ions, whilst preventing the translocation of microbes to systemic organs. The intestinal epithelial barrier is formed of a monolayer of columnar intestinal epithelial cells (IECs). IECs are sealed to each other by tight junctions (TJs) formed of transmembrane proteins such as zonula occludins (ZO-1, ZO-2), claudins, and occludin, that regulate the transport of ions and metabolites through the epithelial barrier[13]. IECs actively contribute to host defence by shedding ly6/PLAUR domain containing 8 (LYPD8) protein to inhibit the invasion of flagellated bacteria[14]. Furthermore, IECs can express pattern recognition receptors (PRRs) such as toll-like receptors (TLRs), which pathogen-associated molecular patterns (PAMPs) or host damage-associated molecular patterns (DAMPs) can bind to and trigger downstream host defence pathways[15].

The gut vascular barrier (GVB) is the next physical line of defence for the systemic organs located just beyond the intestinal epithelial barrier[16]. The GVB is composed of endothelial cells tightened to one another through proteins such as TJs and adherens junctions (AJ)[17]. The TJs expressed in the gut endothelium are occludin, ZO-1, junctional adhesion molecule-A (JAM-A) and claudin-5, which primarily regulate paracellular permeability and maintain cell polarity[18]. Among the AJs

present in the gut endothelium, vascular endothelial (VE)-cadherin is the most represented and acts as a regulator of cell-cell adhesion[19]. Under homeostatic conditions, the permeability of the GVB allows for luminal and dietary antigens required to maintain tolerance to be transported through the systemic circulation[17]. During homeostasis commensals can occasionally cross the intestinal epithelial barrier and, from the LP, are then drained through the lymphatic system by the mLNs, protecting the systemic blood circulation from bacterial invasion[20].

1.1.2 The innate immune response

If the intestinal barrier is breached, the host can activate an innate immune response in the LP, whereby specific innate immune cells can be recruited to prevent invading bacteria from driving disease[21]. Indeed, neutrophils are short-lived phagocytic cells that play an important role in both protecting the host from pathogen invasion, as well as clearing up dying and injured host cells[22]. During intestinal inflammation, neutrophils are recruited to the LP by cytokines, and use several mechanisms of bacterial killing to control infection. These mechanisms include production of reactive oxygen species (ROS) and metal-binding proteins such as calprotectin[23].

Intestinal mononuclear phagocytes (MNPs) include DCs and macrophages, and perform complementary yet differing functions to support the maintenance of intestinal homeostasis. Intestinal DCs are involved in the uptake of antigen in the LP followed by chemokine-dependent migration *via* the lymphatics to the mesenteric lymph nodes (mLNs) where they present processed antigen to T cells[24]. Intestinal DCs express a range of cytokine receptors and PRRs, and can produce a wide array of cytokines, allowing them to orchestrate downstream immunological responses[25]. Intestinal CX_3CR1+ macrophages can also capture microbial and food antigen but remain in the LP and are involved in driving tolerance to innocuous antigen[26]. CX_3CR1+ macrophages sample luminal antigen *via* the extension of transepithelial dendrites that penetrate the epithelial barrier, and captured antigen is then shuttled to DCs for presentation to T cells[27]. Intestinal macrophages also boost tolerance through their production of the regulatory cytokine IL-

10, which promotes the survival and secondary expansion of T_{reg} cells[28]. MNPs also play an important role in gut barrier reinforcement. For instance, macrophages can employ killing mechanisms such as the secretion of antimicrobial peptides (AMPs) and production of ROS[29].

MNPs can be modulated by type 3 innate lymphoid cells (ILC3s) to orchestrate adaptive immune responses. ILC3s respond to cytokine signals and microbial compounds to produce cytokines to induce macrophages and DCs, promoting the differentiation of T_{reg} cells. Furthermore, ILC3s can reinforce the intestinal barrier through IL-23-dependent production of IL-22, which can induce AMP secretion from IECs[30,31]. Conversely, ILC3s can limit production of secretory (s)-immunoglobulin A which can bind to bacteria, through the regulation of T follicular helper cell and B cell interactions [32]. ILC3s can also induce tolerance by selecting microbiota specific T_{reg} cells whilst preventing expansion into pro-inflammatory Th17 cells[33].

1.1.3 The adaptive immune response

Adaptive immune responses utilise clonally diverse, antigen-specific receptors on T and B cells to distinguish self from non-self, and to specifically respond to pathogens without attacking host cells[34]. B and T cells in the intestine play an important role in reinforcing the intestinal barrier and in mounting specific responses to microbial infection.

Thymic development of T cells involves the generation of the T cell receptor (TCR) to determine T cell specificity and differential expression of co-stimulatory receptors CD4 and CD8 to determine cell function. Thymic T cell positive selection occurs to ensure the T cell is functional for response against foreign antigens and negative selection eliminates autoreactive T cells[35]. In secondary lymphoid organs, antigen presenting cells (APCs) can present antigen on major histocompatibility molecules (MHC) to the TCR on naïve T cells, which can subsequently differentiate into functionally distinct subsets based upon exposure to cytokines[36]. Th1 and Th2 cells were first described in 1986 and were classified based upon their cytokine secretion[37]. Th1 cells can produce IFNγ, TNFα, and IL-2 and are involved in driving immune responses to bacteria and viruses[38]. Th2 cells can

produce IL-4, IL-5 and IL-13 and are involved in immune responses against parasite infections and are associated with driving allergy[39].

Several years later Th17 cells were first described, which produce the cytokine IL-17 along with other pro-inflammatory cytokines such as IL-22, IL-6, and TNFα whilst expressing the transcription factor RORγt[40]. Th17 cells are important in mucosal immunity against pathogens, and their differentiation is driven by exposure to cytokines including IL-23[41]. Indeed, production of IL-17 by Th17 cells drives the recruitment of neutrophils and induces MNPs to produce pro-inflammatory mediators including cytokines and AMPs to maintain a robust intestinal barrier[42,43]. Contrasting to their barrier-protective role in homeostasis however, Th17 cells can be pathogenic in several inflammatory diseases through their induction of pro-inflammatory responses[44].

T_{reg} cells can produce the anti-inflammatory cytokine IL-10 and express the transcription factor FoxP3. They can be classified into thymic T_{reg} cells and peripheral T_{reg} cells, depending on the site of their differentiation. Thymic T_{reg} cells have a high affinity for self-peptide and drive peripheral tolerance in secondary lymphoid organs by suppressing the differentiation of other T cell subsets[45,46]. Peripherally, conventional CD4+ T cells can differentiate into T_{reg} cells following microbial antigen recognition in the presence of TGF-β and IL-2[47]. Peripheral T_{reg} cells can express the type 17 transcription factor RORγt and secrete IL-10 to induce tolerance to commensal microbiota[48,49].

Another specialised T cell subset are follicular helper (Tfh) cells that can migrate to the germinal centres of lymph nodes to help B cells by providing survival and selection signals, allowing them to develop and carry out their functions, including the production of antibodies to prevent pathogen infiltration[50,51]. In health, B cells can trigger downstream signalling leading to s-IgA production by plasma cells to aid in intestinal barrier function[52]. In this regard, s-IgA is important for the control of host-microbe interactions by binding to microbiota and forming a protective barrier between the host epithelial layer and microbiota[53].

1.2 Microbial calibration of the host immune system

The human intestinal microbiome consists of 500~1000 distinct bacterial species which belong to few known bacterial phyla[54]. In a healthy individual, Bacteroidetes and Firmicutes are the two most predominant phyla in the human intestine, making up around 90% of the bacteria present in the intestine, Actinobacteria, Verrucomicrobia, and Proteobacteria are also present in the intestine[55]. The intestinal microbiome acts as a metabolically active organ that remains dynamic throughout a person's lifetime, and it usually lives in symbiotic harmony with the host immune system as both sides contribute to the maintenance of intestinal homeostasis[54,56].

Microbiota have several mechanisms by which they exert control over the host immune system. For instance, bacteria such as *Faecalibacterium prausnitzii* and *Eubacterium hallii* can produce short chain fatty acids (SCFAs) including butyrate from dietary fibre[57]. Butyrate acts as an energy source for IECs and can reinforce the intestinal epithelial barrier through the upregulation of TJ proteins and induction of antimicrobial macrophages[58,59]. SCFAs can also promote tolerance to commensal and food antigen in the intestine by the induction of T_{reg} cells[60]. Aside from SCFAs, bacteria can produce immunomodulatory compounds through their metabolism of dietary amino acids. For instance, the essential amino acid tryptophan is metabolised by intestinal bacteria to indole and other derivatives including indole-3-acetic acid (IAA) and indole-3-acetaldehyde acid (I3Ald) using tryptophanase, which is only found in bacteria[61]. These serve as ligands for the aryl hydrocarbon receptor (AhR) and signalling involving AhR modulates intestinal homeostasis by regulating ILC3 and Th17 populations to promote barrier function[62]. Other amino acids have also been shown to play an important role in modulating the host immune system. For instance, leucine and glutamine can modulate the differentiation of T cell subsets[63,64]. Furthermore, bacterial-derived polyamines such as spermidine can undergo metabolism and act as a cue to ensure appropriate T cell differentiation[65].

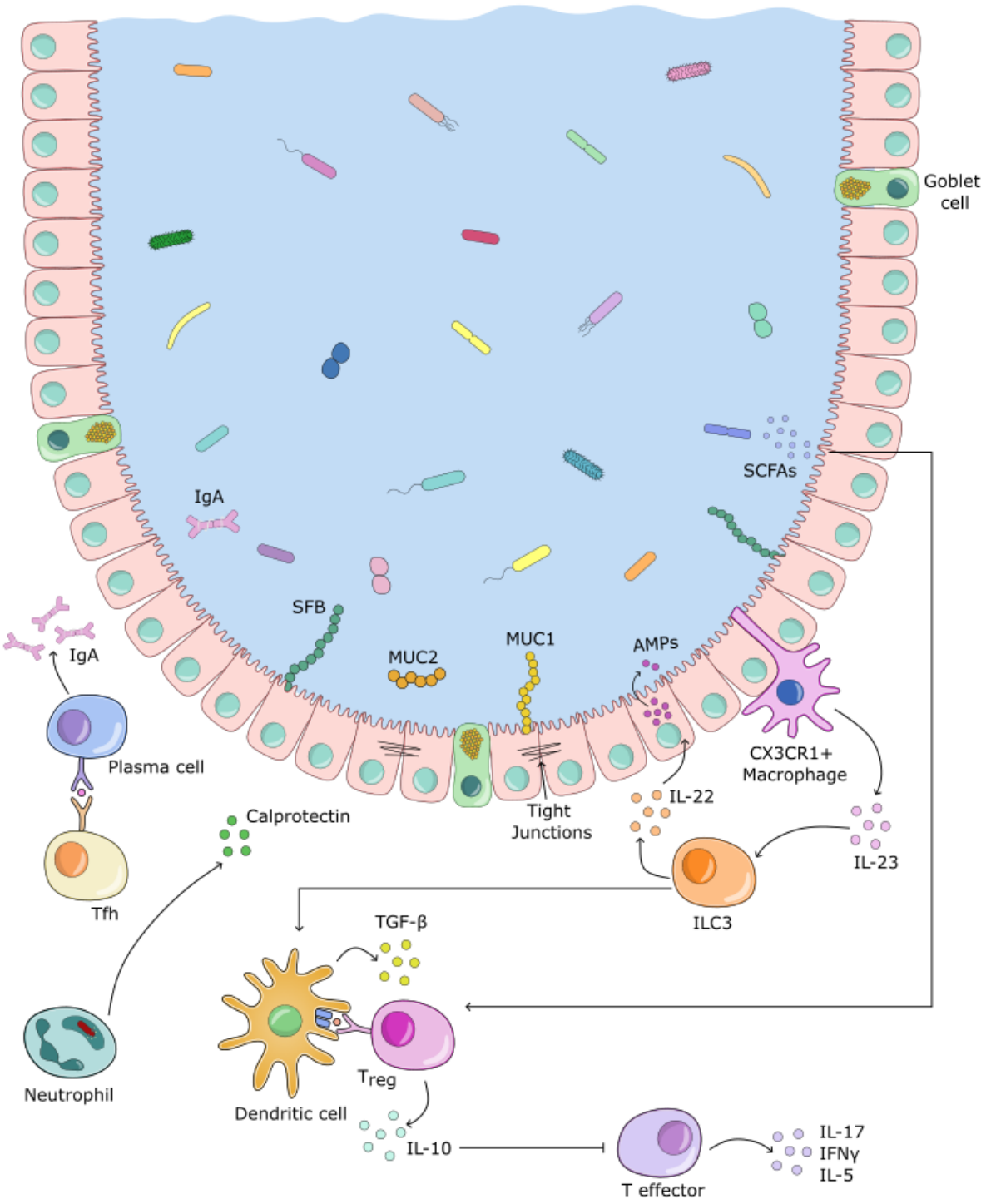


Figure 1.1 Host-microbiota crosstalk in the intestine. The host has evolved several strategies to enable defence against pathogens and tolerance to commensal microbiota. Furthermore, microbiota are able to calibrate the host immune system to further drive host tolerance. A mucus layer comprised of mucins MUC1 and MUC2 form the first defence, followed by the intestinal epithelial layer which is reinforced with tight junctions. ILC3 production of IL-22 can stimulate the production of antimicrobial peptides from intestinal epithelial cells. Neutrophils contribute to antimicrobial activity through their production of metal-binding proteins such as calprotectin. CX_3CR1 macrophages extend transepithelial dendrites to sample luminal antigen and shuttle these to dendritic cells which present them to naïve T cells. A milieu of cytokines drives the differentiation of T cells, and T_{reg} cells specifically drive tolerance through the inhibition of other T cell subsets. Tfh cells drive B cells to produce antibodies including secretory-IgA to bind intestinal bacteria.

Besides metabolite production, microbiota can secrete bacterial components that can influence the host immune system. The most well known are perhaps lipopolysaccharides (LPS); molecules found in the outer bacterial wall membrane of Gram-negative bacteria, which can activate host immune pathways through stimulation of TLRs[66]. Microbiota can secrete components which can also exert immune-suppressive functions. For instance, *Bacteroides fragilis* can promote regulatory responses in the host through its production of polysaccharide A (PSA), which can induce the expansion of IL-10 producing T_{reg} cells through its activation of TLR2[67].

1.3 Spondyloarthritides

Spondyloathritides (SpA) are chronic, destructive autoimmune diseases primarily affecting the sacroiliac joints and include axial spondyloarthritis (AxSpA), psoriatic arthritis (PsA), and reactive arthritis (ReA). SpA has a reported prevalence of between 0.2-1.61% of the population[68]. Several clinical features are shared between diseases classified under the SpA umbrella, including inflammation of the sacroiliac and axial joints, enthesitis, asymmetric oligoarthritis, and dactylitis[69,70]. Several extra-articular manifestations occur in SpA, including anterior uveitis and inflammation of the intestine[71,72]. The prevalence of IBD in patients with SpA is around 7%, and approximately 70% of patients display histological markers of intestinal inflammation[73,74]. SpA is highly associated with genetic factors, most notably the presence of human leukocyte antigen (HLA)-B27. Indeed, HLA-B27 is present in around 90% of patients with AxSpA, and around 60-70% of patients with ReA[75–77]. HLA-B27 positivity is not increased in patients with IBD, but is associated with arthropathy in IBD patients, suggesting its role in potentiating joint disease[78].

1.3.1 Axial spondyloarthritis

AxSpA is a chronic, immune-mediated disease characterised by inflammation of the axial joints and includes patients with both radiographic sacroiliitis and non-radiographic disease[79]. Eventually chronic inflammation that is not controlled by treatment can lead to ankylosis, fusion of the

vertebrae. Onset of AxSpA typically occurs in individuals between the ages of 18-30 and is prevalent in around 0.36-0.7% of the global population[68]. A high level of geographical variation exists in the prevalence of AxSpA, and the highest community prevalence affected being 20% of individuals from Haida[80]. AxSpA has been previously believed to preferentially affect males over females, however recent improvements in diagnosis of AxSpA including early MRI have allowed for recognition of higher disease prevalence in females than historically reported[81]. Treatment of AxSpA involves physiotherapy and non-steroidal anti-inflammatory drugs (NSAIDs) as a first line treatment of choice to reduce pain, followed by disease modifying anti-rheumatic drugs (DMARDs) including methotrexate to delay the progression of disease. Discoveries of biological agents to treat AxSpA are demonstrated to be successful in treating disease and include monoclonal antibodies targeting the cytokines TNF and IL-17A[82,83].

1.3.2 Reactive arthritis

Reactive arthritis (ReA) is a typically self-limiting disease characterised by acute onset oligo-arthritis involving primarily the lower limbs, following gastrointestinal infection with pathogens such as *Salmonella enterotidis,* and *Shigella flexneri,* or urogenitary infection with *Chlamydia trachomatis*[84]. The reported prevalence of ReA varies largely between studies, however, is thought affect up to around 0.2% of the global population[68]. Around 30% of patients develop persistent disease which must then be managed through treatment with NSAIDs initially, followed by DMARDs and occasionally biologic treatment for severe presentation with ReA[84].

1.4 The genetic underpinnings of SpA

The concordance rate of AxSpA is 63% in monozygotic twins, demonstrating a high level of heritability[85]. The MHC molecule HLA-B27 is the strongest known genetic association with SpA, however more recently, extensive genome wide association studies (GWAS) have highlighted several

non-MHC related genetic loci associated with both SpA and IBD, suggesting a gut-joint connection in SpA[86,87].

1.4.1 Major histocompatibility complex genes

The MHC is a group of genes encoding proteins involved in the presentation of antigens to T cells *via* their TCR. These genes are referred to as human leukocyte antigens (HLA) in humans and are highly polymorphic, thus influencing their peptide binding specificity[88]. In the thymus, MHC molecules on thymic epithelial cells present endogenous antigen to the TCR on T cells to facilitate positive or negative selection. Different classes of MHC molecules including class I and class II determine maturation of T cells into CD8+ or CD4+ MHC-restricted T cells, respectively. The high level of polymorphism in HLA molecules is likely an evolutionary advantage to maximise the recognition of any given foreign antigen to ensure some individuals in a population are protected against infectious disease and survive. However, HLA polymorphisms are strongly associated with autoimmune disease, which may be driven by altered HLA-peptide-TCR binding facilitating the thymic escape of T cells from negative selection[35].

HLA-B27 is a surface antigen on the class I MHC, and its primary role is to present endogenous peptides to T cells[89]. The presence of HLA-B27 is the strongest genetic association with SpA, with around 90% of AxSpA patients being HLA-B27+. Approximately 60-70% of patients with ReA are HLA-B27+, and HLA-B27 positivity in ReA is associated with the development of chronic arthritis and is more present in patients with sacroiliitis and spondylitis[75,76]. A causative role for HLA-B27 has been demonstrated through studies in rats transgenic for HLA-B27 that develop SpA-like symptoms including intestinal inflammation[90]. Multiple hypotheses have been postulated for the functional role of HLA-B27 in driving SpA. For instance, the arthritogenic peptide theory suggests that self and arthritogenic antigens are presented by HLA-B27 to autoreactive T cells. Indeed, HLA-B27 restricted pathogen-specific T cells have been identified in the joint of patients with ReA, and bacterial peptides matching the HLA-B27 epitope have been identified in AxSpA patient stool[91,92]. Another

hypothesis postulates that due to a propensity for HLA-B27 to misfold in the endoplasmic reticulum (ER), it can form cell surface homodimers and drive ER stress to facilitate pro-inflammatory responses including IL-23 production[93–96]. Contrary to this hypothesis however, the reduction of HLA-B27 misfolding in transgenic rats drives more severe arthritis and spondylitis, suggesting that although HLA-B27 misfolding may occur, it may not be relevant to disease pathogenesis[97].

1.4.2 Common genetic variants in SpA and IBD

Although HLA-B27 is present in a large majority of patients with SpA, only a small subset of HLA-B27+ individuals develop disease. This suggests that other genetic and environmental factors may play a role in driving SpA pathogenesis. Indeed, GWAS have implicated several common genetic loci between SpA and IBD. Notably, *Il23r;* the gene encoding the IL-23 receptor, *Il12b;* the gene encoding a subunit of the cytokine IL-12*,* and *Card9*; the gene encoding an adaptor molecule involved in the nuclear factor-κB (NFκB) pathway have all been associated with both AxSpA and IBD[86]. Further supporting this gut-joint connection, AxSpA patients with *Nod2* gene polymorphisms have been observed to have a higher risk of developing subclinical intestinal inflammation, and sacroiliitis in IBD patients is linked to *Nod2* polymorphisms[98,99]. NOD2 is an intracellular PRR for bacterial ligands, and upon stimulation can activate NFκB signalling and subsequent pro-inflammatory immune responses to boost barrier defence[100]. Therefore, this induction of barrier-protective responses may also drive deranged pro-arthritogenic responses. Overall, these shared genetic variants in both diseases highlight the overlap between intestinal inflammation and SpA and suggest a shared mechanism involving IL-23 and other pro-inflammatory signalling pathways.

1.5 Animal models of SpA

Despite the strong correlations identified between intestinal and joint inflammation in SpA, the exact mechanisms by which intestinal inflammation and SpA are linked remain largely unclear. However, the use of genetic animal models of arthritis supports the dissection of this relationship.

Genetic models of arthritis encompass both transgenic animals and animals with genetic mutations in pathways involved in driving systemic inflammation and autoimmunity. For example, HLA-B27/hβ2m transgenic rats express human HLA-B27 and MHC class I component β2-microglobulin and this drives spontaneous development of intestinal and joint inflammation that is clinically comparable to SpA in humans[90]. Notably, HLA-B27 transgenic rats develop colitis within 10 weeks of birth, and several weeks later joint inflammation develops, suggesting the potential initiation of disease in the gut followed by transposition to the joint[90]. The K/BxN model involves mice expressing the T cell receptor (TCR) transgene KRN and the MHC class II molecule A(g7) that subsequently develop inflammatory arthritis. Due to the presence of autoantibodies to glucose-6-phosphate isomerase (GPI); a protein that drives the proliferation of synoviocytes, generated in K/BxN mice, serum transfer from K/BxN mice into wild-type mice elicits similar inflammatory arthritis[101,102]. Another model for SpA is the IL-1 receptor antagonist (IL1-Ra) -deficient mouse, which develops inflammatory disease through driving the production of IL-17[82,103].

Few models for ReA involving mucosal infection exist, though the most established involves infection in mice lacking the TNF receptor (TNFR) p55 with *Yersinia enterocolitica* O:3[104]. Indeed, infection with *Yersinia* in TNFRp55-/- mice drives the expansion of intra-articular host-antibodies specific for *Yersinia*, as well as increased levels of IL-17 in the mLNs, which drain the intestine, as well as the joint[104,105]. This mimics human ReA in that *Salmonella*-derived LPS has been identified in the synovium of patients with ReA, reinforcing the presence of a gut-joint connection in driving disease[106].

1.5.1 The SKG mouse model

A widely used genetic model of SpA is the SKG model, whereby a missense mutation in the gene encoding zeta-chain-associated protein kinase 70 (ZAP-70), a TCR signalling molecule, impairs T cell signalling transduction to alter the threshold for T cell selection[107]. This subsequently allows self-reactive T cells to escape negative selection and migrate to the periphery to subsequently skew

towards a Th17 phenotype[108]. T_{reg} functionality is impaired in SKG mice, preventing the suppression of inflammation and the promotion of spontaneous arthritis under conventional microbiome conditions (figure 1.2)[107,109]. Anti-fungal administration to SKG mice results in attenuated arthritis, suggestive of a fungal component in triggering disease[110]. Indeed, under specific pathogen free (SPF) conditions, SKG mice do not develop inflammation unless a fungal component such as curdlan or zymosan is injected intraperitoneally, after which mice develop severe arthritis and intestinal inflammation[110][111]. Curdlan and zymosan act as dectin-1 receptor ligands, which signals through SYK and CARD-9 molecules to activate NF-kB and the production of pro-inflammatory cytokines including IL-23, driving the differentiation of Th17 cells (figure 1.2)[112]. Despite the implication of Th17 responses in the SKG mouse model, mice deficient in IL-17A only have attenuated inflammation rather than total inhibition, and disease is shown to be dependent on the upstream cytokine IL-23[113].

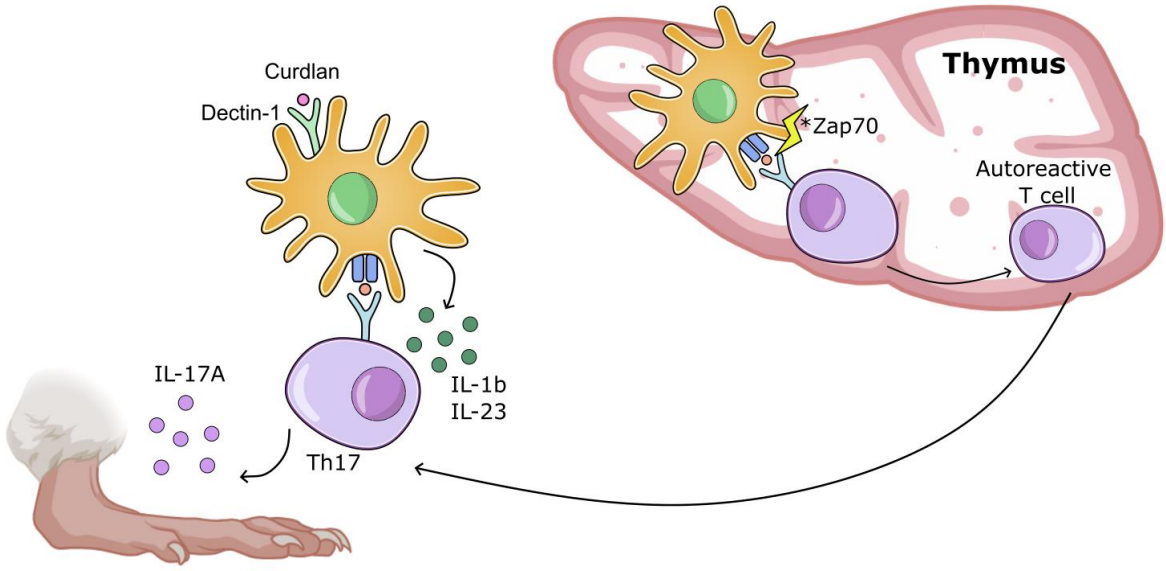


Figure 1.2 The SKG-curdlan mouse model of SpA. SKG mice have a mutation in the gene encoding ZAP-70, a molecule involved in T cell signalling. This mutation leads to an accumulation of self-reactive T cells. SKG mice housed in SPF conditions develop joint and intestinal inflammation following activation of the dectin-1 receptor *via* curdlan. Dectin-1 activation induces the production of IL-1β and IL-23, driving differentiation of the accumulated self-reactive cells into Th17 cells. Th17 cells can thereby potentiate inflammation in the joint.

ReA can be triggered through urogenitary infection with pathogens such as *Chlamydia trachomatis* and is modelled through intravaginal infection of *Chlamydia muridarum* in SKG

mice[114]. Contrasting to curdlan-triggered disease, disease in *C. muridarum*-infected SKG mice is driven primarily *via* TNF signalling, and IL-17 production is impaired[114].

1.6 Aberrant intestinal responses in SpA

A gut-joint axis is clearly associated with SpA through a genetic and clinical overlap with IBD. In addition to these associations, early studies identified histological markers of intestinal inflammation including LP infiltration of inflammatory cells and crypt distortion in SpA[73,115]. Since these observations, several alterations to intestinal barrier function and the intestinal immune landscape have been identified in SpA (figure 1.3).

1.6.1 Impaired barrier integrity in SpA

Mucus layer thinning through goblet cell dysfunction and bacterial mucin consumption in low fibre conditions can allow for inappropriate encroachment of microbiota and the induction of inflammation[116]. This has been highlighted in K/BxN mice that develop joint inflammation alongside a reduction in goblet cells and reduced MUC2 expression as disease progresses[117]. This suggests that the induction of inflammatory arthritis is associated with mucus-layer impairment. Further supporting this, enteropathogens associated with ReA display abilities to interact with the mucus layer to gain access to the intestinal epithelial layer[118,119]. For instance, *Shigella* produces a serine-protease called *Pic* that displays mucolytic activity, allowing it to directly degrade mucins to breach the mucus layer and reach the epithelial layer[118]. Additionally, *Salmonella* has an adhesin that interacts with the mucin MUC1 to gain access to the epithelium and activate the host immune system *via* its type III secretion system[119]. S-IgA contributes to barrier function in the mucus layer by selectively binding to bacteria and preventing their invasion[53].The identification of IgA-coated microbiota has uncovered pathobionts associated with driving joint inflammation in AxSpA and Crohn's disease patients with associated SpA (Crohn's-SpA)[120,121]. This highlights the ability of IgA to selectively bind bacteria with pathogenic potential and suggests their niche to be in the mucus layer, allowing for opportune invasion into the LP.

Disruptions to the intestinal epithelial layer have been associated with SpA. For instance, histological and gene expression analyses on intestinal biopsies from patients with SpA show reductions in claudin and occludin expression, suggesting a deterioration in TJ integrity[122,123]. Furthermore, patients with SpA display increased levels of serum ZO-1 compared to healthy controls, suggesting TJ deterioration and the release of ZO-1[6]. Following intestinal epithelial barrier breakdown, certain bacteria can invade the LP and directly influence gut vascular barrier permeability, assessed by an increase of the detection of protein plasmalemma vesicle-associated protein-1 (PV-1)[124]. For instance, mice infected with *Salmonella* display increased PV-1 detection in blood endothelial cells, indicating its ability to disseminate *via* the bloodstream[16]. In addition, gut vascular barrier TJs and AJs may be impaired in SpA, as patients show significant upregulation of PV-1, and downregulation of the AJs VE-cadherin and JAM-A compared to healthy controls[6]. Notably, host-derived, and bacterial-derived factors can translocate to the systemic circulation when the GVB is impaired[17]. Indeed, host-derived factors intestinal fatty acid binding protein (I-FABP), expressed by IECs and soluble (s)- CD14, released by innate immune cells following LPS activation, as well as LPS and host antibodies to bacteria-derived flagellin have all been detected in the serum of patients with inflammatory arthritis, suggesting that GVB dysfunction is associated with SpA and may allow for the triggering of systemic inflammation[6,123,125].

1.6.2 Innate immune cells may bridge the gut-joint axis

Macrophages are enriched in intestinal biopsies from patients with SpA, and intestinal macrophages from K/BxN mice display reduced expression of IL-10 suggesting a skewing away from an anti-inflammatory phenotype[126,127]. Furthermore, intestinal CX_3CR1+ macrophages are expanded in patients with AxSpA and produce IL-23 which can induce pro-inflammatory Th17 responses, suggesting that pro-inflammatory macrophages are associated with SpA[128]. Macrophages are also potential key players in the joint, and increased frequencies of synovial sublining macrophages are an early marker of joint inflammation[129]. Notably, isolated intestinal macrophages have displayed the ability to bind to vessels isolated from the inflamed synovium of

patients with SpA *in vitro* utilising their adhesion molecules, suggesting that intestinal macrophages are able to gain access to the synovial environment[130]. Indeed, CX_3CR1+ macrophages with the gut-homing marker CCR9 are increased in the synovial fluid and peripheral blood of patients with AxSpA, highlighting a role for macrophages in bridging the gut-joint axis[128]. Notably, ILC3s are also expanded in the intestine and synovial fluid of patients with SpA, and peripheral ILC3s express the gut-homing receptor α4β7[111].

Further evidence supports the role for innate immune cell egress to the joint during disease. For instance, TNFRp55 -/- mice develop severe systemic arthritis when infected with *Yersinia enterocolitica*, and intestinal DCs containing *Yersinia* are present in the joint regional lymph nodes[104,105,131]. In addition, when *Yersinia*-infected mice are treated with FTY720; an immunomodulatory agent that can prevent the egress of immune cells from lymph nodes, numbers of DCs in the joint regional lymph nodes are lowered and arthritis is ameliorated[131].

1.6.3 Skewed T cell responses as a hallmark of SpA

Skewed T cell responses towards a type 17 phenotype play an important role in the pathogenicity of SpA. Indeed, increased frequencies of circulating Th17 cells have been identified in patients with SpA and IL-17 inhibitors are used successfully in the treatment of SpA[82,132,133]. Mouse studies further demonstrate a role for IL-17 in SpA, as IL-17A -/- SKG mice display attenuated joint inflammation[108]. Furthermore, bacteria-driven activation of Th17 cells has been shown to exacerbate joint inflammation in mouse models of arthritis. For instance, segmented filamentous bacteria (SFB), *Bifidobacterium adolescentis*, and IgA-coated *Escherichia coli* have been shown to exacerbate disease in the K/BxN mouse model of arthritis by fostering the skewing of T cells towards a Th17 phenotype[120,134,135]. Th17 cell differentiation is induced by exposure to IL-23, which has been implicated in SpA. Indeed, GWAS have identified common genetic polymorphisms involved in the pathways driving IL-23 signalling including IL23R, IL12B, and CARD9, in SpA and IBD[86]. Further to this, patients with AxSpA have elevated levels of IL-23 in their sera and ileal tissue[136,137]. It has

been suggested that this elevated production of IL-23 may be driven by HLA-B27 misfolding in the ER and driving ER stress[138]. Notably, ReA associated pathogen Salmonella has enhanced replication in the presence of HLA-B27 and is associated with a UPR cellular environment, which drives IL-23 production[139]. Functional mouse studies confirm a crucial role for IL-23 in driving SpA. For instance, administration of anti-IL-23 to SKG mice results in reduced arthritis and ileitis severity, along with increased *Muc2* expression and frequency of goblet cells, suggesting that IL-23 may be involved in tipping the balance of Th17 cells away from being barrier-protective and towards a pathogenic phenotype[113]. Notably, anti-IL23 therapy has been trialled in SpA, and despite its efficacy in IBD, lacks efficacy in patients with SpA[140]. This contrasts with the success of anti-IL17 therapy observed in patients with SpA and suggests a mechanism whereby IL-23 may be involved in initiating the development of SpA in the LPs and drives a deranged, self-reactive Th17 response which persists even in the subsequent absence of IL-23 [82]. Indeed, targeting IL-23 during initiation of disease but not during persistence of disease suppresses inflammation in HLA-B27 transgenic rats[141].

1.7 Postulated mechanisms transposing intestinal disease to the joint

The mechanisms linking the intestine to the joint in SpA have not been fully elucidated, however several hypotheses have been postulated. These mechanisms include egress of lymphocytes from the intestine to the joint, translocation of bacterial components *via* the bloodstream or lymphatics to the joint, and molecular mimicry.

1.7.1 Lymphocyte egress

Lymphocyte egress has been suggested to play a role in potentiating disease in SpA due to the inverse correlation between intestinal intraepithelial lymphocytes and peripheral lymphocyte count, indicating potential migration of intestinal lymphocytes to the periphery[142]. When presenting antigen to T cells in secondary lymphoid organs, DCs can imprint gut homing receptors CCR9 and

α4β7 onto T cells to preferentially attract them to the LP[143]. The detection of lymphocytes with gut homing receptors in peripheral organs suggests their intestinal origin, as well as a hypothesis that intestinal inflammation may be transposed from the intestine *via* lymphocyte egress. Indeed, splenic T cells obtained from K/BxN mice display increased levels of α4β7 compared to control mice and circulating CCR9+ T cell frequencies correlate with measures of disease activity in AxSpA[134,144]. Furthermore, patients with AxSpA display increased expression of α4β7 on peripheral blood ILC3s and intestinal lymphocytes display an ability to bind to synovial vessels *via* α4β7, indicating the potential for intestinal lymphocytes to migrate to the joint environment[111]. Indeed, CX_3CR1+ macrophages expressing CCR9 are expanded in the synovial fluid of patients with AxSpA, further supporting a lymphocyte egress mechanism in driving multi-site inflammation in SpA[128]. There is evidence to suggest that the lymphocyte egress observed in SpA may be associated with intestinal barrier dysfunction allowing microbial invasion and an aberrant innate response. Indeed, K/BxN mice administered the TJ assembly promoting peptide larazotide acetate to reinforce their intestinal barrier displayed reduced frequencies of splenic CCR9+ α4β7+ T cells compared to naïve mice[117].

1.7.2 Translocation of bacterial components

Patients with AxSpA display disrupted intestinal barrier integrity, therefore suggesting that the translocation of microbial components is a conceivable mechanism for the transposition of disease from the intestine to the joint. Some evidence supports this as a mechanism in AxSpA, with anti-flagellin antibodies being identified in sera from AxSpA patients[125]. Studies have suggested a role for translocation of bacterial components in ReA. For instance, *Salmonella*-derived LPS has been identified in the synovium of patients with ReA. Furthermore, *Yersinia*-infected TNFRp55-/- arthritic mice have intra-articular host antibodies against *Yersinia*-derived antigens present in the joint[104]. The mechanisms by which bacterial components can translocate to the systemic environment are currently unknown. Bacteria and their components may be moving freely to translocate, or they may

be loaded into antigen presenting cells for transport to peripheral sites. Indeed, there is evidence to suggest that *Salmonella* can hijack intestinal DCs for migration to lymphoid organs *via* the lymphatic system[145].

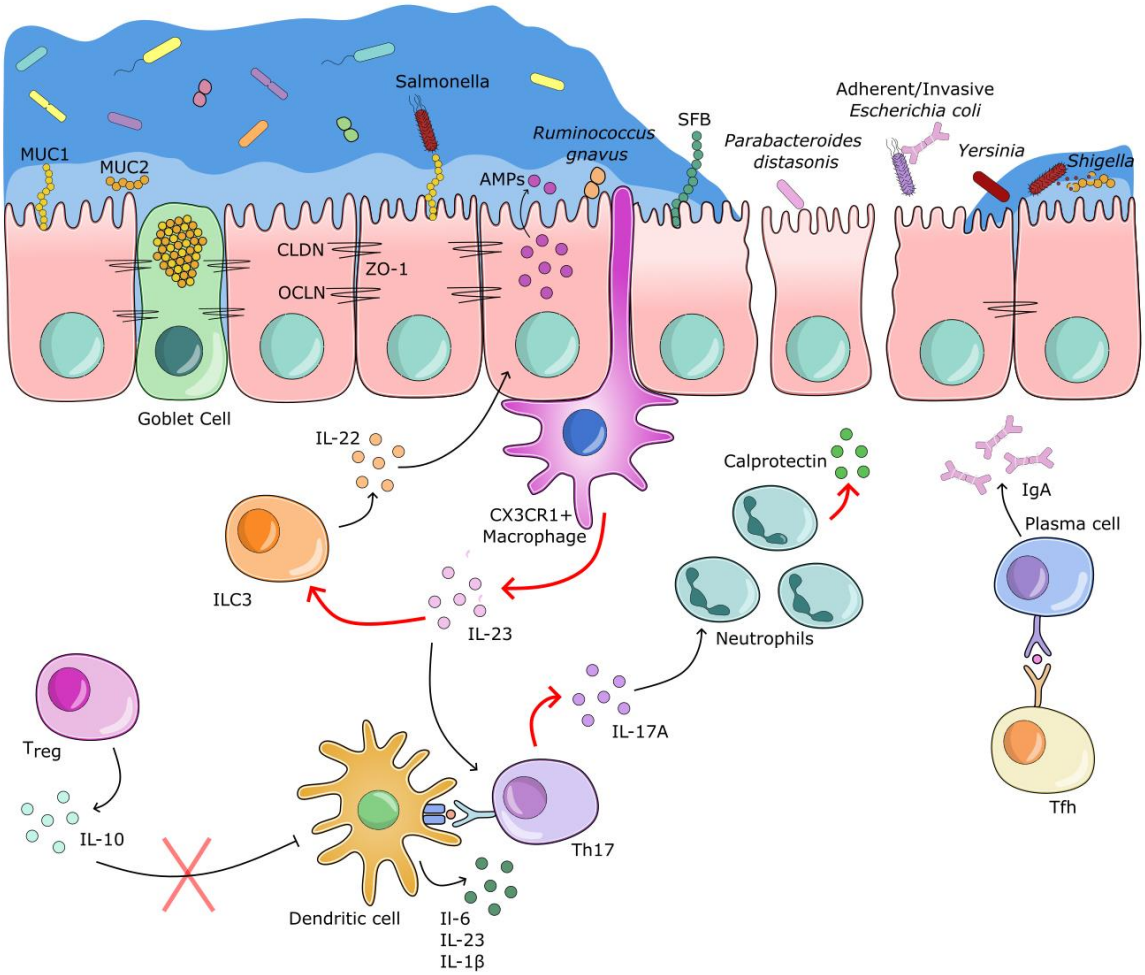


Figure 1.3 Aberrant intestinal responses in SpA. Several typically pro-inflammatory microbiota are associated with human and mouse models of AxSpA and ReA. Pathogens associated with ReA including *Shigella* and *Salmonella* can interact with mucins in the mucus layer to drive mucus degradation. The intestinal epithelial layer is sealed by tight junctions which are disrupted in SpA, driving intestinal permeability and the translocation of microbial components to the bloodstream. CX_3CR1+ macrophages are expanded and produce the pro-inflammatory cytokine IL-23 in SpA. IL-23 and other pro-inflammatory cytokines induce the differentiation of pro-arthritogenic Th17 responses. IL-23 also induces ILC3s which are expanded in SpA. T_{reg} cells can induce tolerance and the production of IL-10 can suppress inflammatory processes, however this is impaired in SpA. Tfh cells interact with B cells to induce the production of IgA, which can preferentially bind to pathobionts associated with SpA.

1.7.3 Molecular mimicry

The movement of bacterial antigen to the joint may also potentiate autoimmune responses by a mechanism called molecular mimicry. Molecular mimicry suggests that a bacterial antigen similar in molecular makeup to self-antigen may trigger an autoimmune response[146]. Molecular mimicry

has been associated with autoimmune diseases such as multiple sclerosis (MS), type one diabetes, and Guillain-Barré syndrome[147–149]. For instance, in the experimental autoimmune encephalomyelitis (EAE) mouse model of MS, a bacterium of the Erysipelotrichaceae family was able to drive Th17 responses whilst *Limosilactobacillus reuteri* contained mimitopes to self-antigen, and co-colonisation of both bacteria induced autoimmune disease to a higher severity than when separately monocolonised[150]. There is some evidence for molecular mimicry in SpA. Indeed, *in vitro* studies isolated bacterial antigen from AxSpA which can mimic the self-antigen type II collagen to trigger IFNɣ secretion[151]. HLA-B27 may be involved in potentiating molecular mimicry through its presentation of microbial peptides that resemble HLA-B27 peptide. For example, an HLA-B27 derived peptide has homology with protein sequences from *Chlamydia trachomatis*, a bacterium associated with urogenitary infection-related ReA[152]. Furthermore, an enrichment in diverse bacterial peptides matching the HLA-B27 epitope has been found in AxSpA patients stool samples, further supporting this hypothesis[91].

1.8 Intestinal microbiome implications in SpA

The concordance rate for AxSpA is only 63% in monozygotic twins, suggesting an interplay between host genetics and environmental factors in driving SpA[85]. Of these environmental factors, altered intestinal microbiota composition, referred to as dysbiosis, has been strongly associated with SpA[151,153]. Dysbiosis refers to changes in the homeostatic composition of the intestinal microbiome, and can be driven by several factors including diet, medication, and gastrointestinal infection[154]. These alterations in the intestinal microbiome are often associated with the development of inflammatory disease, including IBD, colorectal cancer, and inflammatory arthritis[5,155].

The introduction of next-generation sequencing (NGS) technology has allowed for the advancement of our understanding of the role of the microbiome in driving inflammatory disease. These methods include 16S ribosomal RNA (rRNA) sequencing, whereby the bacterial 16S rRNA gene

is amplified and sequenced, shotgun metagenomic sequencing, where all the DNA is sequenced, and RNA sequencing, where the bacterial transcriptome is sequenced[156]. 16S rRNA sequencing provides an affordable method of identifying the bacteria present in a microbial community, and shotgun sequencing allows for increased granularity to strain-level identification of microbes including bacteria, viruses, and parasites. On the other hand, RNA sequencing allows for functionality of the microbiome to be attributed to the community being sequenced. Aside from sequencing of the microbiome, metabolomic analyses of the compounds present in a sample can provide a detailed functional readout for microbial activity.

Microbiome profiling has identified alterations in the intestinal microbiomes of patients with SpA, characterised by a blooming of typically inflammatory taxa and decreased abundance of typical human gut commensals[157]. More specifically, increased abundances of frequently inflammatory bacteria such as *Ruminococcus gnavus, Parabacteroides distasonis, Pseudomonas, and Klebsiella pneumoniae* have been observed in the stool of patients with AxSpA and ReA[5,151,153,158]. Notably, microbiome shifts are associated with disease activity in AxSpA. Microbial dysbiosis is associated with intestinal inflammation in AxSpA, which is also observed in IBD[159,160]. Changes to certain microbiota are associated with joint inflammation in AxSpA; *Dialister* is associated with the AS disease activity score (ASDAS) and *Ruminococcus gnavus* is associated with the Bath Ankylosing Spondylitis Disease Activity Index (BASDAI)[5,161]. Furthermore, patients with AxSpA are observed to have increased levels of sulfate-reducing bacteria, which are typically associated with intestinal inflammation[162].

Conversely, abundances of anti-inflammatory, butyrate-producing bacteria such as *Faecalibacterium prausnitzii* and *Eubacterium hallii* are reduced in patients with AxSpA, and genes involved in butyrate metabolism are downregulated in the microbiome of AxSpA patients[151]. Furthermore, SCFAs butyrate and propionate are reduced in the stool of AxSpA patients[163]. Notably, administration of butyrate to SKG mice attenuates arthritis, implicating the anti-

inflammatory effects butyrate exerts on the host in the suppression of joint inflammation[164]. Metabolites aside from SCFAs have been associated with SpA. Notably, AhR ligands IAA and I3Ald are expanded in the distal colon of patients with AxSpA, compared to patients with IBD and healthy controls[165]. In contrast, another study found that patients with enthesitis-related arthritis (ERA); a juvenile subset of SpA, display lower levels of tryptophan metabolites[166]. Taken together these studies suggest that aberrant tryptophan metabolism may play an important role in SpA, perhaps through the modulation of type 17 responses. Indeed, AhR expression has been observed in ILC3s obtained from the synovium in patients with AxSpA[167]. Amino acid metabolism may also be associated with SpA. For example, amino acid-derived metabolite spermidine is crucial to orchestrating T cell differentiation and has been shown to be upregulated in HLA-B27 transgenic rats alongside the amino acids histidine and tyrosine[168]. Furthermore, the amino acid taurine has been found to be increased in the stool of patients with AxSpA, suggesting a role for intestinal amino acid metabolism in the disease[163].

Studies also demonstrate that HLA-B27 presence influences the intestinal microbiome composition. Indeed, HLA-B27+ healthy controls display alterations in their intestinal microbiome, characterised by a reduction in *Bacteroides ovatus* and increased *Roseburia* species[169]. Furthermore, increased abundances of *Akkermansia muciniphila* and *Prevotella* have been observed in HLA-B27 transgenic rats[170]. HLA-B27 transgenic rats are protected from disease under germ-free conditions and develop disease upon recolonisation with commensal bacteria[171]. The mechanism by which HLA-B27 can shape the intestinal microbiome is unclear. It has been demonstrated that MHC molecules influence antibody responses to intestinal bacteria to drive variation in the intestinal microbiome, and this may be how HLA-B27 is able to alter the microbiome[172]. For instance, HLA-B27-specific antigen presentation may drive differential IgA production and the differentiation of more pathogenic T cell responses, thereby driving an inflammatory environment and shifts to the microbiome.

1.9 Demonstrating a causal role for the microbiome in SpA

Due to the complex interplay of host genetics and the intestinal microbiome in supporting pathology in SpA, mouse models must encompass genetic predisposition as well as easily manipulable microbiota. The conventional environment has the highest level of microbial-diversity for raising laboratory-based animals and these are not routinely screened for the presence of pathogens[173]. Specific pathogen free (SPF) mice are most commonly used mice for laboratory-based animal work. SPF refers to a setting in which animals are maintained that contains pathogens that are routinely screened for, including *Citrobacter rodentium* and *Salmonella* spp., and from some vendors *Helicobacter* spp.[174]. Despite SPF mice providing a model in which the environment is tightly controlled, a high level of variation exists in the SPF microbiome between and within facilities. For instance, the presence of immunogenic bacterium SFB, which plays an important role in driving Th17 responses, is facility-dependent[175]. The SPF microbiome's high level of variability and lack of tractability prevents it from being a meaningful model for ascribing causality to the microbiome. Therefore, gnotobiotic mice; mice which have a defined microbiome, can allow for the attribution of causality to the microbiome and the study of host physiological and pathological processes because of the microbiome[176]. Gnotobiotic studies extend from germ-free mice; void of any microorganisms, to designed communities of bacteria (figure 1.4).

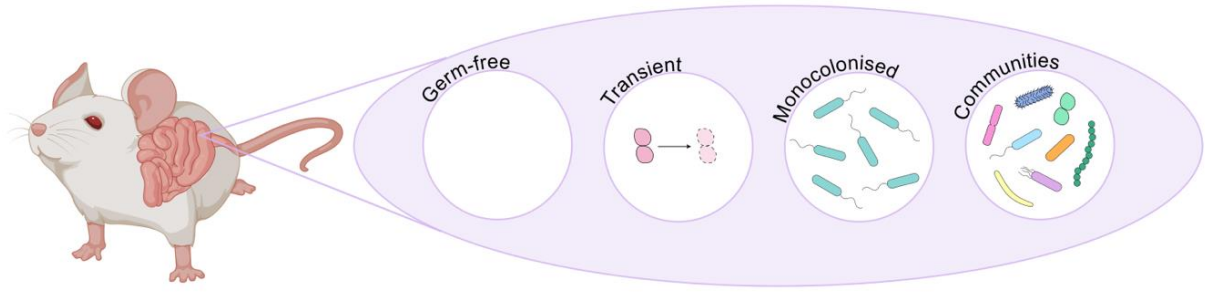


Figure 1.4 Methods of gnotobiology to identify causality in host-microbiome studies. Methods utilised in gnotobiotics to delineate host-microbiota interactions and to definitively determine the role of single or a curated community of microbes on host physiology. These approaches include germ-free mice which lack any microorganisms, transient colonisation of single or multiple microbes to interrogate the contribution of immune system education on host phenotypes, monocolonisation with a single bacterium, and designed communities such as the Oligo-MM^{12}. Figure was adapted from[176,177].

1.9.1 Germ-free animals

Germ-free animals refer to those that lack the colonisation of any microorganisms. Germ-free mice are typically raised in large flexible film isolators which can house several individual open top cages, although the introduction of positive pressured individually sealed cages has increased the accessibility of gnotobiotic research[178]. Several studies in models of arthritis have demonstrated a requirement for the microbiota in permitting the development of joint inflammation by utilising germ-free animals. For instance, HLA-B27 transgenic rats reared under germ-free conditions display an inability to develop intestinal or joint inflammation[171]. Further to this, SKG mice show protection from intestinal inflammation and partial protection from joint inflammation under germ-free conditions[179]. Furthermore, K/BxN mice and IL-1ra $^{-/-}$ mice raised under germ-free conditions display attenuated joint inflammation[134,180]. Together these studies demonstrate a crucial role for the intestinal microbiota in supporting the development of arthritis and suggest its role in shaping the host immune response. Indeed, previous studies have highlighted functional and architectural impairments in the germ-free immune system because of lack of microbial colonisation. For instance, germ-free mice display underdeveloped lymph nodes and small intestinal Peyer's patches, as well as diminished IgA responses[181,182]. Germ-free mice also display a skewing towards Th2 responses which drives hypersensitivity to allergens, and impaired suppressive function of their T_{reg} cells which can be rescued *via* exposure to *Bacteroides fragilis* component PSA[183,184]. Furthermore, Th17 cells are reduced in both germ-free mice and SPF mice without SFB and Th17 cells are reconstituted upon colonisation with SFB[175]. Although some defects in the germ-free immune system are reversible by colonisation at any time, there exists a 'critical window' of colonisation for others. For instance, germ-free mice display increased LP invariant natural killer T (iNKT) cells which are associated with driving IBD, and this phenotype was rescued by microbial colonisation in early-life and not in adulthood[185].

1.9.2 Transient colonisation of microbiota

Given the deficiencies of a germ-free immune system, transient colonisation of microbiota allows for the impact of colonisation on potentiating inflammation and on immune development to be delineated from one another. Broad spectrum antibiotic administration to SPF mice can achieve depletion of the intestinal microbiota, therefore providing a model to determine the influence of removing microbial colonisation on an educated immune system. Antibiotic experiments in animal models of SpA have suggested an importance of continual microbial colonisation on permitting the development of inflammation. For instance, treatment with antibiotics suppresses the differentiation of Th17 cells and Tfh cells to ameliorate arthritis in K/BxN mice[134,186]. Furthermore, antibiotic treatment of IL-1ra -/- mice attenuated arthritis, and this was restored with colonisation of Th17-inducing bacterium SFB[180]. Conversely, antibiotic administration in HLA-B27 transgenic rats is not effective in reducing colitis, but the addition of *Lacticaseibacillus rhamnosus* to antibiotic-treated mice attenuated colitis[187]. Notably, treatment of conventionally raised SKG mice, which develop spontaneous arthritis, with an anti-fungal agent attenuates arthritis[110]. The impact of antibiotic treatment on arthritic symptoms in HLA-B27 transgenic rats and SKG mice has not yet been published. Overall, these studies suggest that continual colonisation of the intestinal microbiota may play an important role in allowing the development of arthritis. However, antibiotic treatment in SPF mice has its pitfalls due to its inability to completely deplete the intestinal microbiota[188,189]. Antibiotic treatment of gnotobiotic mice may allow for the targeted depletion of known bacteria, therefore allowing for more specificity in antibiotic treatment. Furthermore, engineered auxotrophic bacteria can reversibly colonise hosts due to their reliance on nutrients that are not provided by host metabolites, ensuring a bona fide germ-free mouse post-colonisation. This system has been used to study the dynamics of IgA responses and the effects of the maternal microbiota on germ-free offspring immune development[190,191].

1.9.3 Curated communities

To study host-microbiota interactions in a controlled yet physiologically relevant environment, microbial consortia have been developed. One of the pioneering consortia is the Schaedler Flora developed in 1965 which was then optimised to comprise eight bacterial species and named the altered Schaedler flora (ASF) in 1978[192,193]. Notably, germ-free SKG mice recolonised with the ASF develop arthritis and intestinal inflammation, though attenuated in comparison to SPF mice, suggesting a role for species not present in the ASF or a combinatorial effect of the complex SPF microbiome in driving disease development[179].

The Oligo-Mouse Microbiota 12 (Oligo-MM^{12}) includes 12 bacterial species broadly representative of the five major phyla from the mouse intestine[194]. The Oligo-MM^{12} has been demonstrated to be highly reproducible across facilities, stable over several generations, and has a high level of colonisation resistance, highlighted by its ability to prevent *Salmonella* colonisation[194,195]. Furthermore, the Oligo-MM^{12} can reverse the Th2 skewing of the germ-free immune system, whilst the ASF cannot[196]. Despite the Oligo-MM^{12} providing a more relevant community to other minimal microbial communities, it does not fully recapitulate microbiome functionality and immune responses observed in SPF mice. For instance, Oligo-MM^{12} mice are observed to have larger caeca than SPF mice, although smaller than germ-free mice, suggesting that they represent a mid-way point between a void microbiome and a fully complex microbiome in terms of immune maturation[194,197]. Furthermore, the Oligo-MM^{12} lacks both *Enterobacteriaceae* and secondary bile acids (SBA); and addition of a bacterium that can produce SBA was associated with increased protection from *Clostridium difficile* infection. Recently, to overcome these pitfalls in the Oligo-MM^{12}, nine species were used to amend the model to create the Oligo-MM^{19}, a 19-member community including *Enterobacteriaceae* and *Extibacter muris*, which can produce SBA[197]. On the other hand, increasing complexity of a minimal community runs the risk of hindering the reductionist approach that minimal communities provide in delineating host-microbe

interactions. Overall, minimal communities should be selected or curated based upon the research hypothesis and can be edited by the addition or removal of species to develop the most relevant community for the research question.

1.9.4 Modelling ReA using *Citrobacter rodentium*

Few animal models of mucosal infection in ReA exist, and in this thesis, we aim to develop a model of ReA utilising a mouse-adapted pathogen; *Citrobacter rodentium*. *Citrobacter rodentium* is a mouse-specific enteropathogenic bacterium that shares several virulence factors, including the type III secretion system, with pathogens associated with ReA[198]. Upon infection, *C. rodentium* adheres to IECs and forms attaching and effacing lesions. Utilising its type III secretion system, *C. rodentium* injects several effectors into IECs to hijack and mimic host processes to promote its colonisation[199,200]. *C. rodentium* can subsequently disseminate to the systemic environment and in non-obese diabetic mice has been observed to promote islet-specific autoimmunity[201]. In the intestine, *C. rodentium* drives the production of pro-inflammatory cytokines IL-22 and IL-17 from ILC3s and Th17 cells, which trigger the release of AMPs and the recruitment of neutrophils (figure 1.5)[202,203]. In the microbiome, SFB can drive the differentiation of Th17 cells *via* induction of acute phase inflammatory protein serum amyloid A (SAA) from epithelial cells, as well as producing retinoic acid to regulate AMP production by IECs, further driving host defence against *C. rodentium*[175,204]. Clostridiales provide colonisation resistance to *C. rodentium* through their secretion of SCFAs which promote barrier defence[205–208]. In addition, *Escherichia coli* can outcompete *C. rodentium* for nutrients in the intestine, providing another layer of colonisation resistance[209].

C. rodentium infection is typically self-limiting in C57BL/6J mice, and mice fully clear the infection by around 21 days post-infection[210]. In germ-free mice however, due to the lack of colonisation resistance, mice are unable to effectively clear *C. rodentium* from the intestine, though they develop *C. rodentium* inverse dose-dependent disease severity and can resolve disease at similar timepoints

to SPF mice[211]. On the other hand, antibiotic treatment with kanamycin prevented the colonisation of *C. rodentium* through its inhibition of commensal microbiota, suggesting the importance of kanamycin-susceptible commensals in facilitating infection[212].

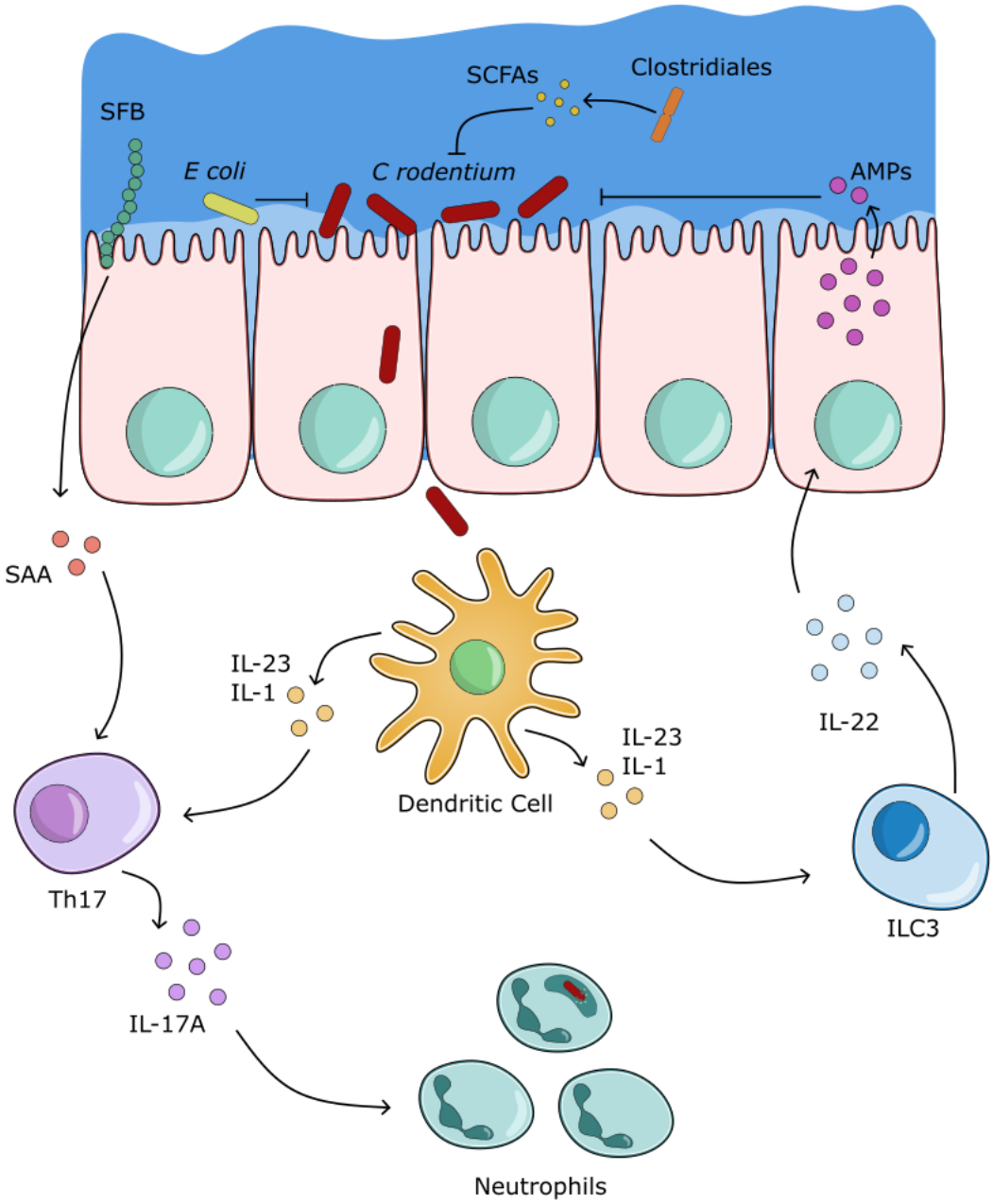


Figure 1.5 Mechanisms of host and microbial defence against *C. rodentium* infection. *C. rodentium* attaches to intestinal epithelial cells and triggers a host immune response. Dendritic cells produce IL-23 and IL-1 to induce the production of IL-22 from ILC3s. IL-22 triggers the release of antimicrobial peptides against *C. rodentium.* Production of IL-23 and IL-1 from dendritic cells, as well as SFB colonisation, drive production of IL-17 from Th17 cells, which aids in recruitment of neutrophils. Neutrophils clear invaded *C. rodentium* through phagocytosis. Colonisation resistance against *C. rodentium* includes commensal *E. coli* which can outcompete *C. rodentium* for nutrients, and Clostridiales which can produce SCFAs to prevent the growth of *C. rodentium.*

1.10 Thesis aims

Though several correlative studies have identified shifts in the microbiome in SpA, and mouse studies identify a crucial role for the intestinal microbiota in permitting pathology, the host-microbe interactions supporting disease are unknown. Therefore, this thesis seeks to determine the role of commensal microbiota in supporting the development of both ReA and AxSpA. This thesis aims to complete the following:

1. Develop a novel murine model of ReA and characterise the microbial and host immune responses in disease.
2. Identify arthritogenic microbiota and their role in supporting the development of AxSpA.
3. Characterise the intestinal and peripheral immune response in human SpA, and to correlate this with stool-derived metabolites.

Chapter 2: Materials and methods

2.1 Patient and control recruitment

Fresh-frozen (n=30) and 100% ethanol-fixed stool (n=53), and peripheral blood (n=46) were obtained from a total of 53 AxSpA patients attending the Oxford University Hospitals National Health Service Foundation Trust. A total of 91 age-matched healthy controls were recruited, with 83 of these healthy controls recruited through the Oxford BioBank. AxSpA patients met Assessment of Spondyloarthritis International Society (ASAS) classification criteria, as shown in Table 2.1. Patients that were pregnant, diagnosed with cancer, presenting with active IBD, or under the age of 18 at the time of recruitment were excluded. Patient and control demographics are shown in Table 2.2. Informed written consent was obtained (Ethics 06/Q1606/139, National Health Service, Health Research Authority, South Central – Oxford C Research Ethics Committee).

Axial Spondyloarthritis (in patients with back pain >3 months and age at onset <45 years)	
A: Sacroiliitis on imaging and ≥1 of:	B: HLA-B27+ and ≥2 of:
• Inflammatory back pain • Arthritis • Enthesitis • Uveitis • Dactylitis • Psoriasis • Crohn's disease/ulcerative colitis • Good response to NSAIDs • Family history of SpA • HLA-B27+ • Elevated C-reactive protein (CRP)	• Inflammatory back pain • Arthritis • Enthesitis • Uveitis • Dactylitis • Psoriasis • Crohn's disease/ulcerative colitis • Good response to NSAIDs • Family history of SpA • Elevated C-reactive protein (CRP)

Table 2.1 Assessment of Spondyloarthritis International Society (ASAS) classification criteria (adapted from [213]).

	AxSpA	Healthy Controls
Number collected	53	91
Age, mean (range)	50.92 (24-74)	52.14 (24-68)
Sex, male/female	40/13	42/49
HLA-B27 -/unknown/+	6/4/43	39/12/40
BASDAI, mean (range)	3.91 (0.6-8.4)	N/A
CRP, mean (range)	5.13 (0.2-31.9)	Not assessed
Disease duration (years), mean (range)	16.95 (0.77-56.96)	N/A
NSAID usage	32	12
Biologic therapy, aTNF/aIL17	17/2	N/A
DMARD therapy	7	N/A
IBD, present/absent	7/46	0/91
Psoriasis, present/absent	9/44	0/91
Uveitis, present/absent	18/35	0/91
Enthesitis, present/absent	7/46	0/91
Dactylitis, present/absent	3/50	0/91

Table 2.2 Patient and control demographics.

2.1.1 Patient and control sample collection

Blood samples were collected from patients at routine clinical visits, and from healthy controls during their visit to the Oxford BioBank. Serum was collected by centrifugation at 2500rpm for 15 minutes and stored at -80^{0}C.

Participants were provided with stool-collection kits during clinic visits. Samples were collected at home using a FecesCatcher (Tag Hemi, Zeijen, Netherlands) and a stool container (Starstedt, Nümbrecht, Germany). Ethanol-fixed stool samples were collected into 5mL molecular biology grade 100% ethanol (Sigma-Aldrich, MO, US) and mailed to the Kennedy Institute of Rheumatology by next-day Royal Mail delivery. Fresh-stool samples were placed inside disposable Styrofoam containers with ice packs and returned to clinic in-person on the same day as collection. Samples

were frozen at -80^{0}C immediately (<30 minutes) upon arrival. Fresh-frozen stool was pulverised utilising a Biopulverizer (Stratech, Cambridge, UK), then cooled in liquid nitrogen prior to aliquoting. All assays were performed on freshly thawed aliquots within 6 months of freezing.

2.2 Mice

SKG mice (BALB/c-*zap70*^{W163C}) were kindly provided by Prof. Ranjeny Thomas (Queensland, Australia). All mice were maintained in SPF or germ-free conditions in licensed animal facilities in the Kennedy Institute of Rheumatology at the University of Oxford. All procedures were conducted in accordance with the requirements of the UK Animals (Scientific Procedures) Act 1986. Females and males aged over 6 weeks were used in experiments as indicated. Mice were caged based upon experimental groups.

2.2.1 Generation and maintenance of Oligo-MM^{12} SKG mice

Oligo-MM^{12} colonised SKG mice were generated through single oral gavage of cecal contents from Oligo-MM^{12} C57BL/6J mice kindly provided by Prof. Andrew Macpherson (Bern, Switzerland), into germ-free SKG breeding pairs. To confirm colonisation, breeder stools were collected 3 days post-gavage and sent for metagenomic sequencing by Transnetyx (TN, US). Subsequent litters were used for all Oligo-MM^{12} experiments or to maintain the colony. All Oligo-MM^{12} breeding, and stock cages were maintained in flexible film isolators and screened for contamination through metagenomic sequencing by Transnetyx.

2.2.2 Generation of monocolonised SKG mice

Germ-free SKG breeding and stock cages were maintained in flexible film isolators and regularly screened for aerobic and anaerobic contaminants by culturing, and 16S qPCR. Once litters were weaned at three weeks of age, they were transferred into germ-free positive pressured individually sealed cages to carry out experiments. Monocolonised SKG mice were generated through single oral gavage of 5x10^9 colony forming unit (CFU) indicated bacteria into experimental 3-week-old germ-

free mice. To confirm colonisation, cage-pooled stools were collected 1-3 days post-gavage, homogenised in 1mL of sterile PBS (Life Technologies, CA, US), 10-fold serially diluted and then plated in bacteria-specific growth conditions (as detailed in section 2.3). Additionally, bacterial DNA was extracted from stools (as detailed in section 2.11.1) and bacteria of interest were quantified by qPCR (as detailed in section 2.11.3). Monocolonised mice were colonised for 3 weeks before being used in experiments.

2.2.3 Antibiotic administration

Bifidobacterium animalis monocolonised mice or germ-free mice were administered ampicillin (Sigma-Aldrich, MO, US) and erythromycin (Sigma-Aldrich, MO, US) in their drinking water, each at a final concentration of 1g/L. Antibiotic water was changed to freshly diluted antibiotics weekly. Mice were kept on antibiotics until the end of the experiment, unless otherwise indicated.

2.2.4 Administration of heat-killed bacteria

Bifidobacterium animalis was grown in 50mL liquid culture for 3 days and centrifuged at 4000 x *g* (av) for 10 minutes. The bacterial pellet was resuspended in 2mL of sterile PBS and heated to 95^0C for 1 hour. The bacterial suspension was then centrifuged at 4000 x *g* (av) for 10 minutes and prepared in sterile PBS at $1x10^9$ CFU for oral gavage. Gavage inoculum was plated on Wilkins-Chalgren anaerobe agar (Merck, Darmstadt, Germany) supplemented with 5% laked horse blood (Merck, Darmstadt, Germany) for 3 days to ensure bacterial death.

2.3 Bacterial Culture

2.3.1 Citrobacter rodentium

Citrobacter rodentium (strain ATCC51459) was grown from glycerol stocks on LB agar (Merck, Darmstadt, Germany) supplemented with 50 µg/mL nalidixic acid (Merck, Darmstadt, Germany) aerobically overnight at 37°C. A single colony was then isolated and inoculated into LB broth (Merck,

Darmstadt, Germany) supplemented with 50 µg/mL nalidixic acid (Merck, Darmstadt, Germany), and incubated aerobically in a shaking (200rpm) incubator set to 37°C overnight.

2.3.2 Parabacteroides distasonis

Parabacteroides distasonis (strain ATCC8503) was grown from glycerol stocks on Wilkins-Chalgren anaerobe agar plates supplemented with 5% laked horse blood at 37°C under anaerobic conditions (0% O_2, 10% CO_2, 10% H_2, 80% N_2) in a Coy vinyl anaerobic chamber (Coy Laboratory products, MI, US) for 3 days. A single colony was isolated and inoculated into Wilkins-Chalgren anaerobe broth (Merck, Darmstadt, Germany) supplemented with 5% laked horse blood (Merck, Darmstadt, Germany) and grown at 37°C under anaerobic conditions for 3 days.

2.3.3 Leuconostoc citreum

Leuconostoc citreum (strain DSM5577) was grown from glycerol stocks on MRS agar (BD Difco, NJ, US) at 30°C for 2 days. A single colony was isolated and inoculated into MRS broth (Thermo Scientific, MA, US) and incubated in a shaking (200rpm) incubator set to 30°C for 2 days.

2.3.4 Oligo-Mouse-Microbiota members

Bifidobacterium animalis (strain YL2, DSM number 26074) was grown from glycerol stocks on Wilkins-Chalgren anaerobe agar plates supplemented with 5% laked horse blood at 37°C under anaerobic conditions (0% O_2, 10% CO_2, 10% H_2, 80% N_2) in a Coy vinyl anaerobic chamber (Coy Laboratory products, MI, US) for 3 days. A single colony was isolated and inoculated into Wilkins-Chalgren anaerobe broth supplemented with 5% laked horse blood and grown at 37°C under anaerobic conditions for 3 days.

Limosilactobacillus reuteri (strain I49, DSM number 32035) was grown from glycerol stocks on MRS agar (BD Difco, NJ, US) at 37°C for 2 days. A single colony was isolated and inoculated into MRS broth (Thermo Scientific, MA, US) and incubated in a non-shaking incubator set to 37°C for 2 days.

2.4 Arthritis induction and animal models

2.4.1 Curdlan

Arthritis was induced in 6–12-week-old SKG mice by a single intraperitoneal injection of 300uL at 10µg/µL of the β-1,3-Glucan, curdlan (Wako Chemicals, Neuss, Germany). Curdlan-treated mice were compared to healthy untreated SKG controls which do not develop arthritis under SPF or germ-free conditions. Body weight and disease was monitored weekly and scoring of joint swelling was completed as detailed in section 2.4.3.

2.4.2 Citrobacter rodentium

Citrobacter rodentium was grown as described in section 2.3.1. On the day of mouse inoculation, the bacterial culture was diluted to 0.1 OD in LB broth supplemented with 50 µg/mL nalidixic acid and incubated at 37°C in a shaking incubator (200rpm) until the sub-culture reached logarithmic phase (OD 1-1.5, around 2-2.5 hours). Mice were orally gavaged with $5x10^9$ CFU in 200µL sterile PBS (Life Technologies, CA, US). CFU was calculated from OD using the following equation: CFU/mL = $5x10^7$ x log phase OD – $3x10^7$. *Citrobacter rodentium* infected mice were compared to healthy uninfected SKG controls which do not develop arthritis under SPF or germ-free conditions. Body weight and disease was monitored weekly, ankles were measured using callipers, and scoring of joint swelling was completed as detailed in section 2.4.3.

2.4.3 Paw swelling quantification

Scoring of the paw swelling was completed using the following system scoring from 0-4 in increments of 0.5: 0 = no swelling or redness, 1 = mild swelling of the wrists and/or ankle joints, 2 = moderate swelling of the wrist and/or ankle joints, 3 = moderate - substantial swelling of the wrist and/or ankle joints, 4 = substantial swelling of the wrist and/or ankle joints, not inhibiting normal mobility, feeding, and drinking. Scores of forepaws and hind paws were combined for each mouse to give a total score out of 16.

2.5 Histopathological scoring

2.5.1 Colon scoring

Colon (proximal, distal, and mid) sections were fixed in 3.7% formalin for 1 day and stored in 70% ethanol until histological processing and staining. Colon sections were paraffin-embedded in triplicate by in-house facilities and stained with hematoxylin and eosin (H&E). Sections were scored blinded, using the scoring system detailed in table 2.3.

Area	Criteria	Score
Epithelium	None	0
	Mild hyperplasia (1.5x) and/or goblet cell depletion (25%)	1
	Moderate hyperplasia (2-3x) and/or goblet cell depletion (25=50%)	2
	Severe hyperplasia (>3x) and/or substantial goblet cell depletion (>50%)	3
Inflammatory infiltrate	None – few leukocytes	0
	Mild – some increase in leukocytes at the tips of the crypts or many lymphoid follicles	1
	Moderate – marked infiltrate (notable broadening of crypt)	2
	Severe – dense infiltrate throughout	3
Area affected	None	0
	Up to 25%	1
	25-50%	2
	>50%	3
Markers of severe inflammation	None	0
	Submucosal inflammation or few crypt abscesses (<5)	1
	• Submucosal inflammation and few crypt abscesses (<5) • Many crypt abscesses(>5), extensive submucosal inflammation or crypt branching	2
	• Many crypt abscesses (>5) and extensive submucosal inflammation or crypt branching • Ulceration or extensive fibrosis	3

Table 2.3 Scoring system used for histopathology of colon tissue.

2.5.2 Small intestine scoring

Small intestine (ileum, jejunum, duodenum) sections were fixed in 3.7% formalin for 1 day and stored in 70% ethanol until histological processing and staining. Small intestine sections were paraffin-embedded in triplicate by in-house facilities and stained with H&E. Sections were scored blinded, using the scoring system detailed in table 2.4.

Area	Criteria	Score
Villous Distortion	Absent	0
	Villus height increased or decreased by <1/3 of normal	1
	Villus height increased or decreased by 1/3-2/3 of normal	2
	Villus height increased or decreased by >2/3 of normal	3
Inflammatory Infiltrate	Absent	0
	Scattered leukocytes in the lamina propria involving <5 intercryptal spaces contiguously involved in an area	1
	Increased leukocytes in the lamina propria and/or submucosa involving >5 intercryptal spaces contiguously involved in an area and ± crypt abscesses and areas of crypt/villous loss <5 crypt widths	2
	Extensive transmural inflammatory infiltrate and areas of crypt/villous loss >5 crypt widths and/or confluent areas of crypt abscesses and/or mucosal erosion/ulceration	3
Granulatoma	Absent	0
	Aggregation of cells not definitely a granuloma	1
	A definite granuloma formation present	2
	Multiple granulomas present	3
Area affected	<1%	0.5
	1-25%	1
	25-50%	2
	50-75%	3
	75-100%	4

Table 2.4 Scoring system used for histopathology of small intestine tissue (adapted from [214]).

2.5.3 Paw scoring

Hind paws were fixed in 3.7% formalin for 1 day and stored in 70% ethanol until histological processing and staining. Paws were decalcified in 10% neutral buffered EDTA for 4 weeks before

being paraffin-embedded by in-house facilities. Sections were then stained with H&E. Sections were scored blinded, using the scoring system detailed in table 2.5.

Features	Score
Few infiltrating immune cells	1
Small patches of inflammation	2
Inflammation throughout the ankle joint	3
Inflammation in soft tissue/entheses/fasciitis	4

Table 2.5 Scoring system used for histopathology of arthritis.

2.6 ELISA

2.6.1 Stool supernatant preparation

~100mg of pulverised human stool or 1 pellet of mouse stool was added to 1mL of cOmplete ULTRA tablets EDTA-free (Roche, Basel, Switzerland) using screw cap O-ring microcentrifuge tubes (ThermoFisher Scientific, MA, US) and homogenised in a TissueLyser II (Qiagen, Manchester, UK) at 30Hz for 10 minutes, before centrifugation (10,000 x *g* (av) for 3 minutes at 4°C). Supernatants were then filtered using 70µm cell strainers (Fisher Scientific, NH, US) and filtered supernatants were stored at -80°C until quantification by ELISA.

2.6.2 Human stool inflammatory marker quantification

Levels of inflammatory proteins (full list detailed in table 2.6) were assessed in the stool supernatant by ELISA following the manufacturer's instructions, incubating samples, and standards overnight at 4^0C. Plates were read at 450nm.

2.6.3 Intestinal barrier marker quantification in human serum

Levels of LPS binding protein (LBP), soluble (s)-CD14, and iFABP were assessed in serum using ELISA following the manufacturer's instructions (R&D Systems, MN, US) and plates were read at 450nm.

Protein	Supplier
Calprotectin (S100A8/9)	BioLegend
GM-CSF	Sigma-Aldrich
IFNγ	Sigma-Aldrich
IL-5	R&D Systems
IL-6	Sigma-Aldrich
IL-10	Sigma-Aldrich
IL-17A	Sigma-Aldrich
IL-17F	R&D Systems
IL-21	Sigma-Aldrich
IL-22	Sigma-Aldrich
IL-23	Sigma-Aldrich
Myeloperoxidase (MPO)	BioLegend
Oncostatin M (OSM)	R&D Systems
TNFα	Sigma-Aldrich

Table 2.6 Proteins quantified by stool ELISA on patients with AxSpA and healthy controls.

2.6.4 Mouse Lipocalin-2 (LCN-2) ELISA

Levels of Lipocalin-2 were assessed in mouse stool using the LCN-2 Mouse ELISA Kit (ThermoFisher Scientific, MA, US) according to manufacturer's instructions and plates were read at 450nm.

2.7 Bacterial CFUs from systemic organs

Livers, spleens, mesenteric lymph nodes (mLNs), and popliteal lymph nodes (pLNs) were aseptically harvested from mice and added to CK14 soft tissue homogenisation tubes (Precellys, PA, US) containing sterile PBS. Paws were sprayed with 70% ethanol and deskinned with digits removed before being added to hard tissue reinforced metal bead tubes (VWR International, PA, US) containing sterile PBS. Tissues were then homogenised for 10 minutes at 30Hz using a TissueLyser II, and subsequently plated on Wilkins-Chalgren anaerobe agar plates supplemented with 5% laked horse blood and incubated both aerobically and anaerobically (0% O_2, 10% CO_2, 10% H_2, 80% N_2) in a Coy vinyl anaerobic chamber for 5 days at 37°C. To identify bacterial colonies, single colonies were

picked and resuspended in 1mL of sterile PBS. Bacterial suspensions were then centrifuged, and pellets were kept at -20°C until DNA extraction (detailed in section 2.11.2).

2.8 Assessment of immune cell populations by flow cytometry

2.8.1 PBMC isolation from human blood

Blood was diluted 1:1 in RPMI-1640 (ThermoFisher Scientific, MA, US) before peripheral blood mononuclear cells (PBMCs) were isolated using histopaque density gradient centrifugation at 2000rpm for 20 minutes without the break (Sigma-Aldrich, MO, US). Isolated PBMCs were stored in liquid nitrogen until flow cytometric staining and analysis.

2.8.2 Isolation of leukocytes from mouse tissue

Cell suspensions were prepared from spleens by passing them through 70µm cell strainers (Fisher Scientific, NH, US) into PBS supplemented with 5% BSA. To lyse splenic red blood cells, spleen cell preparations were resuspended in 1mL ACK lysis buffer and incubated for 1 minute at room temperature before quenching the reaction with 10mL of PBS/BSA and centrifuging at 500 x *g* (av) for 5 minutes. 1/5 of splenic cell suspensions were prepared in PBS/BSA ready for staining detailed in section 2.8.4.

Colonic sections were opened using scissors and washed twice with Roswell Park Memorial Institute medium (RPMI)-1640 (Merck, Darmstadt, Germany) supplemented with 5% fetal bovine serum (FBS) (Bio-Techne, Abingdon, UK) and 5mM EDTA in a shaking incubator set to 37^0C. Colonic tissue was then digested with 1mg/mL collagenase type VIII (Merck, Darmstadt, Germany) diluted in RPMI-1640 supplemented with 5% FBS and 15mM HEPES (Merck, Darmstadt, Germany) for ~60 minutes in a shaking incubator set to 37^0C. Digested preparations were quenched with EDTA and then passed through 70µm cell strainers and resuspended in 4mL of 37.5% Percoll (VWR International, PA, US) and centrifuged at 500 x *g* (av) for 5 minutes. Entire leukocyte pellets were then resuspended in PBS/BSA for staining.

Small intestinal sections were opened using scissors and excess mucus and fat was removed, tissues were then washed twice with RPMI-1640 supplemented with 5% FBS and 5mM EDTA in a shaking incubator set to 37^0C. Small intestinal tissue was then digested with 0.5mg/mL collagenase type VIII and 0.5mg/mL DNase I (Merck, Darmstadt, Germany) diluted in RPMI-1640 supplemented with 5% FBS for ~35 minutes in a shaking incubator set to 37^0C. Digested preparations were then passed through 70µm cell strainers and resuspended in 4mL of 37.5% Percoll and centrifuged at 500 x *g* (av) for 5 minutes. Entire leukocyte pellets were then resuspended in PBS/BSA for staining.

Fur, skin, and digits were removed from hind paws and the tissue was cut into 3 pieces and collected in 2mL of PBS/BSA. Paw tissue was then digested in 0.1mg/mL DNase I and 0.3mg/mL Liberase (Roche, Basel, Switzerland) for 90 minutes at 37^0C. Digested tissues were quenched in EDTA and then passed through 70µm cell strainers and entire leukocyte pellets were resuspended in PBS/BSA for staining.

2.8.3 Intracellular staining of human PBMCs

PBMCs from AxSpA patients and healthy controls were stimulated with phorbol myristate acetate (125ng/ml; Sigma-Aldrich, MO, US) and ionomycin (1µg/ml; Sigma-Aldrich, MO, US) in the presence of Golgiplug (Brefeldin A) and Golgistop (Monensin) (both from BD Biosciences, NJ, US diluted according to the manufacturer's instructions) and incubated for four hours at 37^0C in 5% CO_2. Cells were stained for surface markers (antibodies shown in table 2.6) for 20 minutes on ice, and then permeabilised using Cytofix/Cytoperm fixation and permeabilisation solution (BD Biosciences, NJ, US). Cells were then stained to identify production of the following cytokines (antibodies shown in table 2.7); IL-17A, IL-17F, IL-5, IL-10, IFNγ, GM-CSF for 30 minutes at room temperature.

Flourophore	Marker	Clone	Supplier
BV786	CD3	OKT3	BioLegend
BV510	CD4	RPA-T4	BioLegend
PerCP/Cy5.5	CD8	RPA-T8	BioLegend
eFluor780	Fixable viability dye	N/A	ThermoFisher
BV711	IL-10	JES3-9D7	BD Biosciences
BV650	IL-17A	N49-653	BD Biosciences
PE	IL-17F	O33-782	BD Biosciences
AF700	IFNγ	B27	BioLegend
APC	IL-5	TRFK5	BD Biosciences
PE-CF594	GM-CSF	BVD2-21C11	BD Biosciences

Table 2.7 Antibodies used for intracellular staining of human PBMCs.

2.8.4 Staining of mouse leukocytes

Cell suspensions were stained for surface markers using antibodies diluted in PBS/BSA for 20 minutes on ice. In experiments where intracellularly staining was not completed, cells were fixed using Cytofix/Cytoperm fixation solution for 30 minutes at room temperature and resuspended in 200µL PBS/BSA with 3µL per sample of CountBright™ absolute counting beads (Life Technologies, CA, US) added for acquisition. In experiments where intracellular staining was completed, cells were permeabilised in Foxp3/transcription factor fixation/permeabilisation solution (ThermoFisher Scientific, MA, US) for 30 minutes at room temperature. Intracellular antibodies were prepared in 1X permeabilisation buffer (ThermoFisher Scientific, MA, US) and cells were stained for 30 minutes at room temperature. Cells were resuspended in PBS/BSA with 3µL per sample of CountBright™ absolute counting beads added for acquisition. Surface and intracellular antibodies used for flow cytometric staining are shown in table 2.8.

2.8.5 Data acquisition

Flow cytometry was performed on a BD LSR II flow cytometer calibrated with calibration and tracking beads (BD Biosciences, NJ, US). Data was analysed using FlowJo™ v10 software (BD Biosciences, NJ, US).

Surface antibodies			
Fluorophore	**Marker**	**Clone**	**Supplier**
FITC/ BV711	TCRβ	H57-597	BioLegend
BV510/BV650/ BV785	CD4	RM4-5	BioLegend
BV605/ PE-Cy7/ BV510	CD45	30-F11	BioLegend
APC	CD103	M290	BD Bioscience
BV421	CD11c	3.9	BioLegend
BV510	MHC II	M5/114.15.2	BioLegend
BV605	CD11b	M1/70	BioLegend
BV650	Ly6G	1A8	BioLegend
BV711	F4/80	BM8	BioLegend
FITC	CD206	C068C2	BioLegend
PerCP/Cy5.5	Ly6C	HK1.4	BioLegend
Fixable viability dye	eFluor780	N/A	ThermoFisher
Intracellular antibodies			
Flourophore	**Marker**	**Clone**	**Supplier**
PE	RORγt	Q31-378	BD Bioscience
BV421/ APC	FoxP3	FJK-16s	BioLegend

Table 2.8 Antibodies used for flow cytometric staining of murine leukocytes.

2.9 Bacterial flow cytometry

2.9.1 Immunoglobulin bacterial surface staining

~30mg of frozen stool or intestinal contents from mice were transferred into 1mL sterile PBS and rehydrated on ice for 10 minutes. Samples were then vortexed for 1 minute to homogenise bacteria, and then centrifuged at 100 x *g* (av) for 2 minutes. Supernatants were taken as bacterial suspensions and passed through 70µm cell strainers to remove debris. Samples were then blocked with 10% rat serum (Sigma-Aldrich, MO, US) for 10 minutes on ice, before being stained with antibodies to either IgA or IgG (Table 2.9) diluted in sterile PBS/BSA for 30 minutes on ice. Samples were then stained with SYBR green (Life Technologies, CA, US) for 10 minutes at room temperature in the dark. Data was acquired on a BD Fortessa, or a BD LSR II flow cytometer calibrated with calibration and tracking beads. Data was analysed using FlowJo™ v10 software.

Flourophore	Marker	Clone	Supplier
PE	IgA	mA-6E1	BioLegend
PE	IgG	Poly4053	BioLegend
FITC	SYBR	N/A	ThermoFisher

Table 2.9 Antibodies used for bacterial flow cytometric staining.

2.10 Host RNA analysis

2.10.1 Host RNA Extraction

Colon and small intestine tissues were frozen in RNAlater/RNAprotect (Qiagen, Manchester, UK) and stored at -80^{0}C until extraction. Samples were thawed and tissues were opened using scissors. Samples were then homogenised using CK14 soft tissue homogenisation tubes in RLT lysis buffer (Qiagen, Manchester, UK) containing 1% β-mercaptoethanol (Merck, Darmstadt, Germany) using a TissueLyser II for 10 minutes at 30Hz. Samples were then processed using the RNEasy miniprep kit (Qiagen, Manchester, UK) to extract RNA according to manufacturer's instructions. RNA was then stored at -80^{0}C until converting to cDNA.

2.10.2 qRT-PCR

1µg of RNA was reverse transcribed using a High-capacity cDNA reverse transcription kit with 5% Rnase inhibitor (Applied Biosystems, MA, US) according to manufacturer's instructions. Real time (RT)-PCR was performed on the C1000 Touch^{TM} Thermal Cycler (Bio-Rad, CA, US). cDNA was then diluted 1:10 using nuclease-free water prior to quantitative PCR (qPCR). qPCR was carried out using the Viia7 real-time PCR detection system (Applied Biosystems, MA, US) using TaqMan assays detailed in table 2.10 (Applied Biosystems, MA, US) and PrecisionPlus mastermix (PrimerDesign, Hampshire, UK). *Hprt* was the housekeeping control gene, with relative expression of genes of interest calculated using the equation $2^{-\Delta CT}$ where ΔCT = gene of interest CT – housekeeping gene CT.

Gene	Assay ID
Hprt	Mm01545399_m1
Cldn1	Mm00516701_m1
Ocln	Mm00500912_m1
Clec7a	Mm01183349_m1
Tlr2	Mm00442346_m1
Tlr4	Mm00445273_m1
Tlr5	Mm07297422_m1

Table 2.10 Taqman probes used for quantitative PCR.

2.11 Bacterial DNA analysis

2.11.1 DNA extraction from stool or intestinal contents

Mouse stool pellets were processed using the Dneasy Powersoil Pro kit (Qiagen, Manchester, UK) according to manufacturer's instructions to extract bacterial DNA. Homogenisation was completed at 30Hz for 10 minutes using a TissueLyser II with kit supplied lysis buffer and bead beating tubes.

2.11.2 DNA extraction from bacterial colonies

Single colonies were resuspended in 1mL of sterile PBS and centrifuged at 10,000 x *g* (av) for 3 minutes. Bacterial pellets were then resuspended in 200µL of nuclease-free water and heated to 100^0C for 5 minutes. Immediately following heating, samples were then cooled to -20^0C for 10 minutes. After cooling, samples were centrifuged at 10,000 *g* (av) for 3 minutes and supernatant was taken as bacterial DNA for downstream analysis.

2.11.3 Quantification of Oligo-Mouse-Microbiota members

Oligo-MM^{12} members were quantified by qPCR using primers and probes 5'-labelled with 6-carboxyfluorescein (FAM) and conjugated with a 3' fluorescent quencher (TAMRA dye) shown in table 2.11 with specificity to each Oligo-MM^{12} member as previously published [215] diluted in Takyon Low ROX Probe 2X MasterMix (Eurogentec, Seraing, Belgium) using the Viia7 real-time PCR detection system. Standard curves were generated from linearised plasmids containing 16S

sequences of Oligo-MM^{12} members which were kindly gifted by Professor Bärbel Stecher (Munich, Germany). [215] Plasmid stocks were maintained by transforming Subcloning Efficiency DH5α Competent Cells (ThermoFisher Scientific, MA, US) in SOC media (ThermoFisher Scientific, MA, US) according to manufacturer's instructions. Following the transformation, cells were plated on LB agar supplemented with 100µg/mL of ampicillin overnight at 37^{0}C. A single colony of transformed cells was inoculated into LB broth supplemented with 100µg/mL of ampicillin and incubated at 37^{0}C overnight. DNA was extracted from transformed cells using the Isolate II Plasmid Mini Kit (Meridian Bioscience, OH, US) according to manufacturer's instructions. Plasmid DNA was linearised using restriction digest with NotI, HindIII, or NcoI enzymes (New England Biolabs, MA, US) as appropriate for each Oligo-MM^{12} member primer/probe set and according to manufacturer's instructions. Plasmid standards were prepared using 10-fold serial dilutions from 2 x 10^8 copies/µL.

Bacterium	Forward sequence	Reverse sequence	Probe sequence
I46	CGGATCGTAAAGCTCTGTTGTAAG	GCTACCGTCACTCCCATAGCA	AAGAACGGCTCATAGAGG
I49	GCACTGGCTCAACTGATTGATG	CCGCCACTCACTGGTGATC	CTTGCACCTGATTGACGA
YL58	GAAGAGCAAGTCTGATGTGAAAGG	CGGCACTCTAGAAAAACAGTTTCC	TAACCCCAGGACTGCAT
YL27	TCAAGTCAGCGGTAAAAATTCG	CCCACTCAAGAACATCAGTTTCAA	CAACCCCGTCGTGCC
YL31	AGGCGGGATTGCAAGTCA	CCAGCACTCAAGAACTACAGTTTCA	CAACCTCCAGCCTGC
YL32	AATACCGCATAAGCGCACAGT	CCATCTCACACCACCAAAGTTTT	CGCATGGCAGTGTGT
KB1	CTTCTTTCCTCCCGAGTGCTT	CCCCTCTGATGGGTAGGTTACC	CACTCAATTGGAAAGAGGAG
YL2	GGGTGAGTAATGCGTGACCAA	CGGAGCATCCGGTATTACCA	CGGAATAGCTCCTGGAAA
KB18	TGGCAAGTCAGTAGTGAAATCCA	TCACTCAAGCTCGACAGTTTCAA	CTTAACCCATGAACTGC
YL44	CGGGATAGCCCTGGGAAA	GCGCATTGCTGCTTTAATCTTT	TGGGATTAATACCGCATAGTA
YL45	AGACGGCCTTCGGGTTGTA	CGTCATCGTCTATCGGTATTATCAA	ACCACTTTTGTAGAGAACGA
I48	GGCAGCATGGGAGTTTGCT	TTATCGGCAGGTTGGATACGT	CAAACTTCCGATGGCGAC

Table 2.11 Primers and probes used to quantify Oligo-MM^{12} members by quantitative PCR.

2.11.4 Sanger sequencing

DNA from unknown bacterial colonies was amplified using 27F/1492R primers that cover the length of the 16S gene (table 2.12) diluted in 5PRIME HotMasterMix (VWR International, PA, US) using the C1000 Touch™ Thermal Cycler. Amplified DNA was then cleaned using the UltraClean 96 PCR Cleanup Kit (Qiagen, Manchester, UK) and sent to Source BioScience for Sanger sequencing using 27F/1492R primers. Sequences were aligned using SnapGene version 6.2, and aligned sequences were identified using Basic Local Alignment Search Tool (BLAST)[216].

Primer	Sequence
27-forward	AGAGTTTGATCMTGGCTCAG
515-forward	GTGCCAGCMGCCGCGGTAA
805-reverse	GACTACCAGGGTATCTAAT
1492-reverse	GGTTACCTTGTTACGACTT

Table 2.12 Primers used to quantify/amplify the 16S gene.

2.11.5 16S sequencing

V4 region of the 16S gene was amplified using barcoded 515F/806R primer pairs diluted in 5PRIME HotMasterMix. Amplicons were then cleaned using the UltraClean PCR Clean-Up Kit (Qiagen, Manchester, UK) according to manufacturer's instructions and quantified using the Quant-iT dsDNA high-sensitivity kit (ThermoFisher, MA, US) in triplicate according to manufacturer's instructions. Samples were then pooled, and the pooled library was precipitated in 100% ethanol and 0.2M NaCl for 45 minutes on ice. The DNA pellet was then washed in 70% ethanol and then air dried to remove residual ethanol prior to resuspension in nuclease-free water. Gel clean-up was performed using the QIAquick Gel Extraction kit (Qiagen, Manchester, UK) and the library was then sequenced in the MiSeq (Illumina) platform to generate 2 x 250 base pair paired end reads.

2.11.6 16S sequencing analysis

Initial demultiplexing was completed by Dr Nick Ilott. Adaptor sequences were removed and reads trimmed for quality using EasyMAP[217]. Amplicon sequence variants (ASVs) were annotated

from the SILVA V4 database using EasyMAP. Downstream analysis was completed in R v4.2.1. Colour palettes for compositional plots were assigned using randomcoloR v1.1.0.1. Principle component analysis (PCA) was performed using phyloseq version 1.40[218]. Statistical analysis was completed using student's t-test using rstatix v0.7.2[219]. All p values were corrected for multiple testing using Benjamini-Hochberg approach.

2.11.7 Shotgun metagenomic sequencing analysis

Mouse stool pellets were collected using Transnetyx microbiome sample collection kits which contain barcoded sample collection tubes (Transnetyx Microbiome, TN, US). Stool pellets from each mouse were placed in collection tubes which contain DNA stabilisation buffer and shipped to Transnetyx for DNA extraction, library preparation, and shallow shotgun whole-genome sequencing. Gene annotation was completed using the One Codex software database consisting of >115,000 whole microbial reference genomes. Downstream analysis was completed in R v4.2.1. PCA was carried out using phyloseq version 1.40[218]. Statistical testing was completed using lmerTest v3.1-3 for linear modelling (Abundance ~ Treatment * Experiment + (1|SampleID)) and emmeans v1.8.7 for post-hoc estimated means testing[220,221]. All p values were corrected according to the Benjamini-Hochberg approach for multiple testing.

2.12 Bacterial fluorescent in-situ hybridisation

Distal colon, ileum, and caecum tissues were collected with contents remaining in the lumen and fixed in methacarn fixative (60% methanol (Fisher Scientific, NH, US), 30% chloroform (Fisher Scientific, NH, US), 10% acetic acid (Fisher Scientific, NH, US)) for 48 hours. Samples were then washed sequentially in methanol, ethanol (Sigma-Aldrich, MO, US), and xylene (Fisher Scientific, NH, US) before being embedded in paraffin wax. Paraffin-embedded tissues were sectioned to 5µm thickness. Tissue sections were washed in xylene, followed by ethanol. The probe used (Table 2.13) was EUB338 designed to target the bacterial 16S ribosomal RNA. Sections were then incubated with 10ng/µL of each probe diluted in prewarmed hybridisation buffer (0.9M NaCl (Sigma-Aldrich, MO,

US), 20mM Tris-HCl (Sigma-Aldrich, MO, US) pH 7.4, 10% formamide (Sigma-Aldrich, MO, US), 0.01% SDS (ThermoFisher Scientific, MA, US) overnight at 50^0C in a humid hybridisation chamber. Tissue sections were then washed in pre-warmed washing buffer (0.9M NaCl and 20mM Tris-HCl, pH 7.4) for 20 minutes at 50^0C. Tissue sections were then counterstained with DAPI at 1:500 dilution for 1 hour at 4^0C and mounted using VECTA SHIELD Mounting Medium (Vector Laboratories, CA, US). Confocal images were acquired as z stacks using a Zeiss 980 confocal microscope through 20X or 40X objective.

Primer	Specificity	Sequence	Fluorophore
Eub338	All bacteria	GCTGCCTCCCGTAGGAGT	Cy3

Table 2.13 DNA probe used for bacterial fluorescent in-situ hybridisation.

2.13 Metabolomics

2.13.1 NMR metabolomics on human stool samples

The following methods were completed by collaborator Professor Stephen Young (Birmingham, UK).

Ethanol-fixed stool samples were dried down under vacuum (18-24hrs Speedivac) to remove the preserving ethanol until the weight was constant. Tubes were weighed and water (2ml/gm solid material) was added along with two 7mm stainless steel balls (Qiagen). The tubes were then shaken vigorously in a bead mill (low setting Qiagen Tissuelyzer II) for 5 mins to disperse the dried faeces to a homogenous suspension. Tubes were centrifuged (13,000 x *g* (av) 15 mins 4^0C) and supernatants re-centrifuged (13,000 x *g* (av) for 30min at 4^0C). The supernatant was diluted in a 1:3 ratio with NMR buffer containing 1.6mM Difluorotrimethylsilylmethylphosphonic acid (DFTMP, Manchester Organics, Manchester, UK), 400mM phosphate, 40% D2O, 0.4% azide and 2mM 3-(Trimethylsilyl)-1-propanesulfonic acid-d6 sodium salt (DSS-d6, all from Merck). An aliquot (60ul) was removed to glass champagne vials (Cole-Parmer) and stored at -80°C until analysis. Samples were defrosted and transferred to 1.7mm NMR tubes (Bruker Biospin) using an Anachem Autosampler. After capping the

tubes and wiping with dust-free paper, one-dimensional 1H spectra were acquired at 300K using a standard 1D-1H-Nuclear Overhauser Effect spectroscopy (NOESY) pulse sequence with water saturation using pre-sat in a Bruker AVANCE II 600 MHz NMR spectrometer (Bruker Corp.) equipped with a 1.7 mm cryoprobe. Spectral width was set to 12 ppm and the scans were repeated 128 times. Samples were loaded into racks and held at 6^0C in the SampleJet sample handing device until processed. Spectra were read into Chenomx NMR Suite v8.6 and each manually compared with a library of metabolites NMR spectra to identify the major metabolites.

2.13.2 NMR downstream analysis

The following analysis was completed by collaborator Dr Kelsey Thompson (Boston, US).

NMR data was analyzed for associations with the patients immunophenotypes in R v4.1.2[222], using R Studio. Ethanol was removed as a component of the analysis due to the sample storage in EtOH before extraction. Processed NMR data was median normalized with the limma:normalizeMedianValues function[223]. Per-feature models were then constructed using the defaults in MaAsLin 2 v1.8.0[224]. Briefly, this included log transforming the data and then constructing a linear model for each feature adjusting for the NMR batch with the formula: feature ~ IL23 (fecal) + MBX batch.

2.14 General data analysis

Multiple correlations and t-tests were completed with patient and control metadata. To correct for multiple comparisons in these cases, Benjamini-Hochberg approach was used to identify significant comparisons with a false discovery rate set to 10%.

Sample size for mouse experiments were guided by previous mouse experiments in the laboratory. Results are represented as mean ± standard error mean (SEM). Student's t-test, one-way or two-way ANOVA, or linear modelling was performed as noted in figure legends. All data for results chapters 3 and 4 were processed, graphs produced, and statistical analyses completed in R

version 4.2.1. Data for results chapter 5 was processed, graphs produced, and statistical analyses completed in both R version 4.2.1 and GraphPad Prism version 9.2. Axis breaks were completed in R version 4.2.1 using ggbreak v0.1.2[225].

2.15 Diagrams

Inkscape v1.2 was used to draw each diagram. Some complex aspects of diagrams are added from BioRender.com.

Chapter 3: *Citrobacter rodentium* infection serves as a murine model for ReA

3.1 Introduction

Several spondyloarthritides are associated with the intestinal microbiome, particularly reactive arthritis (ReA), which is diagnosed following joint inflammation as a result of enteric or genitourinary infection[226]. Although ReA is typically a self-limiting disease, around 50% of patients develop persistent symptoms and the mechanisms behind this persistence are unknown[227]. HLA-B27+ individuals are around 50% more likely to develop ReA, however ReA is prevalent in geographical populations where HLA-B27 positivity is low, suggesting that other factors can influence its development[84,228]. The commensal intestinal microbiome may play a role in driving the development of arthritis in ReA. Indeed, shifts in the intestinal microbiome of patients with ReA have been demonstrated, with increased abundances of typically pathogenic taxa such as *Pseudomonas* and *Erwinia* and decreased abundances of taxa associated with the production of anti-inflammatory metabolites such as *Colinsella* and *Roseburia*[153]. The enteropathogens associated with ReA are known to disrupt the intestinal barrier and include *Salmonella, Yersinia, and Shigella*[84]. Furthermore, increased intestinal permeability has been demonstrated in patients with SpA[6,123]. Synovial fluid obtained from patients with ReA has been found to contain bacterial DNA, antigenic proteins, and LPS, suggesting a role for the intestinal barrier in transposing disease to the joint[106,229].

Despite a well-known association of enteral infection and ReA development, current murine models of ReA do not allow for mechanistic study into the host-microbiota interactions involved in disease. Indeed, HLA-B27/hβm transgenic rats provide a robust model for studying the gut-joint axis in AxSpA as they develop joint and intestinal inflammation, however infection is not involved in triggering their disease and therefore renders them less relevant in the study of ReA[90]. *Yersinia*-infected TNFRp55-/- mice provide a model for studying ReA, however disease is very severe and

leads to an 80% rate of mortality in infected mice, making it less relevant to clinical ReA[104]. The SKG mouse model involves a point mutation in the gene encoding ZAP-70, a TCR signalling molecule, thereby driving the accumulation T cells that have escaped negative selection[107]. SKG mice provide a robust model for studying host-microbial interactions involved in AxSpA development, however the trigger is delivered *via* intraperitoneal injection and does not recapitulate mucosal infection observed in ReA[113]. A model for genitourinary infection associated ReA was developed by infecting SKG mice with *Chlamydia muridarum* intravaginally with resulting joint inflammation[114]. This suggests that a microbial trigger delivered mucosally may be sufficient to induce the development of arthritis in SKG mice. Notably, mice in this study were first primed with medroxyprogesterone acetate to impair the vaginal epithelial barrier, suggesting that impaired barrier function influences joint disease during infection[114]. We therefore sought to utilise SKG mice to model ReA development following gastrointestinal infection.

Utilising human pathogens associated with ReA such as *Salmonella, Shigella,* and *Yersinia* in murine models poses several challenges. For instance, *Salmonella* cannot robustly colonise mouse strains which possess the host-resistance gene *Nramp1* for long periods, and SKG mice are positive for *Nramp1*[230]. Furthermore, the use of mouse-adapted pathogens is preferable as they permit the evolution of host-microbiota association to be maintained, thereby allowing for more physiologically relevant interactions to be identified. *Citrobacter rodentium* is an enteric mouse-adapted pathogen that forms attaching and effacing lesions on the intestinal epithelial layer, disrupting the intestinal barrier[231]. *C. rodentium* infection in wild-type C57BL/6J mice is characterised by the recruitment of Th17 cells to the intestine through the production of IL-23 from dendritic cells, where barrier protective Th17 production of IL-22 and IL-17 drives the secretion of antimicrobial peptides (AMPs)[231]. Furthermore, the production of IL-23-dependent Th17 cells is a hallmark of disease in curdlan-triggered SKG arthritis, suggesting that use of *C. rodentium* may provide a Th17 trigger required for disease in the SKG model[113]. *Citrobacter rodentium* has previously been associated with driving disease in the nonobese diabetic model of diabetes, as it

promotes islet-specific T-cells in the pancreatic lymph nodes, which drive autoimmunity in the pancreas[201]. The ability of *C. rodentium* to drive autoimmune responses suggest its relevance in the SKG model for studying host-microbe interactions relevant to ReA.

Inferring causality in microbiome studies is a challenge due to the vast range and number of bacteria present in the intestinal lumen. Therefore, gnotobiotic models provide a method of reducing the complexity associated with microbiome research[193]. The Oligo-MM^{12} community provides a robust model to study host-microbiota interactions *in vivo*[194]. Thus, the aim of this chapter is to develop a model of ReA which can be further modelled in the Oligo-MM^{12} to delineate interactions supporting disease.

3.2 Aim

In this chapter we aimed to develop a model for ReA utilising *Citrobacter rodentium* in SKG mice. We further sought to characterise the microbial changes associated with this mouse model, and to identify how crucial the microbiota is in permitting arthritis. Finally, we generated Oligo-MM^{12} SKG mice and aimed to assess our ReA model in Oligo-MM^{12} mice to reduce the complexity associated with studying the microbiome.

3.3 Results

3.3.1 A novel model for ReA with enteric *Citrobacter rodentium* infection in SKG mice

Patients with ReA develop joint inflammation following enteric infection with *Enterobacteriaceae* including *Salmonella, Shigella, and Yersinia*[84]. To develop a murine model for ReA, we sought to identify a murine enteric pathogen that would elicit joint inflammation in a mouse model of arthritis. We orally gavaged SKG mice with *C. rodentium* and culled them at 2 weeks and 4 weeks post-infection. We found that the mice infected with *C. rodentium* developed persistent arthritis over 4 weeks (figure 3.1A-C).

C. rodentium drives colonic inflammation in C57BL/6J and Balb/C mice, so we measured the neutrophil-associated protein, lipocalin-2 (LCN-2) by ELISA in the stool of mice infected with *C. rodentium* to assess intestinal inflammation[232]. We found that LCN-2 peaked in the stool in mice 2 weeks-post infection, around the same time stool *C. rodentium* load peaked (figure 3.1D, E). Furthermore, we determined the effects of *C. rodentium* on colon histopathology by assessing H&E-stained colon tissues for evidence of disease according to section 2.5.1. We observed colon histopathology peak 2 weeks post-infection with *C. rodentium* (figure 3.1F, G). Thus, *C. rodentium* can colonise and initiate colitis in SKG mice, and this colitis is reduced when *C. rodentium* burden is clearing. However, systemic joint inflammation persists following infection resolution, suggesting that continued *C. rodentium* colonisation is not required for the persistence of arthritis.

3.3.2 *C. rodentium*-infected SKG mice display increased colonic and paw RORγt+ T cells

C. rodentium was able to elicit both paw and colon inflammation in SKG mice, so we sought to characterise the immune response at these sites. The SKG-curdlan model of arthritis is associated with increased Th17 and impaired T_{reg} responses, and *C. rodentium* elicits Th17 responses in the colon during infection in C57BL/6J mice [109,113,233]. Thus, we characterised Th17 and Treg responses in the colon and the paws of SKG mice infected with *C. rodentium* by flow cytometry staining of T cell transcription factors. Transcription factor gating strategy is outlined in appendix figure 3.1, informed by fluorescence minus one (FMO) controls. At 2 weeks post-infection frequencies of colonic RORγt+ T helper cells were significantly increased compared to uninfected mice (figure 3.2B). Notably, frequencies of paw RORγt+ T helper cells were also elevated compared to uninfected mice demonstrating that *C. rodentium* infection is able drive Th17 responses in the paw of SKG mice (figure 3.2F). We observed that frequencies and numbers of colon and paw FoxP3+ T helper cells were significantly reduced 4 weeks post-infection, compared to mice 2 weeks post-infection (figure 3.2A, C, E, G). Furthermore, we observed a similar reduction in the frequencies and numbers of colon and paw RORγt+ T helper cells 4 weeks post-infection, compared to 2 weeks post-

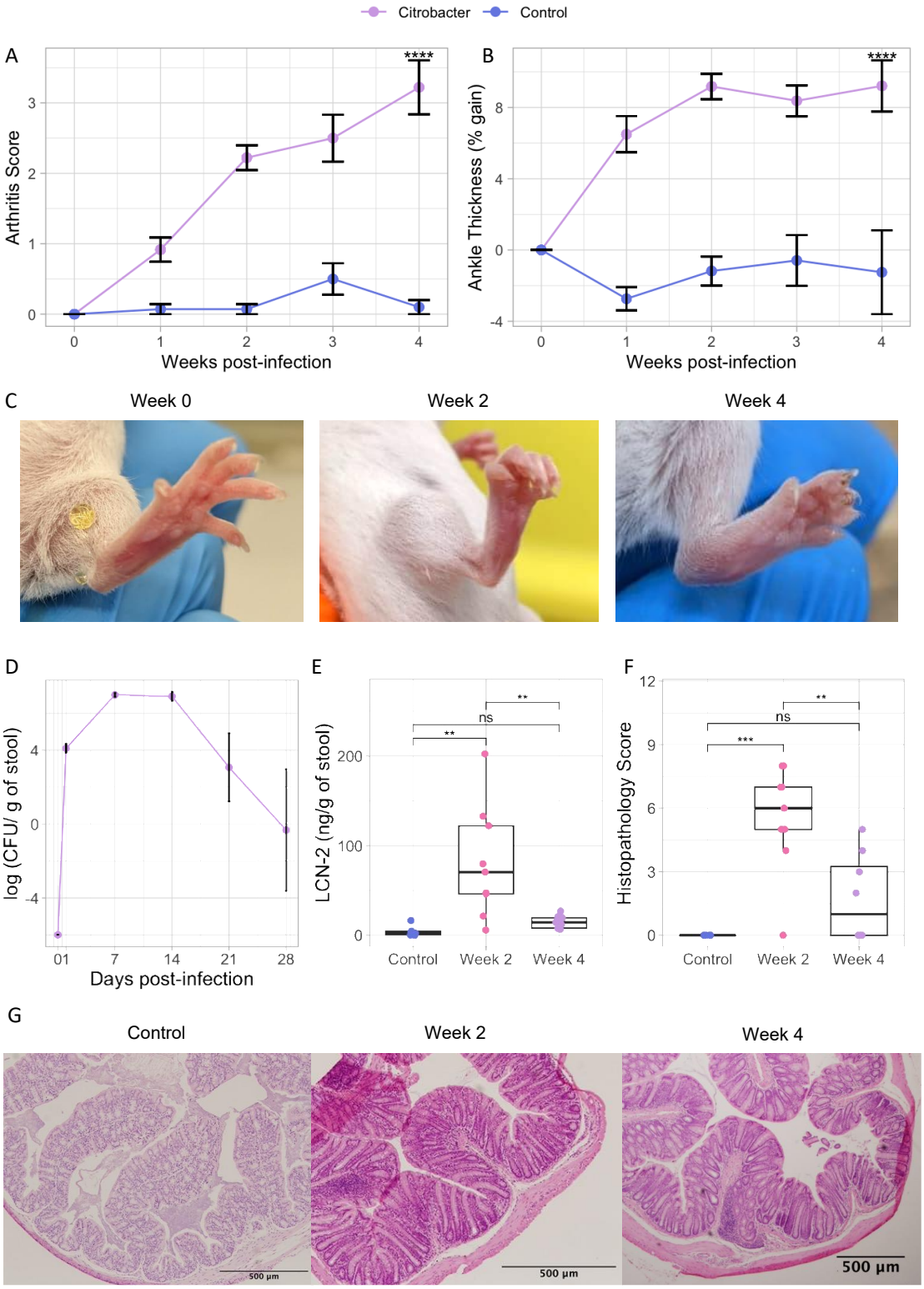


Figure 3.1 A novel model for ReA with enteric *Citrobacter rodentium* infection in SKG mice. SKG mice were orally gavaged with $5x10^9$ CFU *C. rodentium* and culled at 2 weeks and 4 weeks post-infection. A) Arthritis scores in infected and uninfected SKG mice. B) Ankle thickness in infected and uninfected SKG mice. C) Representative images of SKG mice paws prior to infection, 2 weeks post-infection, and 4 weeks post-infection. D) *C. rodentium* load in the stool of infected SKG mice. CFU = colony forming units. E) Stool lipocalin-2 levels (ng/g of stool) in infected and uninfected SKG mice. F) Colon histopathology scoring in infected and uninfected SKG mice. G) Representative microscopy images of H&E-stained colon tissue sections prior to *C. rodentium* infection, 2 weeks post-infection, and 4 weeks post-infection. ****p<0.0001, ***p<0.001, **p<0.01, ns=not significant. A) and B) mixed linear effects modelling. E) and F) one-way ANOVA with Tukey's post-hoc testing. Points in line graphs represent average score + standard error. Boxplots denote median + interquartile range and individual data points are shown. Data obtained from two experiments.

infection (figure 3.2B, D, F, H). These data, accompanied by the increases in stool *C. rodentium* and colonic inflammation at 2 weeks post-infection, suggest that increased RORγt+ T helper cells are a hallmark of *C. rodentium* infection in SKG mice, as they are in C57BL/6J mice. These data also suggest that paw RORγt+ T helper cells do not remain elevated after *C. rodentium* is cleared, despite joint inflammation persisting. Together these data suggest that triggering of disease may involve RORγt+ T helper cells in the joint and that maintenance may be acting *via* different mechanisms.

3.3.3 SKG mice infected with *C. rodentium* display no detectable changes to microbiome composition

Patients with ReA display shifts in their intestinal microbiome, specifically an increase in typically pathogenic taxa, so we wanted to determine whether *C. rodentium* infection in SKG mice altered the intestinal microbiome throughout disease duration[153]. We completed 16S rRNA sequencing on stool from *C. rodentium* infected SKG mice at weekly timepoints. We also analysed samples from uninfected and *C. rodentium* infected mice obtained 2 weeks post-infection with *C. rodentium,* when intestinal inflammation peaks. Microbiome composition analysis did not yield detectable differences in microbiome composition across each weekly timepoint, or at week 2 between infected mice and uninfected mice (figure 3.3A). Additionally, we completed principal component analyses (PCA) on mice at weekly timepoints as well as at 2 weeks post-infection (figure 3.3B). We did not find any clear clustering of disease groups or timepoints in our mice. These data suggest that *C. rodentium* infection in SKG mice does not drive obvious changes to the overall composition of the microbiome.

3.3.4 Several bacteria are elevated in the stool of *C. rodentium* infected mice

Since we did not observe shifts in overall composition of the microbiome in *C. rodentium* infected mice compared to uninfected mice, we decided to look at specific bacterial changes both longitudinally in infected mice, and between infected and uninfected mice at 2 weeks post-infection.

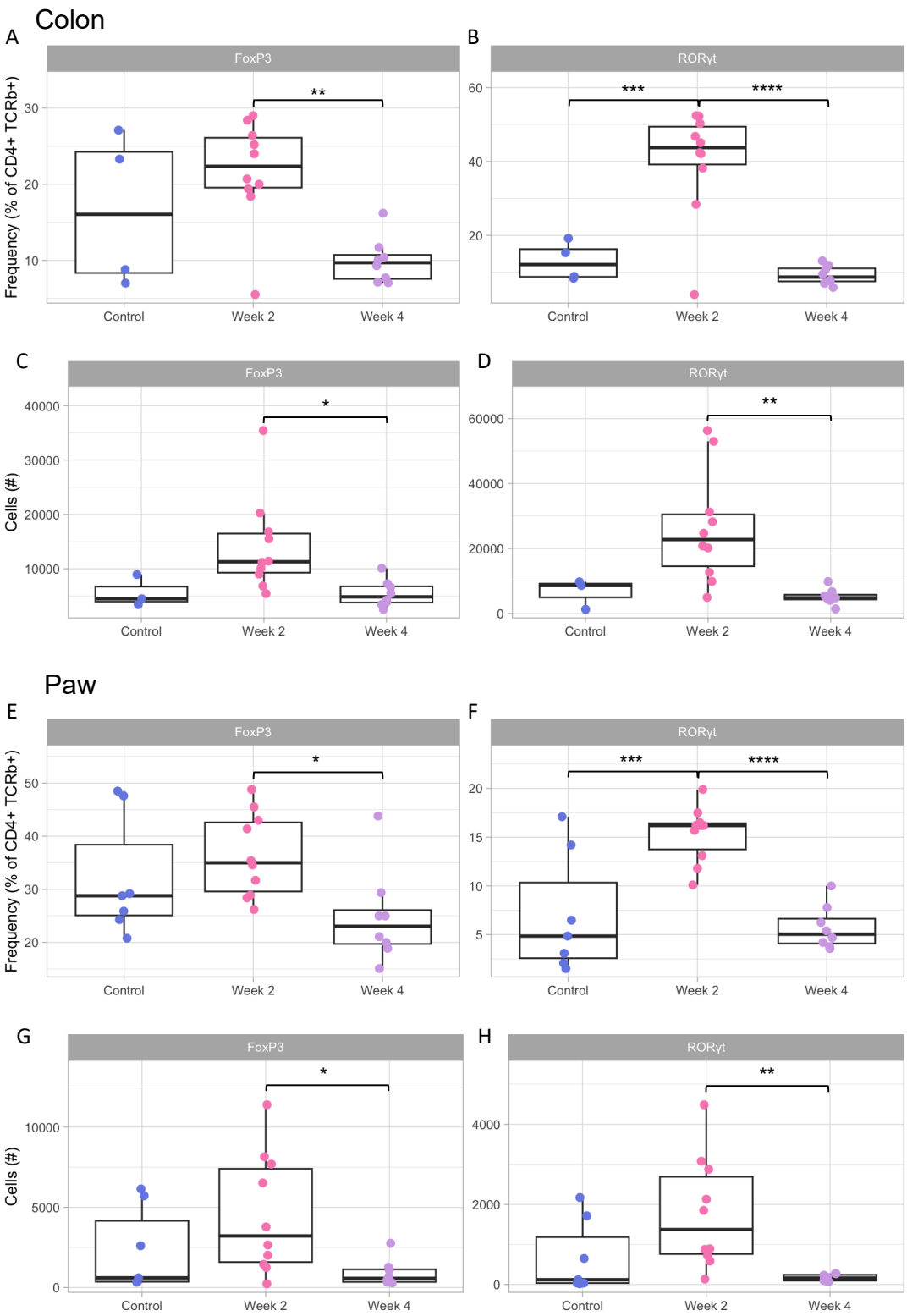


Figure 3.2 *C. rodentium* infected SKG mice display increased colonic and paw RORγt+ T cells. T cell subsets were quantified by flow cytometry in SKG mice infected with *C. rodentium* compared to uninfected SKG controls. Gating strategy is outlined in appendix figure 3.1. A) Frequencies of colonic FoxP3+ T helper cells. B) Frequencies of colonic FoxP3- RORγt+ T helper cells. C) Absolute numbers of colonic FoxP3+ T helper cells. D) Absolute numbers of colonic FoxP3- RORγt+ T helper cells. E) Frequencies of paw FoxP3+ T helper cells. F) Frequencies of paw FoxP3- RORγt+ T helper cells. G) Absolute numbers of paw FoxP3+ T helper cells. H) Absolute numbers of paw FoxP3- RORγt+ T helper cells. Frequencies are denoted as percentage of CD4+ TCRβ+ cells. ****p<0.0001, ***p<0.001, **p>0.01, *p>0.05. One-way ANOVA with Tukey's post-hoc testing was completed for all plots. Boxplots denote median + interquartile range and individual data points are shown. Data obtained from one experiment.

Longitudinal analysis of the 10 highest abundance taxa identifies a reduction in the abundance of Bacteroidales at 3 weeks post-infection in SKG mice infected with *C. rodentium* (figure 3.4A).

We completed statistical testing on each bacterium between infected and uninfected mice at 2 weeks post-infection and identified four bacteria significantly elevated in *C. rodentium*-infected SKG mice compared to uninfected SKG mice (figure 3.4B). *Enterobacteriaceae* were not present in control mice and were elevated in infected mice. Indeed, *C. rodentium* is from the *Enterobacteriaceae* family, and this elevation is explained by the presence of *C. rodentium* in infected mice at 2 weeks post-infection. Further to this, we found that *Staphylococcus* was increased in *C. rodentium*-infected SKG mice compared to uninfected SKG control. Indeed, *C. rodentium* may therefore create an ideal niche for *Staphylococcus* to bloom. Finally, we found that an uncultured Bacteroidales and an unidentified Clostridiales were significantly elevated in *C. rodentium*-infected mice compared to uninfected mice. Taken together, these data suggest that the intestinal microbiome may play a role in *C. rodentium* driven arthritis in SKG mice.

3.3.5 Commensal intestinal bacteria translocate to the systemic organs in SKG mice

Citrobacter rodentium is an attaching and effacing bacterium that can translocate from the intestinal lumen to systemic organs such as the liver and the spleen in C57BL/6J mice[234]. As we identified specific changes in the microbiome of *C. rodentium*-infected SKG mice, we wondered whether *C. rodentium* infection led to the dissemination of itself or commensal microbiota. We cultured bacteria from the liver, spleen, mesenteric lymph nodes (mLN), popliteal lymph nodes (pLN), and paws from SKG mice infected with *C. rodentium* and uninfected SKG controls. We plated on both *C. rodentium*-specific agar, as well as non-specific blood agar for other commensal bacterial growth. Firstly, we found that *C. rodentium* translocated to the liver and the spleen but not the mLNs or the pLNs in SKG mice and was present in these organs 2 weeks post-infection, but not 4 weeks post-infection (figure 3.5A). It is therefore likely that as *C. rodentium* is cleared from the

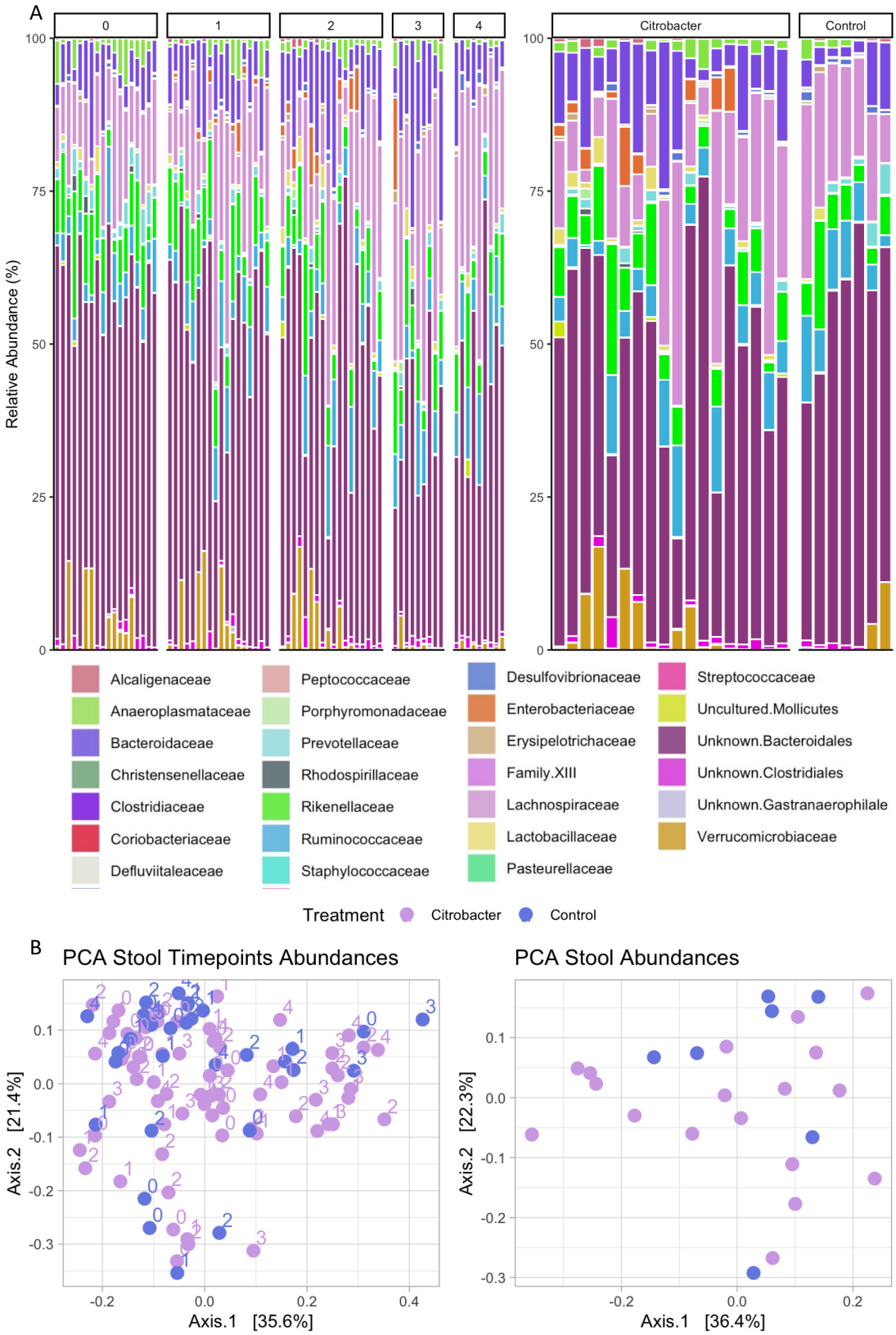


Figure 3.3 SKG mice infected with C. rodentium display no detectable changes to microbiome composition. Stool from SKG mice infected with *C. rodentium* and uninfected SKG mice at weekly timepoints was collected and sequenced by 16S rRNA sequencing. A) Microbiome composition plots at family-level, comparing each timepoint during infection, as well as between infected and uninfected mice at 2 weeks post-infection. Each family is expressed as a relative abundance to the entire population in each sample. B) Principal component analysis of weekly timepoints post-infection in infected and uninfected mice (numbers indicate weeks post-infection), as well as infected and uninfected mice 2 weeks post-infection. Distance = Bray-Curtis.

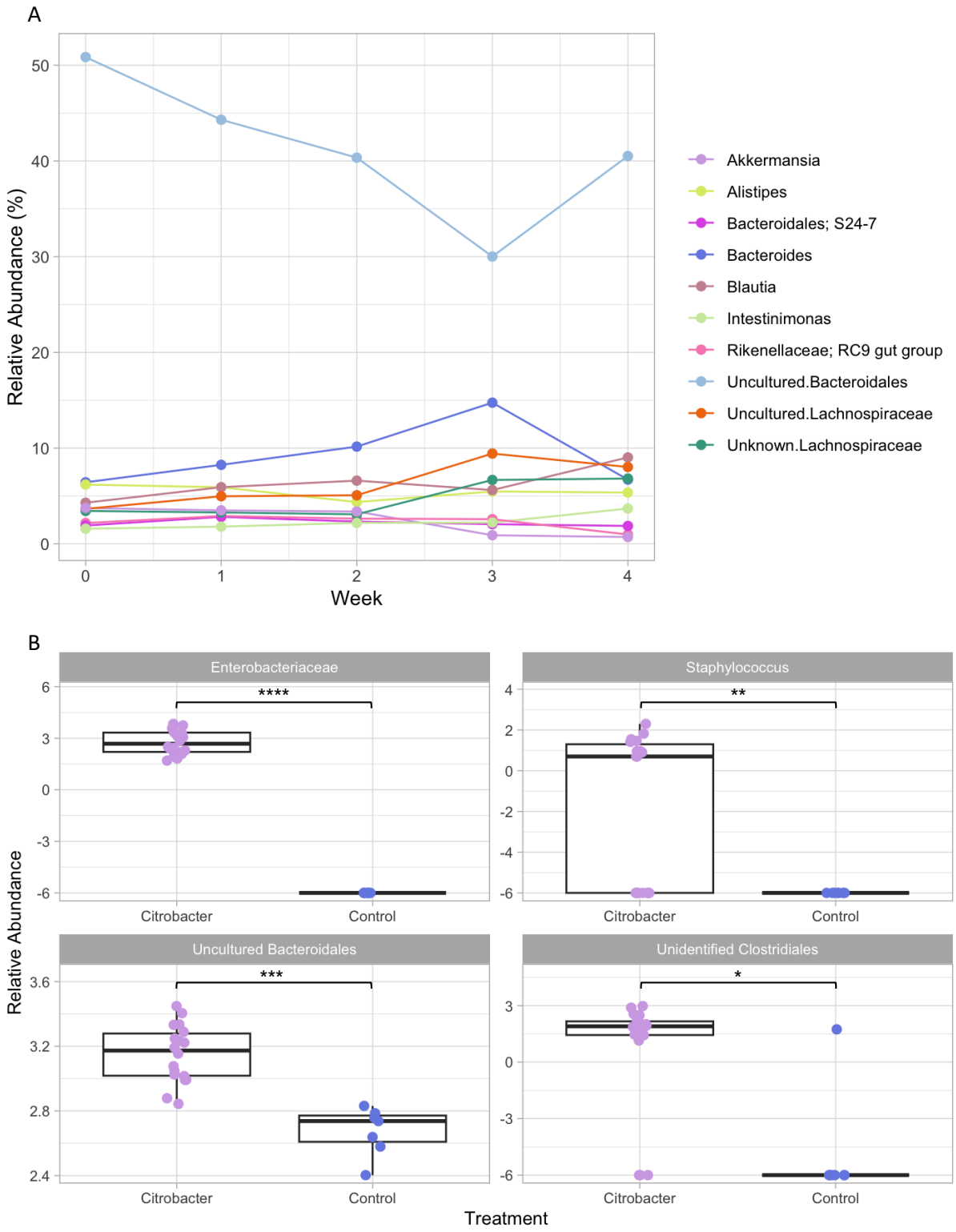


Figure 3.4 Several bacteria are elevated in the stool of *Citrobacter rodentium* infected mice. Further analysis of individual bacteria from 16S rRNA sequencing of stool from *C. rodentium*-infected mice at weekly timepoints, as well as *C. rodentium*-infected mice and uninfected mice at 2 weeks post-infection. A) Longitudinal analysis of the bacteria with the top 10 relative abundance over 4 weeks post-infection. Each point represents mean abundance. B) Bacteria significantly elevated in *C. rodentium*-infected SKG mice compared to uninfected SKG mice 2 weeks post-infection (*Enterobacteriaceae*, *Staphylococcus*, Uncultured Bacteroidales, Unidentified Clostridiales). Boxplots denote median + interquartile range and individual data points are shown. ****p<0.0001, ***p<0.001, **p<0.01, *p<0.05. Student's t-test with Benjamini-Hochberg correction was completed on each bacterium.

intestinal lumen at 4 weeks, it is also cleared from the systemic organs. Furthermore, translocation to the liver and spleen but not the lymph nodes suggests that *C. rodentium* disseminates *via* the blood and not the lymphatics. We hypothesised that *Citrobacter rodentium* may also allow for the translocation of commensal microbiota to the systemic organs, which may be involved in driving systemic joint disease in our model. We plated organs on non-specific blood agar and counted colonies based upon morphology. To ensure we did not count *C. rodentium* colonies in our analysis, we took representative colony swabs of each morphology and sent them for sequencing for strain identification before removing *C. rodentium* colonies from our analysis. We found that commensals could translocate to the liver and the spleen in both uninfected and infected mice, suggesting that *C. rodentium* is not required to facilitate translocation (figure 3.5B). However, we found that despite *C. rodentium* being unable to translocate to the mLNs during infection, commensals colonised the mLNs 4 weeks post-infection, but not in uninfected mice or mice 2 weeks post-infection (figure 3.6B). Upon sequencing of the commensal colonies cultured from both uninfected and infected organs, we identified *Staphylococcus saprophyticus* and *Ligilactobacillus murinus* to be colonising the systemic organs. This is unsurprising, as we identified *Staphylococcus* to be increased in abundance during *C. rodentium* infection, and these bacterial genera are known to disseminate systemically *in vivo*[235,236]. Taken together, these data support the hypothesis that SKG mice themselves may have elevated intestinal permeability, which allows for commensals to colonise the systemic organs without the need for infection with a pathogen to disrupt the intestinal barrier.

3.3.6 Intestinal commensal bacteria translocate to the systemic organs in Balb/C and SKG mice

After demonstrating that commensal bacteria can colonise the systemic organs in uninfected SKG mice, we hypothesised that SKG mice may have elevated intestinal permeability compared to wild-type mice, due to their mutation in *Zap70*, and this may be facilitating inflammation in SKG mice during infection. We assessed intestinal permeability in SKG and wild-type Balb/C mice and tested whether Balb/C mice develop joint inflammation following *C. rodentium* infection.

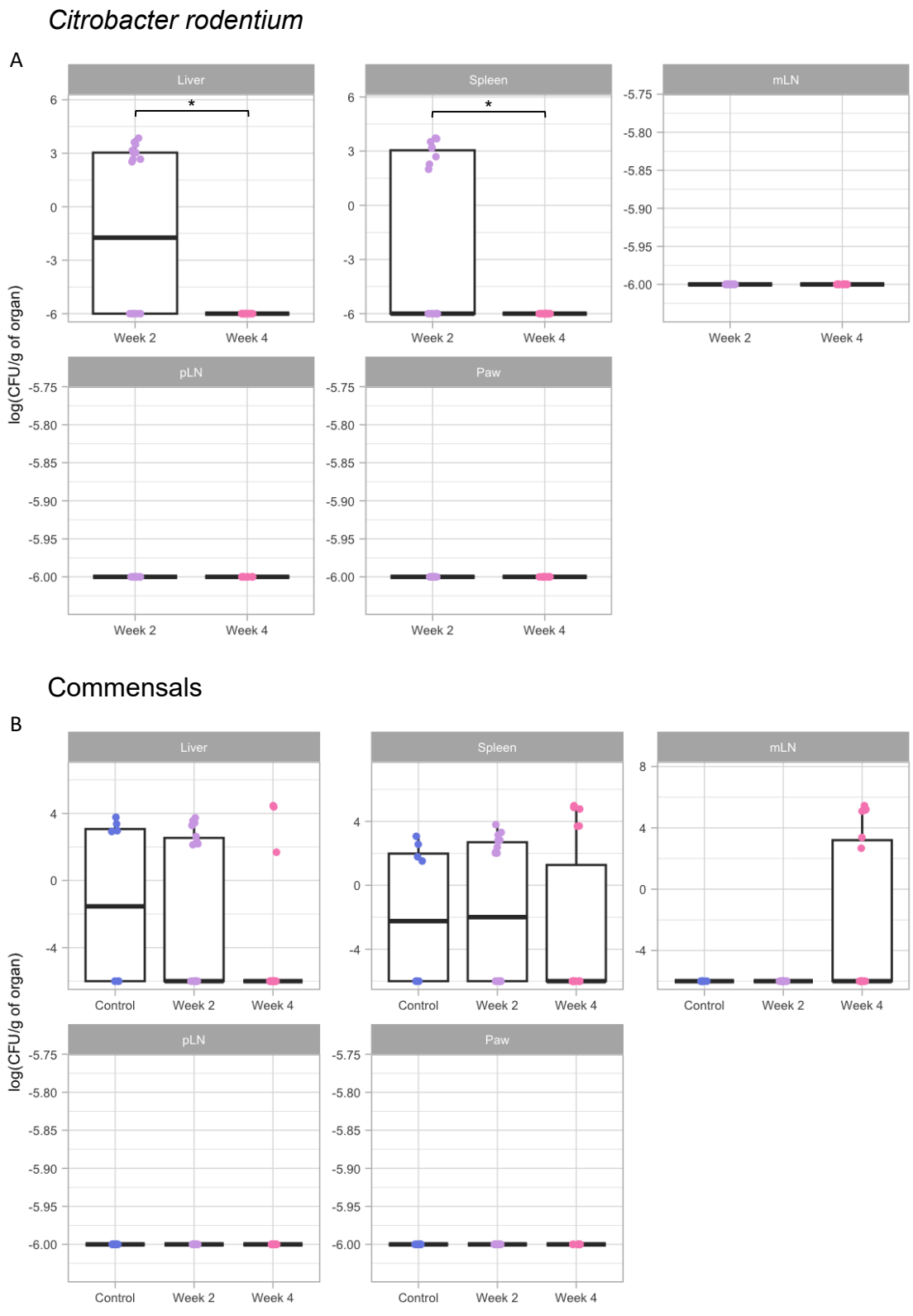


Figure 3.5 Intestinal commensal bacteria translocate to the systemic organs in SKG mice. Livers, spleens, mesenteric lymph nodes (mLNs), popliteal lymph nodes (pLNs), and paws were plated on *C. rodentium*-specific and non-specific agar to assess translocation of bacteria to systemic organs. A) *Citrobacter rodentium* colonisation in the liver, spleen, mLN and pLN at 2 weeks post-infection and 4 weeks post-infection. B) Commensal colonisation in the liver, spleen, mLN, pLN, and paw in uninfected mice, and mice 2 weeks and 4 weeks post-infection with *C. rodentium*. Colonisation is denoted as log (CFU per gram of organ). Boxplots denote median + interquartile range and individual data points are shown. **p<0.01, *p<0.05, ns = not significant. Unpaired student's t-test was completed with Welch's correction on each organ. Data obtained from two experiments.

Previous studies have shown a susceptibility for Balb/C mice to develop colitis following *C. rodentium* infection[237]. To assess whether wild-type Balb/C mice can develop joint inflammation following infection with *C. rodentium*, we infected Balb/C mice and followed them for 4 weeks to monitor joint inflammation. We found that Balb/C mice infected with *C. rodentium* do not develop arthritis (figure 3.6A). This suggests that a mutation *Zap70* in SKG mice driving the accumulation of self-reactive T cells is crucial to the development of arthritis in *C. rodentium* infection.

To determine whether SKG mice have increased intestinal permeability than Balb/C mice, we cultured livers and spleens from naïve SKG mice and Balb/C mice and measured intestinal barrier-associated genes in RNA extracted from colon tissue. We found that commensal microbiota were able to colonise the livers and spleens in both Balb/C and SKG mice (figure 3.6B). Furthermore, qPCR analysis of *Ocln*; the gene encoding the tight junction protein occludin, and *Cldn1*; the gene encoding the tight junction protein claudin, revealed that colon tissue from uninfected Balb/C and SKG mice had similar levels of both proteins (figure 3.6C). Taken together, we suggest that SKG mice do not display increased intestinal permeability when compared to wild-type Balb/C controls, and both SKG and Balb/C mice may both have a baseline level of translocation of commensals to their systemic organs. However, we cannot definitively conclude this as we did not assess a positive control for intestinal permeability such as DSS administration and did not complete functional measures of intestinal permeability such as FITC-dextran permeability assays due to constraints with removing food from our mice.

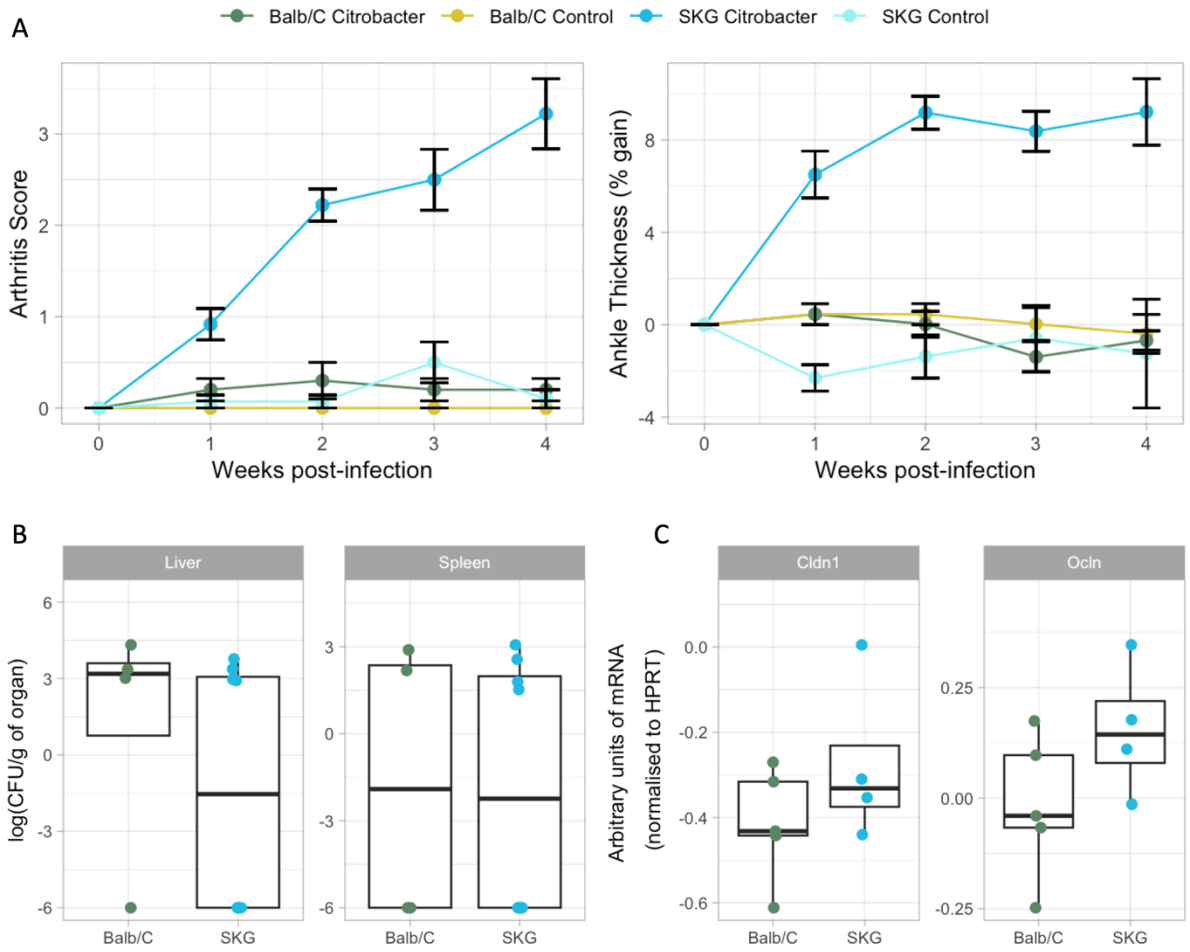


Figure 3.6 Intestinal bacteria translocate to the systemic organs in Balb/C and SKG mice. Balb/C mice were infected with *Citrobacter rodentium* and followed for 4 weeks. A) Arthritis scores and ankle thickness of Balb/C mice infected with *C. rodentium* compared to uninfected Balb/C controls and both infected and uninfected SKG mice. Ankle thickness is denoted as percentage gain. B) Colonisation of commensal microbiota in uninfected Balb/C mice compared to uninfected SKG mice. Colonisation is denoted as log (CFU per gram of organ). C) Expression of *Cldn1* and *Ocln* in the colonic tissue from uninfected Balb/C mice compared to uninfected SKG mice. Expression is denoted as arbitrary units of mRNA, normalised to the house-keeping gene *Hprt.* Points in line graphs represent average score + standard error. Boxplots denote median + interquartile range and individual data points are shown. Data obtained from one experiment.

3.3.7 *C. rodentium* requires intestinal commensals to drive arthritis and colitis in SKG mice

We identified changes to specific intestinal bacteria during *C. rodentium* infection, so we tested whether the intestinal microbiota is required to permit arthritis and colitis in SKG mice. To do this, we infected germ-free SKG mice with *Citrobacter rodentium* and culled them 2 weeks post-infection and 4 weeks post-infection and assessed their arthritis weekly. Firstly, we found that *C. rodentium* colonised germ-free SKG mice at a similar level compared to SPF SKG mice, however, it did not clear from the stool by 4 weeks post-infection as it did in SPF SKG mice (figure 3.7A). This is likely due to a

lack of colonisation resistance from intestinal commensals. Notably, despite the ability for *C. rodentium* to colonise germ-free SKG mice, it was unable to elicit increased arthritis scores or ankle thickness (figure 3.7B). This suggests that commensals are crucial to supporting *C. rodentium* driven arthritis in SKG mice.

To assess whether *C. rodentium* can drive intestinal inflammation in germ-free SKG mice, we measured LCN-2 in the stool as well as histopathology scoring of H&E-stained colon tissue. We found that germ-free SKG mice infected with *C. rodentium* did not display any differences in LCN-2 compared to uninfected germ-free SKG mice, whereas *C. rodentium* infection led to elevated LCN-2 levels 2 weeks post-infection in SPF SKG mice (figure 3.7C). Furthermore, we found that although some germ-free SKG mice infected with *C. rodentium* displayed some level of histopathological inflammation, it was not significantly increased compared to uninfected germ-free controls (figure 3.7D, E). Taken together, these data suggest that *C. rodentium* requires the presence of intestinal commensals to drive both colitis and arthritis in SKG mice.

3.3.8 *C. rodentium* can drive local and systemic T cell responses in the absence of commensals despite not inducing inflammation

We aimed to assess whether T cell responses in SKG mice were associated with disease or just *C. rodentium* colonisation. To do so, we stained colonic and paw lymphocytes obtained from uninfected and *C. rodentium*-infected germ-free SKG at 2 weeks post-infection and 4 weeks post-infection for T helper cell transcription factors by flow cytometry.

At 2 weeks post-infection, we observed that *C. rodentium* was still able to increase the frequencies of colon RORγt+ T helper cells at 2 weeks post-infection in germ-free SKG mice compared to uninfected germ-free controls. This suggests that RORγt+ responses in the intestine are not solely responsible for driving intestinal inflammation (figure 3.8B). In the paw, we observed no changes in any either FoxP3+ T helper cells or RORγt+ T helper cells 2 weeks post-infection, indicating that in the absence of commensals, *C. rodentium* is unable to recapitulate paw T cell

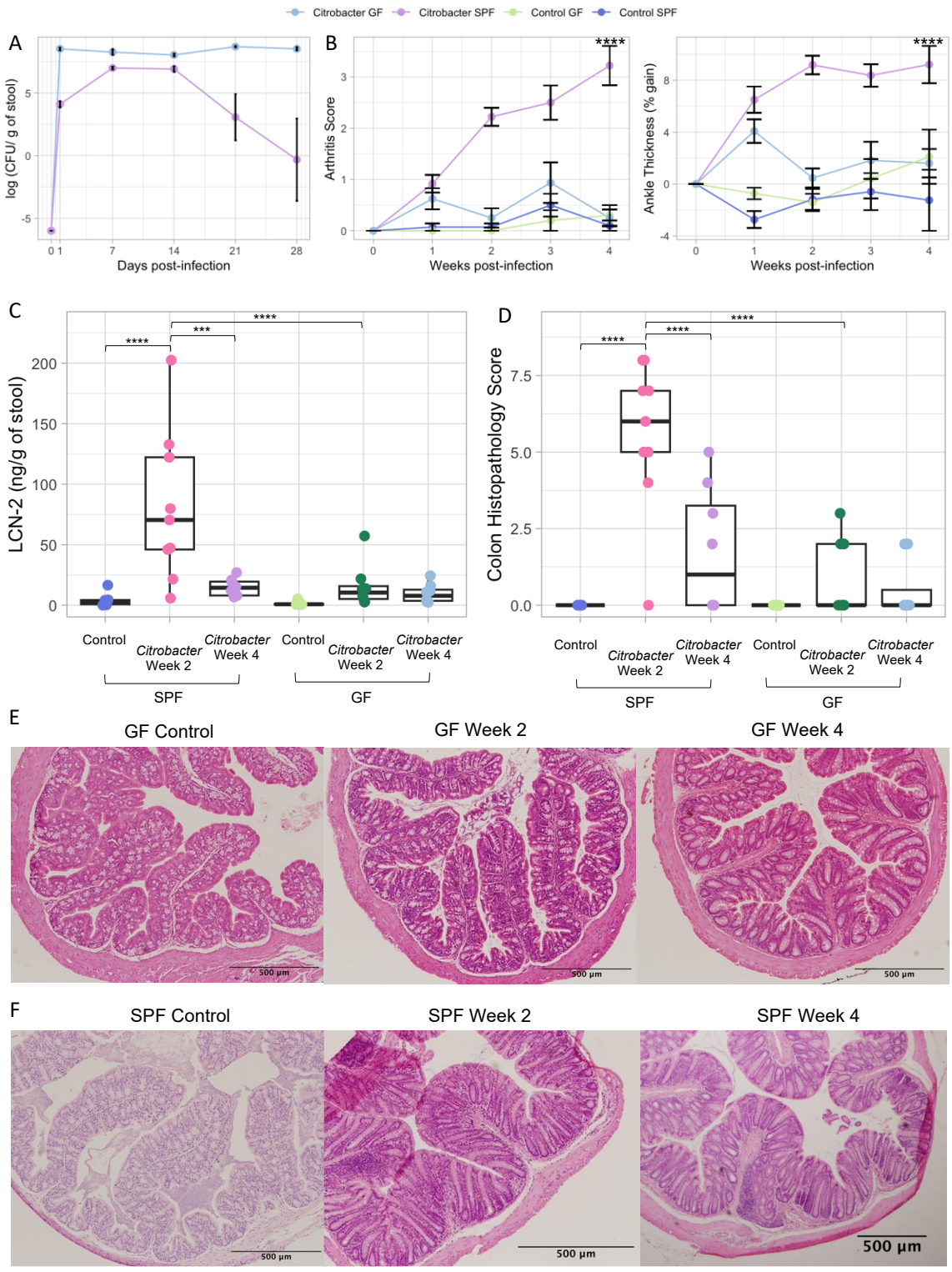


Figure 3.7 *Citrobacter rodentium* requires intestinal commensals to drive arthritis and colitis in SKG mice. Germ-free SKG mice were infected with *C. rodentium* and culled at 2 weeks and 4 weeks post-infection. A) *C. rodentium* load in the stool of germ-free and SPF SKG mice. *C. rodentium* load is denoted as log (CFU per gram of stool). CFU = colony forming units. B) Arthritis scoring and ankle thickness of infected and uninfected germ-free and SPF SKG mice. Ankle thickness is denoted as percentage gain. C) Stool lipocalin-2 levels of infected and uninfected germ-free and SPF SKG mice. D) Colon histopathology scoring for infected and uninfected germ-free and SPF SKG mice. E) Representative microscopy images of H&E-stained colon tissues taken from uninfected and infected germ-free SKG mice 2 weeks and 4 weeks post-infection with *C. rodentium.* F) Representative microscopy images of H&E-stained colon tissues taken from uninfected and infected SPF SKG mice 2 weeks and 4 weeks post-infection with *C. rodentium.* ****p<0.0001, ***p<0.001. B) Mixed linear effects modelling. C) and D) one-way ANOVA with Tukey's post-hoc testing. Points in line graphs represent average score + standard error. Boxplots denote median + interquartile range and individual data points are shown. Data obtained from two experiments.

responses that it drives in SPF mice at 2 weeks (figure 3.8E-H). At 4 weeks post-infection, we observed a significant decrease in the frequency of colonic and paw FoxP3+ T helper cells, similar to SPF mice, indicating that *C. rodentium* can affect T_{reg} cell frequencies in the absence of commensal microbiota (figure 3.8A, E). We observed reduced frequency of RORγt+ T helper cells in the colon 4 weeks post-infection, recapitulating that seen in SPF mice, despite continued *C. rodentium* colonisation in the intestine (figure 3.8B). We found overall increases in the number of FoxP3+ T helper cells and RORγt+ T helper cells in the colon 4 weeks post-infection, suggesting that immune cell infiltration to the lamina propria may occur despite a lack of inflammation (figure 3.8C, D). In the paw, we observed a significant increase in the frequency and number of RORγt+ T helper cells 4 weeks post-infection compared to uninfected germ-free mice (figure 3.8F, H). This suggests that despite being unable to elicit joint inflammation in germ-free mice, *C. rodentium* can modulate joint T cell responses.

3.3.9 *C. rodentium* can translocate to systemic organs in germ-free SKG mice

Having shown that *C. rodentium* can colonise germ-free SKG mice but cannot drive arthritis or colitis, we hypothesised that this was due to a lack of translocation to systemic sites. To test this, we cultured spleens, livers, and mLNs from germ-free SKG mice infected with *C. rodentium* at 2 weeks and 4 weeks post-infection. We observed that *C. rodentium* translocated to the livers, spleens, and mLNs at 2 weeks and 4 weeks post-infection in a small proportion of germ-free SKG mice (figure 3.9). Though only a minority of mice displayed translocation of *C. rodentium,* it demonstrates that *C. rodentium* cannot drive pathology in the absence of commensals despite its ability to disseminate to systemic organs.

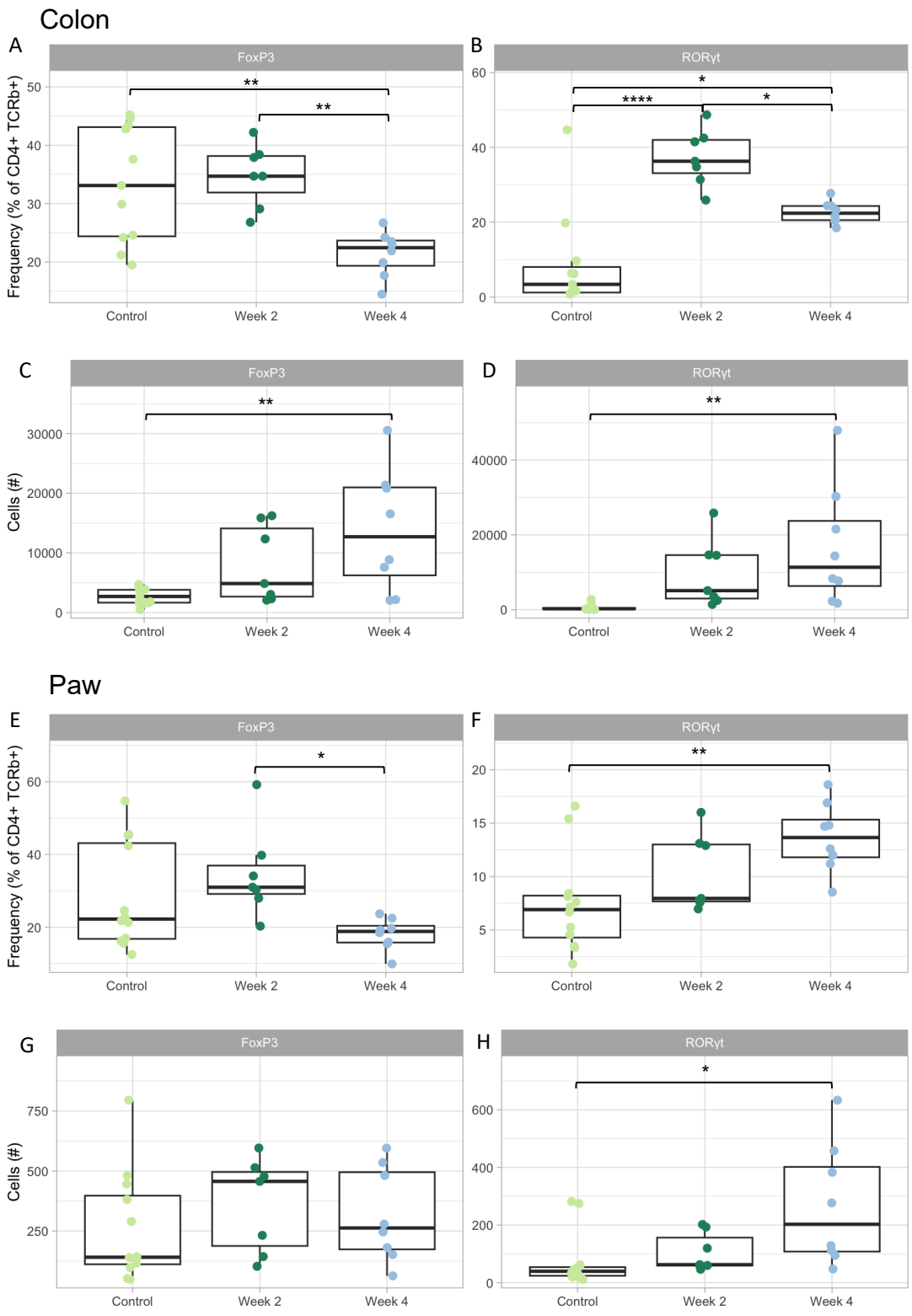


Figure 3.8 *Citrobacter rodentium* can drive local and systemic T cell responses in the absence of commensals despite not inducing inflammation. Colon and paw tissue from germ-free SKG mice infected with *C. rodentium* was obtained and stained for T cell transcription factors by flow cytometry. Gating strategy is outlined in appendix figure 3.1. A) Frequencies of colonic FoxP3+ T helper cells. B) Frequencies of colonic FoxP3- RORγt+ T helper cells. C) Absolute numbers of colonic FoxP3+ T helper cells. D) Absolute numbers of colonic FoxP3- RORγt+ T helper cells. E) Frequencies of paw FoxP3+ T helper cells. F) Frequencies of paw FoxP3- RORγt+ T helper cells. G) Absolute numbers of paw FoxP3+ T helper cells. H) Absolute numbers of paw FoxP3- RORγt+ T helper cells. Frequencies are denoted as percentage of CD4+ TCRβ+ cells. Boxplots denote median + interquartile range and individual data points are shown. ****p<0.0001, **p>0.01, *p>0.05. One-way ANOVA with Tukey's post-hoc testing was completed for all plots. Data obtained from one experiment.

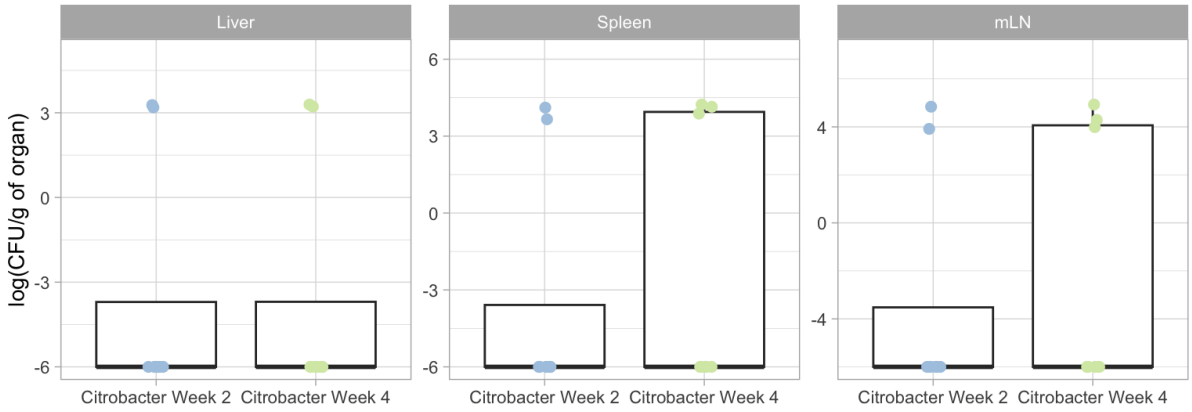


Figure 3.9 *Citrobacter rodentium* can translocate to systemic organs in germ-free SKG mice. *C. rodentium* growth cultured from livers, spleens and mLNs obtained from germ-free SKG mice infected with *C. rodentium* 2 weeks and 4 weeks post-infection. *C. rodentium* growth is denoted as log (CFU per gram of organ). CFU = colony forming units. Boxplots denote median + interquartile range and individual data points are shown. Data obtained from one experiment.

3.3.10 The Oligo-MM^{12} community colonises SKG mice

We sought to reduce the complexity associated with delineating host-microbiota interactions to enable further characterisation of our model. Thus, we utilised the Oligo-MM^{12} community, which has been shown to be functionally and compositionally representative of a normal murine intestinal microbiome[194]. We generated an Oligo-MM^{12} SKG mouse colony by co-housing germ-free SKG mice with Oligo-MM^{12} colonised C57BL/6J mice kindly gifted by Professor Andrew Macpherson (Bern, Switzerland), and orally gavaged a single dose of Oligo-MM^{12} C57BL/6J caecal contents. We confirmed strain adherence to the microbiome through shallow shotgun sequencing of stool from mice 3 weeks following gavage as well as C57BL/6J microbiome donors (figure 3.10). We identified 10 of the 12 Oligo-MM^{12} strains by sequencing but did not pick up *Turicimonas muris* YL45 and *Acutalibacter muris* KB18 in either our SKG colony or our C57BL/6J colony. Further quantitative PCR using strain-specific primers on small intestinal contents from Oligo-MM^{12} SKG mice identified *Turicimonas muris* and *Acutalibacter muris* presence, likely due to a low level of colonisation.

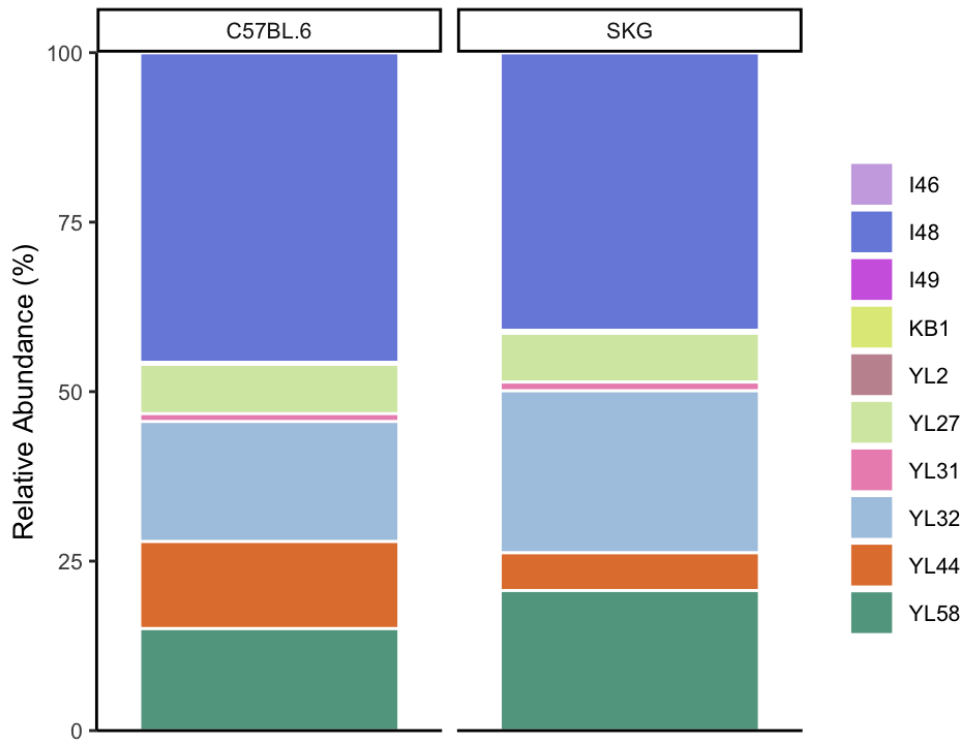


Figure 3.10 The Oligo-MM^{12} community colonises SKG mice. Community composition plot generated from shallow shotgun sequencing data of stool obtained from SKG Oligo-MM^{12} recipient mice and C57BL/6J Oligo-MM^{12} donor mice. SKG recipient mice are pooled from 2 cages of 3 mice each, and C57BL/6J is pooled from 2 donor mice.

3.3.11 The Oligo-MM^{12} community is a useful model for studying *C. rodentium* infection in SKG mice

Next, Oligo-MM^{12} SKG mice were infected with *C. rodentium* and culled them 2 weeks and 4 weeks post-infection. To ensure *C. rodentium* was able to colonise the Oligo-MM^{12} mice, we measured *C. rodentium* by qPCR in the stool of SKG Oligo-MM^{12} mice 2 weeks post-infection and 4 weeks post-infection. We found that *C. rodentium* robustly colonises the Oligo-MM^{12}, however we did not observe clearance of *C. rodentium* by 4 weeks post-infection (figure 3.11A). We measured *C. rodentium* DNA by qPCR rather than live *C. rodentium* by plating, which could explain an apparent lack of clearance. Oligo-MM^{12} SKG mice infected with *C. rodentium* displayed progressive arthritis (figure 3.11B). This suggests that commensal microbiota present in the Oligo-MM^{12} are sufficient to permit *C. rodentium*-driven arthritis. We then measured LCN-2 levels in the stool of uninfected and infected Oligo-MM^{12} SKG mice. We found that, similar to SPF *C. rodentium*-infected mice,

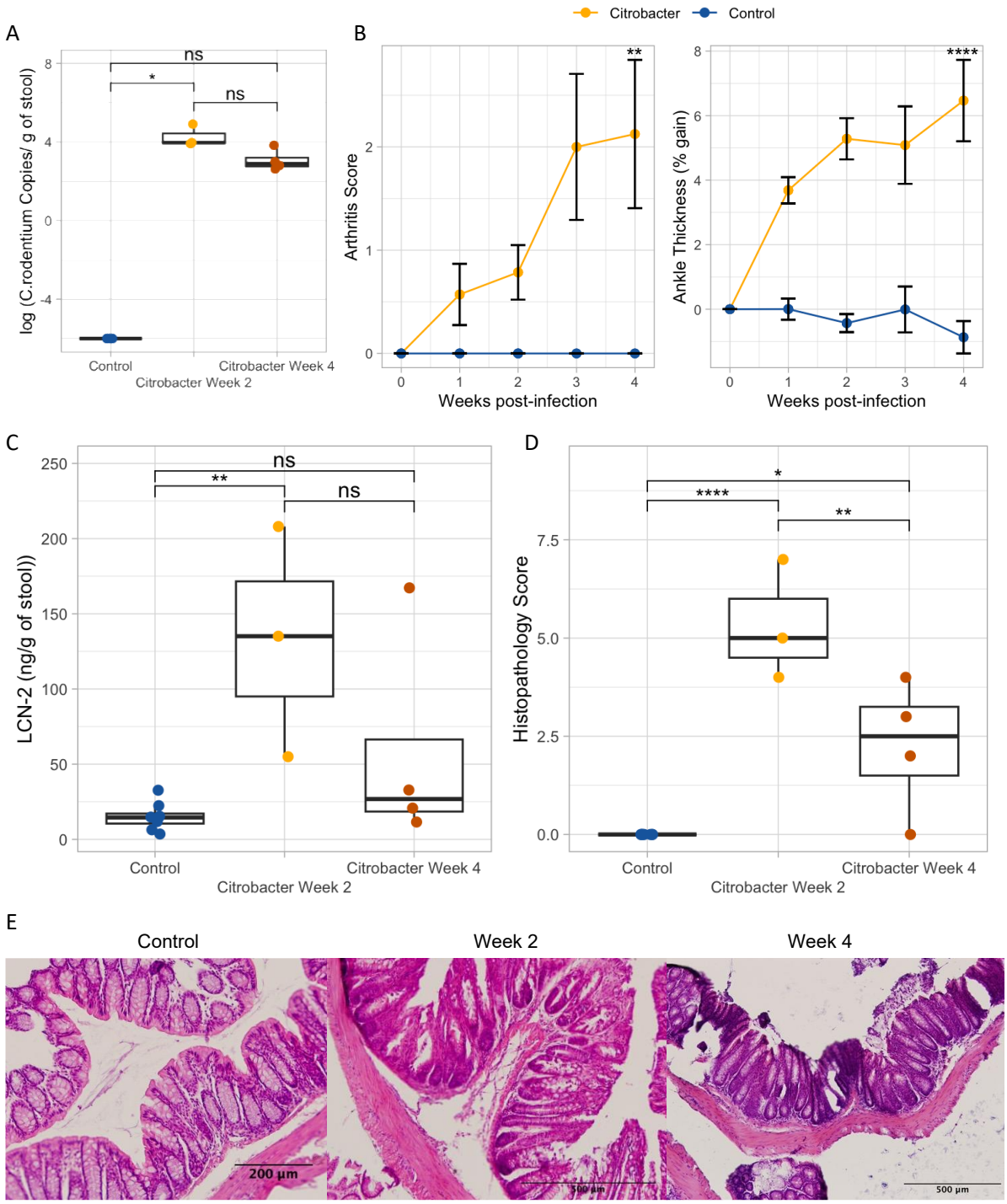


Figure 3.11 The Oligo-MM^{12} community is a useful model for studying *C. rodentium* infection in SKG mice. Oligo-MM^{12} SKG mice were infected with *C. rodentium* and culled at 2 weeks post-infection and 4 weeks post-infection. A) *C. rodentium* gene *Rpod* expression in the stool of uninfected and infected Oligo-MM^{12} SKG mice. Gene expression is denoted as log(bacterial copies per gram of stool). B) Arthritis scoring and ankle thickness of uninfected and infected Oligo-MM^{12} SKG mice. Ankle thickness is denoted as percentage gain. C) Stool LCN-2 levels of uninfected and infected Oligo-MM^{12} SKG mice. D) Histopathology scoring of H&E-stained colon tissue obtained from uninfected and infected Oligo-MM^{12} SKG mice. E) Representative microscopy images of H&E-stained colon tissues taken from Oligo-MM^{12} SKG mice 2 weeks and 4 weeks post-infection with *C. rodentium* compared to uninfected Oligo-MM^{12} SKG mice. B) Points in line graphs represent average score + standard error. ****p<0.0001, **p>0.01. Mixed linear effects modelling. A), C), D) Boxplots denote median + interquartile range and individual data points are shown. ****p<0.0001, **p>0.01, *p<0.05, ns = not significant. One-way ANOVA with Tukey's post-hoc testing. Data obtained from one experiment.

C. rodentium-infected Oligo-MM^{12} mice have elevated stool LCN-2 levels at 2 weeks post-infection (figure 3.11C). In addition, we observed increased histopathology scores for H&E-stained colon tissue obtained from Oligo-MM^{12} mice 2 weeks post-infection with *C. rodentium* (figure 3.11D,E). Notably, paw histopathology scores did not return to baseline 4 weeks post-infection in Oligo-MM^{12} mice, as observed in SPF mice (figure 3.12D). Taken together, these data suggest that members of the Oligo-MM^{12} are able to permit *C. rodentium*-driven disease in SKG mice, and that Oligo-MM^{12} SKG mice can closely model *C. rodentium* infection from SPF mice.

3.3.12 *C. rodentium* elicits RORγt responses in the colon but not the paw of Oligo-MM^{12} SKG mice

Following our observation of the Oligo-MM^{12} and its ability to permit *C. rodentium* driven arthritis and colitis in SKG mice, we sought to determine whether the adaptive T cell responses in the colon and the paw observed in *C. rodentium* infected SPF SKG mice were recapitulated in *C. rodentium* infected Oligo-MM^{12} SKG mice. We stained lymphocytes isolated from colon and paw tissue for T helper cell transcription factors by flow cytometry.

We observed a significant increase in the frequency of RORγt+ T helper cells in the colon 2 weeks post-infection compared to uninfected Oligo- MM^{12} mice, in line with that observed in SPF mice (figure 3.12B). However, at 4 weeks post-infection, we observed a further increase in colonic RORγt+ T helper cell frequencies, in contrast to the reduction we observed in SPF mice (figure 3.13B). This may be explained by the failed clearance of *C. rodentium* infection by 4 weeks post-infection. We observed a reduction in the frequency of FoxP3+ T helper cells in the colon 4 weeks-post infection, which recapitulates that observed during infection in SPF and germ-free mice (figure 3.12A). Crucially, in the paw we did not observe any changes to the frequencies of either FoxP3+ T helper cells or RORγt+ T helper cells at any point during infection with *C. rodentium* (figure 3.13E, F). This is despite an ability for the Oligo-MM^{12} to support the development of joint inflammation, suggesting a Th17-independent mechanism of arthritis.

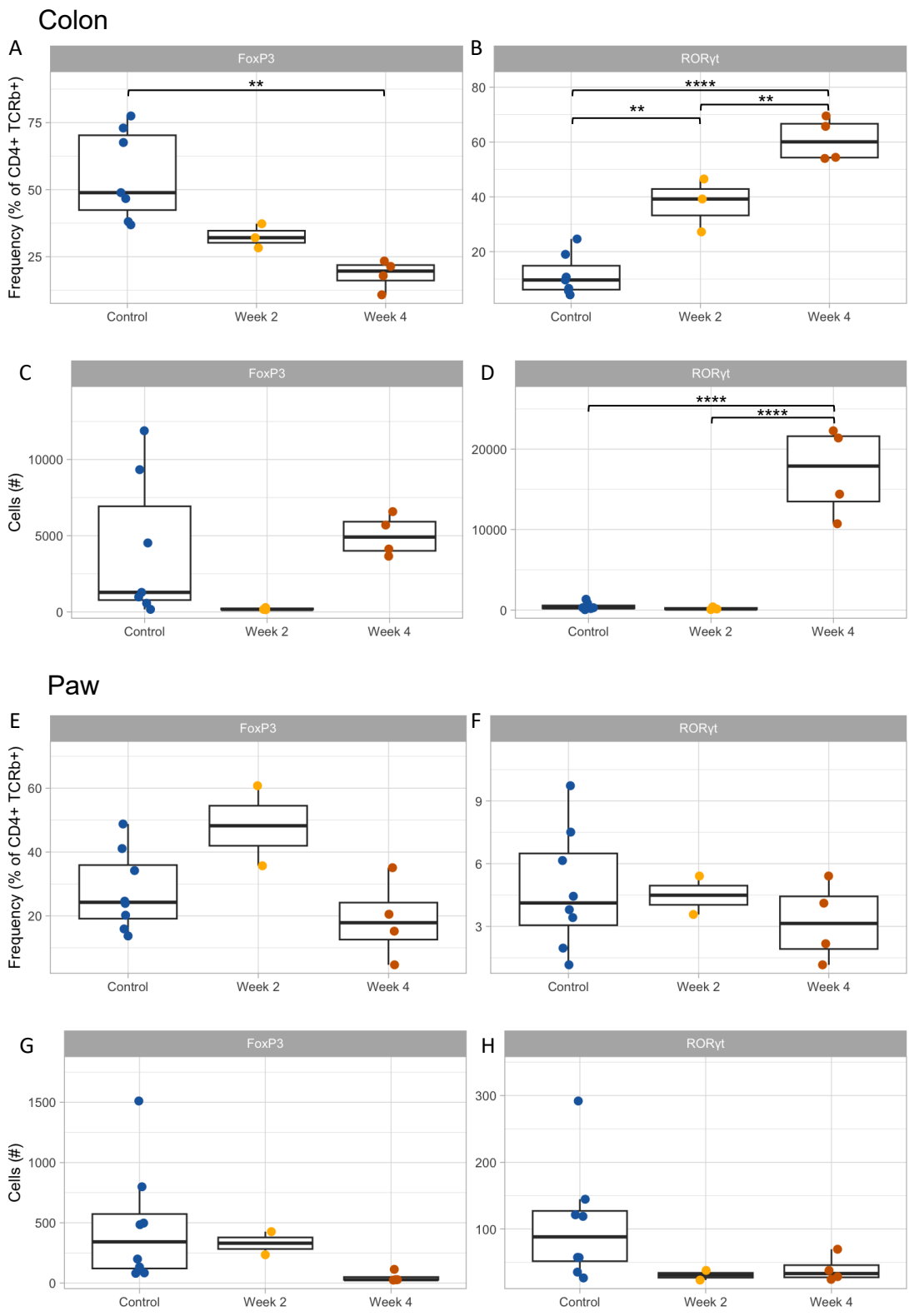


Figure 3.12 *Citrobacter rodentium* elicits RORγt responses in the colon but not the paw of Oligo-MM^{12} SKG mice. Colon and paw tissue from Oligo-MM^{12} SKG mice infected with *C. rodentium* was obtained and stained for T cell transcription factors by flow cytometry. Gating strategy is outlined in appendix figure 3.1. A) Frequencies of colonic FoxP3+ T helper cells. B) Frequencies of colonic FoxP3- RORγt+ T helper cells. C) Absolute numbers of colonic FoxP3+ T helper cells. D) Absolute numbers of colonic FoxP3- RORγt+ T helper cells. E) Frequencies of paw FoxP3+ T helper cells. F) Frequencies of paw FoxP3- RORγt+ T helper cells. G) Absolute numbers of paw FoxP3+ T helper cells. H) Absolute numbers of paw FoxP3- RORγt+ T helper cells. Frequencies are denoted as percentage of CD4+ TCRβ+ cells. Boxplots denote median + interquartile range and individual data points are shown. ****p<0.0001, **p>0.01. One-way ANOVA with Tukey's post-hoc testing was completed for all plots. Data obtained from one experiment.

3.3.13 SKG Oligo-MM^{12} mice infected with *C. rodentium* do not display altered intestinal microbiome composition

We previously demonstrated that *C. rodentium* requires intestinal commensals to support arthritis and colitis in SKG mice. Furthermore, in SPF mice infected with *C. rodentium*, we observed specific changes in intestinal bacteria as a consequence of *C. rodentium* infection. We therefore wanted to determine whether changes in Oligo-MM^{12} composition occurred during *C. rodentium* infection in Oligo-MM^{12} SKG mice. We completed qPCR using strain-specific primers for each Oligo-MM^{12} member and *C. rodentium* on colon contents collected from *C. rodentium* infected and uninfected Oligo-MM^{12} SKG mice. Compositional analysis of the microbiome did not reveal obvious changes to the composition of the microbiome (figure 3.13A). This was further demonstrated by PCA which revealed no alteration in the microbiome of *C. rodentium* infected mice compared to uninfected controls (figure 3.13B). Together, these analyses suggest that *C. rodentium* is not able to shift the microbiome composition of Oligo-MM^{12} SKG mice, recapitulating the lack of compositional changes observed in SPF mice.

3.3.15 Numbers of specific Oligo-MM^{12} members are altered during *C. rodentium* infection in SKG mice

As we did not identify changes to the overall composition of the Oligo-MM^{12} during *C. rodentium* infection, we sought to determine which specific members of the Oligo-MM^{12} were altered during infection. We completed statistical testing on absolute numbers and relative abundances of Oligo-MM^{12} members. We did not observe any changes to the relative abundances of any Oligo-MM^{12} members, further supporting our previous observation of a lack of compositional changes by *C. rodentium* in the Oligo-MM^{12} (appendix figure 3.2).

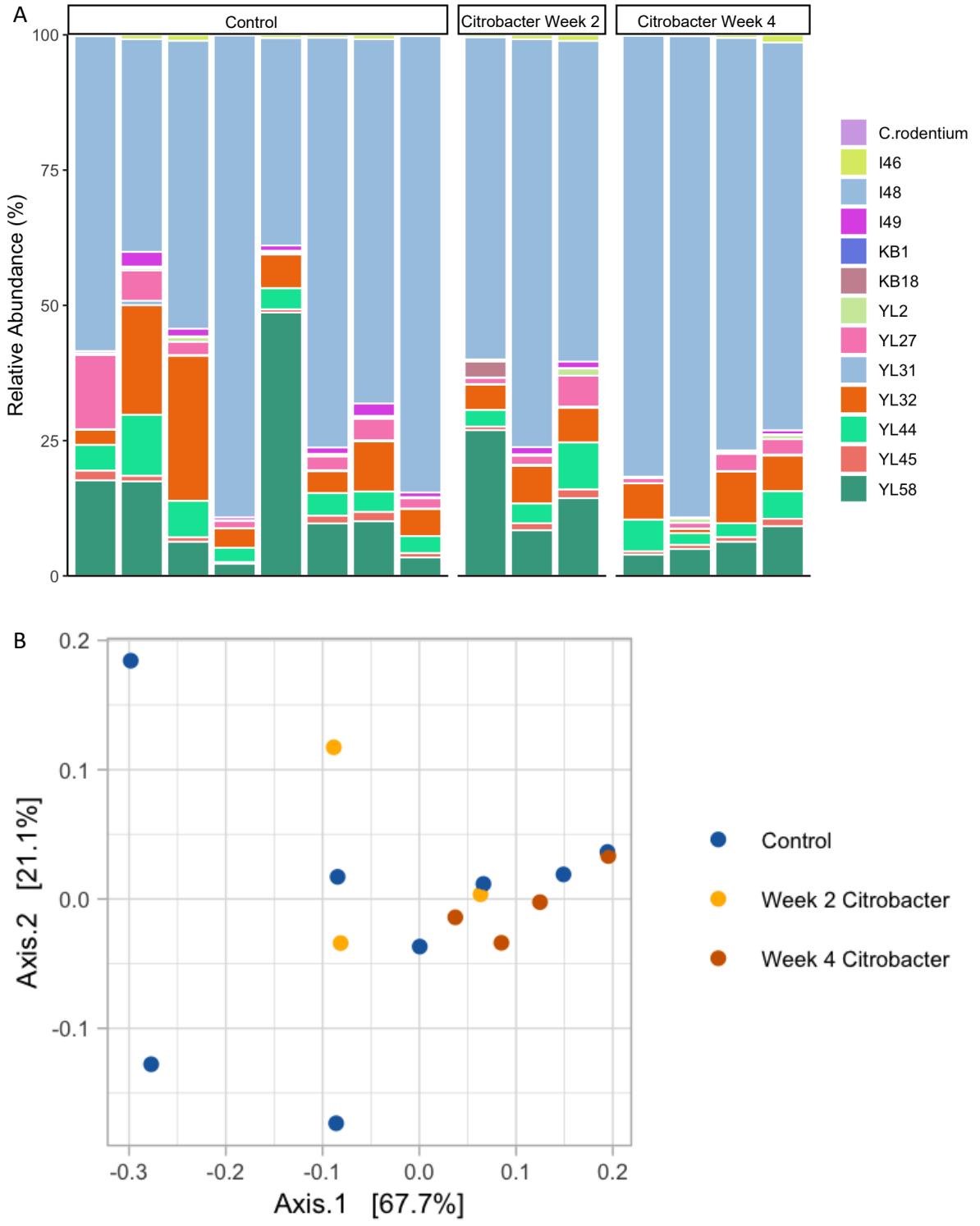


Figure 3.13 SKG Oligo-MM^{12} mice infected with *Citrobacter rodentium* do not display altered intestinal microbiome composition. Colon contents from Oligo-MM^{12} SKG mice 2 weeks and 4 weeks post-infection with *C. rodentium* and uninfected Oligo-MM^{12} SKG mice were obtained, and qPCR was completed using strain-specific primers for Oligo-MM^{12} members and *C. rodentium*. A) Microbiome composition plot comparing control Oligo-MM^{12} mice and Oligo-MM^{12} mice 2 weeks and 4 weeks post-infection with *C. rodentium*. B) Principal component analysis of uninfected Oligo-MM^{12} mice and Oligo-MM^{12} mice 2 weeks and 4 weeks post-infection with *C. rodentium*. Distance = Bray-Curtis. Data obtained from one experiment.

When we completed statistical testing on the absolute numbers of Oligo-MM12 members, we found 4 members that were significantly altered during *C. rodentium* infection. *Clostridium innocuum* I46 was significantly increased in Oligo-MM^{12} SKG mice 4 weeks post-infection with *C. rodentium* (figure 3.14A). Both *Bacteroides caecimuris* I48 and *Turicimonas muris* YL45 were elevated 4 weeks post-infection with *C. rodentium* compared to uninfected controls (figure 3.14B, D). There was a clear trend of increase for I48 and YL45 at 4 weeks post-infection compared to 2 weeks post-infection, although not significant. I46, I48, and YL45 all increased in numbers when *C. rodentium* infection appeared to be clearing. It is possible that these bacteria are aiding in the clearance of *C. rodentium* or are simply replacing the niche *C. rodentium* was occupying. Numbers of *Enterococcus faecalis* KB1 trended towards a decrease 2 weeks post-infection with *C. rodentium* compared to uninfected mice and returned to their original levels 4 weeks post-infection (figure 3.14C). This reduction in KB1 may be because it competes with *C. rodentium* for space or nutrients, or it may be translocating to the systemic environment. This experiment needs to be repeated for increased power to draw definitive conclusions about KB1 changes as a result of *C. rodentium* infection. Boxplots for the numbers of the remaining Oligo-MM12 members can be found in appendix figure 3.3.

3.3.15 *E. faecalis* and *L. reuteri* translocate to the systemic organs in Oligo-MM^{12} SKG mice

C. rodentium can colonise the systemic organs in both SPF and germ-free SKG mice. We therefore wanted to determine whether the Oligo-MM^{12} supported this during infection. We cultured livers, spleens, and mLNs on *C. rodentium*-specific agar from *C. rodentium* infected Oligo-MM^{12} SKG mice 2 weeks and 4 weeks post-infection, as well as uninfected Oligo-MM^{12} mice. We found that *C. rodentium* translocated to both the spleen and the liver 2 weeks and 4 weeks post-infection in a large majority of mice, but not to the mLNs (figure 3.15A). This reproduced what we observed in SPF mice, where *C. rodentium* could colonise the livers and spleens but not the mLNs during infection (figure 3.5A).

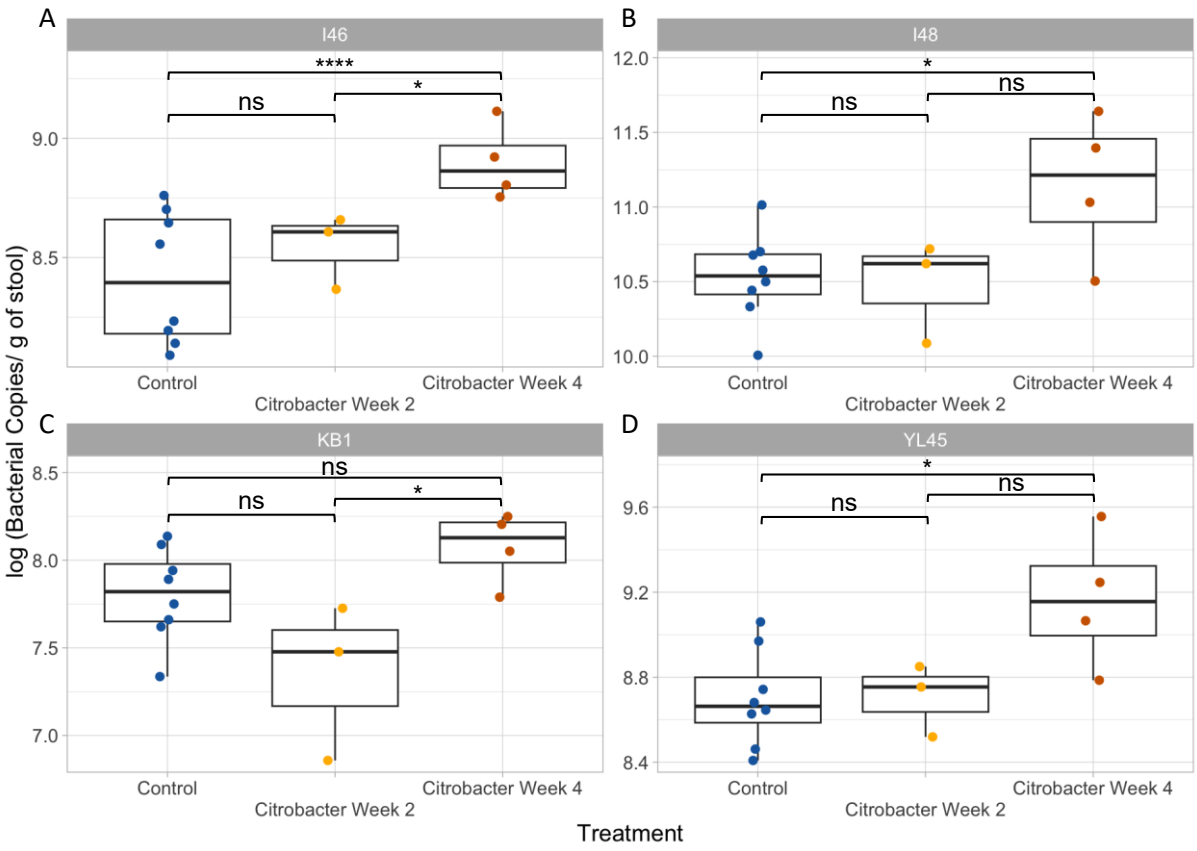


Figure 3.14 Numbers of specific Oligo-MM^{12} members are altered during *Citrobacter rodentium* infection in SKG mice. Colon contents from Oligo-MM^{12} SKG mice 2 weeks and 4 weeks post-infection with *C. rodentium* and uninfected Oligo-MM^{12} SKG mice were obtained, and qPCR was completed using strain-specific primers for Oligo-MM^{12} members and *C. rodentium.* One-way ANOVA with Tukey's post-hoc testing was completed for all bacteria with Benjamini-Hochberg correction to identify members of the Oligo-MM^{12} that were altered during infection. A) *Clostridium innocuum* I46. B) *Bacteroides caecimuris* I48. C) *Enterococcus faecalis* KB1. D) *Turicimonas muris* YL45. Number of bacteria are denoted as log (bacterial copies per gram of stool). Boxplots denote median + interquartile range and individual data points are shown.****p<0.0001, *p<0.05, ns = not significant. Data obtained from one experiment.

We sought to determine whether Oligo-MM^{12} members were able to colonise the systemic organs, as commensals could in SPF mice. We previously found that commensal microbiota were able to colonise the systemic organs in uninfected SPF SKG mice, and we found that those commensals were *Staphylococcus saprophyticus* and *Limosilactobacillus murinus* (figure 3.5B). We therefore cultured livers, spleens, and mLNs obtained from uninfected Oligo-MM^{12} SKG mice and Oligo-MM^{12} SKG mice 2 weeks and 4 weeks post-infection with *C. rodentium* on non-specific blood agar. We found that Oligo-MM^{12} members could colonise the livers and spleens of mice 2 weeks and 4 weeks post-infection with *C. rodentium*, as well as of uninfected Oligo-MM^{12} mice (figure 3.15B). Overall, this suggests that Oligo-MM^{12} SKG mice possess the same level of baseline intestinal permeability as SPF SKG and Balb/C mice. Upon sequencing of the isolated colonies cultured from

the livers and spleens of *C. rodentium*-infected Oligo-MM^{12} SKG mice, we identified these colonies as *Enterococcus faecalis* and *Limosilactobacillus reuteri*. This is unsurprising as they are taxonomically similar to the isolates *Staphylococcus saprophyticus* and *Ligilactobacillus murinus* cultured from organs obtained from SPF *C. rodentium* infected mice.

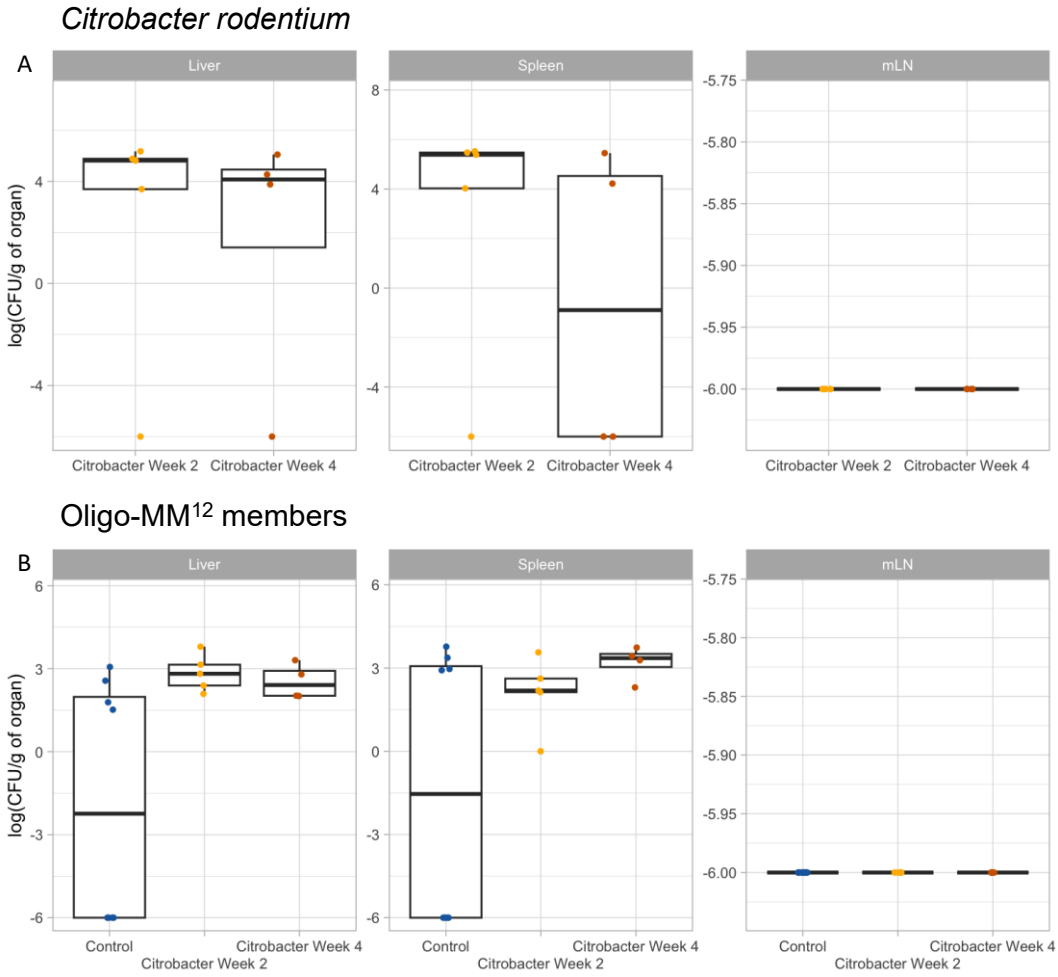


Figure 3.15 *Enterococcus faecalis* and *Limosilactobacillus reuteri* translocate to the systemic organs in Oligo-MM^{12} SKG mice. Livers, spleens, and mLNs from Oligo-MM^{12} SKG mice 2 weeks and 4 weeks post-infection with *C. rodentium* as well as uninfected Oligo-MM^{12} SKG controls were plated on *C. rodentium*-specific and non-specific agar to assess translocation of bacteria to systemic organs. A) *Citrobacter rodentium* colonisation in the liver, spleen, and mLN in uninfected Oligo-MM^{12} mice, and Oligo-MM^{12} mice 2 weeks and 4 weeks post-infection with *C. rodentium*. B) Oligo-MM^{12} member colonisation in the liver, spleen, and mLN of uninfected Oligo-MM^{12} mice, and Oligo-MM^{12} mice 2 weeks and 4 weeks post-infection with *C. rodentium*. Colonisation is denoted as log(CFU per gram of organ). Boxplots denote median + interquartile range and individual data points are shown. Data obtained from one experiment.

3.4 Discussion

In this chapter we developed a novel murine model for ReA that recapitulates the disease phenotypes and immune responses observed in patients. We found that disease was dependent on the presence of a commensal microbiome, and that when modelled in a minimal microbiome community, disease recapitulated SPF mice. We further characterised the microbiome changes in the SKG model in response to *C. rodentium* infection in Oligo-MM^{12} mice and SPF mice and found similar changes in specific microbes that are either typically pathogenic or known to aid in the clearance of *C. rodentium* infection. We found that commensal microbiota could colonise the systemic organs, suggesting a level of intestinal permeability in SKG mice that may contribute to the development of arthritis. We put forward a hypothesis suggesting that intestinal commensals with potential mimitopes to joint antigen are transported to secondary lymphoid organs and presented to T cells that have escaped negative selection due to a mutation in *Zap70*. *C. rodentium* may then provide a microbial trigger to drive pro-inflammatory cytokine production which differentiate these cells into either pathogenic Th17 cells or other T cell subsets, which then migrate to the joint and potentiate joint disease.

3.4.1 *Citrobacter rodentium* infection in SKG mice as a model for ReA

C. rodentium infection in SKG mice can trigger arthritis as well as colitis, recapitulating pathology observed in patients with ReA[84]. Previous studies in the SKG mouse model of arthritis have induced arthritis with a systemic priming trigger, and we showed for the first time in SKG mice that an enteral infection alone can trigger systemic joint inflammation[110]. We also modelled disease in a minimal microbiome community and found that Oligo-MM^{12} mice developed arthritis and colitis following *C. rodentium* infection. In SPF mice, we found that colitis peaked at 2 weeks and resolved alongside clearance of infection, but arthritis persisted after *C. rodentium* clearance. In Oligo-MM^{12} mice however, *C. rodentium* was not cleared and colitis had not returned to baseline by 4 weeks post-infection suggesting that intestinal inflammation resolution is dependent on *C. rodentium* clearance. Indeed, clearance of *C. rodentium* has been shown to be aided by *Enterobacteriaceae,*

which is not present in the Oligo-MM^{12}, and may explain the lower colonisation resistance we observed[209]. We observed increases in *Enterobacteriaceae* following infection with *C. rodentium* in SPF mice but could not delineate whether these reads were solely *C. rodentium* or whether they also accounted for commensal *Enterobacteriaceae* which may have bloomed to clear *C. rodentium.* The Oligo-MM^{19} community provides a model microbiome with higher complexity and presence of *Enterobacteriaceae*[197]. Modelling *C. rodentium* infection in Oligo-MM^{19} mice alongside Oligo-MM^{12} mice with added *Enterobacteriaceae* would assess the requirement for *Enterobacteriaceae* against the combinatorial influence of a complex microbiota in permitting disease.

Aside from *Enterobacteriaceae,* we observed changes to intestinal microbes that may be involved in clearance of *C. rodentium.* For instance, Bacteroidales and Clostridiales in both the SPF microbiome and the Oligo-MM12 community (*Bacteroides caecimuris* I48 and *Clostridium innocuum* I46) were altered following infection with *C. rodentium.* Increased Bacteroidales and Clostridiales is expected following infection with *C. rodentium*, as it has previously been demonstrated that neonates lacking *Bacteroidales* and *Clostridiales* display increased susceptibility to *C. rodentium* infection, and the readministration of *Clostridiales* leads to partial protection against *C. rodentium* infection[206]. Indeed, *Clostridium innocuum* can produce butyrate which can directly inhibit *C. rodentium* growth *in-vitro* and confers protection to mice *in-vivo*[205,238]. Thus, Clostridiales may bloom to help clear *C. rodentium* infection through production of metabolites.

After identifying changes in the intestinal microbiome following *C. rodentium* infection, we assessed how crucial the microbiota is to supporting disease in our model by utilising gnotobiotic mice. We found that *C. rodentium* was unable to drive either colitis or arthritis in the absence of commensal microbiota despite colonising robustly. Previously published data demonstrated that germ-free C57BL/6J mice develop colitis to a similar severity as SPF mice, though they cannot clear the infection[211]. Furthermore, colitis in C57BL/6J mice is attenuated upon higher dosage of *C. rodentium,* due to high bacterial density driving lowered virulence[211]. The reason we did not

observe. colitis in germ-free SKG mice may be due to a high dosage of *C. rodentium* used to remain consistent with our SPF infection protocol. Therefore, repeating this experiment with a lower dose (10^4 CFU rather than 10^9 CFU) may yield colitis.

C. rodentium infection in the absence of commensals is not sufficient to induce the development of arthritis, indicating that commensals are either required to confer virulence to *C. rodentium* or to interact with the host immune system to promote arthritis following *C. rodentium* colonisation. Furthermore, *C. rodentium* colonisation is not required for the persistence of arthritis, suggesting that *C. rodentium* may initiate an inflammatory, perhaps Th17, response, which drives arthritis. However, the persistence of arthritis is independent of this, and can be self-maintained.

3.4.2 RORγt responses may be important in triggering but not maintaining arthritis

C. rodentium colonisation in SPF mice is associated with RORγt responses in the intestine and the paw. Upon infection clearance however, RORγt responses were resolved to the levels of uninfected mice. This suggests a mechanism whereby Th17 responses are driven in the intestine to help clear *C. rodentium* infection but are pathogenic in the joint. In this regard, there is clinical evidence to suggest that Th17 responses are barrier-protective in the intestine but pathogenic in the context of arthritis. For instance, IL-17 inhibition is successful in treating AxSpA joint inflammation but exacerbates IBD[82,239].

Upon clearance of *C. rodentium* RORγt responses were reduced in the paw, suggesting alternative mechanisms perpetuating the maintenance of disease. Indeed, SKG mouse studies have demonstrated that disease can depend on different mechanisms. For instance, SKG mice primed with curdlan develop IL-23-dependent disease which is not inhibited in IL-17A-/- mice, and SKG mice infected intravaginally with *Chlamydia* develop TNF-dependent disease[114,179]. Further characterisation of the intestinal and joint immune response in the persistence of arthritis is required to delineate the inflammatory pathways associated with driving arthritis in our model. In addition, IL-23 signalling is associated with SpA, as well as in driving the development of curdlan-

induced SKG disease from the intestine[86,113]. Therefore, in future experiments we aim to measure myeloid cell production of IL-23 in the colon to determine whether it is involved in the induction of *C. rodentium*-driven arthritis. Notably, growing evidence suggests a role for IL-23 signalling in the initiation but not the maintenance of arthritis, and so characterisation of IL-23 signalling in the intestine at early timepoints may be crucial to observing its potential role in the development of disease[141].

3.4.3 *Citrobacter rodentium* and commensal microbiota colonise the systemic organs

in SPF SKG mice we found that *Staphylococcus* was increased in abundance following infection with *C. rodentium,* and *Enterococcus faecalis* KB1 was increased in Oligo-MM^{12} mice following infection. *C. rodentium* may be creating an ideal niche for *Staphylococcus* and *E. faecalis* to thrive, and they may be involved in driving disease, or it may be an unrelated change. Indeed, we found that both *Staphylococcus saprophyticus* and *Enterococcus faecalis* translocated to systemic organs in SPF and Oligo-MM^{12} mice, respectively. Previous studies have demonstrated that reduced colonisation resistance against, and translocation of *Enterococcus faecalis* facilitates susceptibility to *C. rodentium* infection[240]. This suggests that *E. faecalis* and its systemic translocation may confer virulence to *C. rodentium*.

Translocation of commensals including *S. saprophyticus, E. faecalis, L. murinus, and L. reuteri* occurred in uninfected mice, and *C. rodentium* was able to translocate in germ-free mice. Taken together, these data suggest that translocation of only *C. rodentium* or commensal microbiota is not sufficient to support disease. This may be because commensal microbiota confer virulence to *C. rodentium* allowing for induction of disease, but clearance of *C. rodentium* does not resolve arthritis. Therefore, it may be that *C. rodentium* is only required to initiate disease, and that arthritis is then self-maintained. Another hypothesis is that commensal microbiota provide molecular mimitopes to self-antigen, which are presented to self-reactive SKG T cells, to drive an autoimmune response in the joint. *Enterococcus* and *Lactobacillus* have both been demonstrated to induce liver autoimmune

disease in predisposed hosts by translocating to the liver and secondary lymphoid organs, highlighting their role as autoimmune-related microbiota [241,242]. *C. rodentium* may provide a pro-inflammatory trigger required for the differentiation of these bacteria-specific autoreactive T cells to become arthritogenic. Evidence supporting this hypothesis has been demonstrated in EAE mice, whereby *L. reuteri* contained mimitopes to self-antigen, and an *Erysipelotrichaeceae* bacterium was able to elicit Th17 responses to drive disease[150]. We suggest a similar mechanism in our model whereby *Enterococcus/Staphylococcus* or *Lactobacillus*-specific autoreactive T cells drive arthritis following induction of their differentiation into pathogenic T cells following *C. rodentium* trigger. Functional *in vivo and in vitro* experiments should be performed to investigate this hypothesis. For instance, whether T cells are specific for self and bacterial antigen can be delineated by pulsing of APCs and paw T cells obtained from SKG mice with bacterial and self-antigen to measure cytokine production. Furthermore, transfer of translocating commensal-specific T cells will delineate their involvement in the development of arthritis in our model.

The mechanism by which microbiota translocate to the systemic organs, whether it be freely or by specialised immune cells such as macrophages or DCs should be determined. *C. rodentium* and commensals were able to colonise the liver, spleen, and mLNs suggesting that they can translocate *via* both the bloodstream and the lymphatic system [243]. One way to determine whether immune cells can transport microbes to systemic organs and to characterise these cells is to fluorescently label *C. rodentium* or other translocating commensals prior to infection or monocolonisation and to sort lymphocytes based upon their fluorescence. These sorted cells can subsequently be sequenced by RNA sequencing or qPCR can be completed to identify gene expression changes in the cells that have phagocytosed *C. rodentium.* By identifying these cell types and their localisation, we can target their functionality with the aim to modulate disease.

Aside from intestinal commensals providing molecular mimitopes, lack of immune education by commensal microbiota may explain why germ-free mice do not develop arthritis following infection.

Indeed, germ-free mice display impairment in the development of several lymphocyte subsets as well as a reduction in IgA production from B cells [182,244,245]. As such, microbial colonisation can induce the development of T cell subsets important for both the prevention of pathogen colonisation, as well as the induction of autoimmune disease [134,135,246,247]. One way to determine whether immune education plays a role in our model is to remove the intestinal microbiota through the administration of antibiotics. Another way is to use auxotrophic bacteria, which can reversibly colonise germ-free mice, to educate the host immune system before infection with *C. rodentium*[190,191].

3.5 Conclusion

Overall, in this chapter we have developed a novel model for ReA utilising *C. rodentium* infection in a genetic mouse model for SpA. This model is dependent on the commensal microbiota and involves translocation of both commensals and *C. rodentium* to systemic sites. We suggest a mechanism whereby T cells specific for commensal bacteria with mimitopes to self-antigen are skewed towards a pathogenic phenotype by *C. rodentium*-driven pro-inflammatory responses. Further functional studies are required to delineate the mechanisms perpetuating the persistence of arthritis in this model and to gain insight into potential therapeutic targets in the treatment of ReA.

Chapter 4: *Bifidobacterium* programs the host immune system to support arthritis

4.1 Introduction

The gut-joint axis in AxSpA is clearly supported by its clinical overlap with IBD, and around 70% of patients with AxSpA displaying subclinical intestinal inflammation[73,248]. Furthermore, analysis of the microbiome has identified shifts in the intestinal microbiome of patients with AxSpA, more specifically observing expansion in species such as *Parabacteroides distasonis* which has displayed both protective and pathological effects in inflammatory diseases, and *Ruminococcus gnavus*, a more typically pathogenic bacterium[5,151,249,250]. AxSpA development is highly associated with genetic factors, most notably HLA-B27, suggesting that the interplay of the host genetics, intestinal microbiome, and host immune system may all contribute to the development of joint inflammation[87]. Indeed, mouse models of AxSpA demonstrate an importance of the intestinal microbiome and host genetic predisposition in development of arthritis. For instance, SKG mice with a mutation in the gene encoding the T cell signalling protein ZAP-70 are protected from curdlan-induced intestinal inflammation and partially protected from joint inflammation when maintained in germ-free conditions[179]. Such studies support the presence of a link between the intestinal microbiome, host genetic factors, and the onset of joint inflammation. However, further studies are required to identify the causal cellular and molecular pathways involved.

To begin to investigate the association between the host immune system and the intestinal microbiome, recent studies have focused on identification of host IgA coating, and this has led to the identification of pathobionts in IBD and Crohn's-SpA[120,251]. Previous work in our lab led by Dr Lilian Lam involved sorting intestinal bacteria isolated from curdlan-injected and naïve SKG mice based upon their IgA coating and sequencing them by 16S rRNA sequencing. The genera *Leuconostoc* was found at a higher abundance in the IgA+ population compared to the IgA- population, suggesting a high level of communication with the host immune system (figure 4.1).

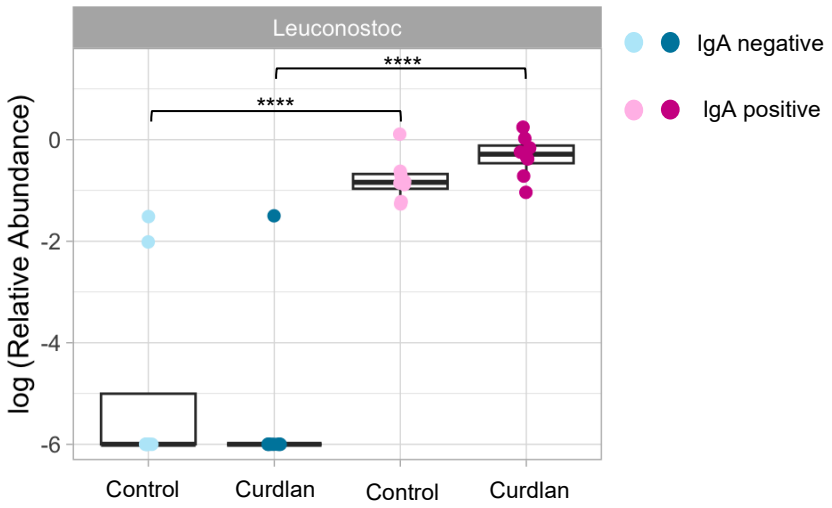


Figure 4.1 *Leuconostoc* is coated in host IgA. Relative abundance of *Leuconostoc* in IgA coated and IgA uncoated populations from small intestinal contents obtained from curdlan-injected and naïve SKG mice. Relative abundance is denoted as log (relative abundance). ****p<0.0001. One-way ANOVA with Tukey's post-hoc testing. Boxplots denote median + interquartile range and individual data points are shown.

Although of interest, these studies do not assess the functional role of bacteria eliciting a humoral response. One approach is the use of gnotobiotic hosts, which allow for a reductionist approach to studying host-microbiota interactions and can range from germ-free animals which lack microorganisms entirely, to monocolonised animals which are colonised with a single bacterial strain, cultured microbial communities such as the Oligo-MM^{12}, as well as transient colonisation to study immune education[176]. Chapter 3 demonstrated that the Oligo-MM^{12} community was able to model *C. rodentium*-driven arthritis in the SKG mouse model, suggesting its utility to study immune pathology in SKG mice. In support of this, SKG mice colonised with the ASF minimal community develop disease following curdlan induction, though it is attenuated compared to SPF mice[179].

Alongside advantages there are also drawbacks of utilising germ-free animals including physiological alterations that arise from a lack of microbial colonisation. Indeed, the intestinal microbiota and its colonisation of mucosal tissues in early life play a crucial role in educating the host immune system. For instance, *Clostridium* species and *Limosilactobacillus reuteri* can drive the development of intestinal T_{reg} cells, enabling tolerance to commensal microbiota[246,247]. However, under certain conditions, microbiota drive intestinal inflammatory responses and development of colitis[252]. Identifying the key arthritogenic members of the intestinal microbiome and how they

interact with the host immune system is under-researched in SpA, and the role these play in developing the host immune system should be investigated. Therefore, this chapter aims to identify host-microbiota interactions that support the development of joint inflammation utilising the SKG mouse model.

4.2 Aim

In this chapter we aimed to firstly characterise the intestinal microbiome during disease in SKG mice under SPF and Oligo-MM^{12} conditions. Subsequently, we sought to utilise monocolonisations in SKG mice with bacteria of interest with the aim to identify arthritogenic members of the intestinal microbiome. Finally, we aimed to delineate the role of microbiota-driven immune maturation in supporting the development of inflammatory arthritis.

4.3 Results

4.3.1 The SKG mutation in *Zap70* confers susceptibility to arthritis and small intestinal inflammation in mice

The SKG mouse model involves a point mutation in *Zap70* and has been previously shown to confer spontaneous arthritis in conventional mouse facilities as well as arthritis following injection with the dectin-1 ligand curdlan in SPF mouse facilities[107,179]. A high level of microbiome compositional variation exists between SPF facilities, so we first assessed the kinetics of disease pathology in SKG mice in our own SPF facility following induction with curdlan. We injected curdlan intraperitoneally into both Balb/C and SKG mice and followed them for 4 weeks, assessing their arthritis weekly according to section 2.4.3. We observed that SKG mice developed arthritis progressively over 4 weeks post-injection, compared to Balb/C mice that did not develop arthritis (figure 4.2A). Furthermore, we determined the effects of curdlan injection and *Zap70* mutation on paw histopathology by assessing H&E-stained paw tissues for evidence of inflammation according to section 2.5.3. We found that SKG mice injected with curdlan developed significantly higher paw

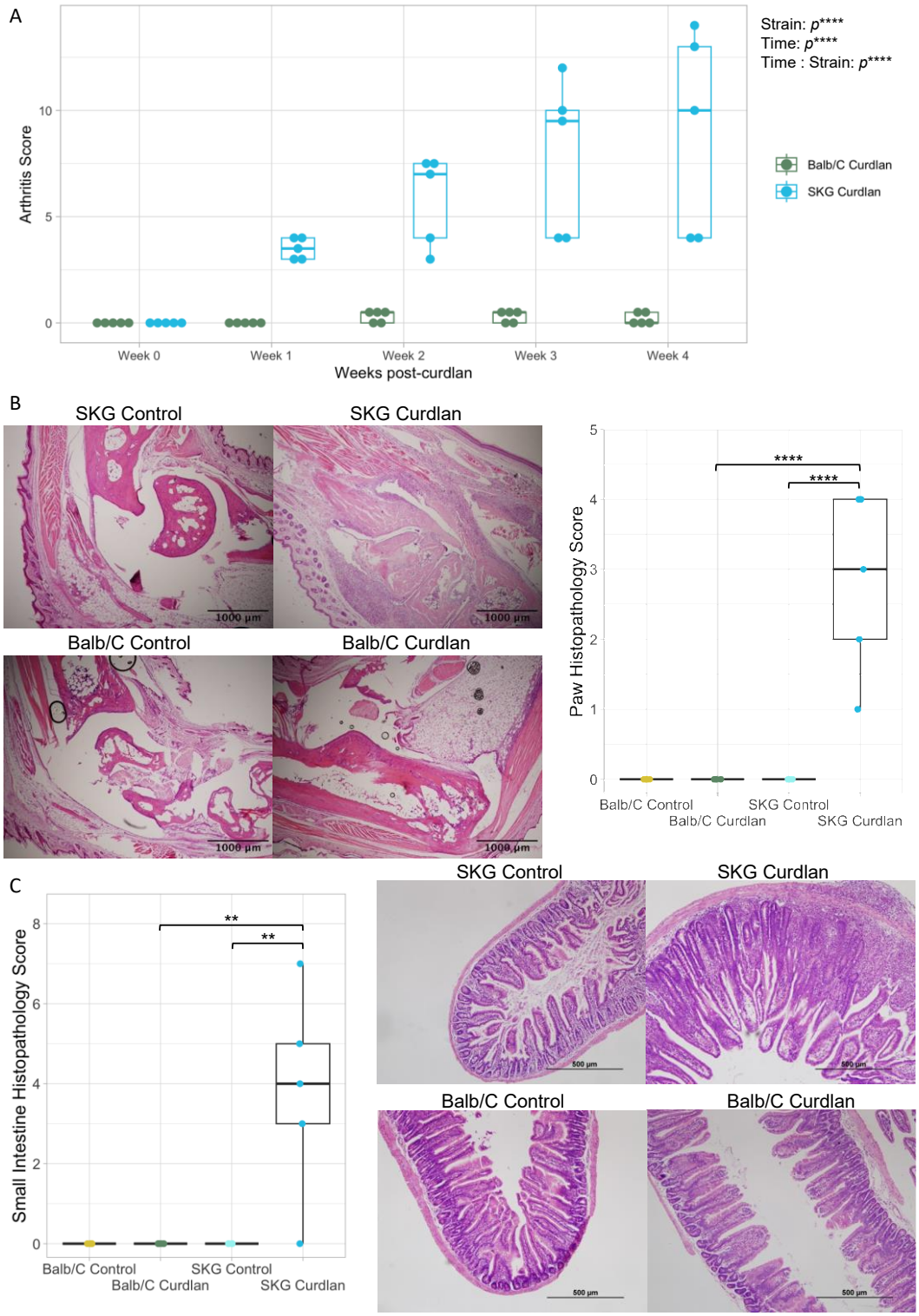


Figure 4.2 The SKG mutation in *Zap70* confers susceptibility to arthritis and small intestinal inflammation in mice. SKG and Balb/C mice were intraperitoneally injected with curdlan and culled 4 weeks post-injection. A) Arthritis scores in SKG mice injected with curdlan compared to Balb/C mice injected with curdlan. Green = Balb/C, blue = SKG. B) Paw histopathology scoring in SKG mice and Balb/C mice injected with curdlan compared to SKG and Balb/C naïve controls with representative microscopy images of H&E-stained paw tissue. C) Small intestine histopathology scoring in SKG mice and Balb/C mice injected with curdlan compared to SKG and Balb/C naïve controls with representative microscopy images of H&E-stained small intestine tissue. ****p<0.0001, **p<0.01. A) Two-way repeated measures ANOVA, factors = mouse strain and weeks post-infection, significance values for effect of each variable and the interaction of the two variables are indicated on the plot. B), C) One-way ANOVA with Tukey's post-hoc testing. Boxplots denote median + interquartile range and individual data points are shown. Data obtained from 1 experiment, replicated once.

histopathology scores when compared to naïve SKG mice and Balb/C mice, characterised by inflammatory infiltrate throughout the ankle joint and in the soft tissue (figure 4.2B). Notably, we observed a larger spread of mice with mild to significant disease compared to previously published data which demonstrates high levels of paw pathology in all mice[179]. This suggests that our SPF facility may lack certain pro-inflammatory microbes that can consistently drive significant disease in all mice.

Previous studies have demonstrated that SKG mice injected with curdlan have small intestinal inflammation [179]. To characterise this in our own facility, we assessed H&E-stained small intestine tissue taken from the ileum, jejunum, and duodenum for signs of intestinal inflammation according to section 2.5.2. We observed that SKG mice injected with curdlan developed significantly more small intestinal inflammation than naïve controls and Balb/C mice injected with curdlan (figure 4.2C). This intestinal inflammation was characterised by extensive inflammatory infiltrate present in the lamina propria and villous distortion (figure 4.2C). Notably, we also observed a spread of intestinal severity in our mice, as seen with paw histopathology. This further supports the hypothesis that our SPF facility lacks certain pro-arthritogenic bacteria required for consistent disease. Overall, we were able to demonstrate that genetic predisposition in the form of *Zap70* mutation alongside dectin-1 priming are required to permit arthritis in our SPF mouse facility.

4.3.2 The Oligo-MM12 community is a useful model for studying curdlan-triggered disease in SKG mice

In Chapter 3, we generated an Oligo-MM^{12} SKG mouse colony as a reductionist approach to studying the microbiome. Here we tested the Oligo-MM^{12} SKG mouse colony to determine whether curdlan-triggered disease in SKG mice was reproducible in a minimal microbiome community. We injected Oligo-MM^{12} SKG mice with curdlan and followed them for 4 weeks post-injection, scoring their arthritis weekly. We found that Oligo-MM^{12} SKG mice injected with curdlan developed similar levels of arthritis compared to SPF mice, although onset of severe arthritis was delayed (figure 4.3A).

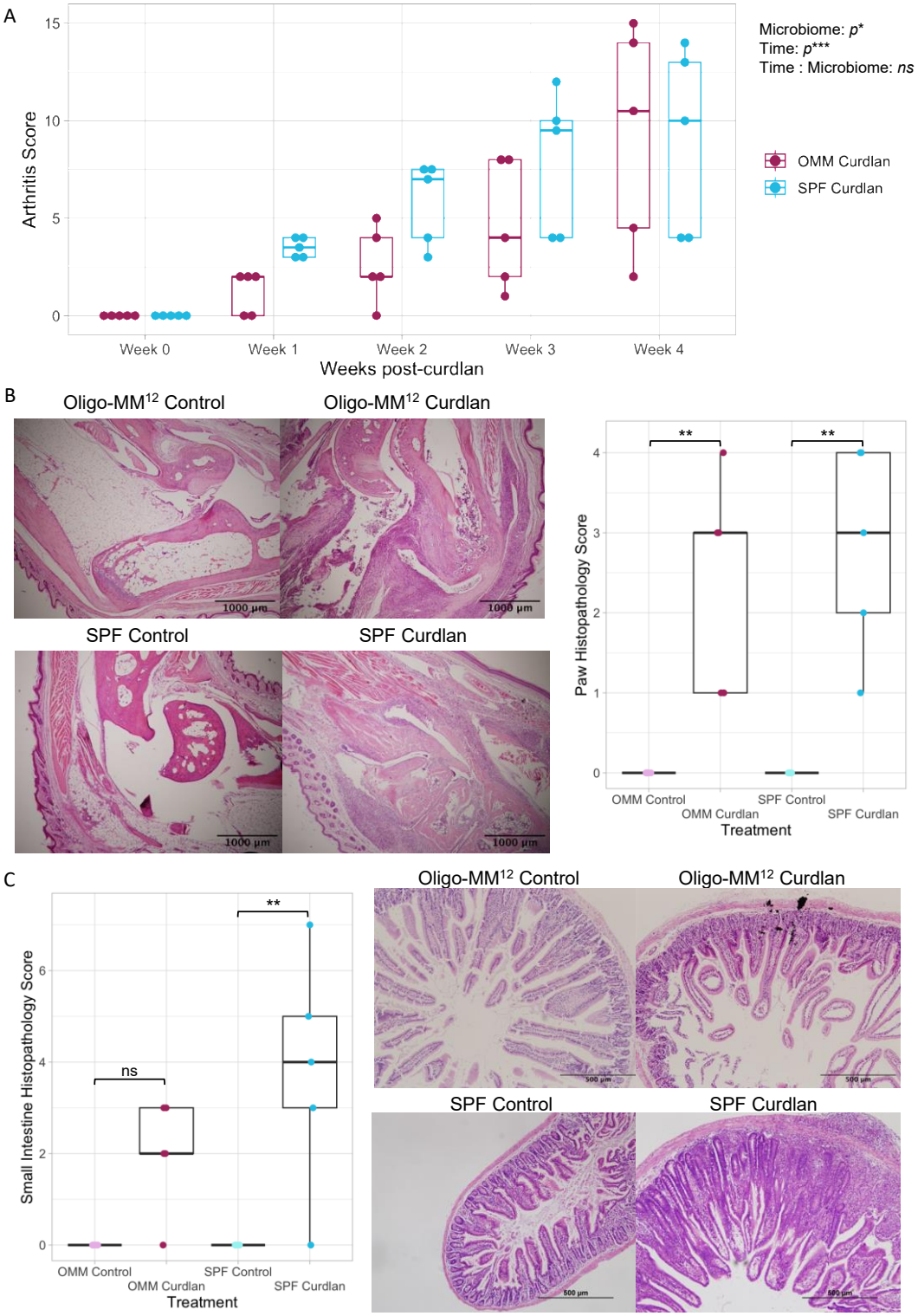


Figure 4.3 The Oligo-MM^{12} community is a useful model for studying curdlan-triggered disease in SKG mice. Oligo-MM^{12} SKG mice were injected with curdlan and culled 4 weeks post-injection. A) Arthritis scores in Oligo-MM^{12} SKG mice injected with curdlan compared to SPF mice injected with curdlan. B) Paw histopathology scoring and representative microscopy images of H&E-stained paw tissue in curdlan-injected and curdlan-naïve Oligo-MM^{12} SKG mice and SPF SKG mice. C) Small intestine histopathology scoring and representative microscopy images of H&E-stained small intestine tissue in curdlan-injected and curdlan-naïve Oligo-MM^{12} SKG mice and SPF SKG mice. ***p<0.001, **p<0.01, *p<0.05, ns = not significant. A) Two-way repeated measures ANOVA, factors = microbiome and weeks post-infection, significance values for effect of each variable and the interaction of the two variables are indicated on the plot. B), C) One-way ANOVA with Tukey's post-hoc testing. Boxplots denote median + interquartile range and individual data points are shown. Data obtained from one experiment, performed once.

We assessed paw histopathology by scoring H&E-stained paw tissue and found that Oligo-MM^{12} SKG mice injected with curdlan developed significantly higher paw histopathology scores compared to naïve Oligo-MM^{12} SKG controls, and similar levels of severity when compared to SPF mice injected with curdlan (figure 4.3B). We also tested whether the Oligo-MM^{12} community was able to permit the development of small intestinal inflammation. We found that Oligo-MM^{12} SKG mice injected with curdlan develop a trend towards higher small intestine histopathology scores compared to naïve Oligo-MM^{12} SKG controls, although not significant, as that seen in SPF SKG mice (figure 4.3C). Taken together, these data suggest that the Oligo-MM^{12} community may replicate the ability of the SPF microbiota to support arthritis and potentially small intestinal inflammation in SKG mice. However, further studies are required to confirm these results.

4.3.3 Paw RORγt responses are associated with disease in SKG mice

Previous studies have demonstrated that the SKG-curdlan mouse model is largely driven by an IL-23-dependent Th17 response[113,253]. To determine whether our Oligo-MM^{12} mice and SPF mice mount similar T cell responses following curdlan injection, we stained paw lymphocytes for FoxP3 and RORγt. We found that FoxP3+ T helper cell frequencies were similar in curdlan-injected and naïve Oligo-MM^{12} SKG mice and SPF SKG mice (figure 4.4A). However, we did find increased frequencies of RORγt+ T helper cells in Oligo-MM^{12} mice and SPF mice following curdlan injection (figure 4.4B). Finally, we found that absolute numbers of RORγt+ T helper cells and FoxP3+ T helper cells were both increased following curdlan injection in Oligo-MM^{12} and SPF mice (figure 4.4C, D). Taken together, Oligo-MM^{12} and SPF SKG mice mount a RORγt T cell response in the paw following induction of disease with curdlan.

4.3.4 Curdlan induces shifts in the microbiome in both SPF and Oligo-MM^{12} SKG mice

Patients with SpA display shifts in their intestinal microbiome, and in Chapter 3 we identified changes in the microbiome of both SPF and Oligo-MM^{12} SKG mice infected with *C. rodentium*[151]. We therefore tested whether curdlan-induced disease was associated with shifts in the intestinal

microbiome in SPF or Oligo-MM^{12} mice. As we found that 16S rRNA sequencing did not allow for adequate depth of sequencing to make consistent species level identification, we performed shallow shotgun sequencing provided by Transnetyx (TN, US) on small intestinal contents taken 4 weeks post-injection from SPF SKG mice. In addition, we completed strain-specific qPCR on each Oligo-MM^{12} member on small intestinal contents from Oligo-MM^{12} SKG mice.

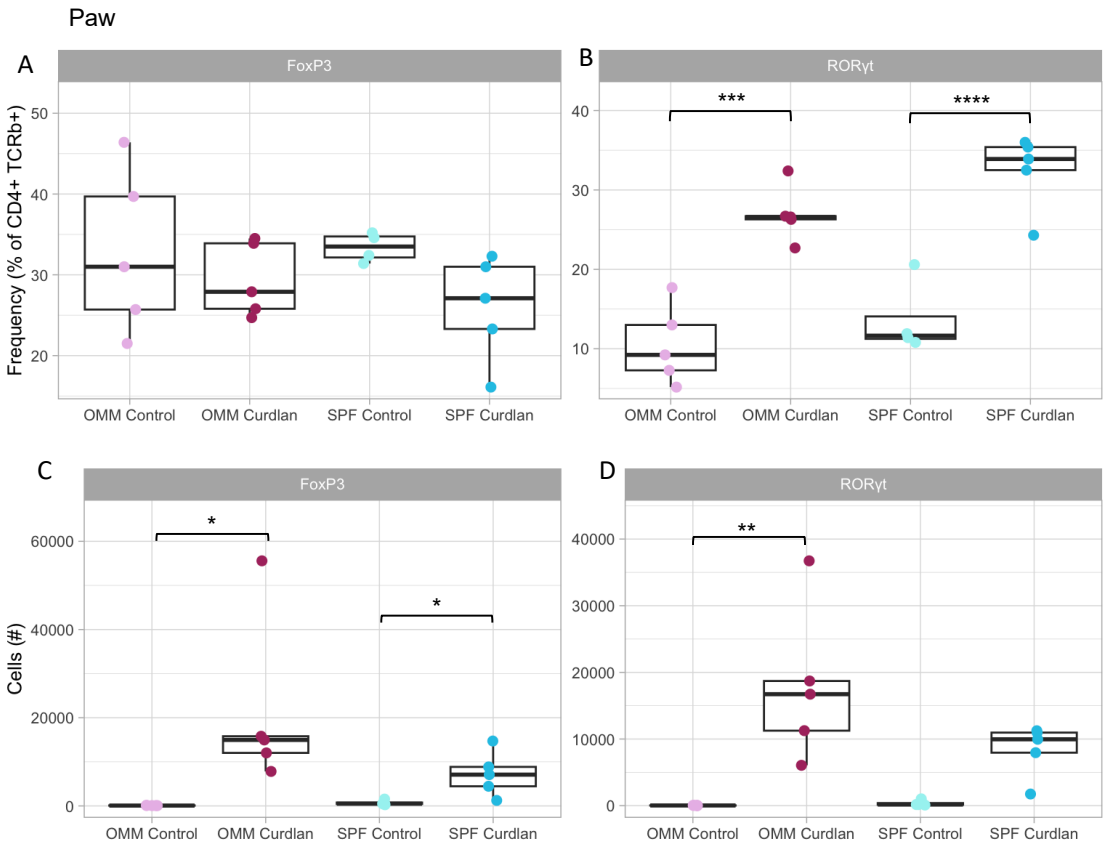


Figure 4.4 Paw RORγt responses are associated with disease in SKG mice. T_{reg} cells and Th17 cells were quantified by flow cytometric staining of the transcription factors FoxP3 and RORγt in the paws of curdlan-injected and naïve Oligo-MM^{12} and SPF SKG mice. Gating strategy is outlined in appendix figure 4.1. A) Frequencies of FoxP3+ T helper cells. B) Frequencies of FoxP3- RORγt+ T helper cells. C) Absolute numbers of FoxP3+ T helper cells. D) Absolute numbers of FoxP3- RORγt+ T helper cells. Frequencies are denoted as % of CD4+ TCRβ+ cells. Boxplots denote median + interquartile range and individual data points are shown. ****p<0.0001, ***p<0.001, **p<0.01, *p<0.05. One-way ANOVA with Tukey's post-hoc testing was completed for all plots. Data obtained from two experiments.

Compositional analysis in SPF and Oligo-MM^{12} SKG mice revealed changes in the overall composition of the microbiome (figure 4.5A, 4.6A). Specifically, there appears to be destabilisation in the abundances of *Lactobacillaceae* in SPF SKG mice injected with curdlan, and *Bacteroides caecimuris* I48 in Oligo-MM^{12} mice injected with curdlan. PCA confirmed microbiome shifts at the

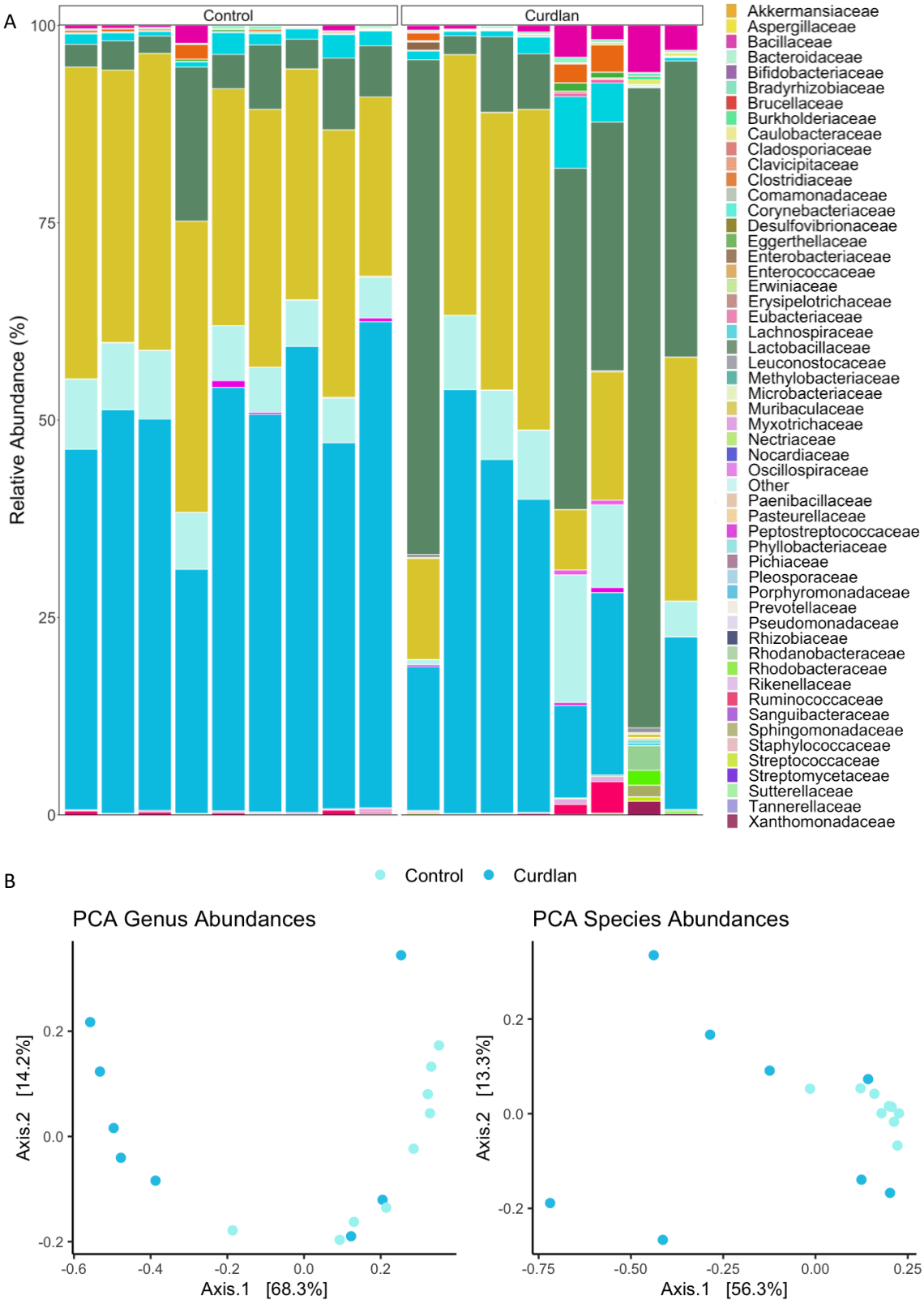


Figure 4.5 Curdlan induces shifts in the microbiome in SPF SKG mice. Small intestine contents 4 weeks post-injection from curdlan-injected and naïve SPF SKG mice were sequenced by shallow shotgun sequencing. A) Microbiome composition plots at family-level, comparing SPF SKG mice injected with curdlan and naïve SPF SKG mice. Each family is expressed as a relative abundance to the entire bacterial population in each sample. B) Principal component analysis at genus-level and species-level of SPF SKG mice injected with curdlan and naïve SPF SKG mice. Distance = Bray-Curtis. Data obtained from two experiments.

genus and species level in SPF SKG mice injected with curdlan compared to naïve SPF SKG mice, as well as at strain-level in Oligo-MM^{12} SKG mice injected with curdlan compared to naïve Oligo-MM^{12} mice (4.5B, 4.6B). Specifically, naïve Oligo-MM^{12} and SPF SKG mice cluster tightly within themselves, whereas curdlan-injected Oligo-MM^{12} and SPF SKG mice appear to have more variation between individual mice. Taken together, these data demonstrate that curdlan-injection is associated with microbiome shifts in the small intestine of SKG mice. Furthermore, they support the use of the Oligo-MM^{12} community in modelling SKG-curdlan disease.

4.3.5 *Weisella* blooms following curdlan injection in SKG mice

To determine changes to specific bacteria, we completed linear modelling at genus-level and species-level in SPF SKG mice. We found that the abundance of the genera *Weisella* was elevated in SPF SKG mice following the injection of curdlan, compared to naïve SPF SKG mice (figure 4.7A). In fact, *Weisella* was not present in naïve SPF SKG controls, suggesting that it blooms specifically during inflammation. At species-level, we found that *Weisella confusa* abundance was elevated in curdlan-injected mice compared to naïve mice (figure 4.8B). It is therefore likely that the species driving the genus-level changes in *Weisella* is *Weisella confusa*.

Statistical analysis of small intestine contents from curdlan-injected and naïve Oligo-MM^{12} SKG mice revealed reductions in the relative abundances of *Akkermansia muciniphila* YL44 and *Turicimonas Muris* YL45 (figure 4.7C, D). Notably, although no other Oligo-MM^{12} members abundances were altered following injection with curdlan, absolute numbers of all Oligo-MM^{12} members that were detected decreased following injection with curdlan (appendix figures 4.2, 4.3). This suggests that the triggering of disease in SKG mice leads to a reduction in overall microbiome density, potentially influencing the intestinal barrier and immune responses.

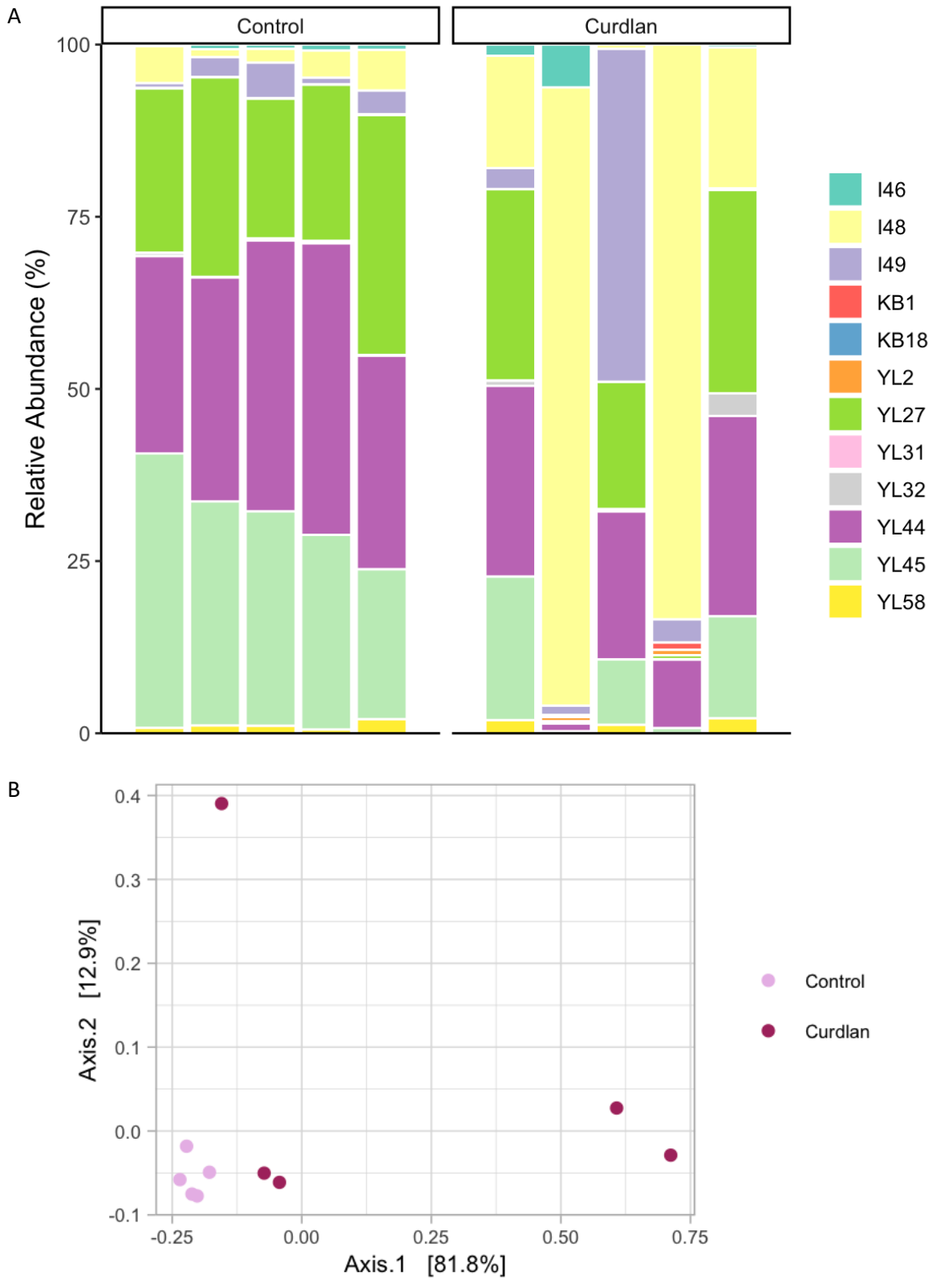


Figure 4.6 Curdlan induces shifts in the microbiome in Oligo-MM^{12} SKG mice. Strain-specific qPCR was completed on small intestine contents 4 weeks post-injection from curdlan-injected and naïve Oligo-MM^{12} SKG mice. A) Microbiome composition plots comparing Oligo-MM^{12} SKG mice injected with curdlan and naïve Oligo-MM^{12} SKG mice. Each strain is expressed as a relative abundance to the entire bacterial population in each sample. B) Principal component analysis of Oligo-MM^{12} SKG mice injected with curdlan and naïve Oligo-MM^{12} SKG mice. Distance = Bray-Curtis. Data obtained from one experiment.

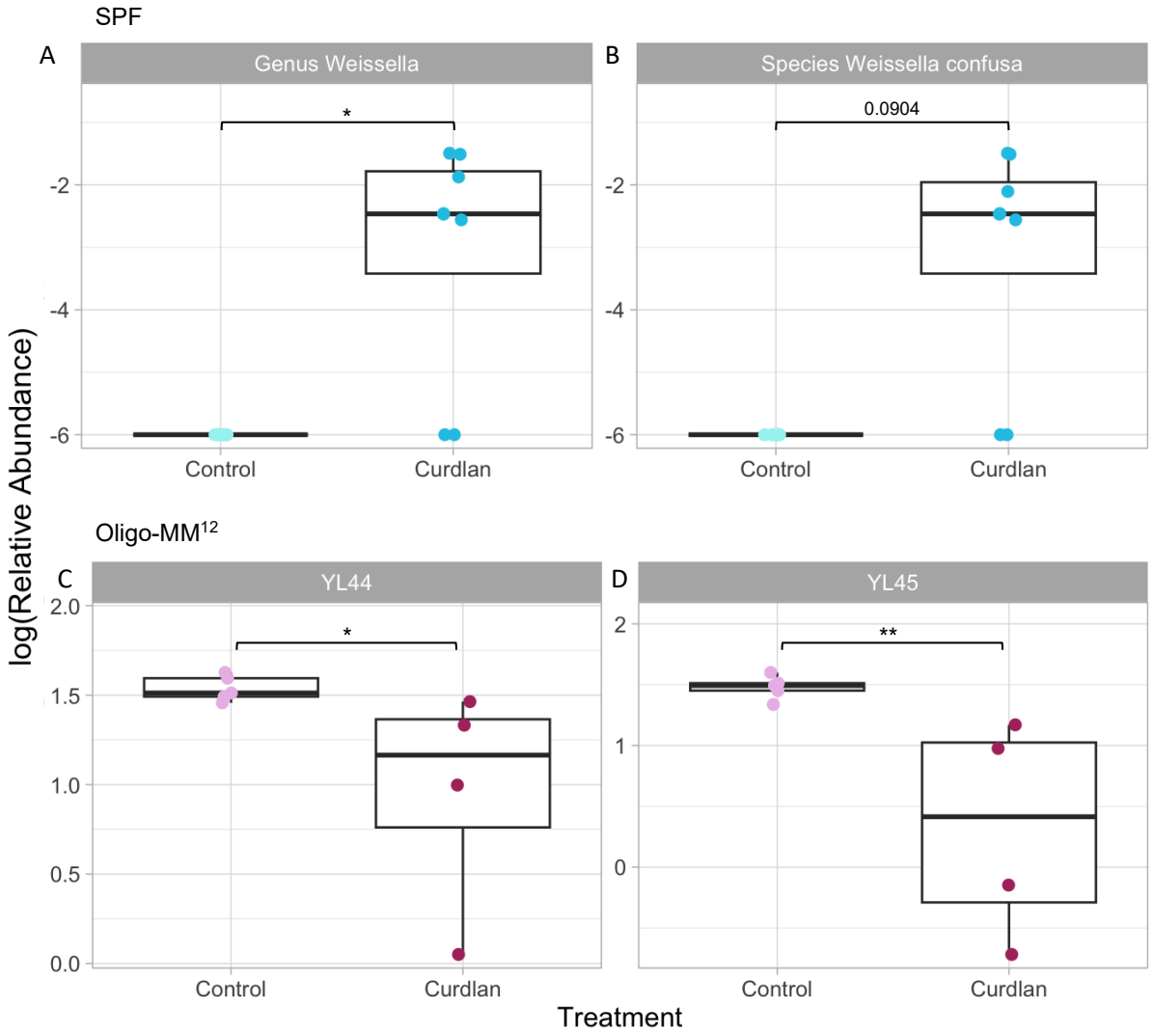


Figure 4.7 *Weisella* blooms following curdlan injection in SKG mice. Statistical testing of individual bacteria from shallow shotgun sequencing or qPCR of small intestine contents taken 4 weeks post-infection from curdlan-injected and naïve SPF and Oligo-MM^{12} SKG mice. A) SPF relative abundance of the genus *Weisella*. B) SPF relative abundance of the species *Weisella confusa*. C) Oligo-MM^{12} relative abundance of *Akkermansia muciniphila* YL44. D) Oligo-MM^{12} relative abundance of *Turicimonas muris* YL45. Boxplots denote median + interquartile range and individual data points are shown. **p<0.01, *p<0.05. A), B) Mixed linear effects modelling with post-hoc estimated marginal means analysis. C), D) Student's t-test with Benjamini-Hochberg correction for multiple testing.

4.3.6 SKG disease is microbiota-dependent

In Chapter 3, we demonstrated a requirement of the intestinal microbiota for *C. rodentium*-induced arthritis and colitis in SKG mice. Furthermore, previously published data demonstrates that germ-free SKG mice have attenuated disease following curdlan injection[179]. The intestinal microbiome was shifted in both SPF and Oligo-MM^{12} SKG mice injected with curdlan, so we sought to assess the role of the intestinal microbiota in permitting pathology. We injected germ-free SKG mice with curdlan and followed them for 4 weeks post-injection, assessing arthritis weekly. We

observed that germ-free SKG mice injected with curdlan did not develop arthritis, compared to SPF SKG mice that developed progressive arthritis (figure 4.8A). We assessed paw histopathology by scoring H&E-stained paw tissue and found that curdlan-injected SPF SKG mice developed significantly higher histopathological disease compared to germ-free SKG mice injected with curdlan (figure 4.8B). Finally, we sought to identify whether small intestinal inflammation was dependent on the microbiota in SKG mice. We assessed small intestinal inflammation by scoring H&E-stained small intestine tissue and found that curdlan-injected SPF SKG mice had significantly elevated histopathology scores compared to germ-free SKG mice injected with curdlan (figure 4.8C). Overall, we have replicated previous findings to demonstrate the dependence of SKG disease on the intestinal microbiota.

4.3.7 Monocolonisation of bacteria permits arthritis in SKG mice

Gnotobiotic colonisation of single microbial organisms allows for a highly reductionist approach to studying host-microbiota interactions. Previous work in the lab identified several bacteria associated with either SpA or anti-inflammatory responses for monocolonisation in SKG mice. Indeed, *Parabacteroides distasonis* was identified as a bacterium of interest as it is increased in abundance in patients with AxSpA compared to healthy controls[151]. In addition, *Bifidobacterium* has been shown to drive Th17 responses in the intestine and drives inflammation in the K/BxN model of arthritis[135]. *Leuconostoc* was identified to be highly IgA-coated, and therefore may be more immune stimulatory. We chose to monocolonise with *Leuconostoc citreum* due to its ability to reduce inflammation in the CIA model of arthritis, suggesting that it may serve as an anti-inflammatory bacterium[254]. Finally, *Limosilactobacillus reuteri* was chosen as a control bacterium that is known to have anti-inflammatory effects on the host-immune system[246,255]. Prior to monocolonising SKG mice with these bacteria of interest, we hypothesised that both *P. distasonis* and *B. animalis* would have the ability to support arthritis in SKG mice due to their associations with arthritis in humans and mice. We further hypothesised that *L. citreum* and *L. reuteri* would not permit the induction of arthritis, due to their anti-inflammatory characteristics.

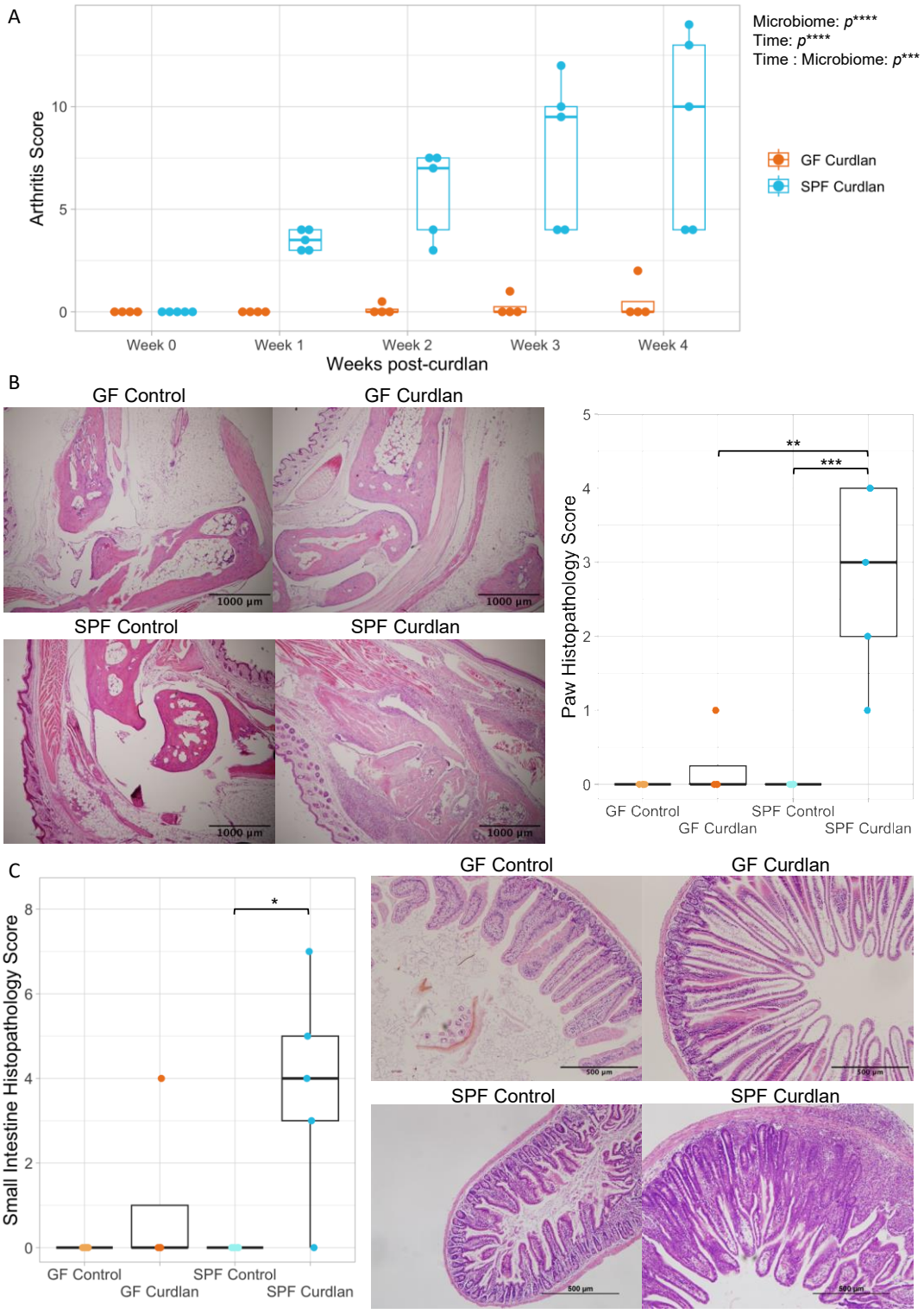


Figure 4.8 SKG disease is microbiota dependent. Germ-free SKG mice were injected with curdlan and culled 4 weeks post-injection. A) Arthritis scores in germ-free SKG mice injected with curdlan compared to SPF SKG mice injected with curdlan. Blue = SPF, orange = germ-free. B) Paw histopathology scoring with representative microscopy images of H&E-stained paw tissue in naïve and curdlan-injected SPF SKG mice compared to naïve and curdlan-injected germ-free SKG mice. C) Small intestine histopathology scoring with representative microscopy images of H&E-stained small intestine tissue in naïve and curdlan-injected SPF SKG mice compared to naïve and curdlan-injected germ-free SKG mice. ****p<0.0001, ***p<0.001, **p<0.01, *p<0.05. A) Two-way repeated measures ANOVA, factors = microbiome status and weeks post-infection, significance values for effect of each variable and the interaction of the two variables are indicated on the plot. B), C) One-way ANOVA with Tukey's post-hoc testing. Boxplots denote median + interquartile range and individual data points are shown. Data obtained from one experiment, replicated twice.

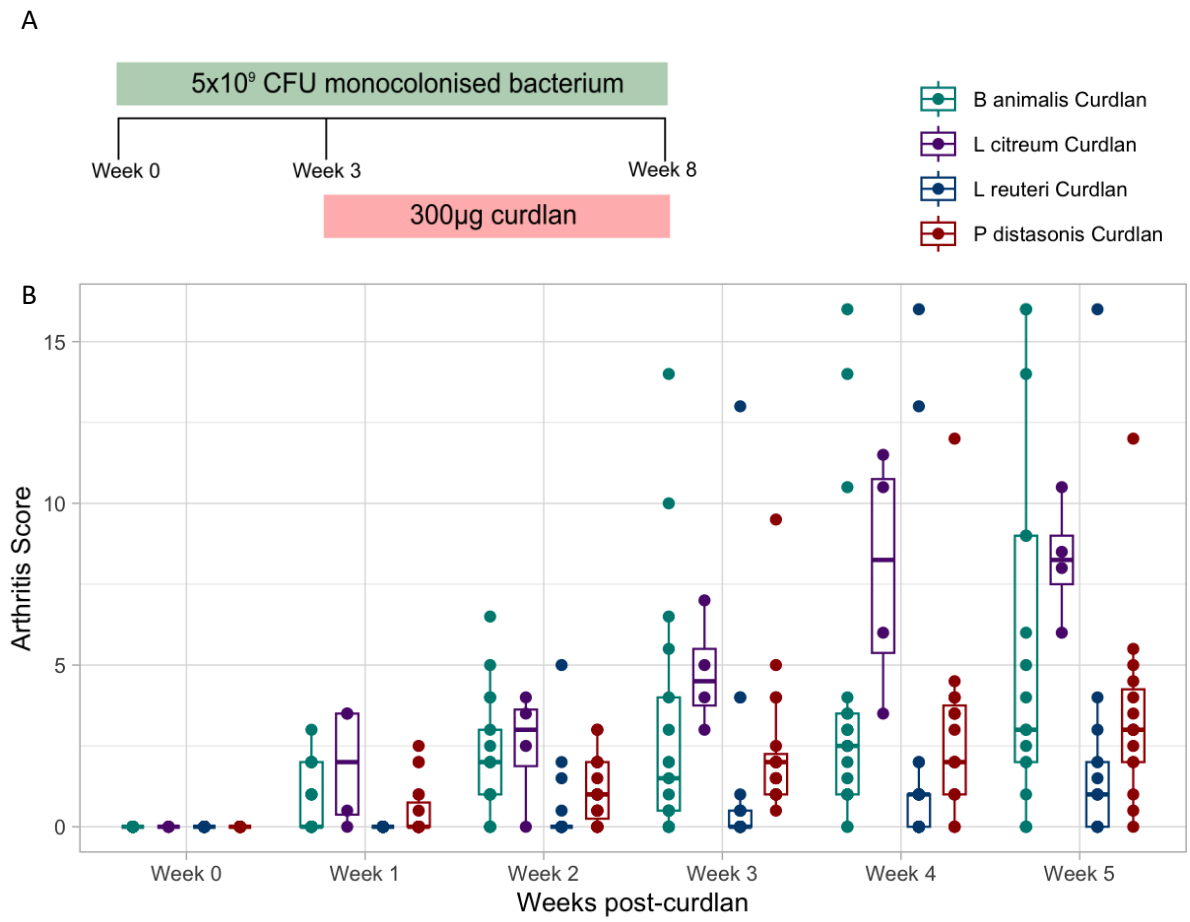


Figure 4.9 Monocolonisation of bacteria permits arthritis in SKG mice. 3-week-old germ-free SKG mice were monocolonised with bacteria of interest *Bifidobacterium animalis, Leuconostoc citreum, Limosilactobacillus reuteri* and *Parabacteroides distasonis* for 3 weeks, and subsequently injected with curdlan. Mice were culled 5 weeks post-injection with curdlan. A) Experimental outline for monocolonisation and subsequent injection with curdlan. B) Arthritis scores for curdlan-injected mono-associated SKG mice. Turquoise = *B. animalis,* purple = *L. citreum*, blue = *L. reuteri*, red = *P. distasonis*. Two-way repeated measures ANOVA, factors = bacterial monocolonisation and weeks post-infection. Boxplots denote median + interquartile range and individual data points are shown. Data obtained from 3 experiments.

To study the effects of these single bacteria, we monocolonised 3-week-old germ-free SKG mice with each bacterium and allowed for stabilisation of bacterial colonisation to occur over 3 weeks. Following this, we injected mice with curdlan and followed them for 5 weeks post-injection, assessing arthritis weekly (figure 4.9A). We found that every bacterium we monocolonised SKG mice with permitted the induction of arthritis, with mice reaching similar score severity to SPF SKG mice (figure 4.9B). We assessed paw histopathology by scoring H&E-stained paw tissue sections and found that *B. animalis, P. distasonis,* and *L. citreum* colonised mice that were injected with curdlan all developed significantly higher paw histopathology compared to naïve monocolonised mice (figure 4.10A, B). Furthermore, *L. reuteri*-associated mice injected with curdlan trended towards increased

paw histopathology scores compared to naïve *L. reuteri*-associated mice (figure 4.10A, B). Together these data demonstrate that each bacterium of interest had the ability to support the induction of joint inflammation in the SKG model. This suggests that early life colonisation with intestinal microbiota may be crucial to form interactions with the host immune system, thereby supporting the induction of disease.

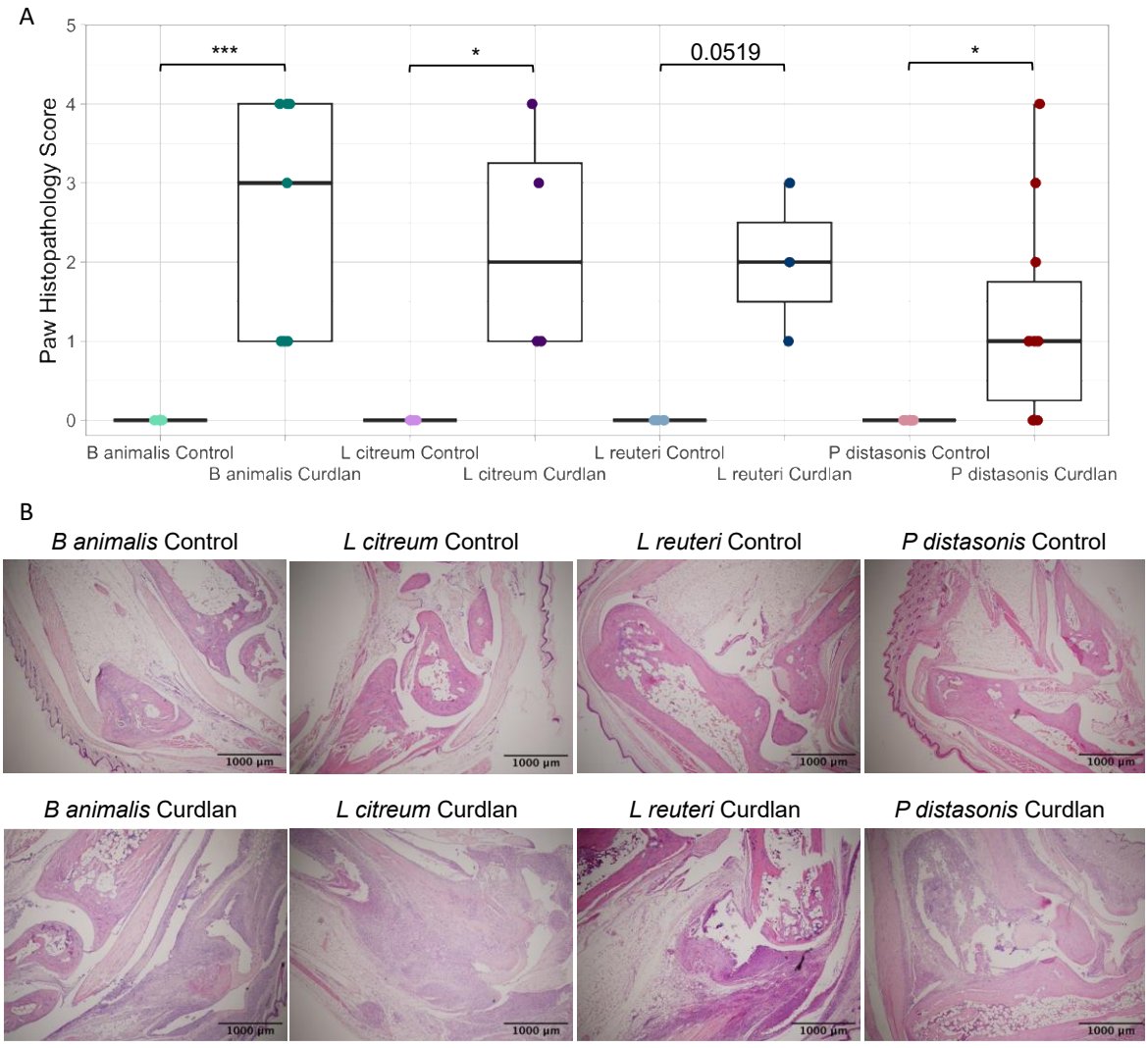


Figure 4.10 Paw histopathology is supported in monocolonised SKG mice. Paw tissue was obtained from curdlan-injected and naïve monocolonised SKG mice, and subsequently sectioned and stained with H&E. A) Paw histopathology scoring for individually monocolonised SKG mice injected with curdlan compared to naïve mono-associated SKG mice. B) Representative microscopy images of H&E-stained paw tissue obtained from curdlan-injected and naïve monocolonised SKG mice. ***p<0.001, *p<0.05. One-way ANOVA with Tukey's post-hoc testing. Boxplots denote median + interquartile range and individual data points are shown. Data obtained from one experiment.

4.3.8 Monocolonisation of bacteria supports intestinal inflammation in SKG mice

After determining that monocolonisation with each bacterium of interest permitted the development of joint inflammation in SKG mice, we sought to identify whether intestinal inflammation was also supported. We found that *B. animalis* and *L. reuteri* colonised SKG mice injected with curdlan developed significantly higher small intestine histopathology scores compared to naïve *B. animalis* and *L. reuteri*-associated SKG mice (figure 4.11A, B). Furthermore, we found that curdlan-injected *L. citreum* and *P. distasonis*-associated SKG mice trended towards increased small

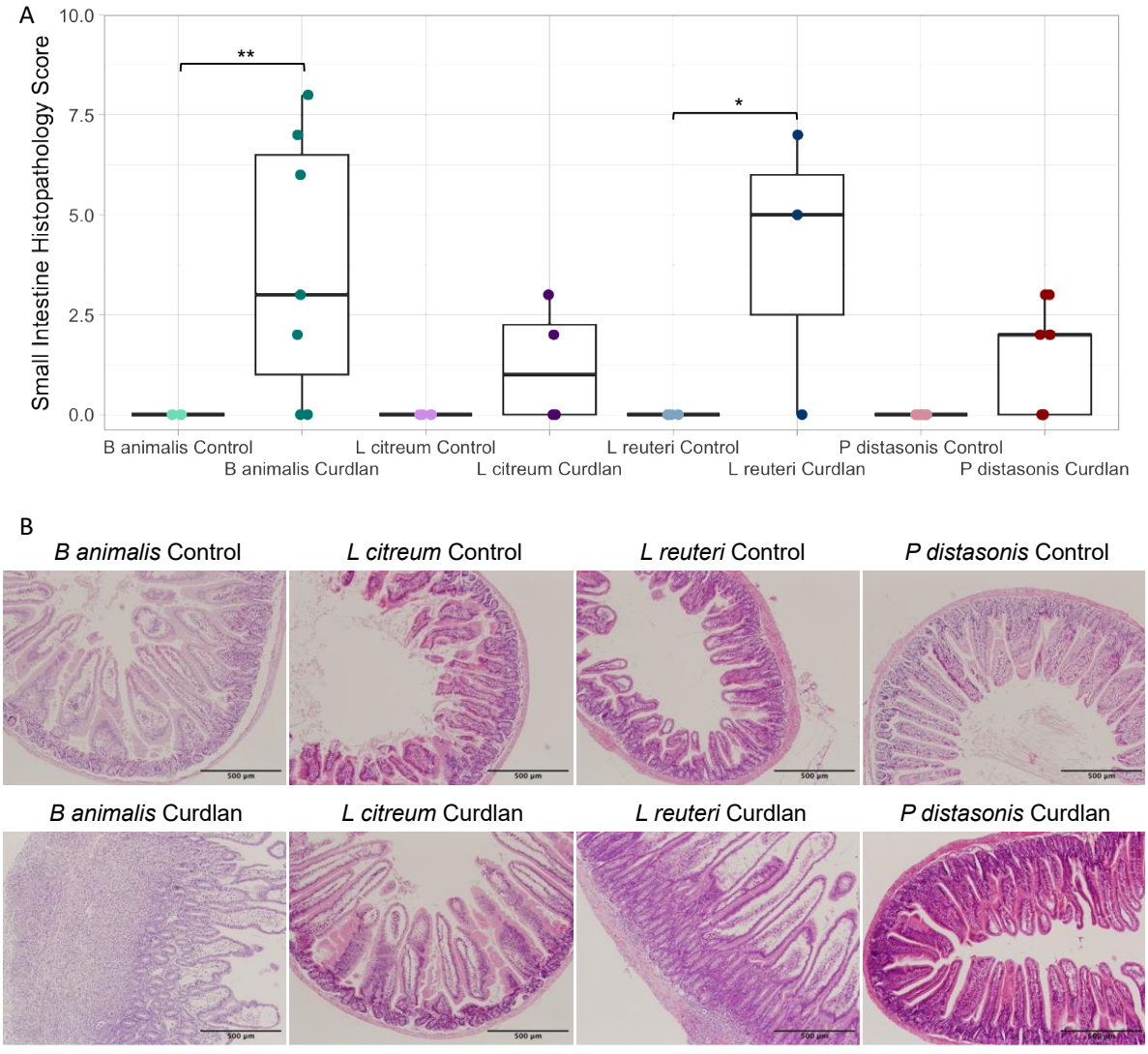


Figure 4.11 Monocolonisation of intestinal microbiota supports intestinal inflammation in SKG mice. Small intestine tissue was obtained from curdlan-injected and naïve monocolonised SKG mice, and subsequently sectioned and stained with H&E. A) Small intestine histopathology scoring for individually monocolonised SKG mice injected with curdlan compared to naïve monocolonised SKG mice. B) Representative microscopy images of H&E-stained small intestine tissue obtained from curdlan-injected and naïve monocolonised SKG mice. **p<0.01, *p<0.05. One-way ANOVA with Tukey's post-hoc testing. Boxplots denote median + interquartile range and individual data points are shown. Data obtained from one experiment.

intestine histopathology compared to naïve *L. citreum* and *P. distasonis*-associated SKG mice. This therefore indicates that each bacterium of interest permitted the development of paw inflammation, and further experiments are required to draw conclusions about their potential to drive intestinal inflammation.

4.3.9 *B. animalis* drives paw RORγt responses

After determining that each of our monocolonised bacteria of interest could permit the development of arthritis and intestinal inflammation in SKG mice, we sought to characterise the T cell responses in the paw of curdlan-injected and naïve monocolonised SKG mice. We hypothesised that increased RORγt responses were associated with inflammation in the paw, and that each of our monocolonised bacteria would recapitulate the T cell responses observed in curdlan-injected SPF SKG mice. We stained the transcription factors RORγt and FoxP3 by flow cytometry on paw lymphocytes from monocolonised SKG mice injected and not injected with curdlan. Contrary to our initial hypothesis, we found that only *B. animalis* drove increased RORγt+ T helper cell frequencies after curdlan-injection when monocolonised in SKG mice (figure 4.12B). Furthermore, only *B. animalis* was able to drive increased paw RORγt+ T helper cell and paw FoxP3+ T helper cell frequencies and numbers after curdlan injection in monocolonised SKG mice (figure 4.12C, D). We did not observe any changes in paw FoxP3+ T helper cell frequencies between curdlan-injected and naïve mono-associated SKG mice (figure 4.12A). These data suggest that increased frequencies of RORγt+ T helper cells in the paw of SKG mice is not always coupled with inflammation, and other mechanisms may drive disease in the presence of different microbes.

4.3.10 *B. animalis* depletion by antibiotics to assess immune priming

Each bacterium of interest that we monocolonised drove joint and intestinal inflammation following injection with curdlan, so we aimed to delineate whether continual or early transient colonisation of microbiota is required to support disease development. To test this, we decided to utilise *Bifidobacterium animalis*, as it elicited the strongest disease and drove paw Th17 responses

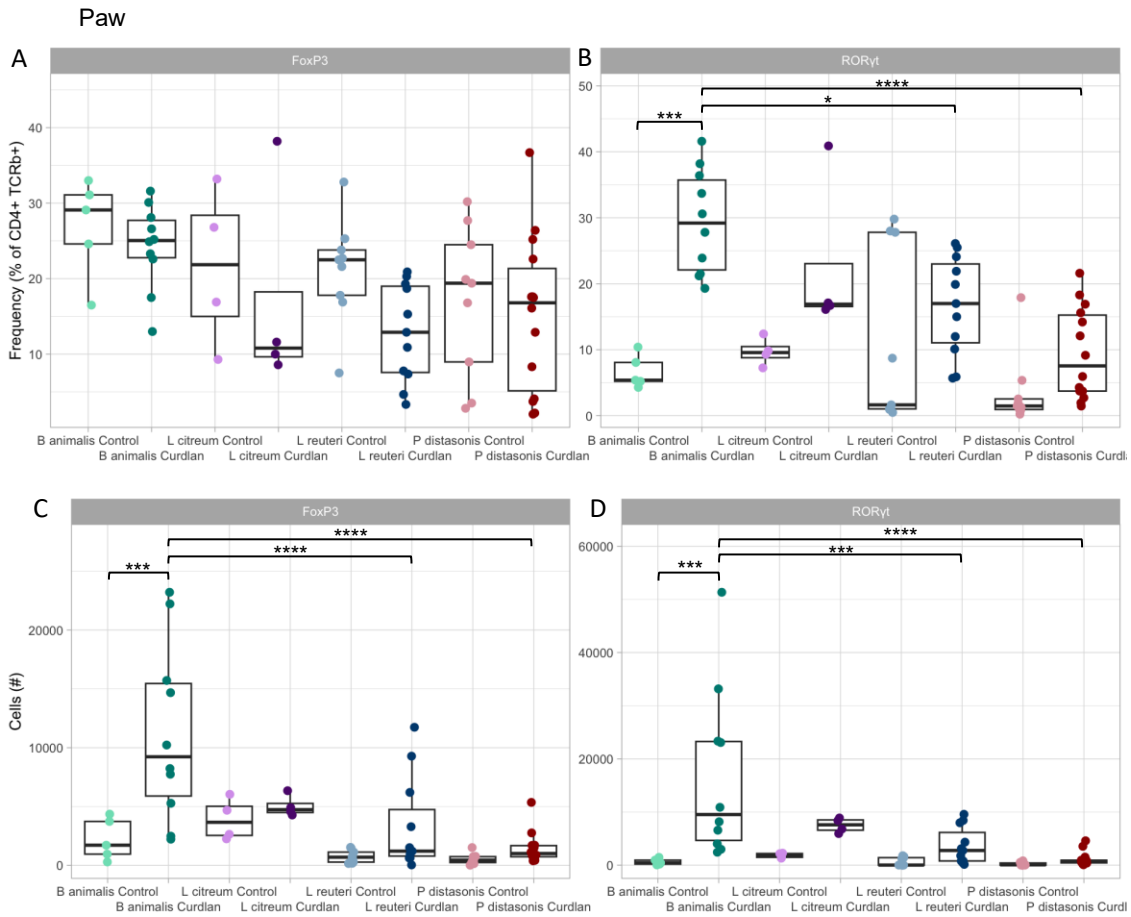


Figure 4.12 *Bifidobacterium animalis* drives paw RORγt responses when monocolonised in SKG mice. T_{reg} cells and Th17 cells were quantified by flow cytometric staining of the transcription factors FoxP3 and RORγt in the paws of curdlan-injected and naïve monocolonised SKG mice. Gating strategy is outlined in appendix figure 4.1. A) Frequencies of FoxP3+ T helper cells. B) Frequencies of FoxP3- RORγt+ T helper cells. C) Absolute numbers of FoxP3+ T helper cells. D) Absolute numbers of FoxP3- RORγt+ T helper cells. Frequencies are denoted as % of CD4+ TCRβ+ cells. Boxplots denote median + interquartile range and individual data points are shown. ****p<0.0001, ***p<0.001, *p<0.05. One-way ANOVA with Tukey's post-hoc testing was completed for all plots. Data obtained from 3 experiments.

after injection with curdlan. We colonised 3-week-old germ-free SKG mice with *B. animalis* for 3 weeks, and then cleared *B. animalis* from the intestine by treating mice with ampicillin and erythromycin for 3 weeks (figure 4.13A). We injected mice with curdlan 3 weeks into their antibiotic treatment and kept them on antibiotics to ensure no recolonisation of *B. animalis* whilst assessing their arthritis weekly (figure 4.13A). To ensure antibiotic treatment was not contributing to disease pathology, we treated germ-free mice with antibiotics and assessed their arthritis weekly (figure 4.13B).

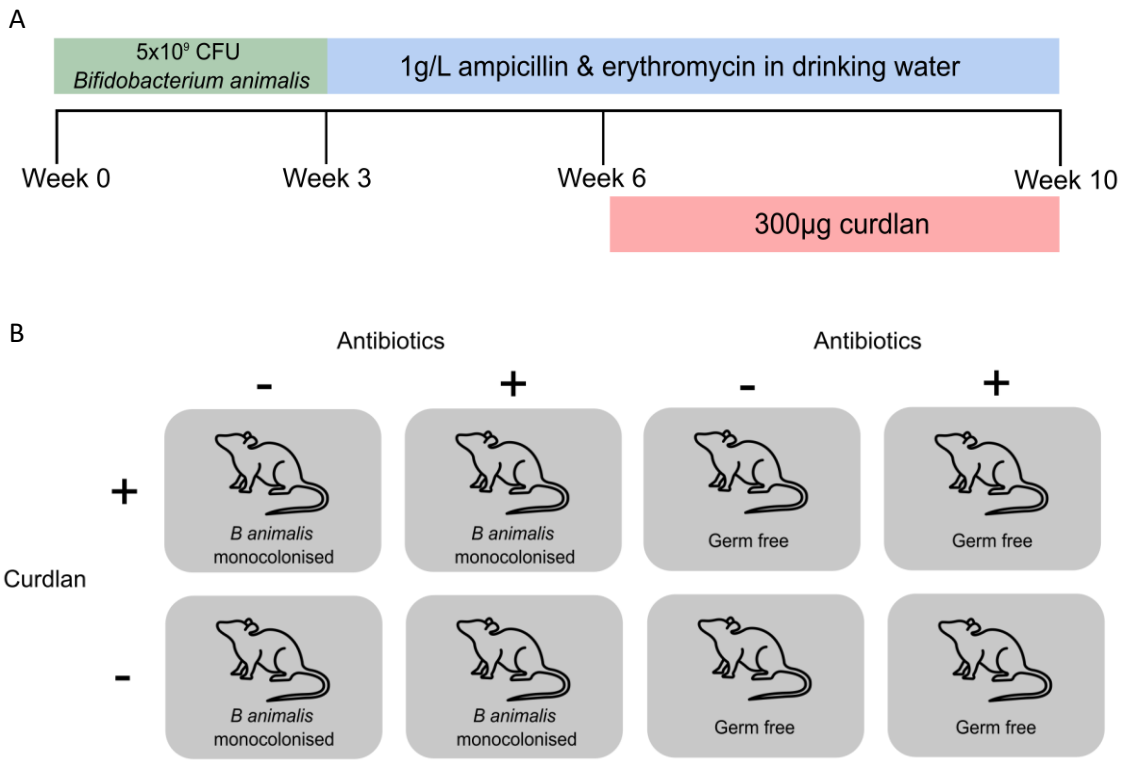


Figure 4.13 *Bifidobacterium animalis* depletion by antibiotics to assess immune priming. *B. animalis*-associated SKG mice were treated with 1g/L ampicillin and 1g/L erythromycin in the drinking water to clear *B. animalis* colonisation prior to injecting mice with curdlan to induce disease. A) Experimental outline of *B. animalis*-SKG antibiotic treatment. B) Experimental groups.

4.3.11 Antibiotic treatment successfully clears *B animalis* from SKG mice

To ensure ampicillin and erythromycin successfully cleared *B. animalis* from SKG mice, we took weekly stool samples from mice and completed strain-specific *B. animalis* qPCR. We confirmed that 3 weeks post-treatment with antibiotics (6 weeks post-bacterial colonisation with *B. animalis*), *B. animalis* is no longer present in the stool of SKG mice (figure 4.14A). To ensure that *B. animalis* is not colonising the intestinal tissue of SKG mice after antibiotic treatment we performed fluorescent in-situ hybridisation (FISH) utilising a pan-bacteria probe on intestinal tissue obtained from *B. animalis* monocolonised mice treated and not treated with antibiotics. We found that *B. animalis* clearly colonises at the intestinal epithelial layer in monocolonised mice not treated with antibiotics and is no longer detectable in antibiotic treated mice (figure 4.14B). Therefore, antibiotic treatment of *B. animalis* monocolonised SKG mice successfully clears *B. animalis* from SKG mice and renders them suitable to test the role of immune priming in supporting the development of arthritis.

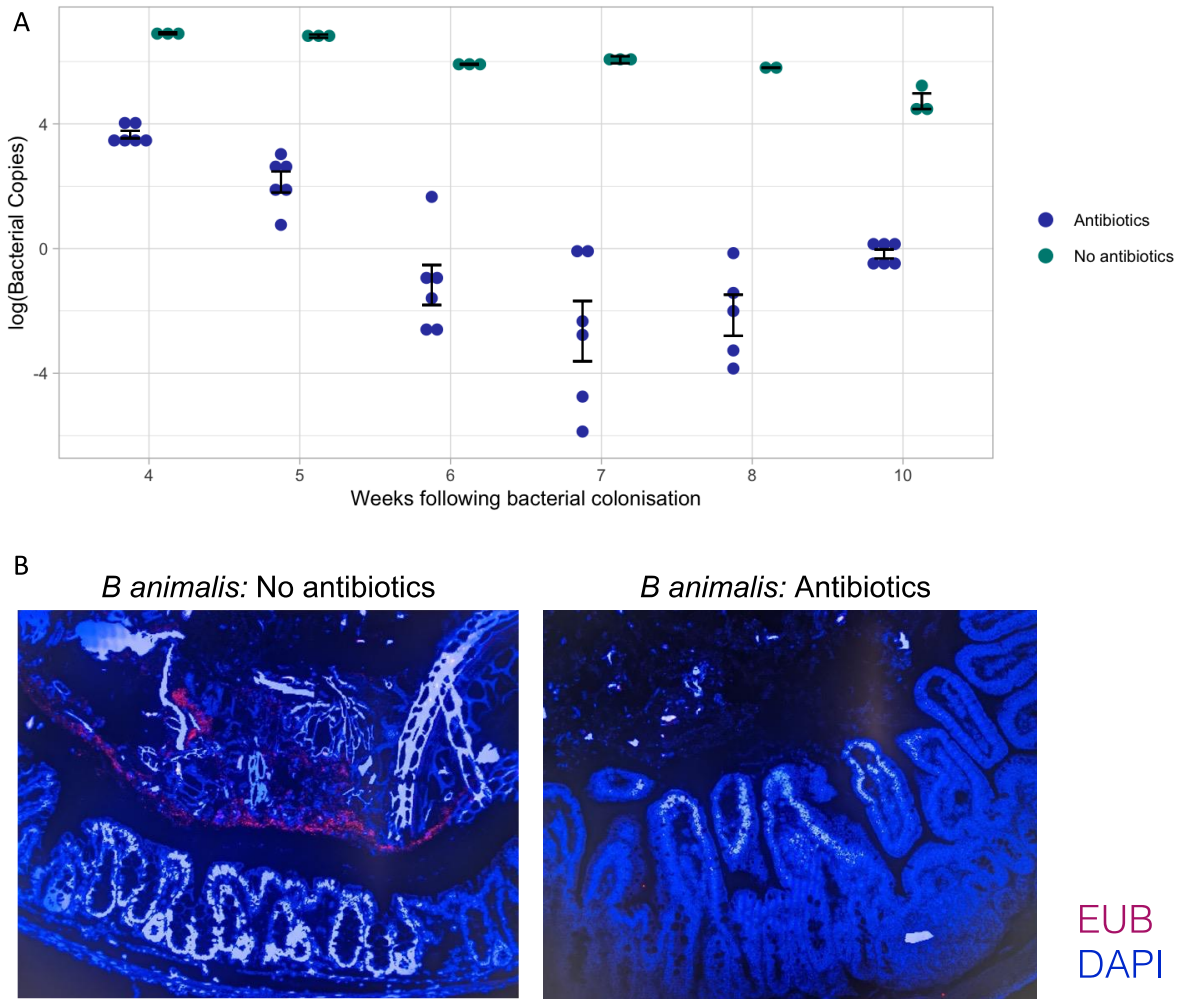


Figure 4.14 Antibiotic treatment successfully clears *Bifidobacterium animalis* from SKG mice. qPCR and fluorescent in-situ hybridisation (FISH) were performed on *B. animalis* monocolonised mice treated and not treated with antibiotics to determine its clearance from the intestine. A) Strain-specific qPCR was completed on stool samples obtained from *B. animalis* monocolonised mice treated and not treated with antibiotics to determine whether erythromycin and ampicillin were able to clear *B. animalis* from the intestine in SKG mice. Blue = antibiotic treated, green = not treated with antibiotics. B) FISH was performed on sections of small intestine and colon using a pan-bacterial probe (EUB) and DAPI to stain for *B. animalis* and any other bacteria present in the intestinal tissue of *B. animalis* monocolonised mice treated and not treated with antibiotics. Red = bacterial probe, blue = DAPI. Dot plot denotes individual data points and whiskers represent standard error of the mean.

4.3.12 Germ-free SKG mice previously monocolonised with *B. animalis* develop arthritis following induction with curdlan

After ensuring that *B. animalis* had been cleared from monocolonised SKG mice through antibiotic treatment, we administered curdlan and followed mice for 4 weeks post-injection. We found that *B. animalis* monocolonised SKG mice treated with antibiotics developed arthritis over 4 weeks post-injection with curdlan to similar severity as *B. animalis* monocolonised mice not treated with antibiotics (figure 4.15A). Furthermore, we assessed paw histopathology on H&E-stained paw tissue and found that curdlan-injected *B. animalis* monocolonised mice treated with antibiotics

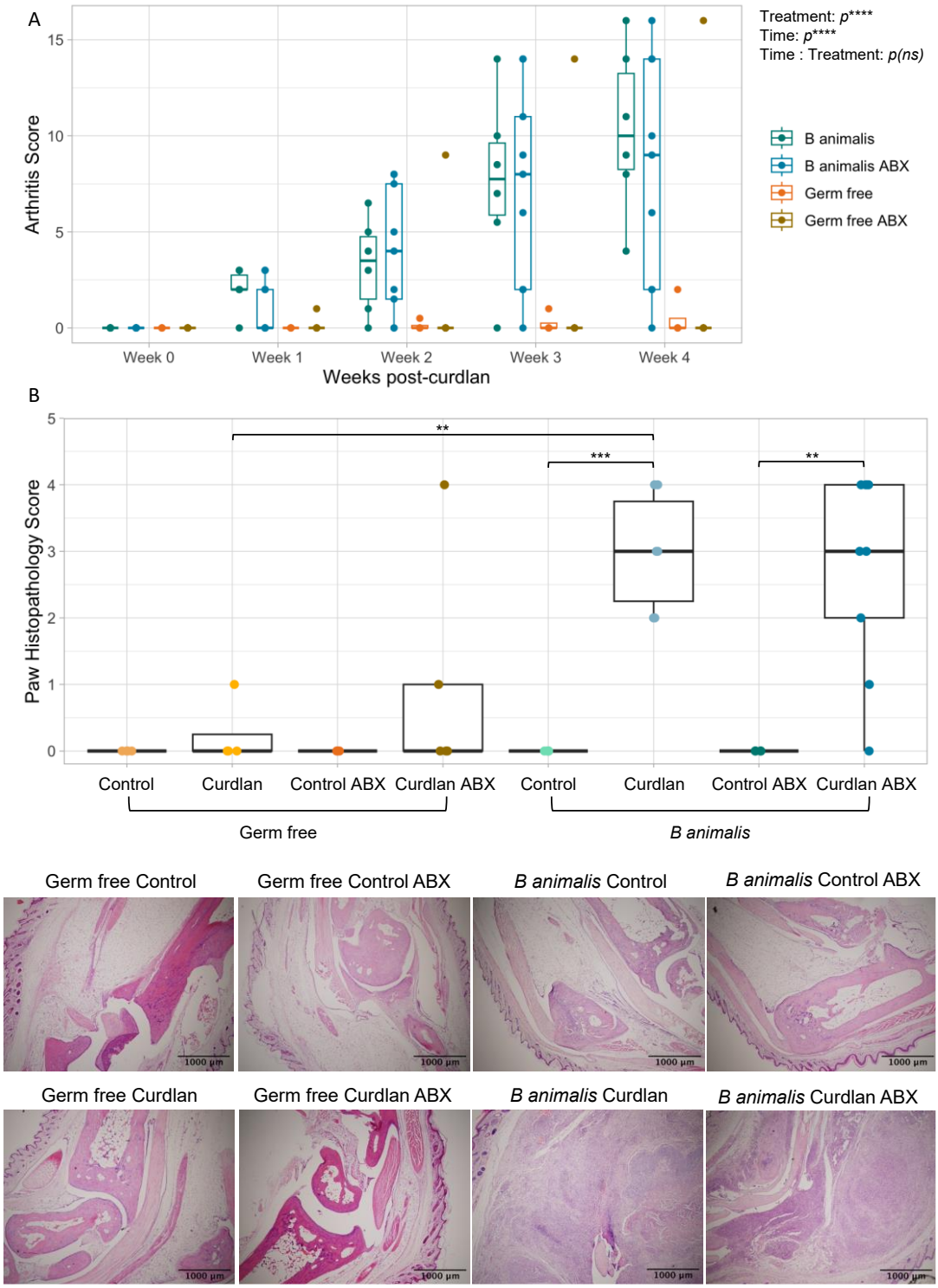


Figure 4.15 Germ-free SKG mice previously monocolonised with *B. animalis* develop arthritis following induction with curdlan. *B. animalis* monocolonised mice were treated with antibiotics and subsequently injected with curdlan. Mice were culled 4 weeks post-injection. ABX = antibiotics. A) Arthritis scores in curdlan-injected germ-free SKG mice treated and not treated with antibiotics and curdlan-injected *B. animalis* monocolonised SKG mice treated and not treated with antibiotics. Turquoise = *B. animalis* monocolonised not treated with antibiotics, blue = *B. animalis* monocolonised treated with antibiotics, orange = germ-free not treated with antibiotics, yellow = germ-free treated with antibiotics. B) Paw histopathology scoring with representative microscopy images of H&E-stained paw tissue in naïve and curdlan-injected mice from the following groups: germ-free treated and not treated with antibiotics, and *B. animalis* monocolonised treated and not treated with antibiotics. ***p<0.001, **p<0.01. A) Two-way repeated measures ANOVA, factors = antibiotic treatment/microbiome status and weeks post-infection, significance values for effect of each variable and the interaction of the two variables are indicated on the plot. B) One-way ANOVA with Tukey's post-hoc testing. Boxplots denote median + interquartile range and individual data points are shown. Data obtained from two experiments.

developed significantly higher histopathology scores than naïve controls, replicating those seen in curdlan-injected *B. animalis* monocolonised mice (figure 4.15B). We also found that germ-free SKG mice treated with antibiotics did not develop paw histopathology following treatment with antibiotics, demonstrating that antibiotic treatment does not contribute to disease pathology in SKG mice. These data suggest that transient exposure to *B. animalis* and subsequent removal from the intestine is sufficient to support disease in SKG mice. This suggests a potential priming mechanism whereby *B. animalis* is helping to educate the previously underdeveloped germ-free immune system to respond to curdlan providing an environment permissive for inflammation.

4.3.13 Germ-free SKG mice previously monocolonised with *B. animalis* develop intestinal inflammation following induction with curdlan

As previously monocolonised SKG mice developed joint inflammation after curdlan injection, we wanted to determine whether intestinal inflammation was also supported. We stained small intestine sections from our experimental groups with H&E and assessed their small intestine histopathology scores. We found that there was a trend of increase in small intestine histopathology scores in curdlan-injected *B. animalis* monocolonised mice treated with antibiotics compared to naïve controls (figure 4.16A, B). This may be because live *B. animalis* contributes towards intestinal inflammation, and its removal reduces the likelihood of intestinal inflammation occurring.

4.3.14 Administration of heat-killed *B. animalis* is sufficient to support arthritis in SKG mice

We have demonstrated that exposure to *B. animalis* and subsequent removal of the bacterium prior to induction of disease with curdlan is sufficient to permit the development of arthritis in SKG mice. This suggests a transient interaction of the bacteria with the host-immune system shapes the immune for subsequent arthritogenic response to curdlan. We hypothesised that this could be due to *B. animalis* metabolic products that are influencing the host immune responses, or due to a component present on the bacterium itself which is interacting with the immune system. To

investigate this, we decided to heat-kill *B. animalis* and subsequently administered this by oral gavage to germ-free SKG mice a single time and waited 3 weeks before injecting them with curdlan and following them for 4 weeks post-injection (figure 4.17A). We confirmed that no live *B. animalis* was present in the heat-killed inoculum by plating it on anaerobic blood agar.

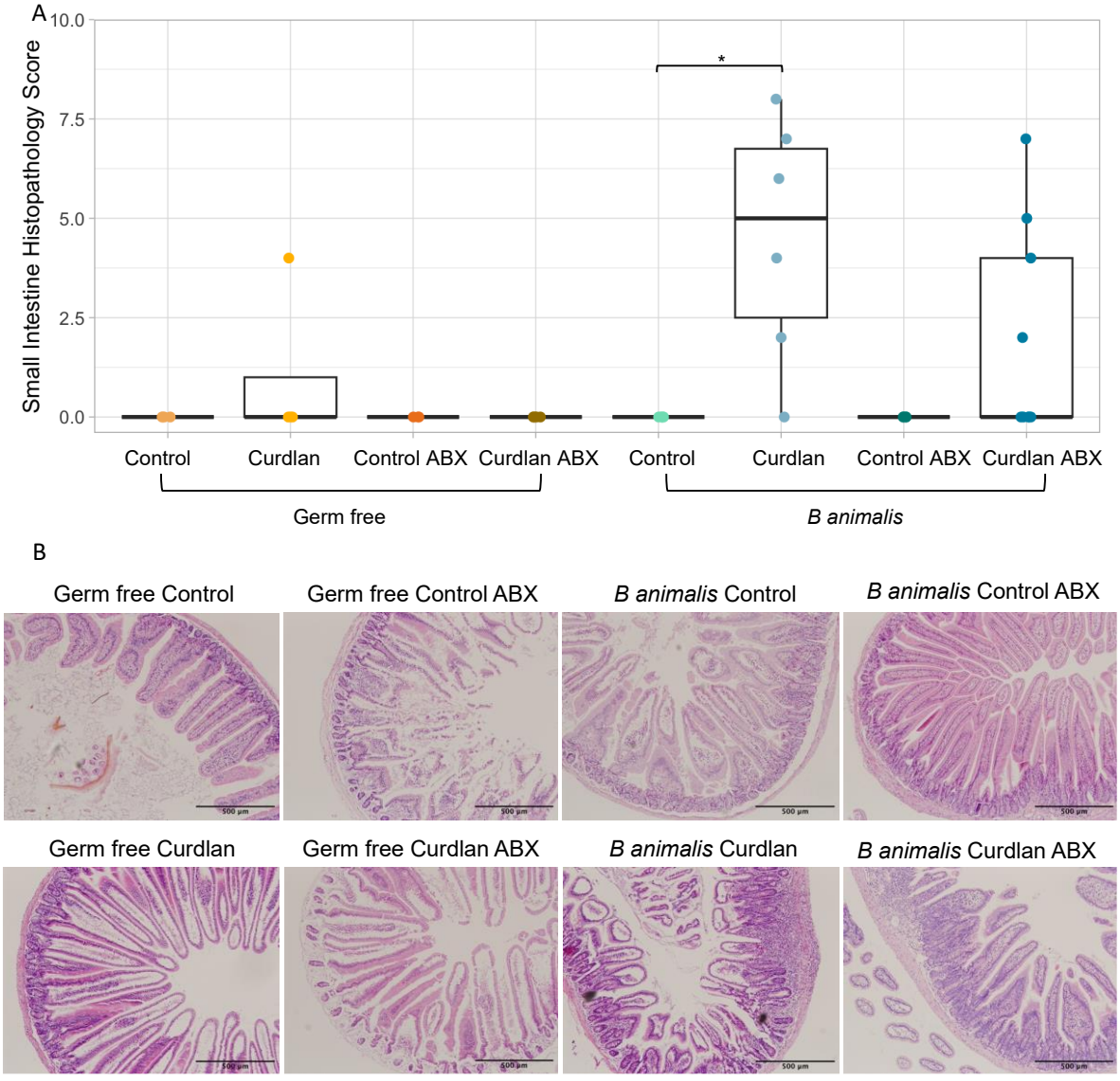


Figure 4.16 Germ-free SKG mice previously monocolonised with *B. animalis* develop intestinal inflammation following induction with curdlan. Small intestine tissue was obtained from the following groups: germ-free treated and not treated with antibiotics, and *B. animalis* monocolonised treated and not treated with antibiotics, and subsequently sectioned and stained with H&E. A) Small intestine histopathology scoring for each experimental group. B) Representative microscopy images of H&E-stained small intestine tissue obtained from each experimental group. *p<0.05. One-way ANOVA with Tukey's post-hoc testing. Boxplots denote median + interquartile range and individual data points are shown. Data obtained from two experiments.

We found that heat-killed *B. animalis* administration followed by curdlan injection was able to drive arthritis in SKG mice (figure 4.17B). We then assessed paw histopathology on H&E-stained paw tissue and found that curdlan-injected mice administered heat-killed *B. animalis* developed paw histopathology to a similar severity as those administered live *B. animalis* (figure 4.18A, B). Taken together, these data demonstrate that exposure to bacterial antigen followed by a 3-week washout period is sufficient to create an arthritogenic environment. This indicates that the host-microbiota interaction driving the development of the host immune system to induce joint inflammation involves a bacterial component present in heat-killed *B. animalis*.

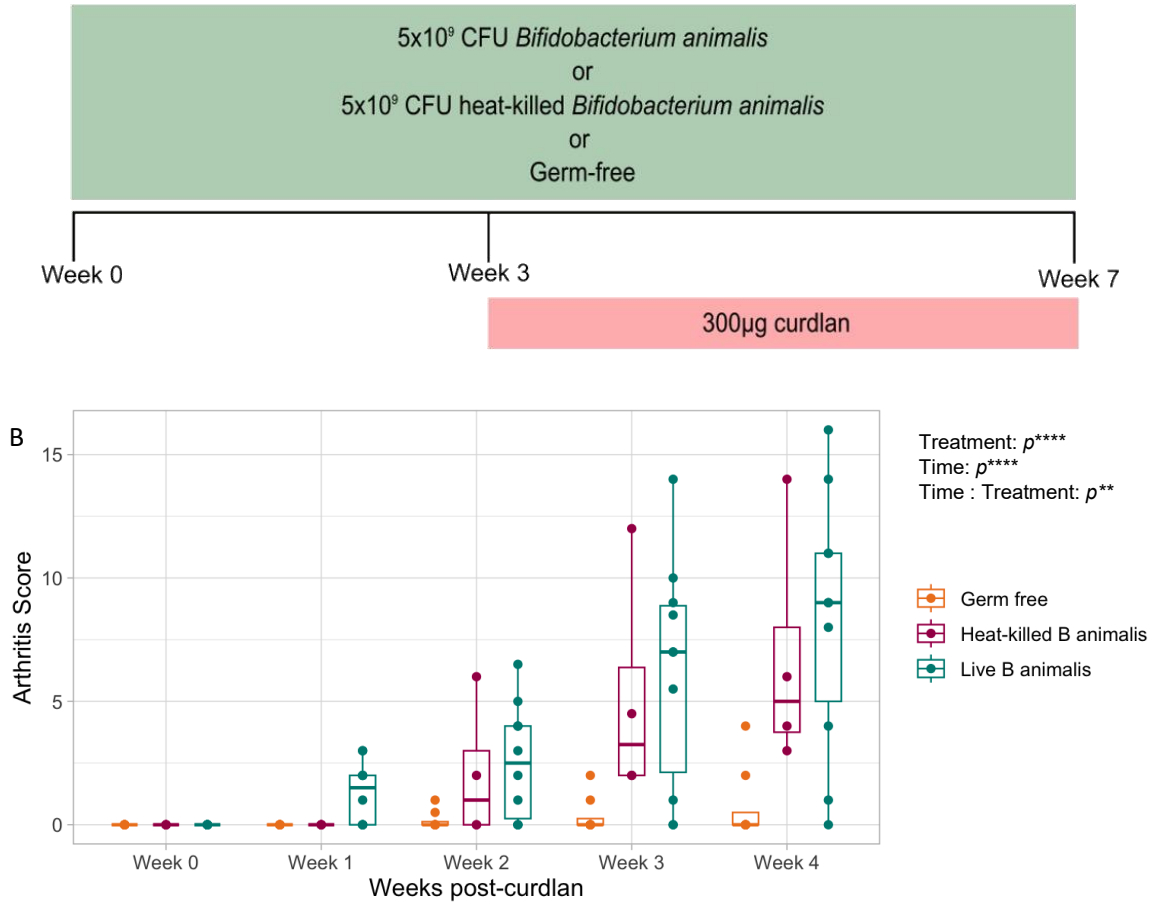


Figure 4.17 Administration of heat-killed *B. animalis* is sufficient to support arthritis in SKG mice. Heat-killed *Bifidobacterium animalis* was administered *via* oral gavage to germ-free SKG mice, and 3 weeks later they were injected with curdlan. Live *Bifidobacterium animalis* was administered to another group of germ-free mice as a control group. A) Experimental outline of heat-killed *B. animalis* experiment. B) Arthritis scores for curdlan-injected germ-free, heat-killed *B. animalis*-administered, and live *B. animalis*-administered SKG mice. Orange = germ-free, maroon = heat-killed *B. animalis*, turquoise = live *B. animalis*. ****p<0.0001, **p<0.01. Two-way repeated measures ANOVA, factors = microbiome status and weeks post-injection, significance values for effect of each variable and the interaction of the two variables are indicated on the plot. Boxplots denote median + interquartile range and individual data points are shown. Data obtained from one experiment.

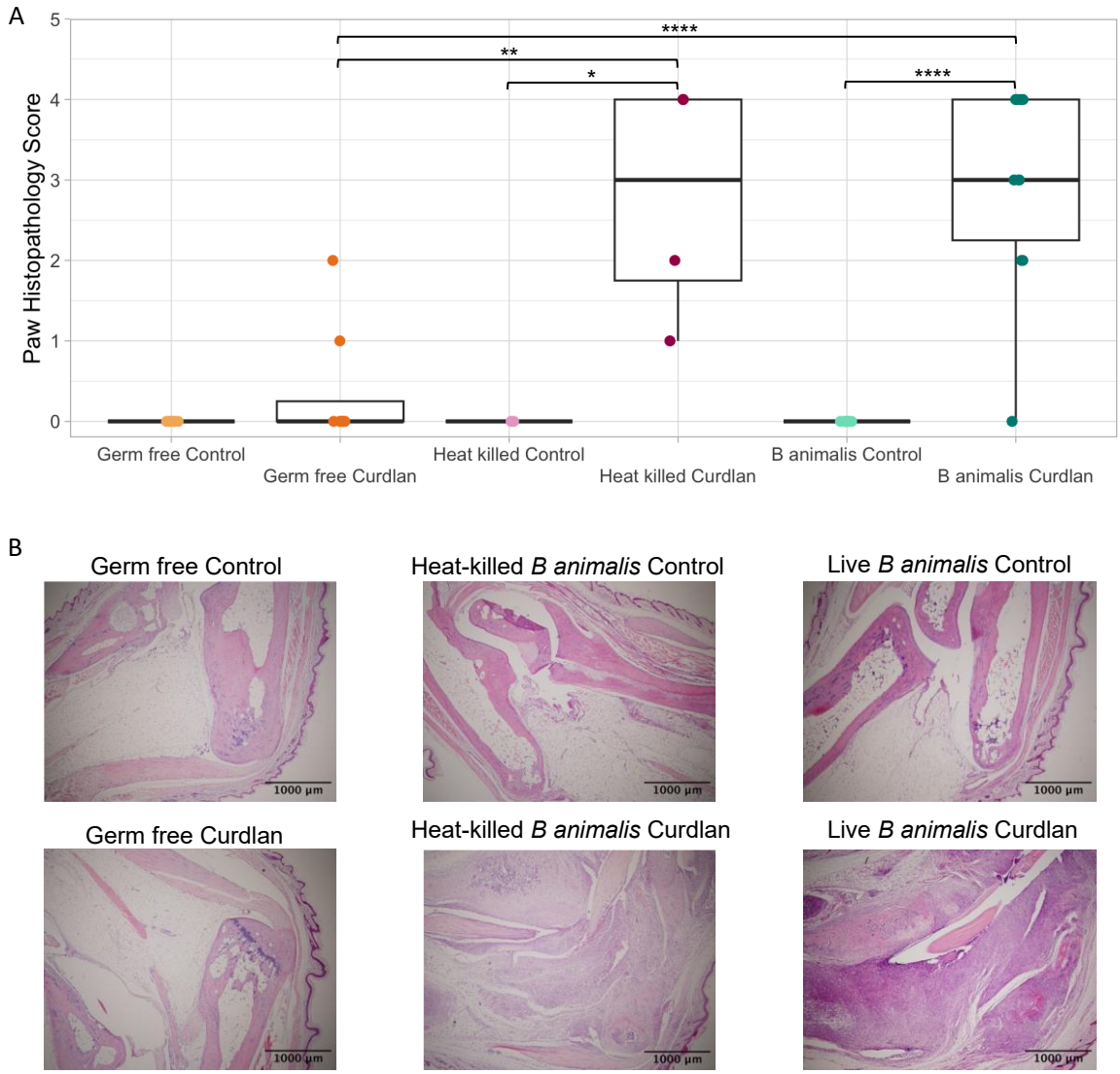


Figure 4.18 Administration of heat-killed *B. animalis* is sufficient to drive paw histopathology in SKG mice. SKG mice were administered heat-killed *B. animalis* by oral gavage and following a 3-week washout period, were injected with curdlan, and culled 4 weeks post-injection. A) Paw histopathology scoring in naïve and curdlan-injected mice from germ-free, heat-killed *B. animalis*-administered, and live *B. animalis*-administered SKG mice. B) Representative microscopy images of H&E-stained paw tissue in naïve and curdlan-injected mice from germ-free, heat-killed *B. animalis*-administered, and live *B. animalis*-administered SKG mice. ****p<0.0001, **p<0.01, *p<0.05. One-way ANOVA with Tukey's post-hoc testing. Boxplots denote median + interquartile range and individual data points are shown. Data obtained from one experiment.

4.3.15 Administration of heat-killed *B. animalis* is sufficient to support intestinal inflammation in SKG mice

We sought to determine whether heat-killed *B. animalis* was able to support the development of intestinal inflammation following curdlan-injection in germ-free SKG mice. We therefore performed H&E staining on small intestine tissue obtained from experimental groups and scored their histopathology. We found that mice administered heat-killed *B. animalis* developed similar levels of small intestinal histopathology compared to mice administered live *B. animalis* following

injection with curdlan (figure 4.19A, B). We observed a trend of increasing histopathology when comparing curdlan-injected and curdlan-naïve mice administered heat-killed *B. animalis* (figure 4.19A, B). This was likely not statistically significant due to the small experimental group numbers, and the experiment must be repeated. Overall, these data demonstrate that the exposure of the host to heat-killed *B. animalis* is sufficient to permit the development of both intestinal and joint inflammation in SKG mice.

4.3.16 Heat-killed *B. animalis* drives paw RORγt responses in SKG mice

We have demonstrated that early life exposure to heat-killed *B. animalis* is sufficient to permit arthritis and small intestinal inflammation in SKG mice, and so we sought to determine whether T cell responses in the paw were similarly skewed as they are in response to live *B. animalis*. We therefore stained for RORγt and FoxP3 by flow cytometry on paw lymphocytes obtained from our experimental groups. We observed that frequencies and absolute numbers of paw RORγt+ T helper cells were significantly elevated in curdlan-injected heat-killed *B. animalis* administered SKG mice compared to naïve controls, to a similar level as curdlan-injected live *B. animalis* administered SKG mice (figure 4.20B, D). By contrast, paw FoxP3+ T helper cell frequencies were significantly reduced in *B. animalis* controls compared to heat-killed *B. animalis* controls and germ-free controls (figure 4.20A). Upon injection with curdlan, frequencies of FoxP3+ T helper cells in the paw of heat-killed *B. animalis* and germ-free mice were reduced to the levels of live *B. animalis* mice. This indicates that the presence of live *B. animalis*, but not the exposure to heat-killed *B. animalis* suppresses T regulatory cell frequencies. Taken together, these data suggest that heat-killed *B. animalis* can elicit Th17 responses similar to those observed in monocolonised mice, but that live bacteria are required to stimulate T regulatory responses in naïve mice.

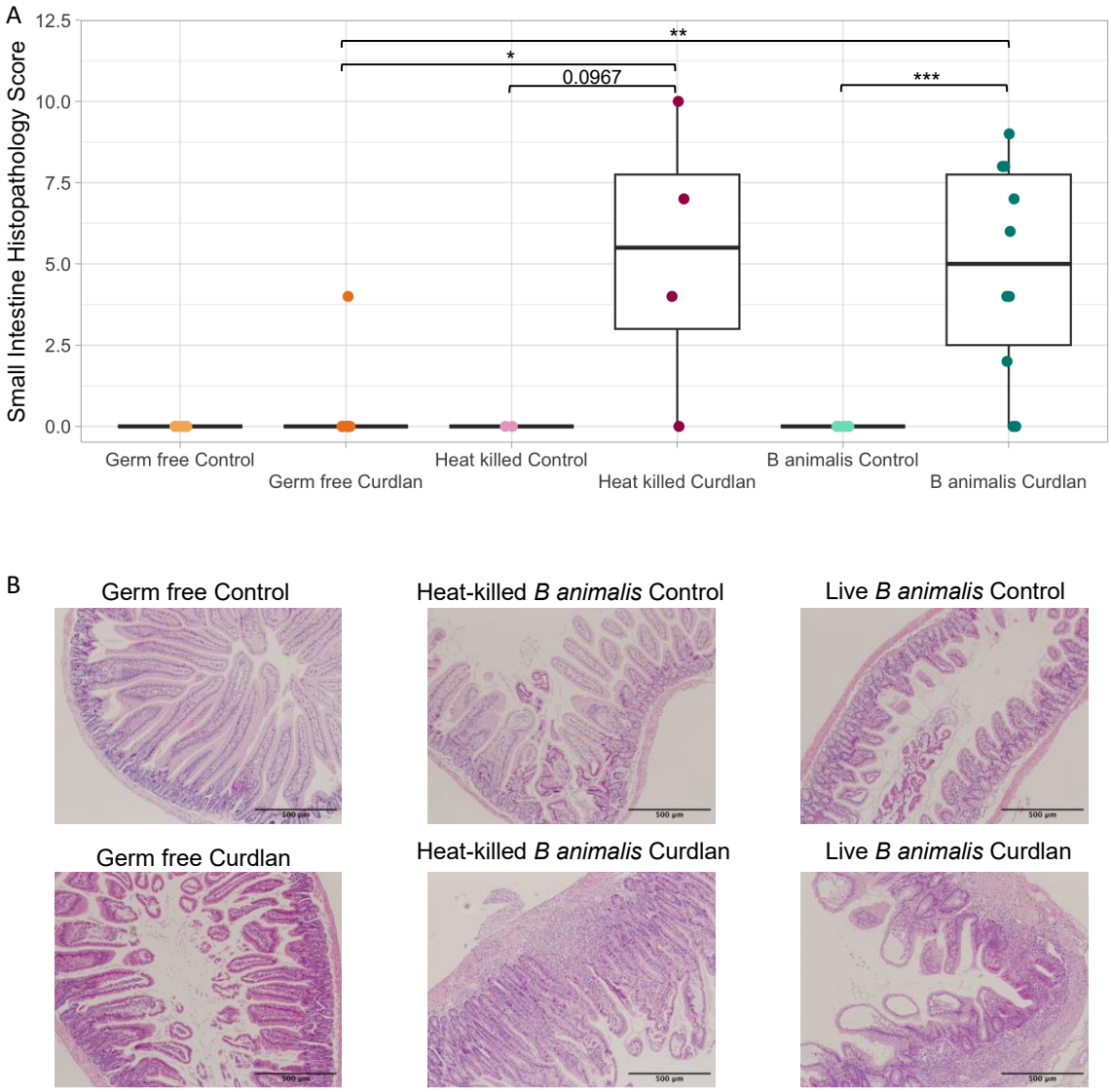


Figure 4.19 Administration of heat-killed *B. animalis* is sufficient to support intestinal inflammation in SKG mice. Small intestine tissue was obtained from curdlan-injected and curdlan-naïve germ-free, heat-killed *B. animalis*-administered, and live *B. animalis*-administered SKG mice, and subsequently sectioned and stained with H&E for small intestine histopathology scoring. A) Small intestine histopathology scoring of curdlan-injected and curdlan-naïve germ-free, heat-killed *B. animalis*-administered, and live *B. animalis*-administered SKG mice. B) Representative microscopy images of H&E-stained small intestine tissue from curdlan-injected and curdlan-naïve germ-free, heat-killed *B. animalis*-administered, and live *B. animalis*-administered SKG mice. ***p<0.001, **p<0.01, *p<0.05. One-way ANOVA with Tukey's post-hoc testing. Boxplots denote median + interquartile range and individual data points are shown. Data obtained from one experiment.

4.3.17 CD206- macrophages expand in the joint during inflammation

We wanted to characterise the innate immune cell component in our mice to determine whether they are associated with disease following administration with heat-killed *B. animalis*. We completed preliminary flow cytometry staining of myeloid cell subsets on lymphocytes isolated from the spleen and paw to explore the subsets that may be involved in potentiating inflammation.

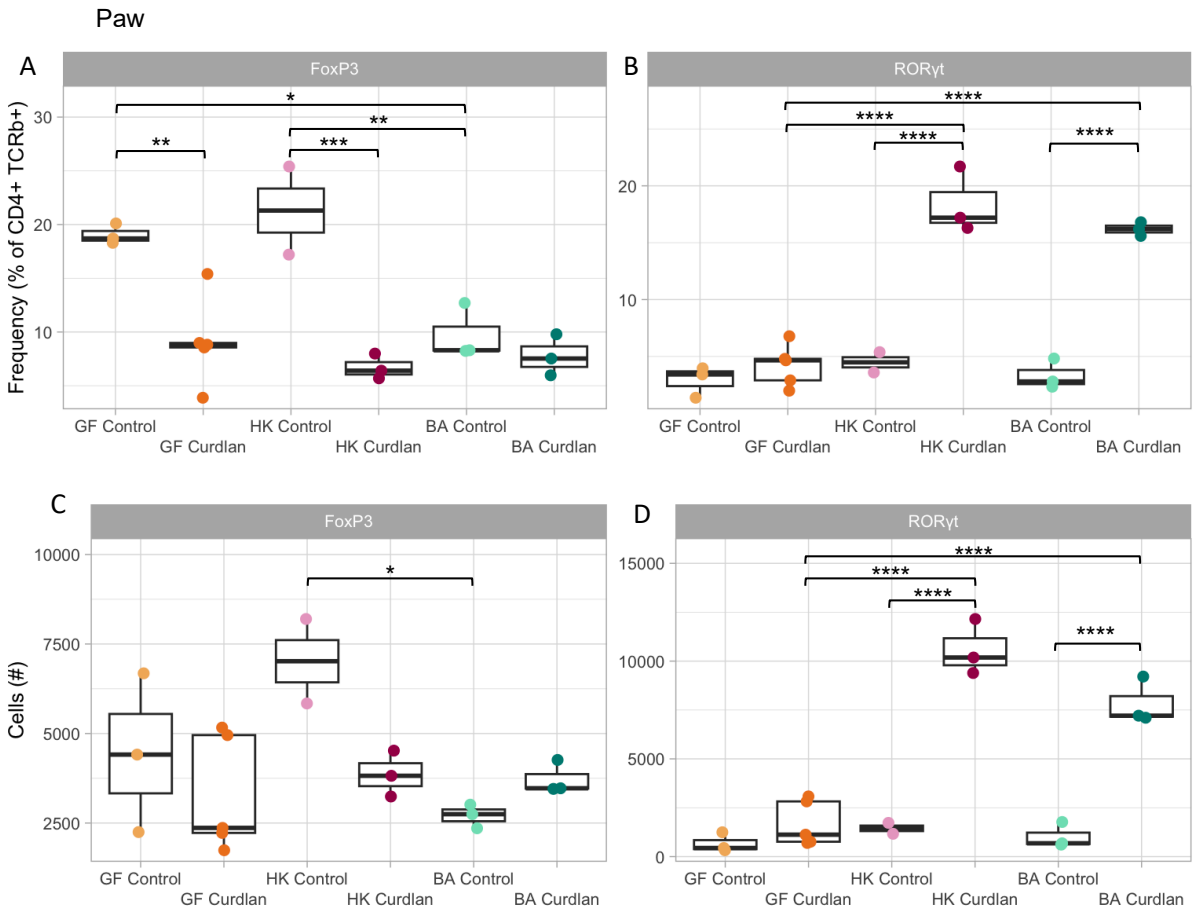


Figure 4.20 Heat-killed *B. animalis* drives paw RORγt responses in SKG mice. T_{reg} cells and Th17 cells were quantified by flow cytometric staining of the transcription factors FoxP3 and RORγt in the paws of curdlan-injected and naïve germ-free, heat-killed *B. animalis*-administered, and live *B. animalis*-administered SKG mice. Gating strategy is outlined in appendix figure 4.1. A) Frequencies of FoxP3+ T helper cells. B) Frequencies of FoxP3- RORγt+ T helper cells. C) Absolute numbers of FoxP3+ T helper cells. D) Absolute numbers of FoxP3- RORγt+ T helper cells. Frequencies are denoted as % of CD4+ TCRβ+ cells. Boxplots denote median + interquartile range and individual data points are shown. ****p<0.0001, ***p<0.001, **p<0.01, *p<0.05. One-way ANOVA with Tukey's post-hoc testing was completed for all plots. Data obtained from one experiment.

We observed interesting trends amongst the data, including an increase in splenic CD103+ DC frequencies following curdlan injection in *B. animalis* colonised SKG mice, but not heat-killed *B. animalis*-administered mice or germ-free mice (figure 4.21A). CD103+ DCs are in the small intestine and ensure tolerance to commensal microbiota, as well as driving T cells to express the molecule α4β7 which drives T cell migration to the gut[256]. We observed that We observed that paw neutrophils are expanded in *B. animalis* colonised and heat-killed *B. animalis*-administered mice following curdlan injection (figure 4.21J). This is in line with the increased level of joint inflammation observed in these mice and suggests that neutrophil infiltration into the joint is associated with arthritis. Splenic neutrophils were expanded in *B. animalis* colonised mice and heat-killed *B. animalis*

colonised mice compared to germ-free mice (figure 4.21E). This indicates that the exposure to *B. animalis* components drive an accumulation of splenic neutrophils, which are unchanged in response to curdlan. Finally, we stained for the presence of CD206 on macrophages, as it differentiates macrophages that have been shown to play different roles in the pathology of inflammatory diseases[257,258]. We observed that CD206- macrophages are expanded in the paw whilst CD206+ macrophages are expanded in the spleen of *B. animalis* colonised and heat-killed *B. animalis* mice following injection with curdlan (figure 4.21C, G).

4.3.18 *B. animalis* colonisation does not upregulate the expression of PRRs in the small intestine of SKG mice

We hypothesised that components present in heat-killed *B. animalis* were able to interact with host myeloid cells *via* PRRs and may upregulate their expression of receptors to curdlan, thereby allowing them to respond to curdlan following injection and initiate arthritis. Curdlan acts *via* the dectin-1 receptor (*Clec7a*) and TLR4[259]. We therefore sought to measure the expression of these molecules and other PRRs in small intestine tissue obtained from germ-free, *B. animalis* monocolonised, and SPF mice using qPCR. We found that expression of *Clec7a*, *Tlr2*, and *Tlr4* were all significantly higher in the small intestinal tissue of SPF mice compared to that obtained from *B. animalis* and germ-free mice (figure 4.22 A, C, D). This is likely due to the high microbial density and complexity present in the SPF microbiome, thereby driving high levels of expression of PRRs. It could therefore be concluded that the mechanism by which *B. animalis* interacts with the host immune system to support the development of arthritis does not involve the upregulation of PRRs. However, it may be that PRRs are upregulated on specific myeloid subsets, and further qPCR or RNA sequencing on sorted myeloid cells should be completed to draw definitive conclusions.

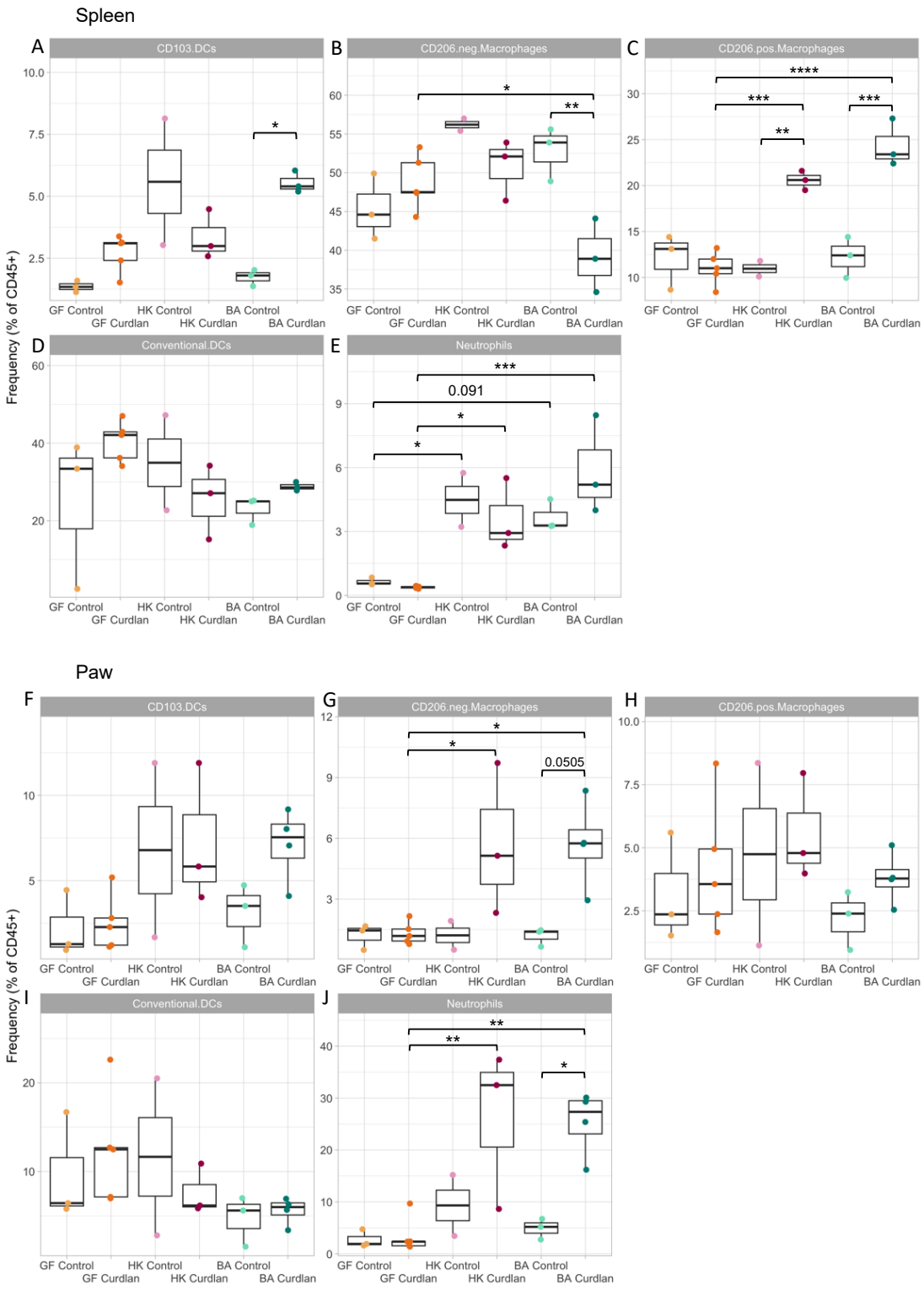


Figure 4.21 CD206- macrophages expand in the joint during inflammation. Lymphocytes isolated from spleens and paws obtained from curdlan-injected and curdlan-naïve germ-free, heat-killed *B. animalis*-administered, and live *B. animalis*-administered SKG mice were stained by flow cytometry for myeloid subset markers. Gating strategy is outlined in appendix figure 4.4. A) Frequencies of splenic CD103+ dendritic cells. B) Frequencies of splenic CD206- macrophages. C) Frequencies of splenic CD206+ macrophages. D) Frequencies of splenic conventional DCs. E) Frequencies of splenic neutrophils. F) Frequencies of paw CD103+ dendritic cells. G) Frequencies of paw CD206- macrophages. H) Frequencies of paw CD206+ macrophages. I) Frequencies of paw conventional DCs. J) Frequencies of paw neutrophils. Frequencies are denoted as % of CD45+ cells. Boxplots denote median + interquartile range and individual data points are shown. ****p<0.0001, ***p<0.001, **p<0.01, *p<0.05. One-way ANOVA with Tukey's post-hoc testing was completed for all plots. Data obtained from one experiment.

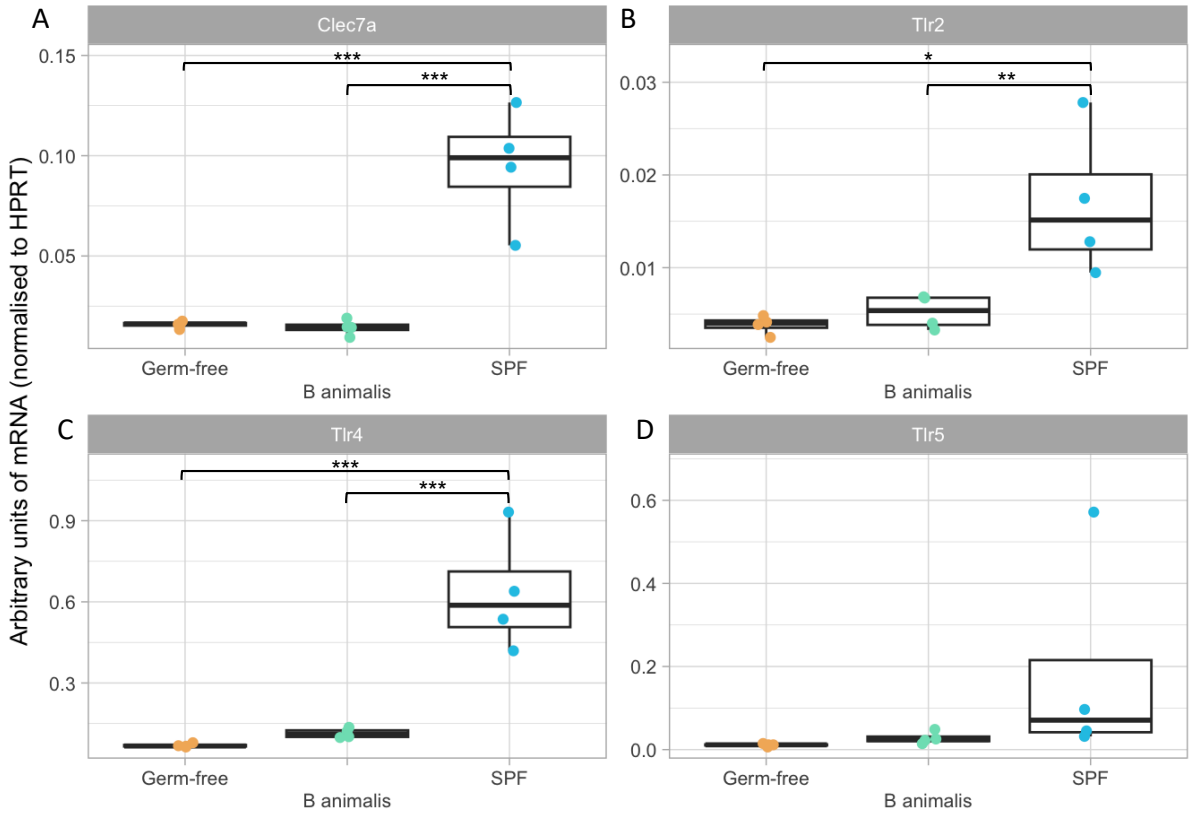


Figure 4.22 *Bifidobacterium animalis* colonisation does not upregulate the expression of PRRs in the small intestine of SKG mice. Small intestinal tissue was obtained from naïve germ-free, *B. animalis* monocolonised, and SPF mice, and qPCR to quantify several PRRs was completed. A) Expression of *Clec7a*. B) Expression of *Tlr2*. C) Expression of *Tlr4*. D) Expression of *Tlr5*. Expression is denoted as arbitrary units of mRNA, normalised to the house-keeping gene *Hprt*. ***p<0.001, **p<0.01, *p<0.05. Boxplots denote median + interquartile range and individual data points are shown. Data obtained from one experiment.

4.4 Discussion

In this chapter we have replicated previous studies demonstrating a crucial role for both host genetic susceptibility and the intestinal microbiota in supporting the development of arthritis in SKG mice. In contrast to expectation, we found that all bacteria tested permitted development of inflammation in monocolonised mice. These results suggest that a shared mechanism such as immune education or training of the underdeveloped germ-free immune system was supporting inflammation. Exposure of the host immune system to both live *B. animalis* and heat-killed *B. animalis* followed by either antibiotic treatment or a washout period, respectively, permitted the development of arthritis. This suggests that a bacterial component present in heat-killed *B. animalis,* rather than a metabolite produced by the bacterium, can program the host immune system to allow for the development of arthritis. Overall, we hypothesise a mechanism whereby a component of *B.*

animalis primes an immune cell population to respond to curdlan and induce the differentiation of pathogenic T cells that are self-reactive, thereby driving destructive inflammation in the joint (figure 4.23).

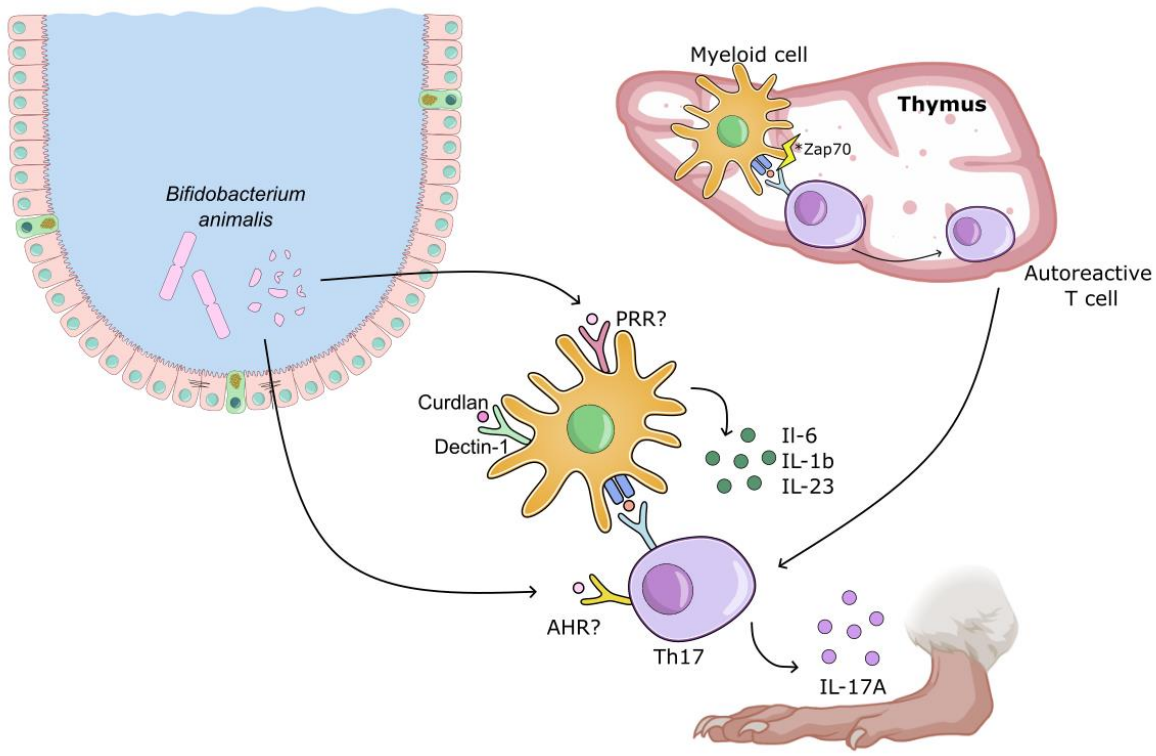


Figure 4.23 Proposed mechanism for *Bifidobacterium animalis* supporting the development of arthritis in SKG mice. *Bifidobacterium animalis* components educate the host immune system, potentially through the priming of myeloid or T cells through PRRs or AhR. Upon injection, curdlan activates the dectin-1 receptor and drives the production of proinflammatory cytokines. Genetic mutation in *Zap70* allows for the escape of T cells from negative selection, which upon presentation with self-antigen and exposure to proinflammatory cytokines drives the differentiation into pathogenic Th17 cells. Th17 cells drive downstream joint disease.

4.4.1 The intestinal microbiome and genetic factors support arthritis

In this chapter we replicated previous studies to demonstrate that host genetics and the intestinal microbiome both play a crucial role in supporting the development of arthritis in a mouse model. SKG mice but not Balb/C mice injected with the fungal wall component, curdlan, were able to develop arthritis and small intestinal inflammation under SPF conditions. Notably, previous studies have demonstrated that Balb/C mice injected with curdlan develop low levels of arthritis compared to SKG mice[179]. This contrasts what we have observed in our SPF facility, whereas Balb/C mice injected with curdlan did not develop any level of arthritis or small intestinal inflammation. This may be explained firstly by the lack of isogenicity within lab mouse strains, as Balb/C mice from different

facilities display genetic variation[260]. This genetic variation may allow for differential immune responses to curdlan, thereby supporting a mild arthritic phenotype. Another explanation for these contrasting results may be that microbiome composition varies between SPF animal facilities and these differences in the microbiome may allow for the development of inflammation in some Balb/C mice but not others.

4.4.2 Induction of inflammation drives dysbiosis in the intestinal microbiome

We observed a clear shift in the composition of the intestinal microbiome upon induction of disease in SKG mice under both SPF and Oligo-MM^{12} conditions. The directionality of this microbiome shift is unknown. It may be that injection of curdlan elicits changes in the intestinal microbiome which subsequently drive the development of arthritis, or it may be that curdlan injection and the subsequent inflammation alter the intestinal environment, thereby shifting the composition of the intestinal microbiome. Upon statistical analysis, we found that *Weisella confusa* blooms following induction of arthritis in SPF mice. This is not a bacterium typically associated with SpA or inflammatory disease, and it may or may not be involved in driving inflammation in the SKG model. For instance, *Weisella* may be blooming as a symptom of inflammation, which may be creating an ideal niche for its growth. On the other hand, *Weisella* may be blooming to control inflammation. Indeed, *Weisella* species have been shown to possess antimicrobial properties to prevent the overgrowth of pathogens such as *Salmonella typhi* and *Listeria monocytogenes*[261]. Notably, *Weisella* can inhibit fungal growth, and may be blooming due to the intraperitoneal introduction of a fungal wall component which induces inflammation[262].

Relative abundance of *Akkermansia muciniphila* was reduced upon curdlan injection in Oligo-MM^{12} mice. *A. muciniphila* is a mucin-degrading bacterium that plays an important role in contributing to intestinal barrier function by increasing mucus thickness and is reduced in abundance in several inflammatory diseases[263,264]. Notably, intestinal barrier dysfunction and the transit of microbial components to the systemic environment has been associated with SpA[6].

In the previous chapter we demonstrated a low level of intestinal permeability present in SKG mice, and this may contribute to disease pathology by allowing microbial and food antigen to enter the lamina propria. We did not assess intestinal barrier function in this chapter, and so its role in potentiating inflammation is unknown and should be further characterised. We hypothesise that a low level of intestinal permeability may contribute to disease by allowing bacterial components to enter the lamina propria to drive host immune responses.

Utilising strain-specific qPCR to characterise the Oligo-MM^{12} microbiome following induction of disease allowed for the quantification of absolute numbers of each community member. SKG mice colonised with the Oligo-MM^{12} community displayed reductions in the numbers of several members following the induction of disease, and no members displayed increased bacterial numbers following curdlan injection. This indicates an overall reduction in microbial density in the intestine during inflammation, which has previously been identified in both Crohn's disease and ulcerative colitis[265]. This may be caused by the inflammatory environment induced in SKG mice which may restrict growth of intestinal microbiota through antimicrobial mechanisms.

4.4.3 RORγt responses are associated with inflammation but do not necessitate it

SpA is closely associated with Th17 responses. Indeed, IL-23R has been identified in GWAS studies as a susceptibility gene, anti-IL-17 therapy successfully treats AxSpA, and circulating Th17 cells are expanded in patients with AxSpA[82,86,133]. Several mouse models of SpA including the SKG mouse model implicate IL-23 signalling and Th17 responses in driving disease, and in this chapter, we demonstrate that T cell responses in the paw of arthritic SKG mice are skewed towards a Th17 RORγt phenotype[113,266]. However, we note that mice monocolonised with *L. citreum, L. reuteri*, and *P. distasonis* develop arthritis with similar severity as SPF mice but do not develop RORγt skewing in their paw T cell compartment. This suggests that although RORγt responses are associated with joint inflammation in the SKG mouse model, their expansion may not be necessary to drive inflammation. Previous studies in IL-17A deficient SKG mice demonstrate a slight reduction

in arthritis severity, but not total protection from disease, suggesting that Th17-independent mechanisms may also play a role in driving disease[113,266]. Our data demonstrate that the intestinal microbiota may play a role in determining which such mechanisms drive disease in SKG mice, as monocolonisation with different bacteria drove differential T cell responses.

Despite our SKG mice displaying clear small intestinal histopathology, we did not identify any changes to RORγt responses in the intestine during induction of arthritis. Therefore, T cell egress from the intestine to the paw may not be a mechanism driving disease in this model. Indeed, previously published data suggests that RORγt+ resident T cells in the enthesis drive inflammation in human SpA, suggesting that myeloid egress or alternate mechanisms are involved in the transposition of inflammation to the joint[267]. Further to this, it has been suggested that Th17 immunity in peripheral sites during arthritis is initiated but not maintained by IL-23 production in the intestine[141]. Therefore, we may identify shifts in IL-23 rather than downstream Th17 cells in the intestine of SKG mice which may be driving the Th17 response we identified in the paw of arthritic mice. Furthermore, we culled mice at 4-5 weeks post-induction of disease, which may be too late to identify meaningful changes to the adaptive immune system in the intestine during the initiation of pathology. Therefore, we aim to measure IL-23 production from myeloid cells in the small intestine during the initiation of pathology in SKG mice to determine whether this is a mechanism inducing arthritis in the presence of differing intestinal microbiota.

We performed preliminary flow cytometry staining on myeloid subsets during disease following administration of heat-killed *B. animalis,* and we did not observe changes to myeloid populations in the small intestine. However, trends emerged in the paw and spleen of arthritic mice that warrant further investigation. For instance, frequencies of paw CD206- macrophages and spleen CD206+ macrophages are increased in arthritic mice exposed to either *B. animalis* or heat-killed *B. animalis.* The presence of CD206 on macrophages has been shown to stratify subsets of macrophages that play different roles in the pathology of inflammatory disease. Indeed, in rheumatoid arthritis,

synovial CD206+ macrophages were associated with disease remission and produce less proinflammatory cytokines upon LPS stimulation than CD206- macrophages, suggesting that CD206+ macrophages have an important role in resolution of inflammation, whilst CD206- macrophages are involved in potentiating inflammation[258]. The potential expansion of proinflammatory macrophages in the paw of our arthritic mice suggest their association with inflammation in this model. However, whether these macrophages are involved in immune development by *B. animalis* components, or whether they are simply driven by downstream inflammatory pathways in disease is unknown. Therefore, further experiments are required to confirm these results. Following this, *in vitro* pulsing of these macrophages with heat-killed *B. animalis* followed by stimulation with curdlan to measure their cytokine production will provide insight into their involvement in pathology.

4.4.4 *Bifidobacterium animalis* developmentally programs the host immune system to drive arthritis

We demonstrated in this chapter that exposure to live or heat-killed *Bifidobacterium animalis* followed by a 3-week washout or antibiotic period was sufficient to permit the development of small intestinal inflammation and arthritis to a similar severity as that observed in SPF SKG mice, following induction with curdlan. Furthermore, T cell responses were similarly skewed to a RORγt phenotype in the paw of SKG mice whether colonised with an SPF microbiome, *Bifidobacterium animalis*, or administered with heat-killed *Bifidobacterium animalis*. These data together suggest that a component of *B. animalis* is able to program the naïve germ-free host immune system to a pro-arthritogenic state, which is then able to respond to curdlan injection and drive T-cell associated inflammation. Early-life colonisation with microbes is important for the development of the immune system to provide tolerance to commensal microbiota and colonisation resistance against pathogens[206,268]. Indeed, germ-free mice display developmental impairments in their intestinal immune system due to a lack of education from microbial colonisation[182,244,245]. Aspects of these developmental impairments can be rescued through exposure to bacteria-derived components. For instance, *B fragilis*-derived polysaccharide A can induce the expansion of IL-10

producing T_{reg} cells *via* TLR activation germ-free mice[183,269]. We hypothesised that *B. animalis* may upregulate the expression of PRRs either for activation with their own components or for curdlan activation to drive the differentiation of Th17 cells. However, we did not find any changes to the expression of the PRRs we assessed upon *B. animalis* colonisation. This is not to suggest that *B. animalis* components do not activate PRRs, it may be that they either do not upregulate their expression, or that a specific cell type upregulates their expression.

Bifidobacterium dominates the neonatal intestinal microbiome and plays a pivotal role in the development of the immune system[270]. A primary way in which it does this is through its production of indole-3-lactic acid which activates the AhR to skew T cell responses[271]. Indeed, activation of AhR can induce the differentiation of T_{reg} cells or Th17s in a ligand-dependent manner[62,272]. Furthermore, although typically metabolism of tryptophan by bacteria leads to production of AhR ligands, heat-killed bacteria such as *Lactobacillus* have been shown to activate the AhR suggestive of bacterial-derived components acting as AhR ligands[273]. Thus, we hypothesise that a component of *B. animalis* has potential to activate the AhR on either APCs or T cells to drive differentiation of arthritogenic Th17 cells. Activation of AhR has been shown to modulate TLR signalling, so another mechanism AhR may be involved in supporting inflammation is by modulating the signalling of curdlan receptors[274,275]. To determine if AhR activation is implicated in the development of disease, we will measure AhR related genes in heat-killed *B. animalis*-administered mice by qPCR. Furthermore, to assess this functionally, we will administer known AhR ligands to germ-free SKG mice prior to curdlan-injection to evaluate the impact on pathology.

Many developmental abnormalities observed in germ-free mice are age-independent, and colonisation of microbiota at any age can drive the development of these immune responses[175]. However, some immunological defects in germ-free mice can only be corrected by colonisation in a critical window in early life. For instance, iNKT cells recognise bacterial and lipid antigen and are hyperresponsive to antigen stimulation in germ-free mice, however colonisation with bacteria

expressing iNKT antigen can rescue this hyperresponsiveness only in the first 2 weeks of life but not thereafter[185]. We performed all monocolonisation experiments and administration of heat-killed *B. animalis* on 3-week-old mice, so it will be important to determine whether colonisation of adult mice affects pathology. Determining whether a critical window of development exists for an arthritic phenotype to be displayed may aid in our understanding of the host-microbiota mechanisms involved in development of the immune system.

4.5 Conclusion

By leveraging gnotobiotic models we have highlighted that exposure of the host immune system to bacterial components of *Bifidobacterium animalis* can support the development of inflammatory arthritis. The component responsible for driving the education of the immune system and the mechanism it utilises are currently unknown, and further functional work is required to delineate this. Furthermore, whether a time-critical window exists for this interaction is not known, and knowledge of this will provide a deeper understanding of early-life maturation of the immune system by intestinal microbiota.

Chapter 5: A stool Th17 inflammatory signature exists in AxSpA

5.1 Introduction

The first two chapters of this thesis demonstrated a crucial role for the microbiota in permitting joint and intestinal inflammation in mouse models of SpA. We further identified a clear Th17 phenotype in the joint tissue in our mouse models of SpA, as well as potential intestinal permeability in SKG mice. Here we set out to see if these traits are recapitulated in human AxSpA, by phenotyping the stool and circulating immune landscape.

There is a well-established clinical overlap between SpA and IBD, and histological markers of intestinal inflammation are present in up to 70% of patients with SpA[73,276]. The measurement of neutrophilic inflammation in patient stool samples is a widely used method to assess intestinal inflammation in IBD, and stool calprotectin; a calcium- and zinc- binding protein released by activated neutrophils, has been shown to be associated with disease activity in AxSpA[277,278]. Stool myeloperoxidase (MPO); a peroxidase enzyme found in neutrophilic granules, has also been identified as a biomarker for IBD, but has not yet been assessed in patients with AxSpA[279].

Intestinal barrier dysfunction presents alongside intestinal inflammation as a feature of AxSpA, with histological and gene expression analyses on intestinal biopsies from patients with AxSpA displaying reductions in expression of claudin and occludin[122,123]. However, less invasive techniques to measure intestinal barrier function can be performed by measuring host-derived and bacterial-derived factors that translocate to the systemic circulation when the intestinal barrier is impaired. These include measurement in the sera of I-FABP; expressed by intestinal epithelial cells, s-CD14; released by innate immune cells following LPS activation, and LBP; an acute-phase protein that binds to bacterial LPS[6,280].

IL-17 and IL-23 have clear roles in the pathogenesis of AxSpA, with GWAS identifying genetic polymorphisms in the IL-23 receptor gene, and anti-IL-17 therapy successfully treating AxSpA[82,86].

In fact, administration of anti-IL-23 to SKG mice results in reduced arthritis and ileitis, alongside increased *Muc2* expression and frequency of goblet cells, suggesting that IL-23 may be involved in tipping the balance of Th17 cells away from being barrier protective and towards a pathogenic phenotype[113]. The circulating immune landscape has been well phenotyped in patients with AxSpA, identifying increased levels of circulating Th17 cells[132,133]. However, phenotyping of the intestinal cytokine response in AxSpA is integral to further dissecting the gut-joint axis. Despite the presence of subclinical intestinal inflammation in a large proportion of patients with AxSpA, access to intestinal tissue biopsies from patients with AxSpA that do not have clinical IBD is limited. Therefore, the assessment of cytokines in stool samples provides a non-invasive method by which to phenotype the intestinal immune landscape in AxSpA[281]. This technique is sparse in the literature and has yet to be used to assess stool cytokines from patients with AxSpA.

The intestinal microbiota can modulate the host immune system in several ways, including through the production of metabolites[59]. Indeed, the downregulation of the SCFAs butyrate and propionate is associated with AxSpA, and administration of butyrate to SKG mice attenuates arthritis[122,282]. Further to this, spermidine, a product of arginine metabolism, is increased in HLA-B27 transgenic rats and is associated with orchestrating the appropriate differentiation of T cell subsets[65]. Therefore, the associations between microbial metabolites and the host intestinal immune response would further our understanding of the gut-joint axis in AxSpA.

5.2 Aim

In this chapter we collected fresh stool, ethanol-fixed stool, and blood samples from patients with AxSpA and age-matched healthy controls (figure 5.1). We quantified several immune parameters in the blood and stool, as well as the stool metabolomic profile. We aimed to characterise the immune phenotype in the stool and the blood of patients with AxSpA, as well as identify any associations between these phenotypes, and with stool metabolites.

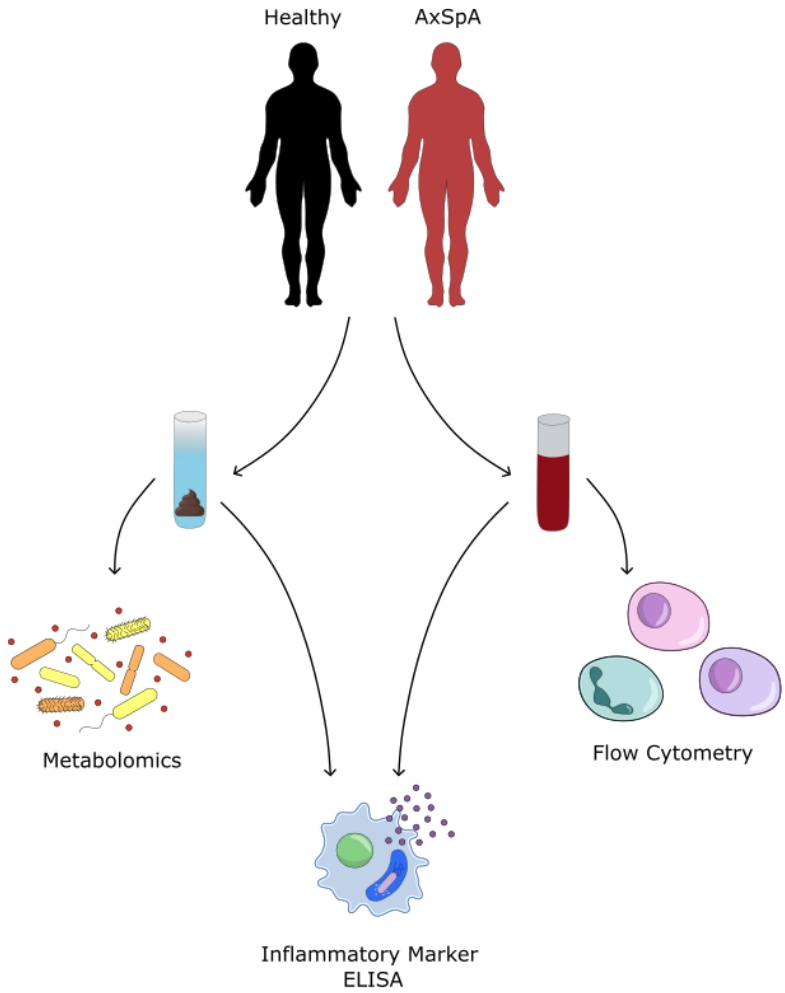


Figure 5.1 Experimental outline to immune phenotype patients with AxSpA. Matched stool and blood samples were obtained from patients with AxSpA and age-matched healthy controls. Metabolomics was performed on ethanol-fixed stool, immune marker ELISAs were performed on fresh stool, and intracellular flow cytometry staining was performed on PBMCs isolated from the blood.

5.3 Results

5.3.1 Markers of intestinal inflammation are elevated in AxSpA

As there is an established clinical overlap between AxSpA and IBD, we sought to determine whether neutrophil-associated molecules indicative of subclinical intestinal inflammation are altered in our AxSpA cohort. We first studied fresh stool samples from 30 AxSpA patients and 84 age-matched healthy donors (see section 2.1.1) and measured levels of calprotectin and myeloperoxidase (MPO) by ELISA. Stool calprotectin and MPO were significantly increased in patients with AxSpA compared to healthy donors (figure 5.2). This suggests that, in accordance with previously published data, subclinical intestinal inflammation is present in patients with AxSpA.

NSAIDs have previously been associated with elevated stool calprotectin levels, and a large proportion of our patients were taking NSAIDs at the time of recruitment [283]. However, neither NSAID usage, nor biologic treatment impacted stool calprotectin levels in our cohort (appendix figure 5.2A).

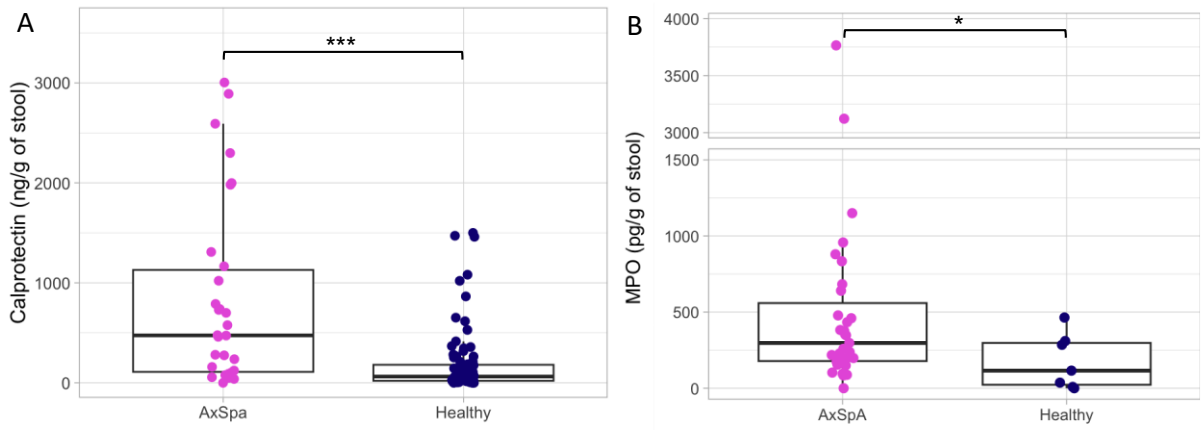


Figure 5.2 Markers of intestinal inflammation are elevated in AxSpA. Fresh stool samples were collected from 30 patients and 84 healthy controls, and stool calprotectin and MPO levels were quantified by ELISA. A) Stool calprotectin (ng/g of stool). B) Stool MPO (pg/g of stool). ***p<0.001, *p<0.05. Unpaired student's t-test with Welch's correction. Boxplots denote median + interquartile range and individual data points are shown.

5.3.2 Serum barrier function proteins are unaltered in AxSpA

Subclinical intestinal inflammation was present in our patient cohort so we hypothesised that our patient cohort would display intestinal barrier function impairment. Serum was collected from 77 patients with AxSpA and 84 age-matched healthy controls, including patients and controls who also donated fresh stool for cytokine and neutrophil protein analysis. We quantified serum levels of s-CD14, LBP, I-FABP. We found no significant differences in these markers of intestinal permeability between patients with AxSpA and healthy controls (figure 5.3). This is not to say that impaired barrier function is not implicated in AxSpA, as we did not complete functional permeability tests such as the lactulose:mannose test; whereby both sugars are consumed by the patient and their excreted ratio is measured in the urine, due to clinical constraints.

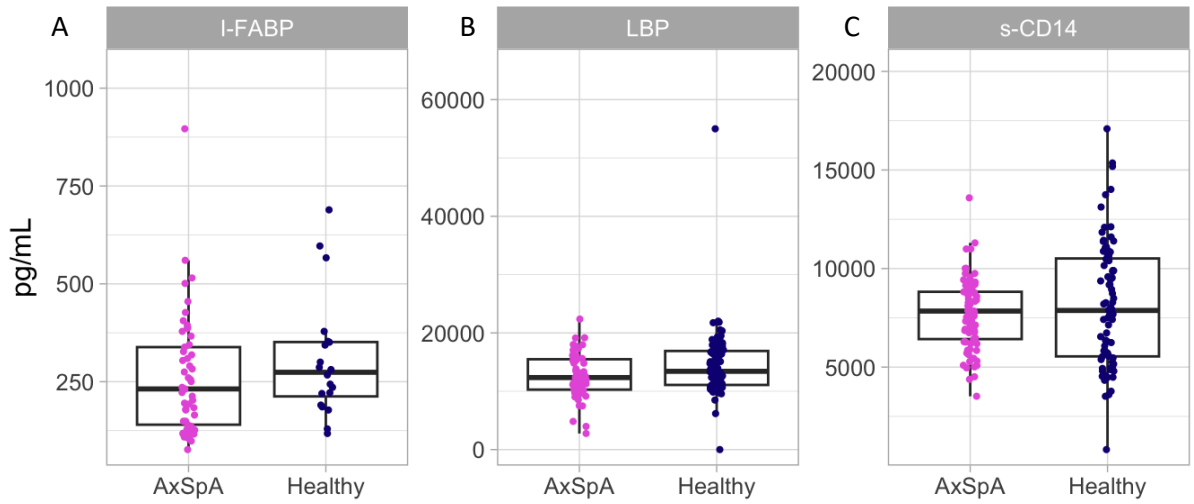


Figure 5.3 Serum barrier functions proteins are unaltered in AxSpA. Serum was collected from 77 AxSpA patients and 84 healthy controls, and intestinal fatty acid binding protein (I-FABP), LPS binding protein (LBP), and soluble (s)-CD14 were quantified by ELISA. A) Serum I-FABP, B) serum LBP, C) serum s-CD14. Protein levels are denoted as pg/mL of sera. Unpaired student's t-test with Welch's correction. Boxplots denote median + interquartile range and individual data points are shown.

5.3.3 Patients with AxSpA display increased frequencies of circulating Th17 cells

Alongside the collection of fresh stools, we collected matched blood samples from our patient and control cohorts to describe the blood immune phenotype. We performed intracellular cytokine staining on *ex vivo* PBMCs from 46 patients with AxSpA and 74 healthy controls (section 2.1.1). IL-17A+ CD4+ (Th17) cells were significantly increased in patients with AxSpA compared to healthy donors (figure 5.4D). IL-17F+ CD4+ cells were also significantly increased in patients with AxSpA (figure 5.4E). We did not observe any differences in the production of IFNγ, IL-10, or GM-CSF from CD4+ cells between AxSpA patients and healthy controls in this cohort (figure 5.4A-C). These data are suggestive of a circulating type-17 environment in AxSpA, which supports previously published data suggesting a pivotal role for the cytokine IL-17A in the disease. We also observed a significant increase in circulating IL-5 producing CD4+ cells in AxSpA compared to healthy controls (figure 5.4F). This has not previously been observed in AxSpA and may suggest a role for Th2 cells in the disease.

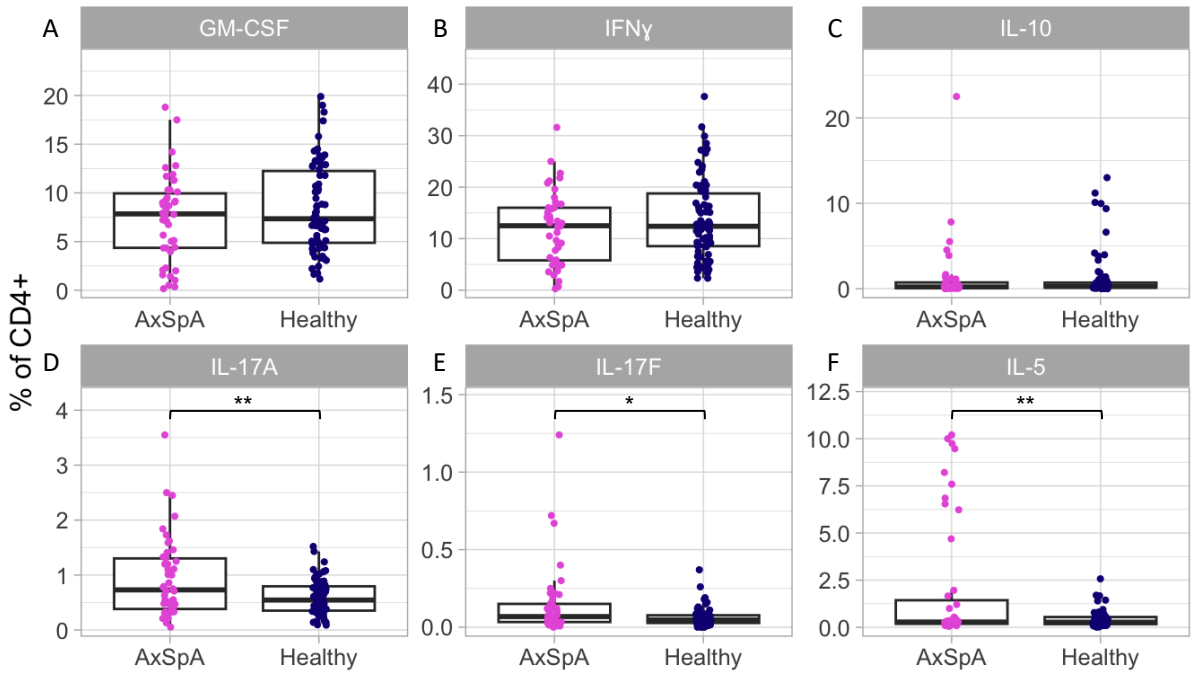


Figure 5.4 Patients with AxSpA display increased frequencies of circulating Th17 cells. Fresh blood was collected from 46 patients with AxSpA and 74 healthy controls, PBMCs were subsequently isolated and intracellular cytokine staining was completed to quantify the production of several cytokines from CD4+ cells. Gating strategy is outlined in appendix figure 5.1. A) GM-CSF+ T helper cells, B) IFNγ+ T helper cells, C) IL-10+ T helper cells, D) IL-17A+ T helper cells, E) IL-17F+ T helper cells F) IL-5+ T helper cells. **p<0.01, *p<0.05. Unpaired student's t-test with Welch's correction and Benjamini-Hochberg correction for multiple testing. Boxplots denote median + interquartile range and individual data points are shown.

5.3.3 Stool Th17 cytokines are elevated in AxSpA

Upon demonstrating elevated stool calprotectin and MPO, we sought to characterise the stool immune phenotype. Patients with AxSpA demonstrate successful response to therapy *via* IL-17 inhibition, but not through inhibition of IL-23[82,284]. Further research alludes to IL-23 implication in the initiation of disease but not the maintenance of disease, so we hypothesised that IL-23 may be elevated in the intestine to drive the initiation of Th17 cell differentiation[141]. We therefore used ELISA to quantify several cytokines, including inflammatory and anti-inflammatory cytokines, Th1, Th2, and Th17 cytokines, in the fresh stool previously obtained from patients and controls (appendix table 5.1). Of these cytokines, stool IL-17A, IL-23, and GM-CSF were all elevated in patients with AxSpA when compared to healthy controls (figure 5.5A, C, D). These elevated cytokines are all associated with type-17 immunity, and thereby these data suggest an IL-23-associated Th17 immune landscape in the stool in AxSpA. Stool IL-10 was unaltered between patients with AxSpA and healthy controls (figure 5.5B).

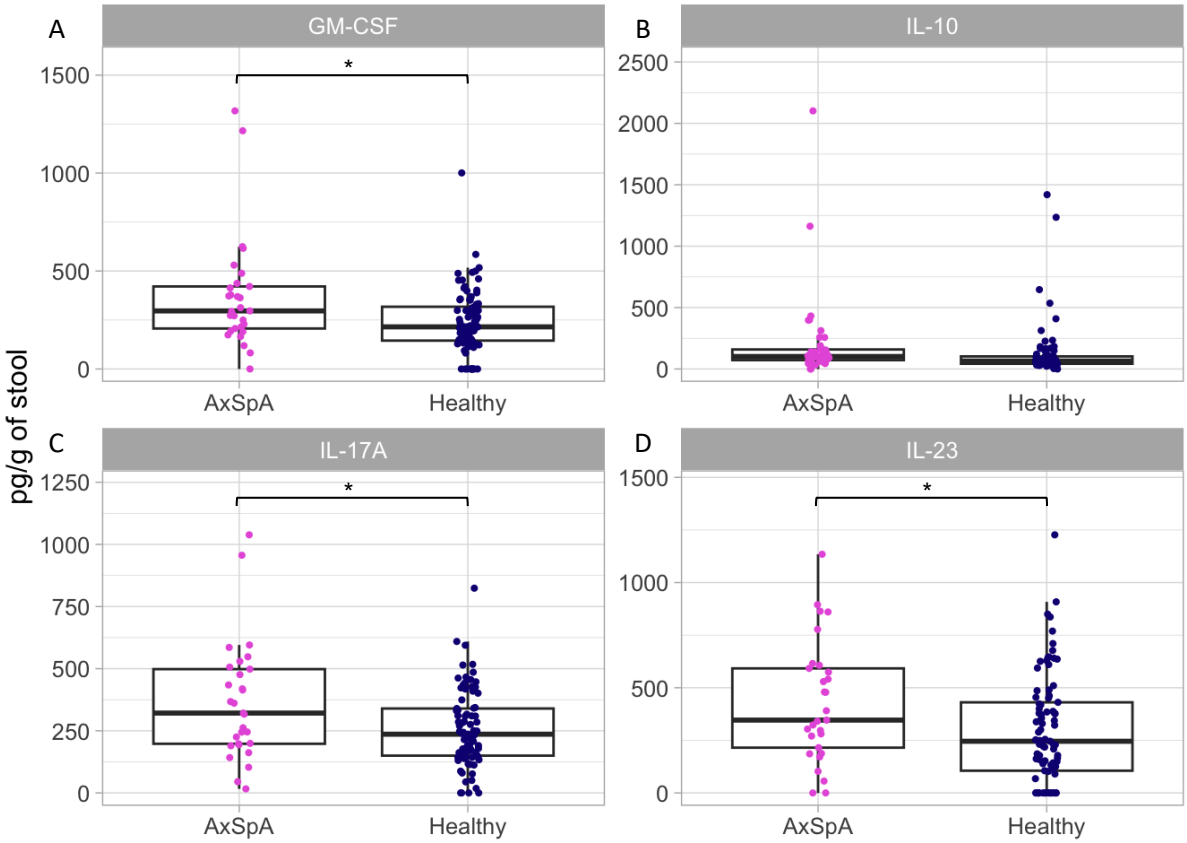


Figure 5.5 Stool Th17 cytokines are elevated in AxSpA. ELISA was completed on fresh stool obtained from 40 patients with AxSpA and 85 healthy controls to quantify cytokine levels. A) Stool GM-CSF, B) stool IL-10, C) stool IL-17A, D) stool IL-23. Cytokine levels are denoted as pg/g of stool. *p<0.05. Unpaired student's t-test with Welch's correction and Benjamini-Hochberg correction for multiple testing. Boxplots denote median + interquartile range and individual data points are shown.

5.3.4 Stool cytokines do not correlate with systemic cytokine production

After observing a type-17 environment in both the stool and the blood of patients with AxSpA, we asked whether cytokine presence in the stool correlated with that produced from circulating CD4+ cells. We found however that the stool cytokines IL-17A and GM-CSF did not associate with production of IL-17A and GM-CSF from circulating CD4+ cells (figure 5.6A-B). These data could suggest that the persistence of Th17 immunity in the gut and the joint are differentially driven.

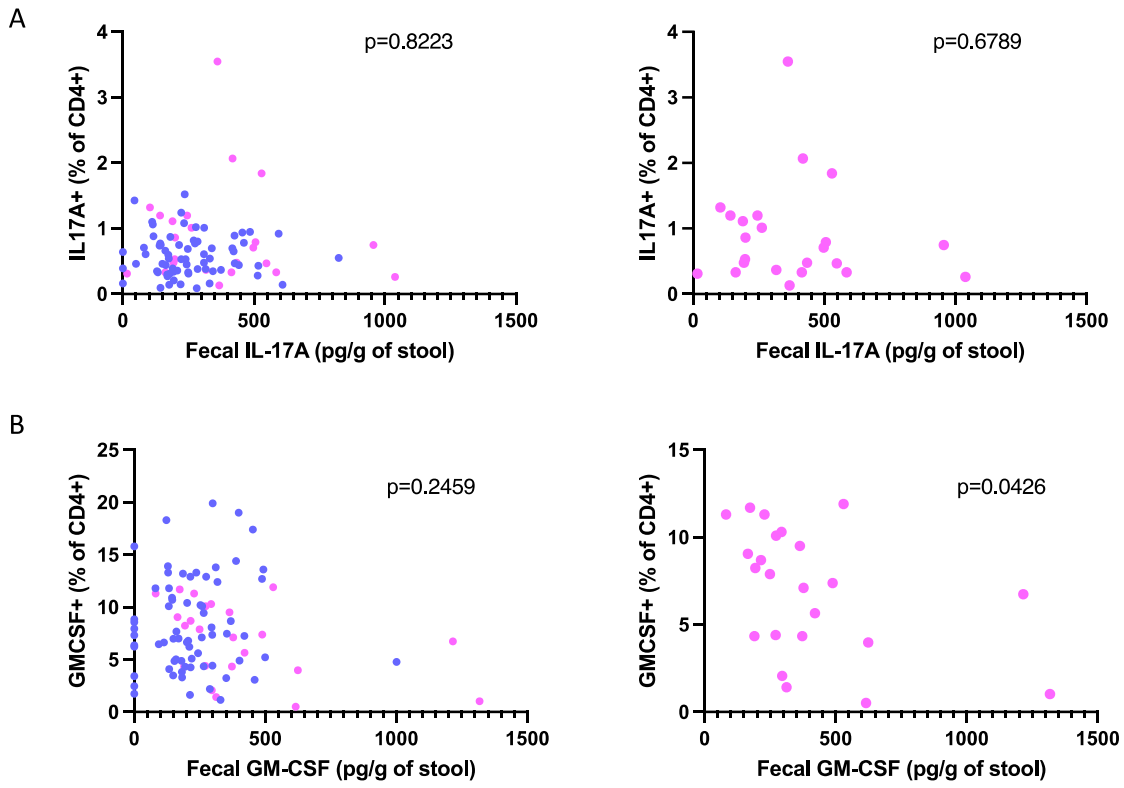


Figure 5.6 Stool cytokines do not correlate with systemic cytokine production. Correlation analyses were completed between stool cytokines and circulating cytokine-producing T helper cells. Left-hand side analyses pool AxSpA and healthy controls, right-hand side analyses include only AxSpA patients. A) IL-17A+ (% of CD4+) and stool IL-17A (pg/g of stool), B) GM-CSF+ (% of CD4+) and stool GM-CSF (pg/g of stool). Pink points refer to patients with AxSpA, purple points refer to healthy controls. Pearson's correlation was carried out with Benjamini-Hochberg adjustment for multiple testing.

5.3.5 Stool calprotectin positively correlates with stool IL-23 levels

As our patient cohort display a type-17 stool immune landscape, we ran multiple correlation tests to determine whether stool calprotectin is associated with any stool cytokine levels or circulating cytokine production. We specifically hypothesised that stool IL-23 would correlate with stool calprotectin levels due to its association with IBD[285]. Indeed, we identified that stool calprotectin is significantly positively correlated with stool IL-23 levels (figure 5.7A). This supports our hypothesis and suggests a role for intestinal inflammation in AxSpA[285]. This association is no longer significant when healthy controls are removed from the analysis, however, as the healthy controls have lower levels of calprotectin, we suggest that the analysis containing only AxSpA patients is underpowered. We also found that stool calprotectin levels are significantly positively correlated with production of IL-17F from circulating CD4+ cells (figure 5.7B). However, this significance is driven by one patient sample, and upon removal is no longer significant.

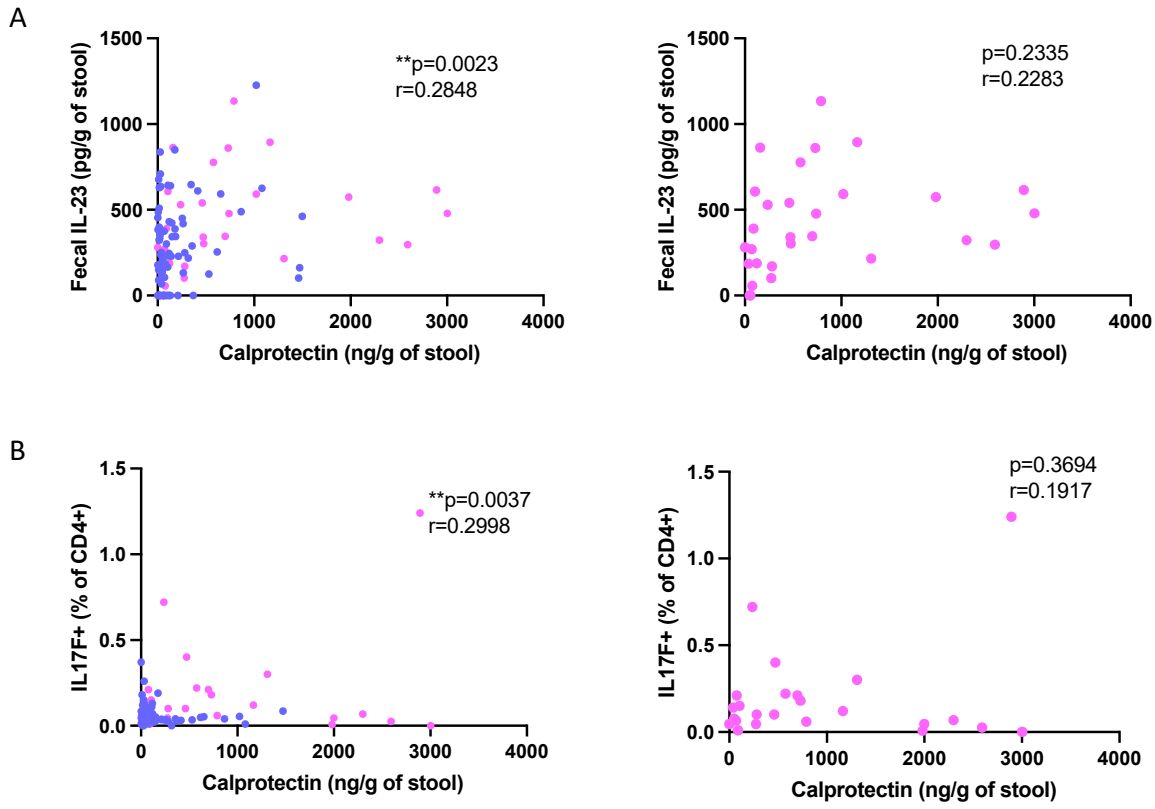


Figure 5.7 Stool calprotectin positively correlates with stool IL-23 levels. Correlation analyses were completed between stool calprotectin and other immune parameters. Left-hand side analyses pool AxSpA and healthy controls, right-hand side analyses include only AxSpA patients. Pink points refer to patients with AxSpA, purple points refer to healthy controls. A) Stool IL-23 (pg/g of stool) (p=0.0023, r=0.2848), B) IL17F+ (% of CD4+) (p=0.0037, r=0.2998). **p<0.01. Pearson's correlation was carried out with Benjamini-Hochberg adjustment for multiple testing. Pearson's correlation coefficient (r) is denoted on each plot.

5.3.6 HLA-B27 presence does not associate with stool and circulating Th17 immune phenotype

Previously published data has demonstrated an expansion of IL-17 producing CD4+ cells in arthritic HLA-B27 transgenic rats, an animal model for AxSpA[286]. We therefore hypothesised that the Th17 phenotype we observed in the stool and blood of patients with AxSpA would be associated with the presence of HLA-B27. We found that HLA-B27 positive patients and controls had elevated levels of stool calprotectin and increased frequencies of circulating IL-17A+ T helper cells (figure 5.8A, B). However, we found that these expansions were primarily driven by diagnosis of AxSpA, as healthy controls do not display any changes in stool calprotectin levels or IL-17A+ T helper cell frequencies (figure 5.8A, B). This is likely due to the association of Th17 immunity with disease, and more HLA-B27- patients are required to interrogate this appropriately. Notably, the previous increased

frequencies of IL-5 producing CD4+ cells we observed between patients with AxSpA and healthy controls (figure 5.3F) seems to be driven by HLA-B27 positivity (figure 5.8C). AxSpA patients and healthy controls together show increased IL-5 production from CD4+ cells, as well as healthy controls alone (figure 5.7C). HLA-B27 positivity did not associate with any other immune parameters measured (appendix figure 5.3).

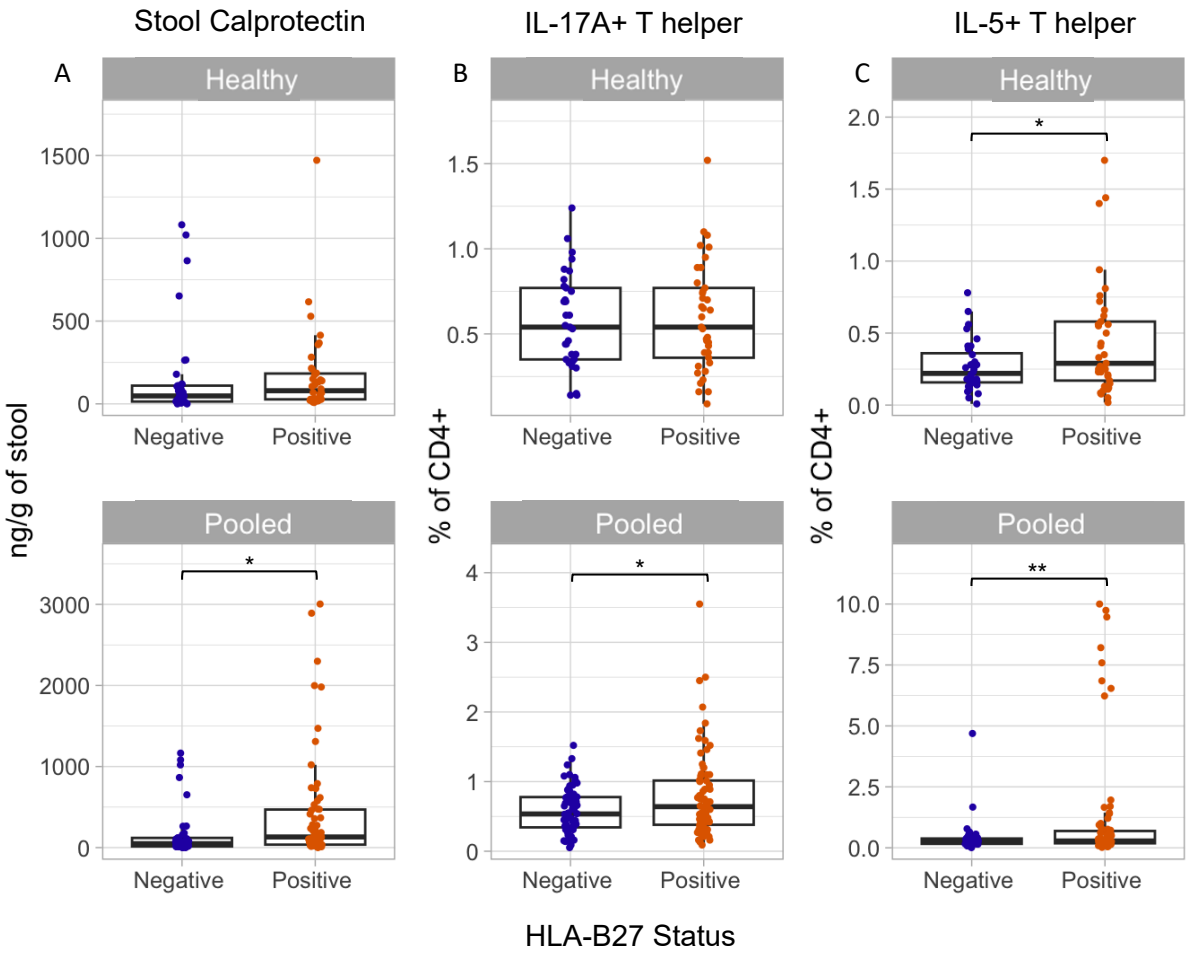


Figure 5.8 HLA-B27 presence does not associate with stool and circulating Th17 immune phenotype. Immune phenotype parameters were analysed based on HLA-B27 positivity in AxSpA patients and healthy controls pooled (bottom), and healthy controls alone (top). A) Stool calprotectin (denoted as ng/g of stool)B) IL-17A+ (denoted as % of CD4+), C) IL-5+ (denoted as % of CD4+). **p<0.01, *p<0.05. Unpaired student's t-test with Welch's correction and Benjamini-Hochberg correction for multiple testing. Boxplots denote median + interquartile range and individual data points are shown.

5.3.8 Markers of disease severity and medications are not associated with immune parameters

We sought to identify the extent to which disease severity associated with the immune parameters we quantified in our patients with AxSpA. We therefore compared 2 measures of

disease, BASDAI and C-reactive protein (CRP), taken at time of recruitment, as well as disease duration. We found no association between BASDAI, CRP, or disease duration with any of the immune parameters that we quantified in our patient cohort (appendix figure 5.4). We hypothesised that this may be because a large proportion of our patients are on treatment (32/54 patients on NSAIDs, and 19/54 patients on biologics), and their disease may be well controlled. However, NSAID and biologic usage did not associate with any of the immune parameters we measured in our AxSpA patients (appendix figure 5.2).

5.3.9 Extra-articular manifestations are associated with altered stool and circulating immune phenotype

Several extra-articular manifestations are associated with AxSpA, including IBD, psoriasis, uveitis, and enthesitis[276]. We therefore stratified our patients with AxSpA by their extra-articular manifestations, to determine whether they associated with the immune parameters we had quantified. A large proportion of our patients had extra-articular manifestations (30/53), with 8/53 patients displaying more than 1 extra-articular manifestation. Surprisingly, IBD was not significantly associated with increased stool calprotectin levels, however the highest levels of stool calprotectin in the cohort were observed in patients with IBD (figure 5.9A). This suggests that the IBD positive patients with low levels of calprotectin have well-controlled inflammation. Conversely, AxSpA patients with psoriasis had lower levels of stool calprotectin compared to AxSpA patients without psoriasis (figure 5.9A). One of our patients was co-diagnosed with IBD and psoriasis. AxSpA patients with psoriasis also had increased levels of circulating GM-CSF producing CD4+ cells compared to AxSpA patients without psoriasis (figure 5.9B). This supports previously published data demonstrating that GM-CSF is elevated in skin biopsies from patients with psoriasis[287]. Patients with enthesitis also displayed increased levels of circulating GM-CSF producing CD4+ cells. However, three of the six patients with enthesitis in this analysis also had psoriasis, and the difference was primarily driven by psoriasis and not enthesitis presence. Notably, AxSpA patients with enthesitis displayed significantly reduced production of IL-5 from circulating CD4+ cells compared to AxSpA

patients without enthesitis (figure 5.9C). This observation was not driven by HLA-B27, as all our patients with enthesitis were HLA-B27 positive. These data have not been shown previously and may indicate a reduction in Th2 immunity in patients with enthesitis manifestation. Extra-articular manifestations did not associate with any other immune parameters that were measured (appendix figure 5.5).

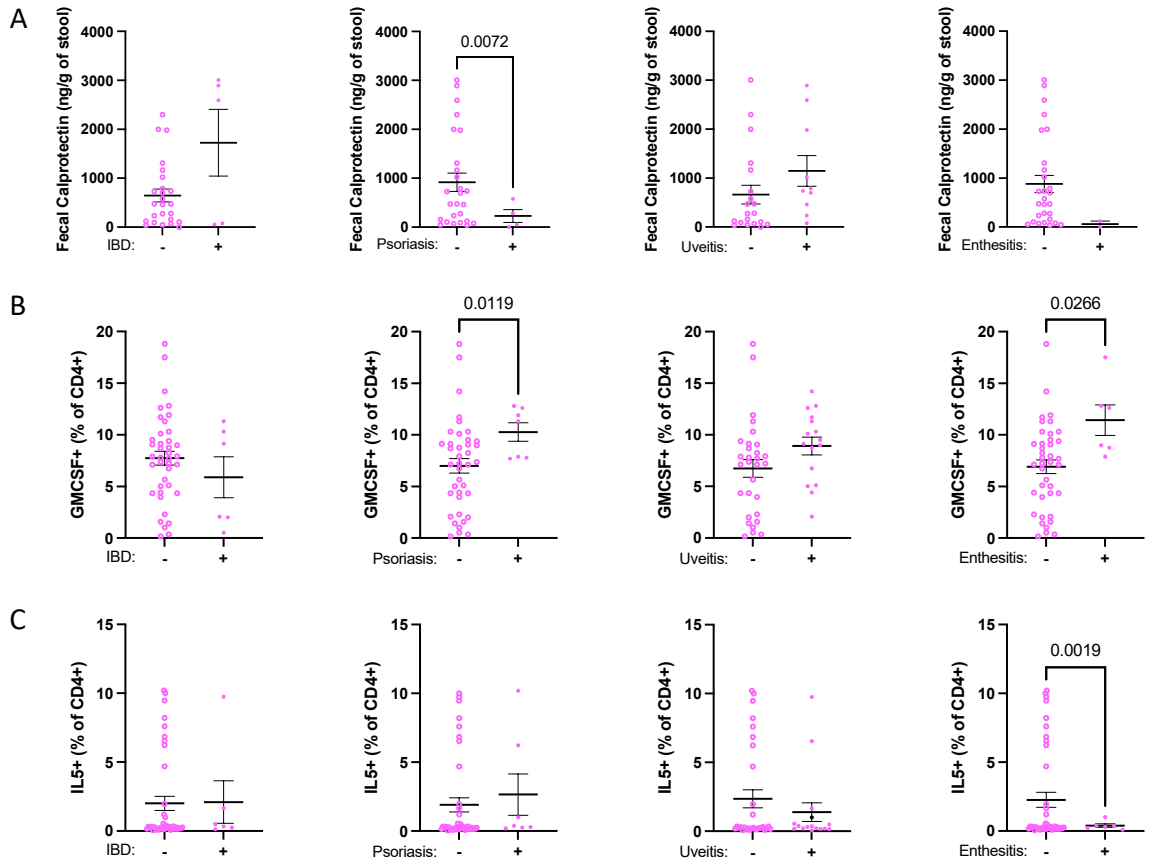


Figure 5.9 Extra-articular manifestations are associated with altered stool and circulating immune phenotype. AxSpA patients were stratified by extra-articular manifestations and immune parameters were compared (from left to right; IBD, psoriasis, uveitis, enthesitis). A) Stool calprotectin (ng/g of stool), B) GM-CSF+ (% of CD4+), C) IL-5+ (% of CD4). Unpaired student's t-test with Welch's correction and Benjamini-Hochberg adjustment for multiple testing. Dotplots denote mean + standard error and individual data points are shown.

5.3.10 Stool amino acid concentrations negatively correlate with stool IL-23 levels

There is clear evidence demonstrating a role for the microbiome in AxSpA, and microbial metabolites have been shown to directly modulate the differentiation and function of T cells[268]. We were therefore interested to understand whether the stool cytokine landscape may be associated with the stool metabolomic signature in our AxSpA patients. To identify stool metabolites, we collected matched ethanol-fixed stool samples from 62 AxSpA patients and 27 age-

matched healthy controls, including patients and controls from our cohort. We subsequently completed NMR spectroscopy on these samples and ran association analyses against our immune parameters. These analyses identified multiple amino acids negatively associating with stool IL-23 levels in patients with AxSpA and healthy controls. Specifically, isoleucine, leucine, valine, threonine, aspartate, and tyrosine were all negatively associated with stool IL-23 levels (figure 5.10A-F).

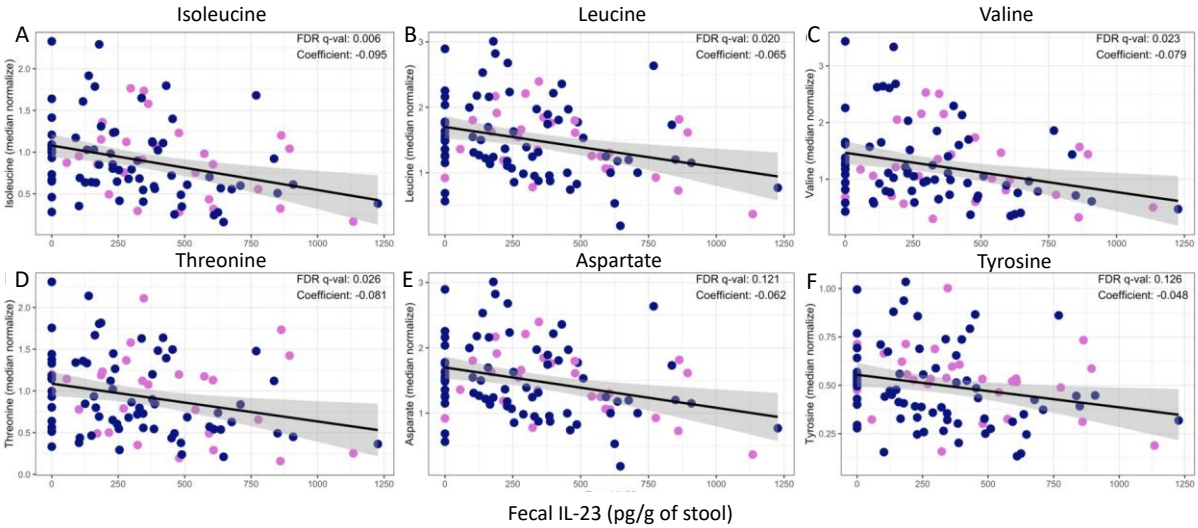


Figure 5.10 Stool amino acid concentrations negatively correlate with stool IL-23 levels. NMR was performed on ethanol-fixed stool samples from patients with AxSpA and healthy controls. Association analyses were completed to identify stool metabolites that are associated with cytokines in the stool or produced in the blood by CD4+ cells. IL-23 was negatively associated with several amino acids. A) Isoleucine, B) leucine, C) valine, D) threonine, E) aspartate, F) tyrosine. Linear modelling was completed. Individual points are shown. Pink= AxSpA, purple = healthy controls.

5.4 Discussion

The results presented in this chapter identify a Th17 signature in both the stool and the blood of patients with AxSpA. Further analysis identified stool IL-23 to be positively correlated with stool calprotectin; a measure of intestinal neutrophilic activity, as well as negatively correlated with several stool amino acids. Taken together, these data suggest a role for IL-23 in intestinal inflammation in AxSpA, and that amino acid metabolism by the microbiota may play a role in modulating IL-23-associated immunity.

5.4.1 Th2 cytokine production is associated with HLA-B27

In this study we observed that HLA-B27 healthy controls displayed increased IL-5 production from T helper cells, suggesting an associated between HLA-B27 and allergic reaction. Indeed, HLA have previously been associated with food allergy, although primarily polymorphisms in the MHC class II region due to preferential presentation of extracellular peptides[288–290]. However, some MHC class I polymorphisms have been associated with allergy. For instance, HLA-B55 has been associated with penicillin allergy, and HLA-B27 is associated with food allergy[291,292]. This may be due to a mechanism whereby the altered peptide binding groove is able to present allergens to CD8+ cells and drive the differentiation of type 2 cytotoxic cells. Further supporting this hypothesis, CD8+ responses have been associated with driving hypersensitivity and may further drive the expansion of IL-5-producing T helper cells we observed[293].

5.4.2 The intestinal barrier is not altered in our AxSpA cohort

Previous studies identify intestinal barrier dysfunction in patients with AxSpA[6]. However, we did not find any differences in serum biomarkers of intestinal permeability between patients with AxSpA and healthy controls. This may be due to other factors and may not indicate a lack of barrier dysfunction in our patients. For example, serum proteins from the intestinal lumen reach the blood *via* the intestinal epithelial layer as well as the gut vascular barrier[16]. It may be that our patients with AxSpA do not have an impaired gut vascular barrier, but do have impairment of the intestinal epithelial layer, thereby showing similar levels of s-CD14, I-FABP, and LBP to healthy controls. In addition, more functional methods of assessment including lactulose-mannose testing may be more accurate in determining intestinal permeability[294].

5.4.3 The IL-23/Th17 axis in SpA may involve the intestinal microbiome

AxSpA is clinically and genetically associated with IBD, and a large subset of AxSpA patients display subclinical intestinal inflammation[73,86,115]. Furthermore, type 17 immunity plays a pivotal role in driving AxSpA pathology, as inhibition of IL-17 is successful in treating disease[82]. We further

support these studies firstly by demonstrating increased levels of neutrophil activity-associated proteins stool calprotectin and MPO in AxSpA compared to healthy controls. In addition, we identify increased IL-17 production from circulating T helper cells and in the stool of patients with AxSpA, implicating type-17 immunity in the intestine and the systemic environment. Th17 cell differentiation is driven by IL-23 production from DCs and prophylactic inhibition of IL-23 in SKG mice and HLA-B27 transgenic rats prevents onset of arthritis[141,179]. We therefore hypothesised that IL-23 would be present in the stool of patients with AxSpA, potentially driving pathogenic Th17 differentiation. We found that stool IL-23 was increased in AxSpA, and correlated with stool calprotectin, suggesting its association with intestinal inflammation. This agrees with clinical data to indicate that IL-23 inhibition is successful in treating IBD, demonstrating its crucial role in driving intestinal inflammation[285]. Conversely, IL-23 inhibition in AxSpA is not effective in treating disease, implying that arthritogenic Th17 responses are IL-23-independent. However, as prophylactic inhibition of IL-23 treats arthritis in mouse models, we hypothesise that IL-23 is involved in induction of Th17 cells which then become deranged and persist independently of IL-23. We note that use of ELISA to detect stool cytokines may be strengthened by the use of experimental positive controls, including the spiking of cytokine into samples to ensure they can be recovered through detection.

The intestinal microbiome plays a crucial role in supporting disease in mouse models of SpA, and microbiome dysbiosis and alterations in stool metabolites are associated with AxSpA[151,163,179,295]. Furthermore, bacteria-derived metabolites can influence the host immune response by skewing the differentiation of T cells[268]. Thus, we completed metabolomic analyses on stool from patients with AxSpA and healthy controls and found that several amino acids negatively correlated with stool IL-23. This may be that increased amino acid metabolism is reducing availability of amino acids in the stool, which could thereby directly or indirectly influence IL-23 production. Indeed, metabolism of tryptophan leads to the production of AhR ligands, which can thereby influence differentiation of T cells through their action on either T cells or APCs[62,272,296]. Thus, increased amino acid metabolism may be driving the production of metabolites able to

influence IL-23 production. Conversely, alterations in amino acid levels may be influenced by IL-23 production and an inflammatory environment in the intestine. Indeed, IL-23 production can drive AMP production by IECs through its induction of IL-22 production from NKT cells and ILC3s, and through its induction of IL-17 from Th17 cells[297]. Therefore, IL-23-mediated production of AMPs may shape the intestinal microbiota to alter amino acid metabolism. Our study is purely correlative and further functional *in vivo* studies utilising amino acid administration should be performed to determine the causality of the amino acid – IL-23 relationship. We also note that although our patients and healthy controls were age-matched, we recruited disproportionate numbers of male AxSpA patients compared to female AxSpA patients, whereas our healthy control recruitment was split equally based upon sex. Therefore, future studies should consider appropriately sex-matching when recruiting healthy controls.

5.5 Conclusion

In this chapter we aimed to clinically recapitulate changes to the immune response and intestinal microbiome that we observed in SKG mouse models of SpA. We found that patients with AxSpA display increased stool neutrophil activity that was correlated with stool IL-23 levels, supporting previously published data associating intestinal inflammation with IL-23. Furthermore, we demonstrated that stool amino acids negatively correlated with stool IL-23, suggesting that amino acid metabolism may be associated with IL-23-mediated immunity. Further functional studies characterising the role of amino acid metabolism in modulating Th17 responses are required to ascribe causality to this relationship.

Chapter 6: General discussion

Recent advancements in microbiome studies have highlighted a clear role for the intestinal microbiota in communicating with the immune system to modulate host health and disease. Alterations to the intestinal microbiome have been identified in several conditions extending from IBD to mental health disorders[298,299]. Studies have demonstrated an important role for the intestinal microbiome in SpA, alongside clinical and genetic overlaps with IBD which have, together, indicated the presence of a gut-joint axis in SpA[5,74,86,151,153,171,179,300]. The microbiome therefore remains an enticing space in which to develop therapies for SpA, however the field currently lacks mechanistic understanding of the host-microbiota interactions driving disease to develop targeted and effective microbiota-based therapies.

6.1 Summary

Overall, this thesis aimed to determine the role of the commensal microbiota in driving immune responses to induce the development of SpA. In this regard, we highlighted a key role for commensal microbiota in programming the host immune system in a genetically susceptible host to respond to an immunogenic trigger and drive both intestinal and joint disease. We hypothesise that an interplay of host genetics, environmental triggers, and the intestinal microbiome supports the host immune system in triggering arthritogenicity (figure 6.1). More specifically, we suggest that the intestinal microbiota imprints the predisposed autoreactive host immune system to become reactive to a pro-inflammatory microbial trigger, driving inflammatory joint disease. Verifying these hypotheses utilising both *in vitro* and *in vivo* experimentation is currently ongoing.

6.2 SpA is driven by host-microbiota interplay

The strong genetic component of SpA, coupled with pathological intestinal manifestations and microbiome shifts led us to hypothesise that an interplay of host genetics and environmental factors can impact on immune responses and the intestinal microbiota, which can thereby drive the

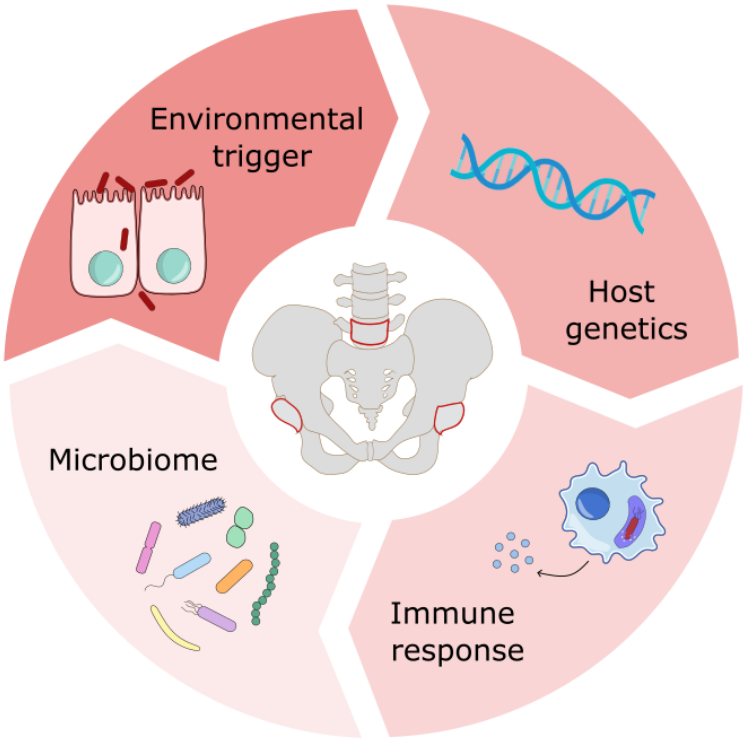


Figure 6.1 Proposed factors influencing SpA pathogenicity. We hypothesise that the interplay between host genetics, the intestinal microbiome, and the immune response drives SpA pathogenicity following an immunogenic environmental trigger.

development of SpA. In this thesis we demonstrated a requirement for a mutation in the T cell signalling molecule ZAP-70 to support the development of both *C. rodentium* and curdlan-triggered arthritis. Aberrant T cell selection from a mutation in ZAP-70 leads to an accumulation of highly self-reactive T cells in SKG mice, and T cells in SKG mice are skewed towards a Th17 phenotype and display T_{reg} cell impairment[108,109]. It may be that HLA-B27 fulfils the role of driving self-reactive T cells in SpA. Indeed, one hypothesis which has been postulated to explain the role of HLA-B27 in SpA is its potential function to present self-antigen or other arthritogenic peptides to T cells, thereby driving a pro-inflammatory response[89]. However, several HLA-B27+ individuals do not develop SpA, and so factors aside from HLA-B27, including other genetic factors, are clearly important in supporting disease. In this thesis we found that mice on a Balb/C background may display a baseline level of intestinal permeability. We suggest that host genetics may also play a crucial role in determining intestinal barrier integrity, perhaps due to dysfunctional barrier site immune responses. In this regard, first degree relatives of patients with SpA also display increased stool calprotectin

levels and serum antibodies to flagellin compared to non-related controls, indicating intestinal barrier impairment[301,302]. Notably, these observations were independent of HLA-B27 status, which indicates that a combinatorial effect of host genetics may support pathology in SpA, but also indicates that barrier defects alone are not sufficient for the development of disease.

In this thesis we also demonstrated that curdlan injection and *C. rodentium* infection were both able to drive the development of joint inflammation in SKG mice. We hypothesise that an immunogenic trigger that stimulates the production of pro-inflammatory cytokines is required to drive the differentiation towards an arthritogenic T cell phenotype. For instance, *C. rodentium* and curdlan are both known to trigger the production of IL-23 and IL-1 through different pathways, which can drive the differentiation of Th17 cells[112,303,304]. Pathogens associated with ReA such as *Shigella* and *Salmonella* are also known to trigger the production of pro-inflammatory cytokines[305–307]. AxSpA is not typically associated with enteral infection, although typically pathogenic bacteria such as *Ruminococcus gnavus* are expanded in AxSpA, which have been demonstrated to pro-inflammatory pathways[308]. Furthermore, HLA-B27 misfolding in the ER can drive the production of IL-23 from DCs, which may act as a trigger to drive the differentiation of arthritogenic T cell responses[93].

6.3 IL-23/Th17 immunity may connect the gut-joint axis in SpA

Th17 responses are strongly associated with SpA, demonstrated with the expansion of circulating Th17 cells and the efficacy of anti-IL-17A therapy in treating disease[82,132]. Data in this thesis supports a clear role for type 17 responses in SpA, as it highlighted increased frequencies of circulating IL-17A and IL-17F producing T helper cells in patients with AxSpA. In addition, we observed expansions of RORγt+ T helper cells associated with disease in SKG mice injected with curdlan or infected with *C. rodentium*. Notably however, we found that disease was not consistently associated with RORγt responses in SKG mice. For instance, RORγt+ T helper cells did not persist in the paw alongside arthritis after *C. rodentium* was cleared, and monocolonisations of SKG mice with

bacteria aside from *B. animalis* did not support the expansion of RORγt+ T helper cells whilst disease was triggered upon curdlan stimulation. This indicates that immune responses aside from RORγt responses are associated with driving inflammation. Indeed, IL-17A -/- in SKG mice has previously been shown to not be protective against arthritis, and only attenuates disease. Similarly, anti-IL-17 therapy is not effective in all patients with AxSpA and indicates heterogeneity in the immune response in SpA. Completing further immune profiling of cytokine production and adaptive responses aside from RORγt and FoxP3 responses will allow for further mechanistic understanding of differential responses to different microbiota.

Although curdlan-triggered disease in SKG mice is not entirely dependent on IL-17A, blockade of IL-23 has been shown to prevent onset of disease[113]. IL-23 production by DCs is upstream of the differentiation of cell types such as of Th17 cells, NKT cells, and ILC3s which can produce IL-17, IL-22, TNFα, and GM-CSF, and is associated with driving IBD[309–311]. Supporting this, we observed elevated stool IL-23 levels in patients with AxSpA that positively correlated with stool calprotectin levels. Furthermore, stool IL-23 was negatively correlated with several stool amino acids, suggesting that increased amino acid metabolism by intestinal microbes may be associated with IL-23 production. *C. rodentium* and curdlan have both been shown to trigger the production of IL-23, though we did not measure this in our model[112,304]. We hypothesise that the production of IL-23 in a complex microbiota or the presence of *B. animalis* may be involved in triggering the differentiation of self-reactive T cells towards a pro-arthritogenic Th17 phenotype, thereby triggering disease. In the absence of bacteria to prime the immune system to support Th17 responses, we suggest that alternate immunological mechanisms drive the differentiation of self-reactive T cells into other pathogenic subsets to drive arthritis. Although targeting IL-23 is efficacious in the treatment of IBD, it is not effective in reducing disease in AxSpA[284]. Conversely, anti-IL-17A therapy has been shown to exacerbate intestinal inflammation, potentially due to the cytokine's role in maintaining barrier function, highlighting independent mechanisms in perpetuating inflammation in the intestine and the joint[239]. Notably, prophylactic inhibition of IL-23 in SKG mice and HLA-B27

transgenic rats prevents the onset of arthritis, whereas therapeutic inhibition of IL-23 does not attenuate arthritis in HLA-B27 rats[141,179]. Taken together we can hypothesise that an immunogenic trigger inducing IL-23 production may be important in the initiation of disease by driving a deranged Th17 response, which is independently maintained, and contributes to joint disease. To delineate this in our models, we will characterise myeloid cell subsets and their production of pro-inflammatory cytokines.

6.4 Microbiota-based therapies to treat established SpA

Manipulation of the intestinal microbiota may unlock therapeutic advancements for the treatment of inflammatory diseases, including SpA. Both broad and targeted approaches to microbiota-based therapeutics exist (figure 6.2), however leveraging gnotobiotic models aids in identifying appropriate targets relevant to the host and disease pathogenicity to prevent potential off target effects.

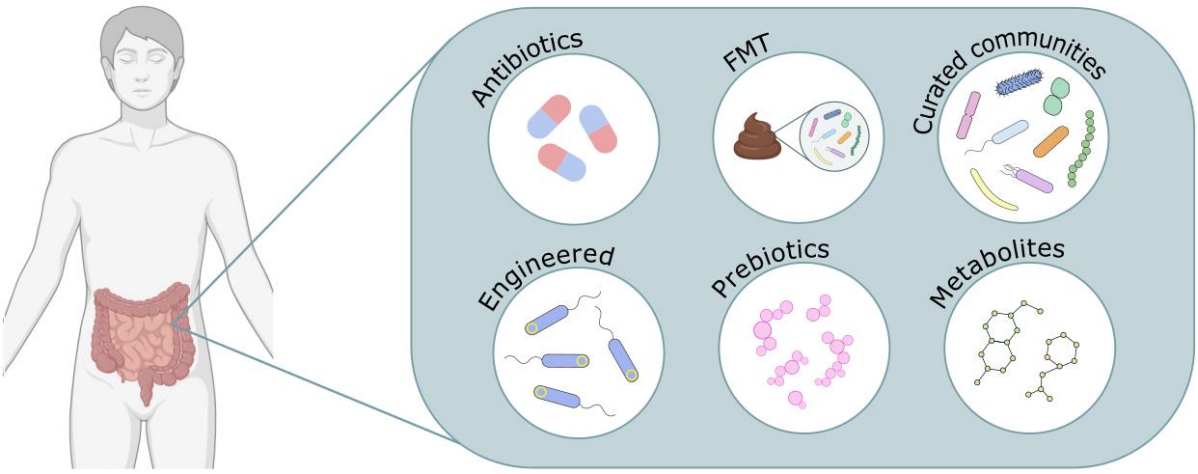


Figure 6.2 Microbiome-based therapies for treating inflammatory disease. Approaches to targeting the microbiome to restore intestinal homeostasis in the treatment of inflammatory disease. From left to right; antibiotics deplete the intestinal microbiota. Faecal microbiota transplant (FMT) involves transfer of an entire microbiota. Curation of communities can involve the administration of bacteria from single isolates to known communities. Bacteria can be engineered to promote a specific bacterial function such as production of a metabolite. Prebiotic treatment involves administration of bacterial substrates to induce beneficial compositional changes to the microbiome. Metabolite administration can target specific host pathways for therapeutic benefit. Figure informed by [312].

In this thesis we demonstrate that removal of the microbiota through antibiotic treatment does not attenuate disease in SKG mice. We further highlight the role of microbiota components in preparing

the immune system to respond to an immunogenic trigger. It may be that on a normal genetic background these immune responses provide protection to the host against pathogen invasion by reinforcing barrier integrity, as colonisation with SFB provides protection against *C. rodentium* infection[175]. On a genetically predisposed individual however, we suggest that these normally barrier-protective immune responses act as a double-edged sword and drive arthritic disease. This suggests that following the activation of these immune responses, targeted depletion of the microbiota would not provide any therapeutic benefit. Furthermore, targeting the microbiota to prevent the education of the immune system in the clinic is not feasible due to the early life stage in which this occurs, and the vulnerability to infection which would occur. Prophylactically preventing the colonisation of pathogens which may provide an immunogenic trigger to disease by manipulation of the commensal microbiota could yield therapeutic advantages, however, would require avoiding the triggering of host pro-inflammatory responses and therefore arthritic disease.

Whilst depletion of the microbiota to prevent the activation of pro-inflammatory pathways may not provide a meaningful therapy for SpA, targeting the microbiota to drive anti-inflammatory pathways may indeed suppress arthritogenic responses. In this regard, SCFAs produced by microbes can induce IL-10 production from T_{reg} cells whilst also reinforcing the intestinal barrier[58–60]. Patients with AxSpA display reduced abundances of butyrate-producing bacteria such as *Faecalibacterium prausnitzii* and *Eubacterium hallii,* as well as reduced potential for butyrate metabolism in the intestine[151]. In addition, SKG mice display impaired T_{reg} function and AxSpA patients display decreased T_{reg} cell frequencies, suggesting that a lack of suppression of arthritogenic T cell responses may contribute to disease pathogenesis[109,313]. Indeed, supplementation of SKG mice with butyrate attenuates arthritis and mice with collagen-induced arthritis also display attenuated disease with butyrate treatment due to an enrichment in regulatory B cells that can promote expansion of T_{reg} cells[164,282]. Overall, targeting the microbiota by either introduction of engineered butyrate “super-producers” or supplementation with butyrate itself may provide a novel therapy to SpA whilst not exacerbating intestinal symptoms, as observed with anti-IL-17

therapy[314]. In this thesis we also identified reductions in stool amino acids were associated with increased levels of the cytokine IL-23 and previous studies have highlighted an ability for amino acids to induce the differentiation of T cell subsets[63,64]. Modulating the availability of amino acids in the intestine may provide another therapeutic avenue to drive regulatory immune responses and the suppression of pro-arthritogenic responses.

6.5 Lessons from utilising germ-free animals

This thesis highlights the importance of considering the impairments of a germ-free immune system in studying the role of the intestinal microbiome in disease. Indeed, gnotobiology can be leveraged to provide significant insight into the causal role of the microbiome, and this role may be in providing education to a naïve immune system rather than a continual pro-inflammatory signal required to drive inflammation. It is important for researchers to recognise the context of the host immune system and predisposing genetics prior to labelling a specific microorganism as "pro-inflammatory" or "pro-arthritogenic". The interactions between the microbiota and the host are highly complex and context-specific, so rational, mechanistic approaches to targeting the microbiome are important in providing relevant therapeutic avenues for SpA.

6.6 Conclusion

Despite several correlative studies identifying a gut-joint connection and a role for the microbiome in SpA, the mechanisms driving these associations are not understood. By employing gnotobiotic techniques we have attributed causality to the microbiome in murine models of AxSpA and ReA and have demonstrated a role for specific bacterial components in programming the host immune system to support arthritis. Going forward, understanding the specific host-microbiota interactions driving the development of inflammatory disease will be crucial to inform the advancement of relevant and targeted microbiota-based therapeutics.

References

1. Hooper L V., MacPherson AJ. Immune adaptations that maintain homeostasis with the intestinal microbiota. *Nat Rev Immunol* 2010;**10**, DOI: 10.1038/nri2710.

2. Hou K, Wu ZX, Chen XY *et al.* Microbiota in health and diseases. *Signal Transduct Target Ther* 2022;**7**, DOI: 10.1038/s41392-022-00974-4.

3. Harrison OJ, Powrie FM. Regulatory T cells and immune tolerance in the intestine. *Cold Spring Harb Perspect Biol* 2013;**5**, DOI: 10.1101/cshperspect.a018341.

4. Cheng HY, Ning MX, Chen DK *et al.* Interactions between the gut microbiota and the host innate immune response against pathogens. *Front Immunol* 2019;**10**, DOI: 10.3389/fimmu.2019.00607.

5. Breban M, Tap J, Leboime A *et al.* Faecal microbiota study reveals specific dysbiosis in spondyloarthritis. *Ann Rheum Dis* 2017;**76**, DOI: 10.1136/annrheumdis-2016-211064.

6. Ciccia F, Guggino G, Rizzo A *et al.* Dysbiosis and zonulin upregulation alter gut epithelial and vascular barriers in patients with ankylosing spondylitis. *Ann Rheum Dis* 2017;**76**, DOI: 10.1136/annrheumdis-2016-210000.

7. Barbara G, Barbaro MR, Fuschi D *et al.* Inflammatory and Microbiota-Related Regulation of the Intestinal Epithelial Barrier. *Front Nutr* 2021;**8**, DOI: 10.3389/fnut.2021.718356.

8. Maloy KJ, Powrie F. Intestinal homeostasis and its breakdown in inflammatory bowel disease. *Nature* 2011;**474**, DOI: 10.1038/nature10208.

9. Ermund A, Schütte A, Johansson MEV *et al.* Studies of mucus in mouse stomach, small intestine, and colon. I. Gastrointestinal mucus layers have different properties depending on location

as well as over the Peyer's patches. *Am J Physiol Gastrointest Liver Physiol* 2013;**305**, DOI: 10.1152/ajpgi.00046.2013.

10. Cone RA. Barrier properties of mucus. *Adv Drug Deliv Rev* 2009;**61**, DOI: 10.1016/j.addr.2008.09.008.

11. Derrien M, Vaughan EE, Plugge CM *et al.* Akkermansia municiphila gen. nov., sp. nov., a human intestinal mucin-degrading bacterium. *Int J Syst Evol Microbiol* 2004;**54**, DOI: 10.1099/ijs.0.02873-0.

12. Johansson MEV, Phillipson M, Petersson J *et al.* The inner of the two Muc2 mucin-dependent mucus layers in colon is devoid of bacteria. *Proc Natl Acad Sci U S A* 2008;**105**, DOI: 10.1073/pnas.0803124105.

13. Paradis T, Bègue H, Basmaciyan L *et al.* Tight junctions as a key for pathogens invasion in intestinal epithelial cells. *Int J Mol Sci* 2021;**22**, DOI: 10.3390/ijms22052506.

14. Okumura R, Kurakawa T, Nakano T *et al.* Lypd8 promotes the segregation of flagellated microbiota and colonic epithelia. *Nature* 2016;**532**, DOI: 10.1038/nature17406.

15. Fukata M, Arditi M. The role of pattern recognition receptors in intestinal inflammation. *Mucosal Immunol* 2013;**6**, DOI: 10.1038/mi.2013.13.

16. Spadoni I, Zagato E, Bertocchi A *et al.* A gut-vascular barrier controls the systemic dissemination of bacteria. *Science (1979)* 2015;**350**, DOI: 10.1126/science.aad0135.

17. Brescia P, Rescigno M. The gut vascular barrier: a new player in the gut–liver–brain axis. *Trends Mol Med* 2021;**27**, DOI: 10.1016/j.molmed.2021.06.007.

18. Bazzoni G. Endothelial Cell-to-Cell Junctions: Molecular Organization and Role in Vascular Homeostasis. *Physiol Rev* 2004, DOI: 10.1152/physrev.00035.2003.

19. Spadoni I, Zagato E, Bertocchi A *et al.* A gut-vascular barrier controls the systemic dissemination of bacteria. *Science* 2015;**350**:830–4.

20. Gautreaux MD, Deitch EA, Berg RD. Bacterial translocation from the gastrointestinal tract to various segments of the mesenteric lymph node complex. *Infect Immun* 1994;**62**, DOI: 10.1128/iai.62.5.2132-2134.1994.

21. Jiao Y, Wu L, Huntington ND *et al.* Crosstalk Between Gut Microbiota and Innate Immunity and Its Implication in Autoimmune Diseases. *Front Immunol* 2020;**11**, DOI: 10.3389/fimmu.2020.00282.

22. Fournier BM, Parkos CA. The role of neutrophils during intestinal inflammation. *Mucosal Immunol* 2012;**5**, DOI: 10.1038/mi.2012.24.

23. Jukic A, Bakiri L, Wagner EF *et al.* Calprotectin: From biomarker to biological function. *Gut* 2021, DOI: 10.1136/gutjnl-2021-324855.

24. Jang MH, Sougawa N, Tanaka T *et al.* CCR7 Is Critically Important for Migration of Dendritic Cells in Intestinal Lamina Propria to Mesenteric Lymph Nodes. *The Journal of Immunology* 2006;**176**, DOI: 10.4049/jimmunol.176.2.803.

25. Kinnebrew MA, Pamer EG. Innate immune signaling in defense against intestinal microbes. *Immunol Rev* 2012;**245**, DOI: 10.1111/j.1600-065X.2011.01081.x.

26. Joeris T, Müller-Luda K, Agace WW *et al.* Diversity and functions of intestinal mononuclear phagocytes. *Mucosal Immunol* 2017;**10**, DOI: 10.1038/mi.2017.22.

27. Schulz O, Jaensson E, Persson EK *et al.* Intestinal CD103+, but not CX3CR1+, antigen sampling cells migrate in lymph and serve classical dendritic cell functions. *Journal of Experimental Medicine* 2009;**206**, DOI: 10.1084/jem.20091925.

28. Krause P, Morris V, Greenbaum JA *et al.* IL-10-producing intestinal macrophages prevent excessive antibacterial innate immunity by limiting IL-23 synthesis. *Nat Commun* 2015;**6**, DOI: 10.1038/ncomms8055.

29. Cruz CM, Rinna A, Forman HJ *et al.* ATP activates a reactive oxygen species-dependent oxidative stress response and secretion of proinflammatory cytokines in macrophages. *Journal of Biological Chemistry* 2007;**282**, DOI: 10.1074/jbc.M608083200.

30. Buonocore S, Ahern PP, Uhlig HH *et al.* Innate lymphoid cells drive interleukin-23-dependent innate intestinal pathology. *Nature* 2010;**464**, DOI: 10.1038/nature08949.

31. Sonnenberg GF, Monticelli LA, Elloso MM *et al.* CD4+ Lymphoid Tissue-Inducer Cells Promote Innate Immunity in the Gut. *Immunity* 2011;**34**, DOI: 10.1016/j.immuni.2010.12.009.

32. Melo-Gonzalez F, Kammoun H, Evren E *et al.* Antigen-presenting ILC3 regulate T cell-dependent IgA responses to colonic mucosal bacteria. *Journal of Experimental Medicine* 2019;**216**, DOI: 10.1084/jem.20180871.

33. Lyu M, Suzuki H, Kang L *et al.* ILC3s select microbiota-specific regulatory T cells to establish tolerance in the gut. *Nature* 2022;**610**, DOI: 10.1038/s41586-022-05141-x.

34. Chaplin DD. Overview of the immune response. *Journal of Allergy and Clinical Immunology* 2010;**125**, DOI: 10.1016/j.jaci.2009.12.980.

35. Dendrou CA, Petersen J, Rossjohn J *et al.* HLA variation and disease. *Nat Rev Immunol* 2018;**18**, DOI: 10.1038/nri.2017.143.

36. Ma H, Tao W, Zhu S. T lymphocytes in the intestinal mucosa: defense and tolerance. *Cell Mol Immunol* 2019;**16**, DOI: 10.1038/s41423-019-0208-2.

37. Mosmann TR, Cherwinski H, Bond MW *et al.* Two types of murine helper T cell clone. I. Definition according to profiles of lymphokine activities and secreted proteins. *The Journal of Immunology* 1986;**136**, DOI: 10.4049/jimmunol.136.7.2348.

38. Flynn JAL, Chan J, Triebold KJ *et al.* An essential role for interferon γ in resistance to mycobacterium tuberculosis infection. *Journal of Experimental Medicine* 1993;**178**, DOI: 10.1084/jem.178.6.2249.

39. Walker JA, McKenzie ANJ. TH2 cell development and function. *Nat Rev Immunol* 2018;**18**, DOI: 10.1038/nri.2017.118.

40. Harrington LE, Hatton RD, Mangan PR *et al.* Interleukin 17-producing CD4+ effector T cells develop via a lineage distinct from the T helper type 1 and 2 lineages. *Nat Immunol* 2005;**6**, DOI: 10.1038/ni1254.

41. Zelante T, De Luca A, Bonifazi P *et al.* IL-23 and the Th17 pathway promote inflammation and impair antifungal immune resistance. *Eur J Immunol* 2007;**37**, DOI: 10.1002/eji.200737409.

42. Martínez-López M, Iborra S, Conde-Garrosa R *et al.* Microbiota Sensing by Mincle-Syk Axis in Dendritic Cells Regulates Interleukin-17 and -22 Production and Promotes Intestinal Barrier Integrity. *Immunity* 2019;**50**, DOI: 10.1016/j.immuni.2018.12.020.

43. Lee JS, Tato CM, Joyce-Shaikh B *et al.* Interleukin-23-Independent IL-17 Production Regulates Intestinal Epithelial Permeability. *Immunity* 2015;**43**, DOI: 10.1016/j.immuni.2015.09.003.

44. Tesmer LA, Lundy SK, Sarkar S *et al.* Th17 cells in human disease. *Immunol Rev* 2008;**223**, DOI: 10.1111/j.1600-065X.2008.00628.x.

45. Sakaguchi S, Sakaguchi N, Shimizu J *et al.* Immunologic tolerance maintained by CD25+ CD4+ regulatory T cells: Their common role in controlling autoimmunity, tumor immunity, and transplantation tolerance. *Immunol Rev* 2001;**182**, DOI: 10.1034/j.1600-065X.2001.1820102.x.

46. Taguchi O, Kontani K, Ikeda H *et al.* Tissue-specific suppressor T cells involved in self-tolerance are activated extrathymically by self-antigens. *Immunology* 1994;**82**.

47. Chen WJ, Jin W, Hardegen N *et al.* Conversion of Peripheral CD4+CD25- Naive T Cells to CD4+CD25+ Regulatory T Cells by TGF-β Induction of Transcription Factor Foxp3. *Journal of Experimental Medicine* 2003;**198**, DOI: 10.1084/jem.20030152.

48. Ohnmacht C, Park JH, Cording S *et al.* The microbiota regulates type 2 immunity through RORγt+ T cells. *Science (1979)* 2015;**349**, DOI: 10.1126/science.aac4263.

49. Yang BH, Hagemann S, Mamareli P *et al.* Foxp3+ T cells expressing RORγt represent a stable regulatory T-cell effector lineage with enhanced suppressive capacity during intestinal inflammation. *Mucosal Immunol* 2016;**9**, DOI: 10.1038/mi.2015.74.

50. Sun L, Kong R, Li H *et al.* The Role of T Follicular Helper Cells and Interleukin-21 in the Pathogenesis of Inflammatory Bowel Disease. *Gastroenterol Res Pract* 2021;**2021**, DOI: 10.1155/2021/9621738.

51. Walker LSK. The link between circulating follicular helper T cells and autoimmunity. *Nat Rev Immunol* 2022;**22**, DOI: 10.1038/s41577-022-00693-5.

52. Hase K, Kawano K, Nochi T *et al.* Uptake through glycoprotein 2 of FimH + bacteria by M cells initiates mucosal immune response. *Nature* 2009;**462**, DOI: 10.1038/nature08529.

53. Phalipon A, Cardona A, Kraehenbuhl JP *et al.* Secretory component: A new role in secretory IgA-mediated immune exclusion in vivo. *Immunity* 2002;**17**, DOI: 10.1016/S1074-7613(02)00341-2.

54. Hooper L V., MacPherson AJ. Immune adaptations that maintain homeostasis with the intestinal microbiota. *Nat Rev Immunol* 2010, DOI: 10.1038/nri2710.

55. Eckburg PB, Bik EM, Bernstein CN *et al.* Microbiology: Diversity of the human intestinal microbial flora. *Science (1979)* 2005;**308**, DOI: 10.1126/science.1110591.

56. Arumugam M, Raes J, Pelletier E *et al.* Enterotypes of the human gut microbiome. *Nature* 2011, DOI: 10.1038/nature09944.

57. Duncan SH, Louis P, Flint HJ. Lactate-utilizing bacteria, isolated from human feces, that produce butyrate as a major fermentation product. *Appl Environ Microbiol* 2004;**70**, DOI: 10.1128/AEM.70.10.5810-5817.2004.

58. Wang HB, Wang PY, Wang X *et al.* Butyrate enhances intestinal epithelial barrier function via up-regulation of tight junction protein claudin-1 transcription. *Dig Dis Sci* 2012;**57**, DOI: 10.1007/s10620-012-2259-4.

59. Schulthess J, Pandey S, Capitani M *et al.* The Short Chain Fatty Acid Butyrate Imprints an Antimicrobial Program in Macrophages. *Immunity* 2019;**50**, DOI: 10.1016/j.immuni.2018.12.018.

60. Sun M, Wu W, Chen L *et al.* Microbiota-derived short-chain fatty acids promote Th1 cell IL-10 production to maintain intestinal homeostasis. *Nat Commun* 2018;**9**, DOI: 10.1038/s41467-018-05901-2.

61. Lee JH, Lee J. Indole as an intercellular signal in microbial communities. *FEMS Microbiol Rev* 2010;**34**, DOI: 10.1111/j.1574-6976.2009.00204.x.

62. Schiering C, Wincent E, Metidji A *et al.* Feedback control of AHR signalling regulates intestinal immunity. *Nature* 2017;**542**, DOI: 10.1038/nature21080.

63. Sinclair L V., Rolf J, Emslie E *et al.* Control of amino-acid transport by antigen receptors coordinates the metabolic reprogramming essential for T cell differentiation. *Nat Immunol* 2013;**14**, DOI: 10.1038/ni.2556.

64. Nakaya M, Xiao Y, Zhou X *et al.* Inflammatory T cell responses rely on amino acid transporter ASCT2 facilitation of glutamine uptake and mTORC1 kinase activation. *Immunity* 2014;**40**, DOI: 10.1016/j.immuni.2014.04.007.

65. Puleston DJ, Baixauli F, Sanin DE *et al.* Polyamine metabolism is a central determinant of helper T cell lineage fidelity. *Cell* 2021;**184**, DOI: 10.1016/j.cell.2021.06.007.

66. Lotz M, Gütle D, Walther S *et al.* Postnatal acquisition of endotoxin tolerance in intestinal epithelial cells. *Journal of Experimental Medicine* 2006;**203**, DOI: 10.1084/jem.20050625.

67. Round JL, Lee SM, Li J *et al.* The toll-like receptor 2 pathway establishes colonization by a commensal of the human microbiota. *Science (1979)* 2011;**332**, DOI: 10.1126/science.1206095.

68. Stolwijk C, van Onna M, Boonen A *et al.* Global Prevalence of Spondyloarthritis: A Systematic Review and Meta-Regression Analysis. *Arthritis Care Res (Hoboken)* 2016;**68**, DOI: 10.1002/acr.22831.

69. Voruganti A, Bowness P. New developments in our understanding of ankylosing spondylitis pathogenesis. *Immunology* 2020;**161**, DOI: 10.1111/imm.13242.

70. Payet J, Gossec L, Paternotte S *et al.* Prevalence and clinical characteristics of dactylitis in spondylarthritis: A descriptive analysis of 275 patients. *Clin Exp Rheumatol* 2012;**30**.

71. Rademacher J, Poddubnyy D, Pleyer U. Uveitis in spondyloarthritis. *Ther Adv Musculoskelet Dis* 2020;**12**, DOI: 10.1177/1759720X20951733.

72. Schwartzman M, Ermann J, Kuhn KA *et al.* Spondyloarthritis in inflammatory bowel disease cohorts: Systematic literature review and critical appraisal of study designs. *RMD Open* 2022;**8**, DOI: 10.1136/rmdopen-2021-001777.

73. Simenon G, Van Gossum A, Adler M *et al.* Macroscopic and microscopic gut lesions in seronegative spondyloarthropathies. *Journal of Rheumatology* 1990;**17**.

74. Stolwijk C, Van Tubergen A, Castillo-Ortiz JD *et al.* Prevalence of extra-articular manifestations in patients with ankylosing spondylitis: A systematic review and meta-analysis. *Ann Rheum Dis* 2015;**74**, DOI: 10.1136/annrheumdis-2013-203582.

75. Leirisalo M, Skylv G, Kousa M *et al.* Followup study on patients with reiter's disease and reactive arthritis, with special reference to HLA—B27. *Arthritis Rheum* 1982;**25**, DOI: 10.1002/art.1780250302.

76. Leirisalo-Repo M, Helenius P, Hannu T *et al.* Long term prognosis of reactive salmonella arthritis. *Ann Rheum Dis* 1997;**56**, DOI: 10.1136/ard.56.9.516.

77. Schlosstein L, Terasaki PI, Bluestone R *et al.* High Association of an HL-A Antigen, W27, with Ankylosing Spondylitis. *New England Journal of Medicine* 1973;**288**, DOI: 10.1056/nejm197304052881403.

78. Mallas EG, Mackintosh P, Asquith P *et al.* Histocompatibility antigens in inflammatory bowel disease; their clinical significance and their association with arthropathy with special reference to HLA B27 (W27). *Gut* 1976;**17**, DOI: 10.1136/gut.17.11.906.

79. Robinson PC, van der Linden S, Khan MA *et al.* Axial spondyloarthritis: concept, construct, classification and implications for therapy. *Nat Rev Rheumatol* 2021;**17**, DOI: 10.1038/s41584-020-00552-4.

80. Gofton JP, Chalmers A, Price GE *et al.* HL-A 27 and ankylosing spondylitis in B.C. Indians. *Journal of Rheumatology* 1984;**11**.

81. Rusman T, van Vollenhoven RF, van der Horst-Bruinsma IE. Gender Differences in Axial Spondyloarthritis: Women Are Not So Lucky. *Curr Rheumatol Rep* 2018;**20**, DOI: 10.1007/s11926-018-0744-2.

82. Baeten D, Sieper J, Braun J *et al.* Secukinumab, an Interleukin-17A Inhibitor, in Ankylosing Spondylitis. *New England Journal of Medicine* 2015;**373**, DOI: 10.1056/nejmoa1505066.

83. Danve A, Deodhar A. Treatment of axial spondyloarthritis: an update. *Nat Rev Rheumatol* 2022;**18**, DOI: 10.1038/s41584-022-00761-z.

84. Pennisi M, Perdue J, Roulston T *et al.* An overview of reactive arthritis. *J Am Acad Physician Assist* 2019;**32**, DOI: 10.1097/01.JAA.0000558320.47868.2f.

85. Brown MA, Laval SH, Brophy S *et al.* Recurrence risk modelling of the genetic susceptibility to ankylosing spondylitis. *Ann Rheum Dis* 2000;**59**, DOI: 10.1136/ard.59.11.883.

86. Burton PR, Clayton DG, Cardon LR *et al.* Association scan of 14,500 nonsynonymous SNPs in four diseases identifies autoimmunity variants. *Nat Genet* 2007;**39**, DOI: 10.1038/ng.2007.17.

87. Arévalo M, Gratacós Masmitjà J, Moreno M *et al.* Influence of HLA-B27 on the Ankylosing Spondylitis phenotype: Results from the REGISPONSER database. *Arthritis Res Ther* 2018;**20**, DOI: 10.1186/s13075-018-1724-7.

88. Robinson J, Soormally AR, Hayhurst JD *et al.* The IPD-IMGT/HLA Database - New developments in reporting HLA variation. *Hum Immunol* 2016;**77**, DOI: 10.1016/j.humimm.2016.01.020.

89. Bowness P. HLA B27 in health and disease: A double-edged sword? *Rheumatology* 2002;**41**, DOI: 10.1093/rheumatology/41.8.857.

90. Hammer RE, Maika SD, Richardson JA *et al.* Spontaneous inflammatory disease in transgenic rats expressing HLA-B27 and human β2m: An animal model of HLA-B27-associated human disorders. *Cell* 1990;**63**, DOI: 10.1016/0092-8674(90)90512-D.

91. Yin J, Sternes PR, Wang M *et al.* Shotgun metagenomics reveals an enrichment of potentially cross-reactive bacterial epitopes in ankylosing spondylitis patients, as well as the effects of TNFi therapy upon microbiome composition. *Ann Rheum Dis* 2020;**79**, DOI: 10.1136/annrheumdis-2019-215763.

92. Hermann E, Meyer zum Büschenfelde KH, Fleischer B *et al.* HLA-B27-restricted CD8 T cells derived from synovial fluids of patients with reactive arthritis and ankylosing spondylitis. *The Lancet* 1993;**342**, DOI: 10.1016/0140-6736(93)91760-J.

93. Mear JP, Schreiber KL, Münz C *et al.* Misfolding of HLA-B27 as a result of its B pocket suggests a novel mechanism for its role in susceptibility to spondyloarthropathies. *J Immunol* 1999;**163**.

94. Goodall JC, Wu C, Zhang Y *et al.* Endoplasmic reticulum stress-induced transcription factor, CHOP, is crucial for dendritic cell IL-23 expression. *Proc Natl Acad Sci U S A* 2010;**107**, DOI: 10.1073/pnas.1011736107.

95. Bird LA, Peh CA, Kollnbeger S *et al.* Lymphoblastoid cells express HLA-B27 homodimers both intracellularly and at the cell surface following endosomal recycling. *Eur J Immunol* 2003;**33**, DOI: 10.1002/eji.200323678.

96. Chan AT, Kollnberger SD, Wedderburn LR *et al.* Expansion and enhanced survival of natural killer cells expressing the killer immunoglobulin-like receptor KIR3DL2 in spondylarthritis. *Arthritis Rheum* 2005;**52**, DOI: 10.1002/art.21395.

97. Tran TM, Dorris ML, Satumtira N *et al.* Additional human β2-microglobulin curbs HLA-B27 misfolding and promotes arthritis and spondylitis without colitis in male HLA-B27-transgenic rats. *Arthritis Rheum* 2006;**54**, DOI: 10.1002/art.21740.

98. Peeters H, Vander Cruyssen B, Laukens D *et al.* Radiological sacroiliitis, a hallmark of spondylitis, is linked with CARD15 gene polymorphisms in patients with Crohn's disease. *Ann Rheum Dis* 2004;**63**, DOI: 10.1136/ard.2004.021774.

99. Laukens D, Peeters H, Marichal D *et al.* CARD15 gene polymorphisms in patients with spondyloarthropathies identify a specific phenotype previously related to Crohn's disease. *Ann Rheum Dis* 2005;**64**, DOI: 10.1136/ard.2004.028837.

100. Inohara N, Ogura Y, Fontalba A *et al.* Host recognition of bacterial muramyl dipeptide mediated through NOD2: Implications for Crohn's disease. *Journal of Biological Chemistry* 2003;**278**, DOI: 10.1074/jbc.C200673200.

101. Ji H, Gauguier D, Ohmura K *et al.* Genetic influences on the end-stage effector phase of arthritis. *Journal of Experimental Medicine* 2001;**194**, DOI: 10.1084/jem.194.3.321.

102. Kouskoff V, Korganow AS, Duchatelle V *et al.* Organ-specific disease provoked by systemic autoimmunity. *Cell* 1996;**87**, DOI: 10.1016/S0092-8674(00)81989-3.

103. Akitsu A, Ishigame H, Kakuta S *et al.* IL-1 receptor antagonist-deficient mice develop autoimmune arthritis due to intrinsic activation of IL-17-producing CCR2 + Vγ6 + γδT cells. *Nat Commun* 2015;**6**, DOI: 10.1038/ncomms8464.

104. Di Genaro MS, Cargnelutti DE, Eliçabe JR *et al.* Role of TNFRp55 in Yersinia enterocolitica O:3-induced arthritis: Triggering bacterial antigens and articular immune response. *Rheumatology* 2007;**46**, DOI: 10.1093/rheumatology/kel348.

105. Eliçabe RJ, Cargnelutti E, Serer MI *et al.* Lack of TNFR p55 Results in Heightened Expression of IFN-γ and IL-17 during the Development of Reactive Arthritis. *The Journal of Immunology* 2010;**185**, DOI: 10.4049/jimmunol.0902245.

106. Granfors K, Jalkanen S, Mäki-Ikola O *et al.* Salmonella lipopolysaccharide in synovial cells from patients with reactive arthritis. *The Lancet* 1990;**335**, DOI: 10.1016/0140-6736(90)90804-E.

107. Sakaguchi N, Takahashi T, Hata H *et al.* Altered thymic T-cell selection due to a mutation of the ZAP-70 gene causes autoimmune arthritis in mice. *Nature* 2003;**426**, DOI: 10.1038/nature02119.

108. Hirota K, Hashimoto M, Yoshitomi H *et al.* T cell self-reactivity forms a cytokine milieu for spontaneous development of IL-17+ Th cells that cause autoimmune arthritis. *Journal of Experimental Medicine* 2007;**204**, DOI: 10.1084/jem.20062259.

109. Tanaka S, Maeda S, Hashimoto M *et al.* Graded Attenuation of TCR Signaling Elicits Distinct Autoimmune Diseases by Altering Thymic T Cell Selection and Regulatory T Cell Function. *The Journal of Immunology* 2010;**185**, DOI: 10.4049/jimmunol.1000848.

110. Yoshitomi H, Sakaguchi N, Kobayashi K *et al.* A role for fungal β-glucans and their receptor Dectin-1 in the induction of autoimmune arthritis in genetically susceptible mice. *Journal of Experimental Medicine* 2005;**201**, DOI: 10.1084/jem.20041758.

111. Ciccia F, Guggino G, Rizzo A *et al.* Type 3 innate lymphoid cells producing IL-17 and IL-22 are expanded in the gut, in the peripheral blood, synovial fluid and bone marrow of patients with ankylosing spondylitis. *Ann Rheum Dis* 2015;**74**, DOI: 10.1136/annrheumdis-2014-206323.

112. LeibundGut-Landmann S, Groß O, Robinson MJ *et al.* Syk- and CARD9-dependent coupling of innate immunity to the induction of T helper cells that produce interleukin 17. *Nat Immunol* 2007;**8**, DOI: 10.1038/ni1460.

113. Benham H, Rehaume LM, Hasnain SZ *et al.* Interleukin-23 mediates the intestinal response to microbial β-1,3-glucan and the development of spondyloarthritis pathology in SKG mice. *Arthritis and Rheumatology* 2014;**66**, DOI: 10.1002/art.38638.

114. Baillet AC, Rehaume LM, Benham H *et al.* High Chlamydia burden promotes tumor necrosis factor-dependent reactive arthritis in SKG mice. *Arthritis and Rheumatology* 2015;**67**, DOI: 10.1002/art.39041.

115. De Vos M, Cuvelier C, Mielants H *et al.* Ileocolonoscopy in seronegative spondylarthropathy. *Gastroenterology* 1989;**96**, DOI: 10.1016/0016-5085(89)91557-6.

116. Chassaing B, Koren O, Goodrich JK *et al.* Dietary emulsifiers impact the mouse gut microbiota promoting colitis and metabolic syndrome. *Nature* 2015;**519**, DOI: 10.1038/nature14232.

117. Matei DE, Menon M, Alber DG *et al.* Intestinal barrier dysfunction plays an integral role in arthritis pathology and can be targeted to ameliorate disease. *Med* 2021;**2**, DOI: 10.1016/j.medj.2021.04.013.

118. Henderson IR, Czeczulin J, Eslava C *et al.* Characterization of Pic, a secreted protease of Shigella flexneri and enteroaggregative Escherichia coli. *Infect Immun* 1999;**67**, DOI: 10.1128/iai.67.11.5587-5596.1999.

119. Li X, Bleumink-Pluym NMC, Luijkx YMCA *et al.* MUC1 is a receptor for the Salmonella SiiE adhesin that enables apical invasion into enterocytes. *PLoS Pathog* 2019;**15**, DOI: 10.1371/journal.ppat.1007566.

120. Viladomiu M, Kivolowitz C, Abdulhamid A *et al.* IgA-coated E. Coli enriched in Crohn's disease spondyloarthritis promote TH17-dependent inflammation. *Sci Transl Med* 2017;**9**, DOI: 10.1126/scitranslmed.aaf9655.

121. Gill T, Stauffer P, Asquith M *et al.* Axial spondyloarthritis patients have altered mucosal IgA response to oral and fecal microbiota. *bioRxiv* 2021.

122. Tajik N, Frech M, Schulz O *et al.* Targeting zonulin and intestinal epithelial barrier function to prevent onset of arthritis. *Nat Commun* 2020;**11**, DOI: 10.1038/s41467-020-15831-7.

123. Luchetti MM, Ciccia F, Avellini C *et al.* Gut epithelial impairment, microbial translocation and immune system activation in inflammatory bowel disease-Associated spondyloarthritis. *Rheumatology (United Kingdom)* 2021;**60**, DOI: 10.1093/rheumatology/keaa164.

124. Stan R v., Tse D, Deharvengt SJ *et al.* The Diaphragms of Fenestrated Endothelia: Gatekeepers of Vascular Permeability and Blood Composition. *Dev Cell* 2012;**23**, DOI: 10.1016/j.devcel.2012.11.003.

125. Wallis D, Asaduzzaman A, Weisman M *et al.* Elevated serum anti-flagellin antibodies implicate subclinical bowel inflammation in ankylosing spondylitis: An observational study. *Arthritis Res Ther* 2013;**15**, DOI: 10.1186/ar4350.

126. Demetter P, De Vos M, Van Huysse JA *et al.* Colon mucosa of patients both with spondyloarthritis and Crohn's disease is enriched with macrophages expressing the scavenger receptor CD163. *Ann Rheum Dis* 2005;**64**, DOI: 10.1136/ard.2003.018382.

127. Flak MB, Colas RA, Muñoz-Atienza E *et al.* Inflammatory arthritis disrupts gut resolution mechanisms, promoting barrier breakdown by Porphyromonas gingivalis. *JCI Insight* 2019;**4**, DOI: 10.1172/jci.insight.125191.

128. Ciccia F, Guggino G, Zeng M *et al.* Proinflammatory CX3CR1+CD59+Tumor Necrosis Factor–Like Molecule 1A+Interleukin-23+ Monocytes Are Expanded in Patients With Ankylosing Spondylitis and Modulate Innate Lymphoid Cell 3 Immune Functions. *Arthritis and Rheumatology* 2018;**70**, DOI: 10.1002/art.40582.

129. Udalova IA, Mantovani A, Feldmann M. Macrophage heterogeneity in the context of rheumatoid arthritis. *Nat Rev Rheumatol* 2016;**12**, DOI: 10.1038/nrrheum.2016.91.

130. Salmi M, Rajala P, Jalkanen S. Homing of mucosal leukocytes to joints: Distinct endothelial ligands in synovium mediate leukocyte-subtype specific adhesion. *Journal of Clinical Investigation* 1997;**99**, DOI: 10.1172/JCI119389.

131. Silva JE, Mayordomo AC, Dave MN *et al.* Dendritic Cells of Mesenteric and Regional Lymph Nodes Contribute to Yersinia enterocolitica O:3–Induced Reactive Arthritis in TNFRp55 −/− Mice . *The Journal of Immunology* 2020;**204**, DOI: 10.4049/jimmunol.1901137.

132. Jandus C, Bioley G, Rivals JP *et al.* Increased numbers of circulating polyfunctional Th17 memory cells in patients with seronegative spondylarthritides. *Arthritis Rheum* 2008;**58**, DOI: 10.1002/art.23655.

133. Shen H, Goodall JC, Hill Gaston JS. Frequency and phenotype of peripheral blood Th17 cells in ankylosing spondylitis and rheumatoid arthritis. *Arthritis Rheum* 2009;**60**, DOI: 10.1002/art.24568.

134. Wu HJ, Ivanov II, Darce J *et al.* Gut-residing segmented filamentous bacteria drive autoimmune arthritis via T helper 17 cells. *Immunity* 2010;**32**, DOI: 10.1016/j.immuni.2010.06.001.

135. Tan TG, Sefik E, Geva-Zatorsky N *et al.* Identifying species of symbiont bacteria from the human gut that, alone, can induce intestinal Th17 cells in mice. *Proc Natl Acad Sci U S A* 2016;**113**, DOI: 10.1073/pnas.1617460113.

136. Wang X, Lin Z, Wei Q *et al.* Expression of IL-23 and IL-17 and effect of IL-23 on IL-17 production in ankylosing spondylitis. *Rheumatol Int* 2009;**29**, DOI: 10.1007/s00296-009-0883-x.

137. Ciccia F, Bombardieri M, Principato A *et al.* Overexpression of interleukin-23, but Not interleukin-17, as an immunologic signature of Subclinical intestinal inflammation in ankylosing spondylitis. *Arthritis Rheum* 2009;**60**, DOI: 10.1002/art.24389.

138. DeLay ML, Turner MJ, Klenk EI *et al.* HLA-B27 misfolding and the unfolded protein response augment interleukin-23 production and are associated with Th17 activation in transgenic rats. *Arthritis Rheum* 2009;**60**, DOI: 10.1002/art.24763.

139. Antoniou AN, Lenart I, Kriston-Vizi J *et al.* Salmonella exploits HLA-B27 and host unfolded protein responses to promote intracellular replication. *Ann Rheum Dis* 2019;**78**, DOI: 10.1136/annrheumdis-2018-213532.

140. Baeten D, Østergaard M, Wei JCC *et al.* Risankizumab, an IL-23 inhibitor, for ankylosing spondylitis: Results of a randomised, double-blind, placebo-controlled, proof-of-concept, dose-finding phase 2 study. *Ann Rheum Dis* 2018;**77**, DOI: 10.1136/annrheumdis-2018-213328.

141. van Tok MN, Na S, Lao CR *et al.* The initiation, but not the persistence, of experimental spondyloarthritis is dependent on interleukin-23 signaling. *Front Immunol* 2018;**9**, DOI: 10.3389/fimmu.2018.01550.

142. Regner EH, Ohri N, Stahly A *et al.* Functional intraepithelial lymphocyte changes in inflammatory bowel disease and spondyloarthritis have disease specific correlations with intestinal microbiota. *Arthritis Res Ther* 2018;**20**, DOI: 10.1186/s13075-018-1639-3.

143. Coombes JL, Powrie F. Dendritic cells in intestinal immune regulation. *Nat Rev Immunol* 2008;**8**, DOI: 10.1038/nri2335.

144. Wright PB, McEntegart A, McCarey D *et al.* Ankylosing spondylitis patients display altered dendritic cell and T cell populations that implicate pathogenic roles for the IL-23 cytokine axis and intestinal inflammation. *Rheumatology (United Kingdom)* 2016;**55**, DOI: 10.1093/rheumatology/kev245.

145. Lim CH, Voedisch S, Wahl B *et al.* Independent Bottlenecks Characterize Colonization of Systemic Compartments and Gut Lymphoid Tissue by Salmonella. *PLoS Pathog* 2014;**10**, DOI: 10.1371/journal.ppat.1004270.

146. Rojas M, Restrepo-Jiménez P, Monsalve DM *et al.* Molecular mimicry and autoimmunity. *J Autoimmun* 2018;**95**, DOI: 10.1016/j.jaut.2018.10.012.

147. Yuki N, Shahrizaila N. Guillain-Barré syndrome animal model: The first proof of molecular mimicry in human autoimmune disorder. *J Biomed Biotechnol* 2011;**2011**, DOI: 10.1155/2011/829129.

148. Wucherpfennig KW, Strominger JL. Molecular mimicry in T cell-mediated autoimmunity: Viral peptides activate human T cell clones specific for myelin basic protein. *Cell* 1995;**80**, DOI: 10.1016/0092-8674(95)90348-8.

149. Coppieters KT, Wiberg A, von Herrath MG. Viral infections and molecular mimicry in type 1 diabetes. *APMIS* 2012;**120**, DOI: 10.1111/apm.12011.

150. Miyauchi E, Kim SW, Suda W *et al.* Gut microorganisms act together to exacerbate inflammation in spinal cords. *Nature* 2020;**585**, DOI: 10.1038/s41586-020-2634-9.

151. Zhou C, Zhao H, Xiao X yue *et al.* Metagenomic profiling of the pro-inflammatory gut microbiota in ankylosing spondylitis. *J Autoimmun* 2020;**107**, DOI: 10.1016/j.jaut.2019.102360.

152. Ramos M, Alvarez I, Sesma L *et al.* Molecular mimicry of an HLA-B27-derived ligand of arthritis-linked subtypes with chlamydial proteins. *Journal of Biological Chemistry* 2002;**277**, DOI: 10.1074/jbc.M205470200.

153. Manasson J, Shen N, Garcia Ferrer HR *et al.* Gut Microbiota Perturbations in Reactive Arthritis and Postinfectious Spondyloarthritis. *Arthritis and Rheumatology* 2018;**70**, DOI: 10.1002/art.40359.

154. Clemente JC, Manasson J, Scher JU. The role of the gut microbiome in systemic inflammatory disease. *BMJ (Online)* 2018;**360**, DOI: 10.1136/bmj.j5145.

155. Janney A, Powrie F, Mann EH. Host–microbiota maladaptation in colorectal cancer. *Nature* 2020;**585**, DOI: 10.1038/s41586-020-2729-3.

156. Durazzi F, Sala C, Castellani G *et al.* Comparison between 16S rRNA and shotgun sequencing data for the taxonomic characterization of the gut microbiota. *Sci Rep* 2021;**11**, DOI: 10.1038/s41598-021-82726-y.

157. Scher JU, Littman DR, Abramson SB. Review: Microbiome in Inflammatory Arthritis and Human Rheumatic Diseases. *Arthritis and Rheumatology* 2016;**68**, DOI: 10.1002/art.39259.

158. Ebringer RW, Cawdell DR, Cowling P *et al.* Sequential studies in ankylosing spondylitis. Association of Klebsiella pneumoniae with active disease. *Ann Rheum Dis* 1978;**37**, DOI: 10.1136/ard.37.2.146.

159. Klingberg E, Magnusson MK, Strid H *et al.* A distinct gut microbiota composition in patients with ankylosing spondylitis is associated with increased levels of fecal calprotectin. *Arthritis Res Ther* 2019;**21**, DOI: 10.1186/s13075-019-2018-4.

160. Qin J, Li R, Raes J *et al.* A human gut microbial gene catalogue established by metagenomic sequencing. *Nature* 2010;**464**, DOI: 10.1038/nature08821.

161. Tito RY, Cypers H, Joossens M *et al.* Brief Report: Dialister as a Microbial Marker of Disease Activity in Spondyloarthritis. *Arthritis and Rheumatology* 2017;**69**, DOI: 10.1002/art.39802.

162. Stebbings S, Munro K, Simon MA *et al.* Comparison of the faecal microflora of patients with ankylosing spondylitis and controls using molecular methods of analysis. *Rheumatology* 2002;**41**, DOI: 10.1093/rheumatology/41.12.1395.

163. Shao T juan, He Z xing, Xie Z jun *et al.* Characterization of ankylosing spondylitis and rheumatoid arthritis using 1H NMR-based metabolomics of human fecal extracts. *Metabolomics* 2016;**12**, DOI: 10.1007/s11306-016-1000-2.

164. Min HK, Na HS, Jhun JY *et al.* Identification of gut dysbiosis in axial spondyloarthritis patients and improvement of experimental ankylosing spondyloarthritis by microbiome-derived butyrate with immune-modulating function. *Front Immunol* 2023;**14**, DOI: 10.3389/fimmu.2023.1096565.

165. Berlinberg AJ, Regner EH, Stahly A *et al.* Multi 'Omics Analysis of Intestinal Tissue in Ankylosing Spondylitis Identifies Alterations in the Tryptophan Metabolism Pathway. *Front Immunol* 2021;**12**, DOI: 10.3389/fimmu.2021.587119.

166. Stoll ML, Kumar R, Lefkowitz EJ *et al.* Fecal metabolomics in pediatric spondyloarthritis implicate decreased metabolic diversity and altered tryptophan metabolism as pathogenic factors. *Genes Immun* 2016;**17**, DOI: 10.1038/gene.2016.38.

167. Blijdorp ICJ, Menegatti S, van Mens LJJ *et al.* Expansion of Interleukin-22– and Granulocyte–Macrophage Colony-Stimulating Factor–Expressing, but Not Interleukin-17A–Expressing, Group 3

Innate Lymphoid Cells in the Inflamed Joints of Patients With Spondyloarthritis. *Arthritis and Rheumatology* 2019;**71**, DOI: 10.1002/art.40736.

168. Asquith M, Davin S, Stauffer P *et al.* Intestinal Metabolites Are Profoundly Altered in the Context of HLA–B27 Expression and Functionally Modulate Disease in a Rat Model of Spondyloarthritis. *Arthritis and Rheumatology* 2017;**69**, DOI: 10.1002/art.40183.

169. Asquith M, Sternes PR, Costello ME *et al.* HLA Alleles Associated With Risk of Ankylosing Spondylitis and Rheumatoid Arthritis Influence the Gut Microbiome. *Arthritis and Rheumatology* 2019;**71**, DOI: 10.1002/art.40917.

170. Gill T, Brooks SR, Rosenbaum JT *et al.* Novel Inter-omic Analysis Reveals Relationships Between Diverse Gut Microbiota and Host Immune Dysregulation in HLA–B27–Induced Experimental Spondyloarthritis. *Arthritis and Rheumatology* 2019;**71**, DOI: 10.1002/art.41018.

171. Rath HC, Wilson KH, Sartor RB. Differential induction of colitis and gastritis in HLA-B27 transgenic rats selectively colonized with Bacteroides vulgatus or Escherichia coli. *Infect Immun* 1999;**67**, DOI: 10.1128/iai.67.6.2969-2974.1999.

172. Kubinak JL, Stephens WZ, Soto R *et al.* MHC variation sculpts individualized microbial communities that control susceptibility to enteric infection. *Nat Commun* 2015;**6**, DOI: 10.1038/ncomms9642.

173. Chen J, Zhang S, Feng X *et al.* Conventional co-housing modulates murine gut microbiota and hematopoietic gene expression. *Int J Mol Sci* 2020;**21**, DOI: 10.3390/ijms21176143.

174. Majlessi L, Sayes F, Bureau JF *et al.* Colonization with Helicobacter is concomitant with modified gut microbiota and drastic failure of the immune control of Mycobacterium tuberculosis. *Mucosal Immunol* 2017;**10**, DOI: 10.1038/mi.2016.140.

175. Ivanov II, Atarashi K, Manel N *et al.* Induction of Intestinal Th17 Cells by Segmented Filamentous Bacteria. *Cell* 2009;**139**, DOI: 10.1016/j.cell.2009.09.033.

176. Thomson CA, Morgan SC, Ohland C *et al.* From germ-free to wild: modulating microbiome complexity to understand mucosal immunology. *Mucosal Immunol* 2022;**15**, DOI: 10.1038/s41385-022-00562-3.

177. Jeffery R. Delineating the causal role of the gut microbiota in experimental colitis. 2022.

178. Yi P, Li LJ. The germfree murine animal: An important animal model for research on the relationship between gut microbiota and the host. *Vet Microbiol* 2012;**157**, DOI: 10.1016/j.vetmic.2011.10.024.

179. Rehaume LM, Mondot S, Aguirre De Cárcer D *et al.* ZAP-70 genotype disrupts the relationship between microbiota and host, leading to spondyloarthritis and ileitis in SKG mice. *Arthritis and Rheumatology* 2014;**66**, DOI: 10.1002/art.38773.

180. Rogier R, Ederveen THA, Boekhorst J *et al.* Aberrant intestinal microbiota due to IL-1 receptor antagonist deficiency promotes IL-17- and TLR4-dependent arthritis. *Microbiome* 2017;**5**, DOI: 10.1186/s40168-017-0278-2.

181. Macpherson AJ, Harris NL. Interactions between commensal intestinal bacteria and the immune system. *Nat Rev Immunol* 2004;**4**, DOI: 10.1038/nri1373.

182. Bunker JJ, Erickson SA, Flynn TM *et al.* Natural polyreactive IgA antibodies coat the intestinal microbiota. *Science (1979)* 2017;**358**, DOI: 10.1126/science.aan6619.

183. Round JL, Mazmanian SK. Inducible Foxp3+ regulatory T-cell development by a commensal bacterium of the intestinal microbiota. *Proc Natl Acad Sci U S A* 2010;**107**, DOI: 10.1073/pnas.0909122107.

184. Stefka AT, Feehley T, Tripathi P *et al.* Commensal bacteria protect against food allergen sensitization. *Proc Natl Acad Sci U S A* 2014;**111**, DOI: 10.1073/pnas.1412008111.

185. Olszak T, An D, Zeissig S *et al.* Microbial exposure during early life has persistent effects on natural killer T cell function. *Science (1979)* 2012;**336**, DOI: 10.1126/science.1219328.

186. Block KE, Zheng Z, Dent AL *et al.* Gut Microbiota Regulates K/BxN Autoimmune Arthritis through Follicular Helper T but Not Th17 Cells. *The Journal of Immunology* 2016;**196**, DOI: 10.4049/jimmunol.1501904.

187. Dieleman LA, Goerres MS, Arends A *et al.* Lactobacillus GG prevents recurrence of colitis in HLA-B27 transgenic rats after antibiotic treatment. *Gut* 2003;**52**, DOI: 10.1136/gut.52.3.370.

188. Garrett WS, Lord GM, Punit S *et al.* Communicable Ulcerative Colitis Induced by T-bet Deficiency in the Innate Immune System. *Cell* 2007;**131**, DOI: 10.1016/j.cell.2007.08.017.

189. Fagarasan S, Muramatsu M, Suzuki K *et al.* Critical roles of activation-induced cytidine deaminase in the homeostasis of gut flora. *Science (1979)* 2002;**298**, DOI: 10.1126/science.1077336.

190. De Agüero MG, Ganal-Vonarburg SC, Fuhrer T *et al.* The maternal microbiota drives early postnatal innate immune development. *Science (1979)* 2016;**351**, DOI: 10.1126/science.aad2571.

191. Hapfelmeier S, Lawson MAE, Slack E *et al.* Reversible microbial colonization of germ-free mice reveals the dynamics of IgA immune responses. *Science (1979)* 2010;**328**, DOI: 10.1126/science.1188454.

192. SCHAEDLER RW, DUBS R, COSTELLO R. ASSOCIATION OF GERMFREE MICE WITH BACTERIA ISOLATED FROM NORMAL MICE. *J Exp Med* 1965;**122**, DOI: 10.1084/jem.122.1.77.

193. Brand MW, Wannemuehler MJ, Phillips GJ *et al.* The altered schaedler flora: Continued applications of a defined murine microbial community. *ILAR J* 2015;**56**, DOI: 10.1093/ilar/ilv012.

194. Brugiroux S, Beutler M, Pfann C *et al.* Genome-guided design of a defined mouse microbiota that confers colonization resistance against Salmonella enterica serovar Typhimurium. *Nat Microbiol* 2016;**2**, DOI: 10.1038/nmicrobiol.2016.215.

195. Eberl C, Ring D, Münch PC *et al.* Reproducible Colonization of Germ-Free Mice With the Oligo-Mouse-Microbiota in Different Animal Facilities. *Front Microbiol* 2020;**10**, DOI: 10.3389/fmicb.2019.02999.

196. Wyss M, Brown K, Thomson CA *et al.* Using Precisely Defined in vivo Microbiotas to Understand Microbial Regulation of IgE. *Front Immunol* 2020;**10**, DOI: 10.3389/fimmu.2019.03107.

197. Afrizal A, Jennings SAV, Hitch TCA *et al.* Enhanced cultured diversity of the mouse gut microbiota enables custom-made synthetic communities. *Cell Host Microbe* 2022;**30**, DOI: 10.1016/j.chom.2022.09.011.

198. Eng VV, Pearson JS. In vivo studies on Citrobacter rodentium and host cell death pathways. *Curr Opin Microbiol* 2021;**64**, DOI: 10.1016/j.mib.2021.09.005.

199. Crepin VF, Habibzay M, Glegola-Madejska I *et al.* Tir triggers expression of CXCL1 in enterocytes and neutrophil recruitment during Citrobacter rodentium infection. *Infect Immun* 2015;**83**, DOI: 10.1128/IAI.00291-15.

200. Nadler C, Baruch K, Kobi S *et al.* The type III secretion effector NleE inhibits NF-κB activation. *PLoS Pathog* 2010;**6**, DOI: 10.1371/journal.ppat.1000743.

201. Pöysti S, Toivonen R, Takeda A *et al.* Infection with the enteric pathogen C. rodentium promotes islet-specific autoimmunity by activating a lymphatic route from the gut to pancreatic lymph node. *Mucosal Immunol* 2022;**15**, DOI: 10.1038/s41385-022-00490-2.

202. Ishigame H, Kakuta S, Nagai T *et al.* Differential Roles of Interleukin-17A and -17F in Host Defense against Mucoepithelial Bacterial Infection and Allergic Responses. *Immunity* 2009;**30**, DOI: 10.1016/j.immuni.2008.11.009.

203. Zheng Y, Valdez PA, Danilenko DM *et al.* Interleukin-22 mediates early host defense against attaching and effacing bacterial pathogens. *Nat Med* 2008;**14**, DOI: 10.1038/nm1720.

204. Woo V, Eshleman EM, Hashimoto-Hill S *et al.* Commensal segmented filamentous bacteria-derived retinoic acid primes host defense to intestinal infection. *Cell Host Microbe* 2021;**29**, DOI: 10.1016/j.chom.2021.09.010.

205. Osbelt L, Thiemann S, Smit N *et al.* Variations in microbiota composition of laboratory mice influence Citrobacter rodentium infection via variable short-chain fatty acid production. *PLoS Pathog* 2020;**16**, DOI: 10.1371/journal.ppat.1008448.

206. Kim YG, Sakamoto K, Seo SU *et al.* Neonatal acquisition of Clostridia species protects against colonization by bacterial pathogens. *Science (1979)* 2017;**356**, DOI: 10.1126/science.aag2029.

207. Zhao Y, Chen F, Wu W *et al.* GPR43 mediates microbiota metabolite SCFA regulation of antimicrobial peptide expression in intestinal epithelial cells via activation of mTOR and STAT3. *Mucosal Immunol* 2018;**11**, DOI: 10.1038/mi.2017.118.

208. Burger-van Paassen N, Vincent A, Puiman PJ *et al.* The regulation of intestinal mucin MUC2 expression by short-chain fatty acids: Implications for epithelial protection. *Biochemical Journal* 2009;**420**, DOI: 10.1042/BJ20082222.

209. Kamada N, Kim YG, Sham HP *et al.* Regulated virulence controls the ability of a pathogen to compete with the gut microbiota. *Science (1979)* 2012;**336**, DOI: 10.1126/science.1222195.

210. Crepin VF, Collins JW, Habibzay M *et al.* Citrobacter rodentium mouse model of bacterial infection. *Nat Protoc* 2016;**11**, DOI: 10.1038/nprot.2016.100.

211. Buschor S, Cuenca M, Uster SS *et al.* Innate immunity restricts Citrobacter rodentium A/E pathogenesis initiation to an early window of opportunity. *PLoS Pathog* 2017;**13**, DOI: 10.1371/journal.ppat.1006476.

212. Mullineaux-Sanders C, Collins JW, Ruano-Gallego D *et al.* Citrobacter rodentium Relies on Commensals for Colonization of the Colonic Mucosa. *Cell Rep* 2017;**21**, DOI: 10.1016/j.celrep.2017.11.086.

213. Rudwaleit M, van der Heijde D, Landewe R *et al.* The development of Assessment of SpondyloArthritis international Society classification criteria for axial spondyloarthritis (part II): validation and final selection. *Ann Rheum Dis* 2009;**68**:777–83.

214. Benham H, Rehaume LM, Hasnain SZ *et al.* Interleukin-23 mediates the intestinal response to microbial β-1,3-glucan and the development of spondyloarthritis pathology in SKG mice. *Arthritis and Rheumatology* 2014;**66**, DOI: 10.1002/art.38638.

215. Brugiroux S, Beutler M, Pfann C *et al.* Genome-guided design of a defined mouse microbiota that confers colonization resistance against Salmonella enterica serovar Typhimurium. *Nat Microbiol* 2016;**2**, DOI: 10.1038/nmicrobiol.2016.215.

216. Blast N. Nucleotide BLAST. *Basic Local Alignment Search Tool* 2020.

217. Hung YM, Lu TP, Tsai MH *et al.* EasyMAP: A user-friendly online platform for analyzing 16S ribosomal DNA sequencing data. *N Biotechnol* 2021;**63**, DOI: 10.1016/j.nbt.2021.03.001.

218. McMurdie PJ, Holmes S. Phyloseq: An R Package for Reproducible Interactive Analysis and Graphics of Microbiome Census Data. *PLoS One* 2013;**8**, DOI: 10.1371/journal.pone.0061217.

219. Kassambara A. Pipe-friendly framework for basic statistical tests [R Package “rstatix” version 0.7. 0]. *R Foundation for Statistical Computing, Vienna* 2021.

220. Kuznetsova A, Brockhoff PB, Christensen RHB. lmerTest Package: Tests in Linear Mixed Effects Models. *J Stat Softw* 2017;**82**, DOI: 10.18637/JSS.V082.I13.

221. Lenth VR. Estimated marginal means, aka least-squares means. *American Statistician* 2023;**34**.

222. R Core Team (2020). R: A language and environment for statistical computing. *R Foundation for Statistical Computing, Vienna, Austria* 2020.

223. Ritchie ME, Phipson B, Wu D *et al.* Limma powers differential expression analyses for RNA-sequencing and microarray studies. *Nucleic Acids Res* 2015;**43**, DOI: 10.1093/nar/gkv007.

224. Mallick H, Rahnavard A, McIver LJ *et al.* Multivariable association discovery in population-scale meta-omics studies. *PLoS Comput Biol* 2021;**17**, DOI: 10.1371/journal.pcbi.1009442.

225. Xu S, Chen M, Feng T *et al.* Use ggbreak to Effectively Utilize Plotting Space to Deal With Large Datasets and Outliers. *Front Genet* 2021;**12**, DOI: 10.3389/fgene.2021.774846.

226. Bentaleb I, Abdelghani K Ben, Rostom S *et al.* Reactive Arthritis: Update. *Curr Clin Microbiol Rep* 2020;**7**, DOI: 10.1007/s40588-020-00152-6.

227. Ngaruiya CM, Martin IBK. A case of reactive arthritis: A great masquerader. *American Journal of Emergency Medicine* 2013;**31**, DOI: 10.1016/j.ajem.2012.04.019.

228. Hayes KM, Hayes RJP, Turk MA *et al.* Evolving patterns of reactive arthritis. *Clin Rheumatol* 2019;**38**, DOI: 10.1007/s10067-019-04522-4.

229. Siala M, Gdoura R, Fourati H *et al.* Broad-range PCR, cloning and sequencing of the full 16S rRNA gene for detection of bacterial DNA in synovial fluid samples of Tunisian patients with reactive and undifferentiated arthritis. *Arthritis Res Ther* 2009;**11**, DOI: 10.1186/ar2748.

230. Vidal SM, Pinner E, Lepage P *et al.* Natural resistance to intracellular infections: Nramp1 encodes a membrane phosphoglycoprotein absent in macrophages from susceptible (Nramp1 D169) mouse strains. *The Journal of Immunology* 1996;**157**, DOI: 10.4049/jimmunol.157.8.3559.

231. Mullineaux-Sanders C, Sanchez-Garrido J, Hopkins EGD *et al.* Citrobacter rodentium–host–microbiota interactions: immunity, bioenergetics and metabolism. *Nat Rev Microbiol* 2019;**17**, DOI: 10.1038/s41579-019-0252-z.

232. Mundy R, MacDonald TT, Dougan G *et al.* Citrobacter rodentium of mice and man. *Cell Microbiol* 2005;**7**, DOI: 10.1111/j.1462-5822.2005.00625.x.

233. Wang Z, Friedrich C, Hagemann SC *et al.* Regulatory T cells promote a protective Th17-associated immune response to intestinal bacterial infection with C. rodentium. *Mucosal Immunol* 2014;**7**, DOI: 10.1038/mi.2014.17.

234. Liu Z, Man SM, Zhu Q *et al.* DOCK2 confers immunity and intestinal colonization resistance to Citrobacter rodentium infection. *Sci Rep* 2016;**6**, DOI: 10.1038/srep27814.

235. Kline KA, Ingersoll MA, Nielsen H V. *et al.* Characterization of a novel murine model of Staphylococcus saprophyticus urinary tract infection reveals roles for Ssp and SdrI in virulence. *Infect Immun* 2010;**78**, DOI: 10.1128/IAI.01235-09.

236. Ma L, Deitch E, Specian R *et al.* Translocation of Lactobacillus murinus from the gastrointestinal tract. *Curr Microbiol* 1990;**20**, DOI: 10.1007/BF02091994.

237. Spahn TW, Ross M, Von Eiff C *et al.* CD4+ T cells transfer resistance against Citrobacter rodentium-induced infectious colitis by induction of Th 1 immunity. *Scand J Immunol* 2008;**67**, DOI: 10.1111/j.1365-3083.2007.02063.x.

238. Weiss AS, Burrichter AG, Durai Raj AC *et al.* In vitro interaction network of a synthetic gut bacterial community. *ISME Journal* 2022;**16**, DOI: 10.1038/s41396-021-01153-z.

239. Burisch J, Eigner W, Schreiber S *et al.* Risk for development of inflammatory bowel disease under inhibition of interleukin 17: A systematic review and meta-analysis. *PLoS One* 2020;**15**, DOI: 10.1371/journal.pone.0233781.

240. Pham TAN, Clare S, Goulding D *et al.* Epithelial IL-22RA1-mediated fucosylation promotes intestinal colonization resistance to an opportunistic pathogen. *Cell Host Microbe* 2014;**16**, DOI: 10.1016/j.chom.2014.08.017.

241. Manfredo Vieira S, Hiltensperger M, Kumar V *et al.* Translocation of a gut pathobiont drives autoimmunity in mice and humans. *Science (1979)* 2018;**359**, DOI: 10.1126/science.aar7201.

242. Zegarra-Ruiz DF, El Beidaq A, Iñiguez AJ *et al.* A Diet-Sensitive Commensal Lactobacillus Strain Mediates TLR7-Dependent Systemic Autoimmunity. *Cell Host Microbe* 2019;**25**, DOI: 10.1016/j.chom.2018.11.009.

243. Fine RL, Manfredo Vieira S, Gilmore MS *et al.* Mechanisms and consequences of gut commensal translocation in chronic diseases. *Gut Microbes* 2020;**11**, DOI: 10.1080/19490976.2019.1629236.

244. Gordon HA. MORPHOLOGICAL AND PHYSIOLOGICAL CHARACTERIZATION OF GERMFREE LIFE. *Ann N Y Acad Sci* 1959;**78**, DOI: 10.1111/j.1749-6632.1959.tb53104.x.

245. Hepworth MR, Monticelli LA, Fung TC *et al.* Innate lymphoid cells regulate CD4 + T-cell responses to intestinal commensal bacteria. *Nature* 2013;**498**, DOI: 10.1038/nature12240.

246. Livingston M, Loach D, Wilson M *et al.* Gut commensal Lactobacillus reuteri 100-23 stimulates an immunoregulatory response. *Immunol Cell Biol* 2010;**88**, DOI: 10.1038/icb.2009.71.

247. Atarashi K, Tanoue T, Shima T *et al.* Induction of colonic regulatory T cells by indigenous Clostridium species. *Science (1979)* 2011;**331**, DOI: 10.1126/science.1198469.

248. Kopylov U, Starr M, Watts C *et al.* Detection of Crohn disease in patients with spondyloarthropathy: The SpACE capsule study. *Journal of Rheumatology* 2018;**45**, DOI: 10.3899/jrheum.161216.

249. Hall AB, Yassour M, Sauk J *et al.* A novel Ruminococcus gnavus clade enriched in inflammatory bowel disease patients. *Genome Med* 2017;**9**, DOI: 10.1186/s13073-017-0490-5.

250. Kverka M, Zakostelska Z, Klimesova K *et al.* Oral administration of Parabacteroides distasonis antigens attenuates experimental murine colitis through modulation of immunity and microbiota composition. *Clin Exp Immunol* 2011;**163**, DOI: 10.1111/j.1365-2249.2010.04286.x.

251. Palm NW, De Zoete MR, Cullen TW *et al.* Immunoglobulin A coating identifies colitogenic bacteria in inflammatory bowel disease. *Cell* 2014;**158**, DOI: 10.1016/j.cell.2014.08.006.

252. Kullberg MC, Ward JM, Gorelick PL *et al.* Helicobacter hepaticus triggers colitis in specific-pathogen-free interleukin-10 (IL-10)-deficient mice through an IL-12-and gamma interferon-dependent mechanism. *Infect Immun* 1998;**66**, DOI: 10.1128/iai.66.11.5157-5166.1998.

253. Maloy KJ, Kullberg MC. IL-23 and Th17 cytokines in intestinal homeostasis. *Mucosal Immunol* 2008;**1**, DOI: 10.1038/mi.2008.28.

254. Kwon MS, Shin MY, Lim SK *et al.* Leuconostoc citreum isolated from kimchi suppresses the development of collagen-induced arthritis in DBA/1 mice. *J Funct Foods* 2019;**63**, DOI: 10.1016/j.jff.2019.103579.

255. Karimi K, Inman MD, Bienenstock J *et al.* Lactobacillus reuteri-induced regulatory T cells protect against an allergic airway response in mice. *Am J Respir Crit Care Med* 2009;**179**, DOI: 10.1164/rccm.200806-951OC.

256. Johansson-Lindbom B, Svensson M, Pabst O *et al.* Functional specialization of gut CD103+ dendritic cells in the regulation of tissue-selective T cell homing. *Journal of Experimental Medicine* 2005;**202**, DOI: 10.1084/jem.20051100.

257. Wright PB, McDonald E, Bravo-Blas A *et al.* The mannose receptor (CD206) identifies a population of colonic macrophages in health and inflammatory bowel disease. *Sci Rep* 2021;**11**, DOI: 10.1038/s41598-021-98611-7.

258. Alivernini S, MacDonald L, Elmesmari A *et al.* Distinct synovial tissue macrophage subsets regulate inflammation and remission in rheumatoid arthritis. *Nat Med* 2020;**26**, DOI: 10.1038/s41591-020-0939-8.

259. Kim HS, Park KH, Lee HK *et al.* Curdlan activates dendritic cells through dectin-1 and toll-like receptor 4 signaling. *Int Immunopharmacol* 2016;**39**, DOI: 10.1016/j.intimp.2016.07.013.

260. Chebib J, Jackson BC, López-Cortegano E *et al.* Inbred lab mice are not isogenic: genetic variation within inbred strains used to infer the mutation rate per nucleotide site. *Heredity (Edinb)* 2021;**126**, DOI: 10.1038/s41437-020-00361-1.

261. Lakra AK, Domdi L, Hanjon G *et al.* Some probiotic potential of Weissella confusa MD1 and Weissella cibaria MD2 isolated from fermented batter. *LWT* 2020;**125**, DOI: 10.1016/j.lwt.2020.109261.

262. Yao D, Wang X, Ma L *et al.* Impact of Weissella cibaria BYL4.2 and its supernatants on Penicillium chrysogenum metabolism. *Front Microbiol* 2022;**13**, DOI: 10.3389/fmicb.2022.983613.

263. Bajer L, Kverka M, Kostovcik M *et al.* Distinct gut microbiota profiles in patients with primary sclerosing cholangitis and ulcerative colitis. *World J Gastroenterol* 2017;**23**, DOI: 10.3748/wjg.v23.i25.4548.

264. Fassatoui M, Lopez-Siles M, Díaz-Rizzolo DA *et al.* Gut microbiota imbalances in Tunisian participants with type 1 and type 2 diabetes mellitus. *Biosci Rep* 2019;**39**, DOI: 10.1042/BSR20182348.

265. Contijoch EJ, Britton GJ, Yang C *et al.* Gut microbiota density influences host physiology and is shaped by host and microbial factors. *Elife* 2019;**8**, DOI: 10.7554/eLife.40553.

266. Pfeifle R, Rothe T, Ipseiz N *et al.* Regulation of autoantibody activity by the IL-23-T H 17 axis determines the onset of autoimmune disease. *Nat Immunol* 2017;**18**, DOI: 10.1038/ni.3579.

267. Sherlock JP, Joyce-Shaikh B, Turner SP *et al.* IL-23 induces spondyloarthropathy by acting on ROR-γt+ CD3+ CD4- CD8- entheseal resident T cells. *Nat Med* 2012;**18**, DOI: 10.1038/nm.2817.

268. Colonic T, Homeostasis C, Smith PM *et al.* The Microbial Metabolites, Short-Chain Fatty Acids, Regulate Colonic Treg Cell Homeostasis. *Science (1979)* 2013;**341**.

269. Mazmanian SK, Round JL, Kasper DL. A microbial symbiosis factor prevents intestinal inflammatory disease. *Nature* 2008;**453**, DOI: 10.1038/nature07008.

270. Milani C, Duranti S, Bottacini F *et al.* The First Microbial Colonizers of the Human Gut: Composition, Activities, and Health Implications of the Infant Gut Microbiota. *Microbiology and Molecular Biology Reviews* 2017;**81**, DOI: 10.1128/mmbr.00036-17.

271. Henrick BM, Rodriguez L, Lakshmikanth T *et al.* Bifidobacteria-mediated immune system imprinting early in life. *Cell* 2021;**184**, DOI: 10.1016/j.cell.2021.05.030.

272. Ehrlich AK, Pennington JM, Bisson WH *et al.* TCDD, FICZ, and other high affinity AhR ligands dose-dependently determine the fate of CD4+ T cell differentiation. *Toxicological Sciences* 2018;**161**, DOI: 10.1093/toxsci/kfx215.

273. Takamura T, Harama D, Fukumoto S *et al.* Lactobacillus bulgaricus OLL1181 activates the aryl hydrocarbon receptor pathway and inhibits colitis. *Immunol Cell Biol* 2011;**89**, DOI: 10.1038/icb.2010.165.

274. Kado S, Chang WLW, Chi AN *et al.* Aryl hydrocarbon receptor signaling modifies Toll-like receptor-regulated responses in human dendritic cells. *Arch Toxicol* 2017;**91**, DOI: 10.1007/s00204-016-1880-y.

275. Lu P, Yamaguchi Y, Fulton WB *et al.* Maternal aryl hydrocarbon receptor activation protects newborns against necrotizing enterocolitis. *Nat Commun* 2021;**12**, DOI: 10.1038/s41467-021-21356-4.

276. Stolwijk C, Essers I, van Tubergen A *et al.* THU0069 The Epidemiology of Extra-Articular Manifestations in Ankylosing Spondylitis: A Population-Based Matched Cohort Study. *Ann Rheum Dis* 2014;**73**, DOI: 10.1136/annrheumdis-2014-eular.2833.

277. Duran A, Kobak S, Sen N *et al.* Fecal calprotectin is associated with disease activity in patients with ankylosing spondylitis. *Bosn J Basic Med Sci* 2016;**16**, DOI: 10.17305/bjbms.2016.752.

278. Sipponen T, Kärkkäinen P, Savilahti E *et al.* Correlation of faecal calprotectin and lactoferrin with an endoscopic score for Crohn's disease and histological findings. *Aliment Pharmacol Ther* 2008;**28**, DOI: 10.1111/j.1365-2036.2008.03835.x.

279. Swaminathan A, Borichevsky GM, Edwards TS *et al.* Faecal Myeloperoxidase as a Biomarker of Endoscopic Activity in Inflammatory Bowel Disease. *J Crohns Colitis* 2022;**16**, DOI: 10.1093/ecco-jcc/jjac098.

280. Mikuls TR, LeVan TD, Sayles H *et al.* Soluble CD14 and CD14 polymorphisms in rheumatoid arthritis. *Journal of Rheumatology* 2011;**38**, DOI: 10.3899/jrheum.110378.

281. Riva A, Gray EH, Azarian S *et al.* Faecal cytokine profiling as a marker of intestinal inflammation in acutely decompensated cirrhosis. *JHEP Reports* 2020;**2**, DOI: 10.1016/j.jhepr.2020.100151.

282. Rosser EC, Piper CJM, Matei DE *et al.* Microbiota-Derived Metabolites Suppress Arthritis by Amplifying Aryl-Hydrocarbon Receptor Activation in Regulatory B Cells. *Cell Metab* 2020;**31**, DOI: 10.1016/j.cmet.2020.03.003.

283. Klingberg E, Strid H, Ståhl A *et al.* A longitudinal study of fecal calprotectin and the development of inflammatory bowel disease in ankylosing spondylitis. *Arthritis Res Ther* 2017;**19**, DOI: 10.1186/s13075-017-1223-2.

284. Mease P. Ustekinumab Fails to Show Efficacy in a Phase III Axial Spondyloarthritis Program: The Importance of Negative Results. *Arthritis and Rheumatology* 2019;**71**, DOI: 10.1002/art.40759.

285. Feagan BG, Sandborn WJ, Gasink C *et al.* Ustekinumab as Induction and Maintenance Therapy for Crohn's Disease. *New England Journal of Medicine* 2016;**375**, DOI: 10.1056/nejmoa1602773.

286. Glatigny S, Fert I, Blaton MA *et al.* Proinflammatory Th17 cells are expanded and induced by dendritic cells in spondylarthritis-prone HLA-B27-transgenic rats. *Arthritis Rheum* 2012;**64**, DOI: 10.1002/art.33321.

287. Kelly R, Marsden RA, Bevan D. Exacerbation of psoriasis with GM-CSF therapy [6]. *British Journal of Dermatology* 1993;**128**, DOI: 10.1111/j.1365-2133.1993.tb00218.x.

288. Hong X, Hao K, Ladd-Acosta C *et al.* Genome-wide association study identifies peanut allergy-specific loci and evidence of epigenetic mediation in US children. *Nat Commun* 2015;**6**, DOI: 10.1038/ncomms7304.

289. Khor SS, Morino R, Nakazono K *et al.* Genome-wide association study of self-reported food reactions in Japanese identifies shrimp and peach specific loci in the HLA-DR/DQ gene region. *Sci Rep* 2018;**8**, DOI: 10.1038/s41598-017-18241-w.

290. Madore AM, Vaillancourt VT, Asai Y *et al.* HLA-DQB1*02 and DQB1*06:03P are associated with peanut allergy. *European Journal of Human Genetics* 2013;**21**, DOI: 10.1038/ejhg.2013.13.

291. Kamanli A, Ardicoglu O, Godekmerdan A. HLA-B27 subtypes in patients with spondylarthropathies, IgE levels against some allergens and their relationship to the disease parameters. *Bratislava Medical Journal* 2009;**110**.

292. Krebs K, Bovijn J, Zheng N *et al.* Genome-wide Study Identifies Association between HLA-B∗55:01 and Self-Reported Penicillin Allergy. *Am J Hum Genet* 2020;**107**, DOI: 10.1016/j.ajhg.2020.08.008.

293. Kalish RS, Askenase PW. Molecular mechanisms of CD8+T cell-mediated delayed hypersensitivity: Implications for allergies, asthma, and autoimmunity. *Journal of Allergy and Clinical Immunology* 1999;**103**, DOI: 10.1016/s0091-6749(99)70489-6.

294. Abu Musa M, Kabir M, Iqbal Hossain M *et al.* Measurement of intestinal permeability using lactulose and mannitol with conventional five hours and shortened two hours urine collection by two different methods: HPAE-PAD and LC-MSMS. *PLoS One* 2019;**14**, DOI: 10.1371/journal.pone.0220397.

295. Rath HC, Herfarth HH, Ikeda JS *et al.* Normal luminal bacteria, especially bacteroides species, mediate chronic colitis, gastritis, and arthritis in HLA-B27/human β2 microglobulin transgenic rats. *Journal of Clinical Investigation* 1996;**98**, DOI: 10.1172/JCI118878.

296. Lamas B, Richard ML, Leducq V *et al.* CARD9 impacts colitis by altering gut microbiota metabolism of tryptophan into aryl hydrocarbon receptor ligands. *Nat Med* 2016;**22**, DOI: 10.1038/nm.4102.

297. Łukasik Z, Gracey E, Venken K *et al.* Crossing the boundaries: IL-23 and its role in linking inflammation of the skin, gut and joints. *Rheumatology (Bulgaria)* 2021;**60**, DOI: 10.1093/rheumatology/keab385.

298. Vich Vila A, Imhann F, Collij V *et al.* Gut microbiota composition and functional changes in inflammatory bowel disease and irritable bowel syndrome. *Sci Transl Med* 2018;**10**, DOI: 10.1126/scitranslmed.aap8914.

299. Zhu F, Ju Y, Wang W *et al.* Metagenome-wide association of gut microbiome features for schizophrenia. *Nat Commun* 2020;**11**, DOI: 10.1038/s41467-020-15457-9.

300. Wen C, Zheng Z, Shao T *et al.* Quantitative metagenomics reveals unique gut microbiome biomarkers in ankylosing spondylitis. *Genome Biol* 2017;**18**, DOI: 10.1186/s13059-017-1271-6.

301. Bjarnason I, Helgason KO, Geirsson ÁJ *et al.* Subclinical Intestinal Inflammation and Sacroiliac Changes in Relatives of Patients with Ankylosing Spondylitis. *Gastroenterology* 2003;**125**, DOI: 10.1053/j.gastro.2003.08.035.

302. Kehl AS, Learch TJ, Li D *et al.* Relationship between the gut and the spine: A pilot study of first-degree relatives of patients with ankylosing spondylitis. *RMD Open* 2017;**3**, DOI: 10.1136/rmdopen-2017-000437.

303. Seo SU, Kuffa P, Kitamoto S *et al.* Intestinal macrophages arising from CCR2+ monocytes control pathogen infection by activating innate lymphoid cells. *Nat Commun* 2015;**6**, DOI: 10.1038/ncomms9010.

304. Aychek T, Mildner A, Yona S *et al.* IL-23-mediated mononuclear phagocyte crosstalk protects mice from Citrobacter rodentium-induced colon immunopathology. *Nat Commun* 2015;**6**, DOI: 10.1038/ncomms7525.

305. Raupach B, Peuschel SK, Monack DM *et al.* Caspase-1-mediated activation of interleukin-1β (IL-1β) and IL-18 contributes to innate immune defenses against Salmonella enterica serovar typhimurium infection. *Infect Immun* 2006;**74**, DOI: 10.1128/IAI.00417-06.

306. Godinez I, Raffatellu M, Chu H *et al.* Interleukin-23 orchestrates mucosal responses to Salmonella enterica serotype typhimurium in the intestine. *Infect Immun* 2009;**77**, DOI: 10.1128/IAI.00933-08.

307. Narayan C, Kant V, Mahajan JK *et al.* Differential dendritic immune cell responses to infection with various serotypes of Shigella. *Indian J Med Microbiol* 2022;**40**, DOI: 10.1016/j.ijmmb.2022.02.007.

308. Haynie T, Gubler S, Drees C *et al.* Synthesis of the pentasaccharide repeating unit from: Ruminococcus gnavus and measurement of its inflammatory properties. *RSC Adv* 2021;**11**, DOI: 10.1039/d1ra01918j.

309. Pastor-Fernández G, Mariblanca IR, Navarro MN. Decoding IL-23 Signaling Cascade for New Therapeutic Opportunities. *Cells* 2020;**9**, DOI: 10.3390/cells9092044.

310. McGovern D, Powrie F. The IL23 axis plays a key role in the pathogenesis of IBD. *Gut* 2007;**56**, DOI: 10.1136/gut.2006.115402.

311. Buonocore S, Ahern PP, Uhlig HH *et al.* Innate lymphoid cells drive IL-23 dependent innate intestinal pathology Europe PMC Funders Group. *Nature* 2010;**464**.

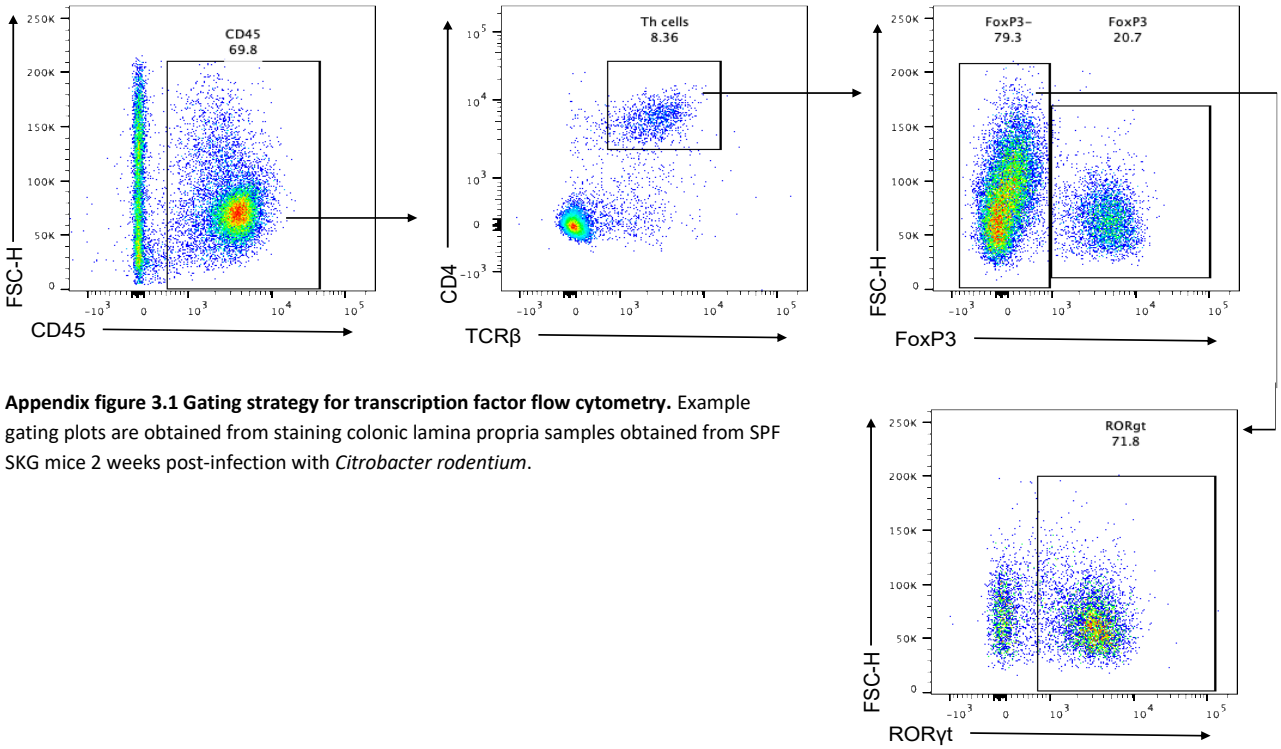
312. Sorbara MT, Pamer EG. Microbiome-based therapeutics. *Nat Rev Microbiol* 2022;**20**, DOI: 10.1038/s41579-021-00667-9.

313. Lai NL, Zhang SX, Wang J *et al.* The Proportion of Regulatory T Cells in Patients with Ankylosing Spondylitis: A Meta-Analysis. *J Immunol Res* 2019;**2019**, DOI: 10.1155/2019/1058738.

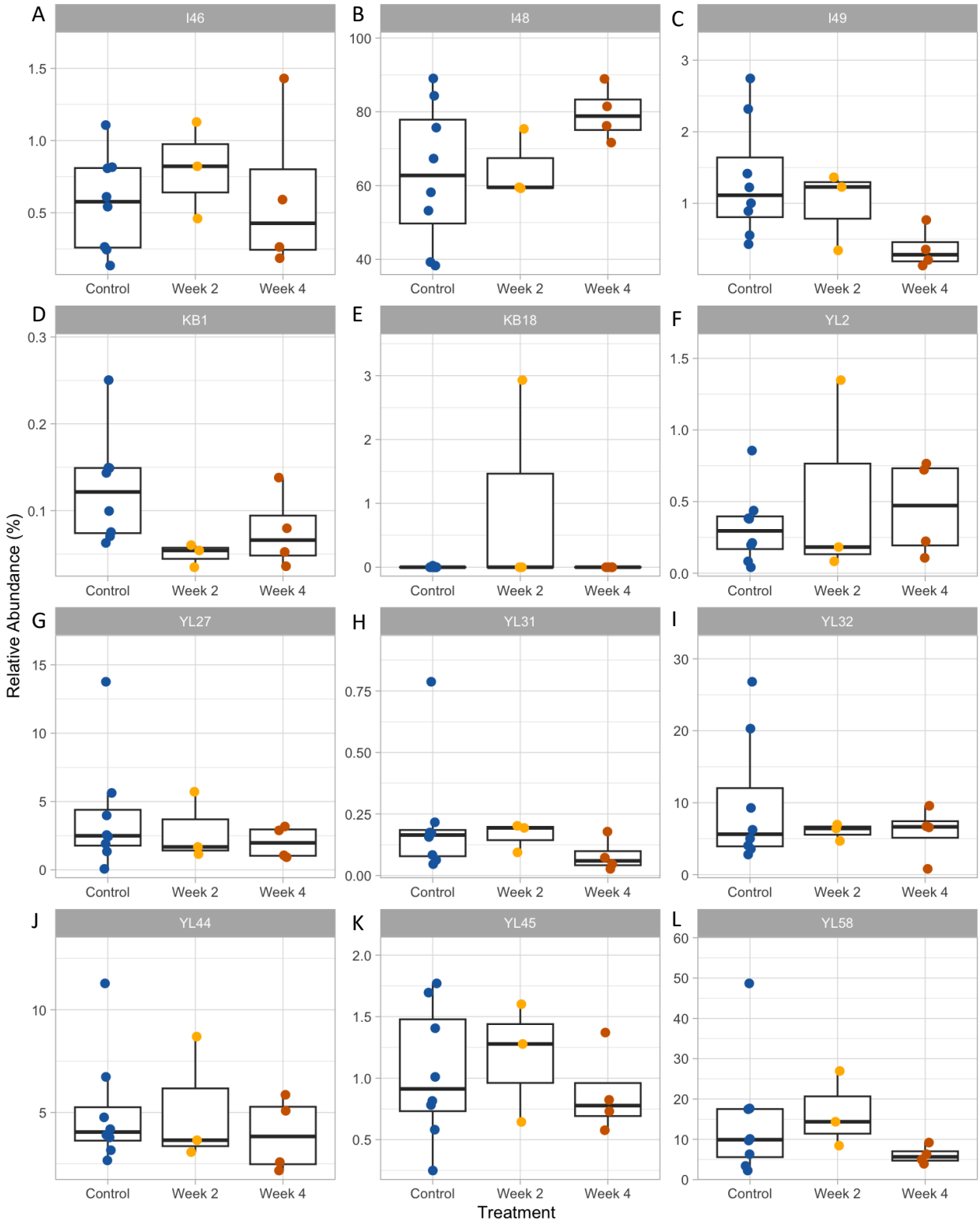
314. Bai L, Gao M, Cheng X *et al.* Engineered butyrate-producing bacteria prevents high fat diet-induced obesity in mice. *Microb Cell Fact* 2020;**19**, DOI: 10.1186/s12934-020-01350-z.

Appendix

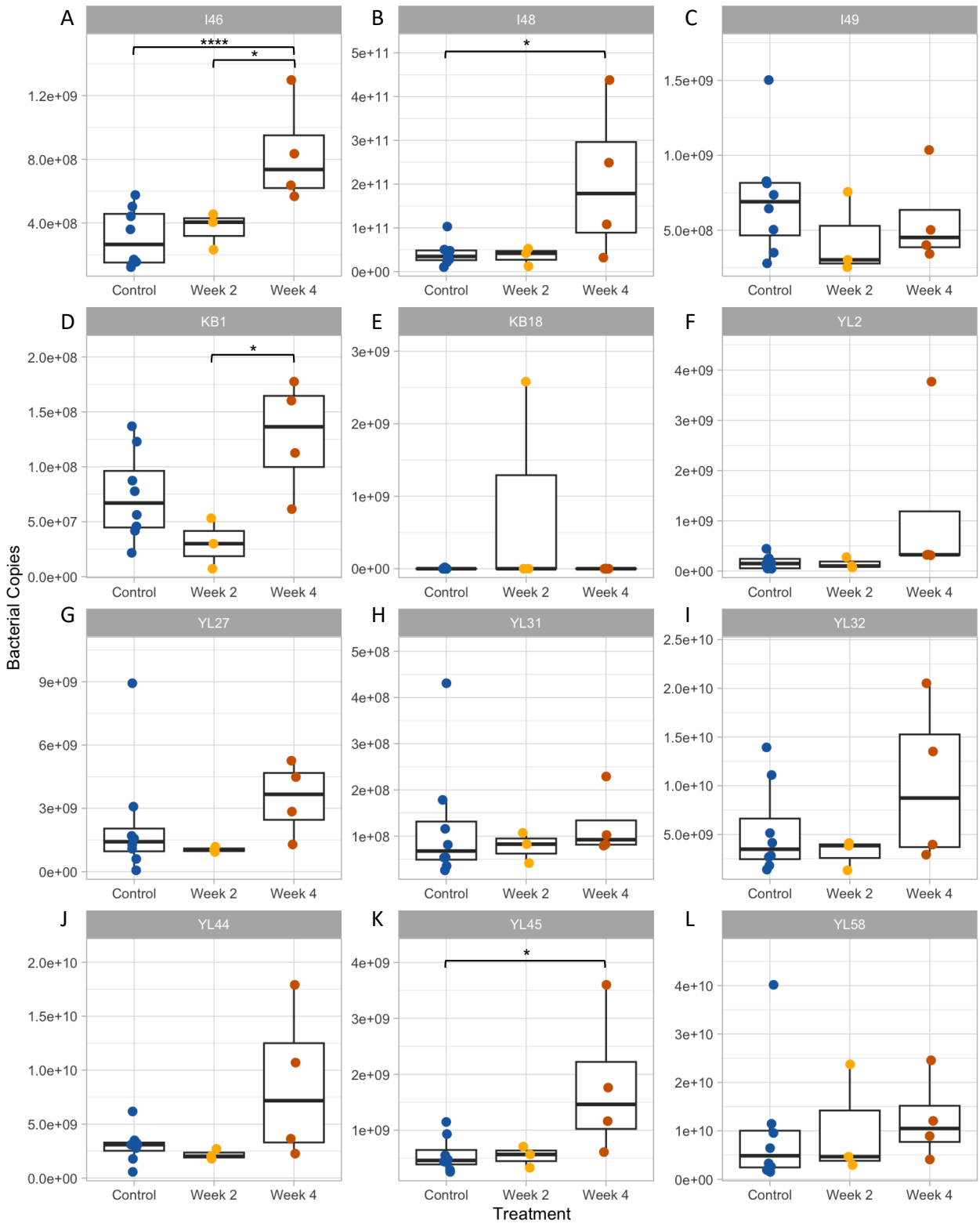
Chapter 3 Appendix:



Appendix figure 3.1 Gating strategy for transcription factor flow cytometry. Example gating plots are obtained from staining colonic lamina propria samples obtained from SPF SKG mice 2 weeks post-infection with *Citrobacter rodentium*.

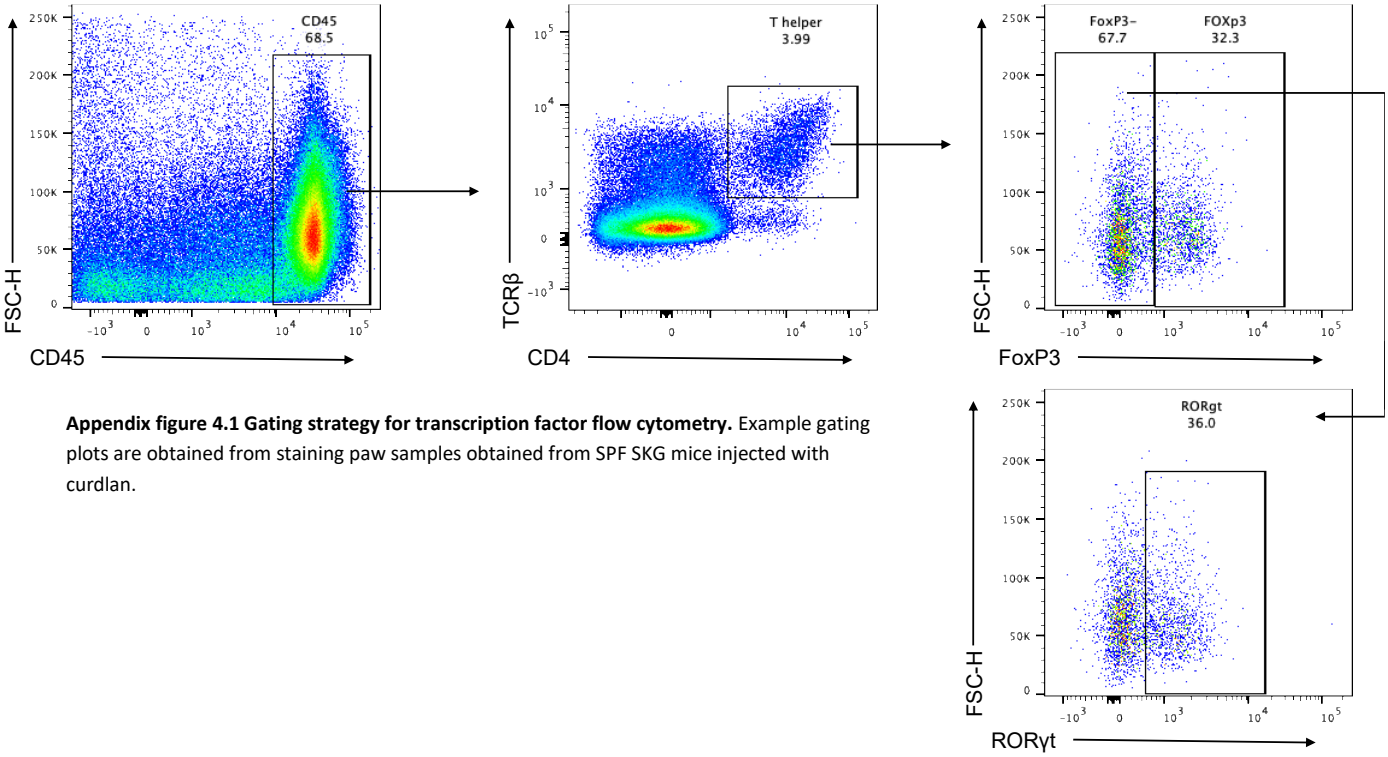


Appendix figure 3.2 Relative abundances of Oligo-MM^{12} members during *C. rodentium* infection in SKG mice. Colon contents from Oligo-MM^{12} SKG mice 2 weeks and 4 weeks post-infection with *C. rodentium* and naïve Oligo-MM^{12} SKG mice were obtained, and qPCR was completed using strain-specific primers for Oligo-MM^{12} members and *C. rodentium.* One-way ANOVA with Tukey's post-hoc testing was completed on relative abundances of all bacteria with Benjamini-Hochberg correction to identify members of the Oligo-MM^{12} that were altered during infection. A) I46, B) I48, C) I49, D) KB1, E) KB18, F) YL2, G) YL27, H) YL31, I) YL32, J) YL44, K) YL45, L) YL58. Boxplots denote median + interquartile range and individual data points are shown.

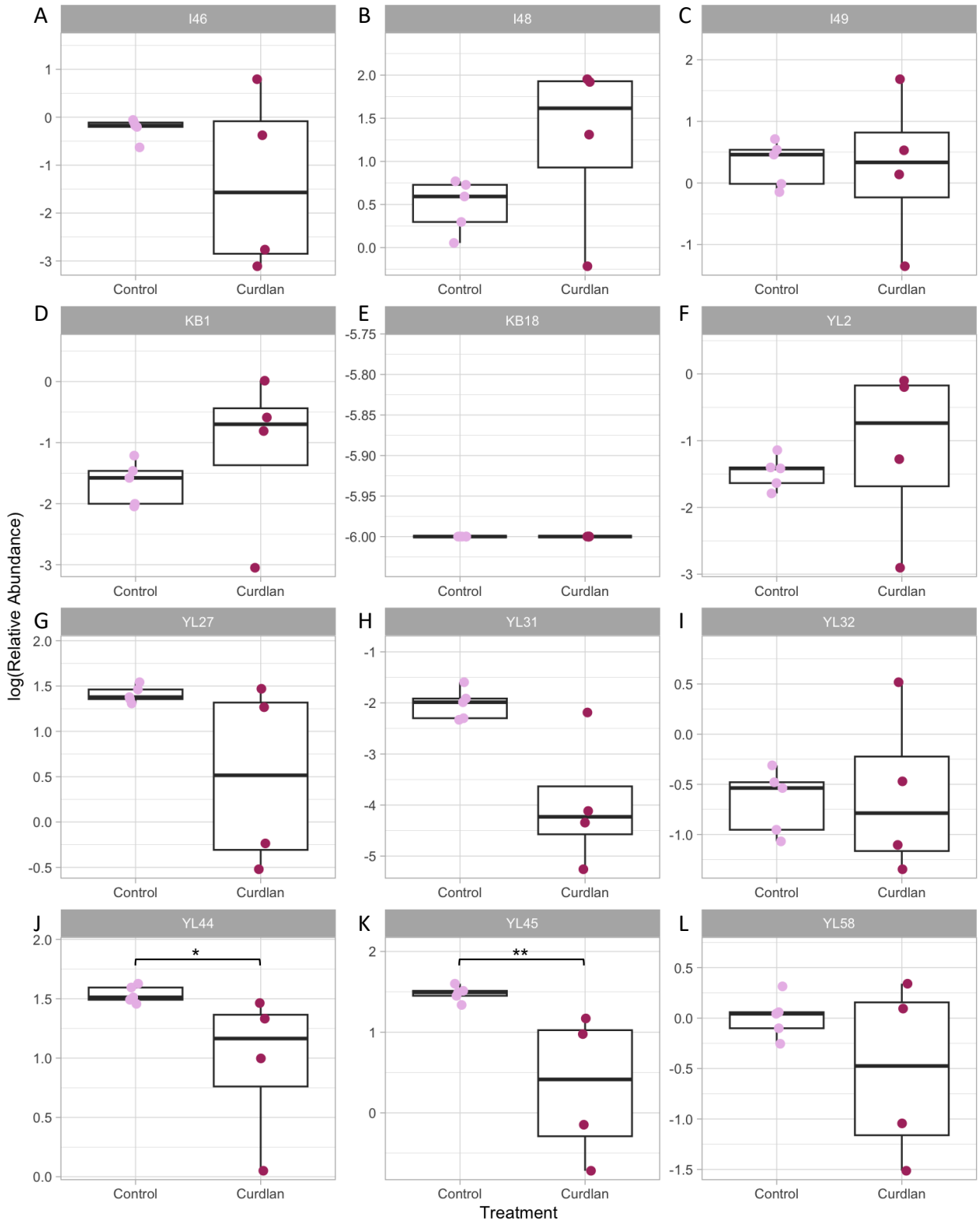


Appendix figure 3.3 Numbers of Oligo-MM^{12} members during *C. rodentium* infection in SKG mice. Colon contents from Oligo-MM^{12} SKG mice 2 weeks and 4 weeks post-infection with *C. rodentium* and naïve Oligo-MM^{12} SKG mice were obtained, and qPCR was completed using strain-specific primers for Oligo-MM^{12} members and *C. rodentium.* One-way ANOVA with Tukey's post-hoc testing was completed on absolute numbers of all bacteria with Benjamini-Hochberg correction to identify members of the Oligo-MM^{12} that were altered during infection. A) I46, B) I48, C) I49, D) KB1, E) KB18, F) YL2, G) YL27, H) YL31, I) YL32, J) YL44, K) YL45, L) YL58. Boxplots denote median + interquartile range and individual data points are shown.****p<0.0001, *p<0.05, ns = not significant

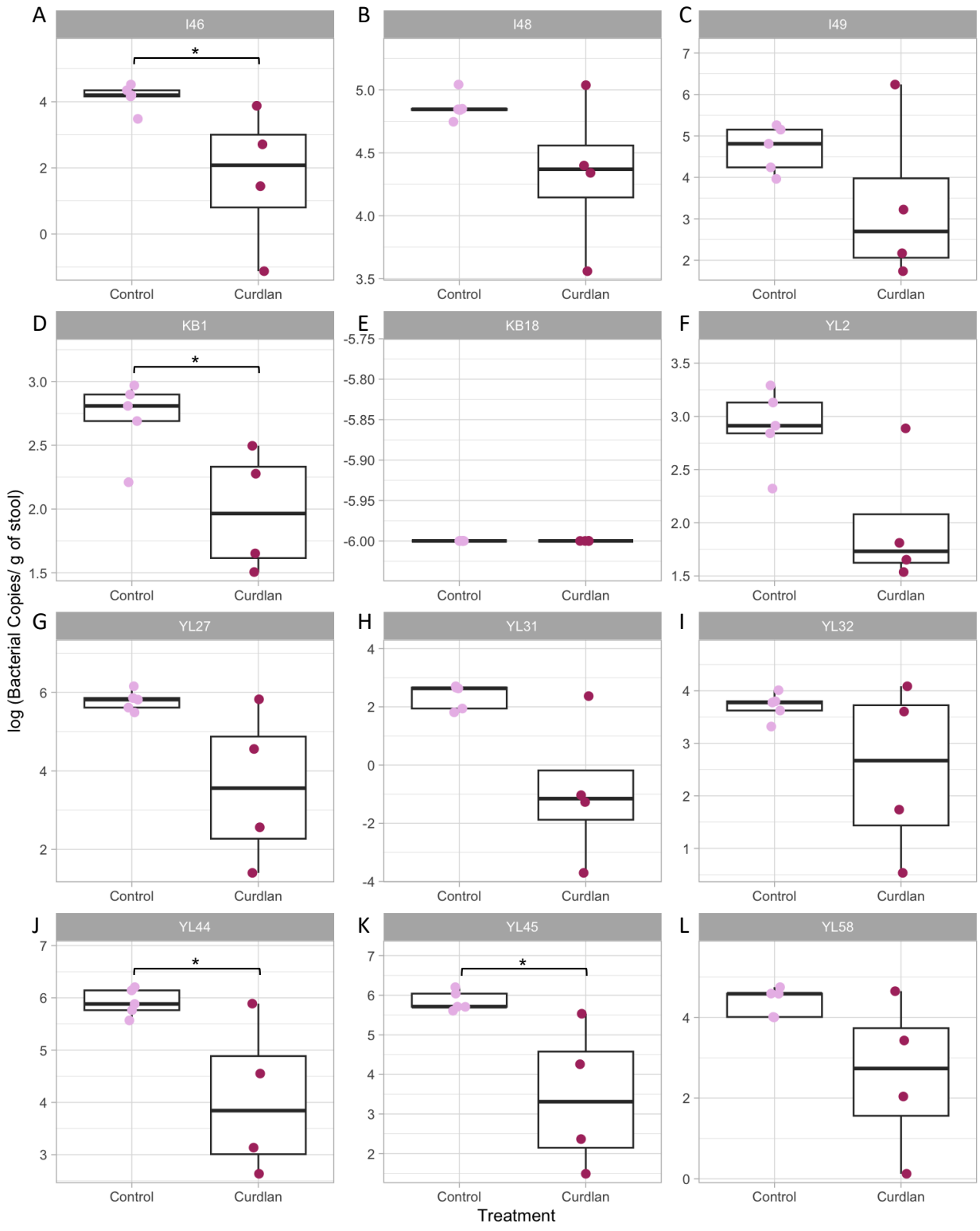
Chapter 4 Appendix:



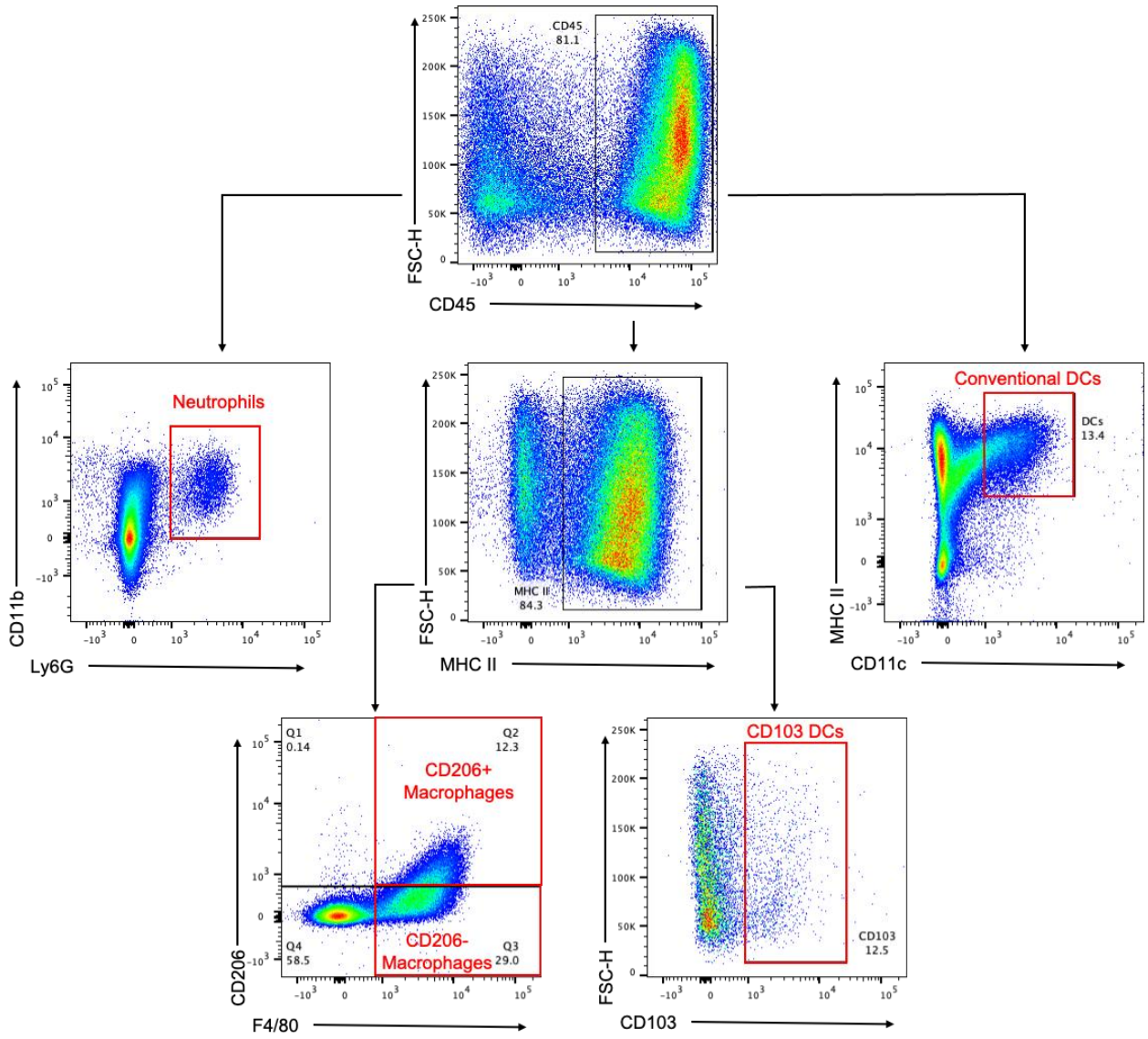
Appendix figure 4.1 Gating strategy for transcription factor flow cytometry. Example gating plots are obtained from staining paw samples obtained from SPF SKG mice injected with curdlan.



Appendix figure 4.2 Relative abundances of Oligo-MM^{12} members from strain-specific qPCR. Strain-specific qPCR was completed on small intestine contents retrieved from Oligo-MM^{12} SKG mice injected with curdlan and naïve Oligo-MM^{12} SKG mice. A) I46, B) I48, C) I49, D) KB1, E) KB18, F) YL2, G) YL27, H) YL31, I) YL32, J) YL44, K) YL45, L) YL58. Relative abundances are denoted as log(relative abundance(%)). **p<0.01, *p<0.05. Student's t-test was completed for each member of the Oligo-MM^{12} with Benjamini-Hochberg correction for multiple testing. Boxplots denote median + interquartile range and individual data points are shown.

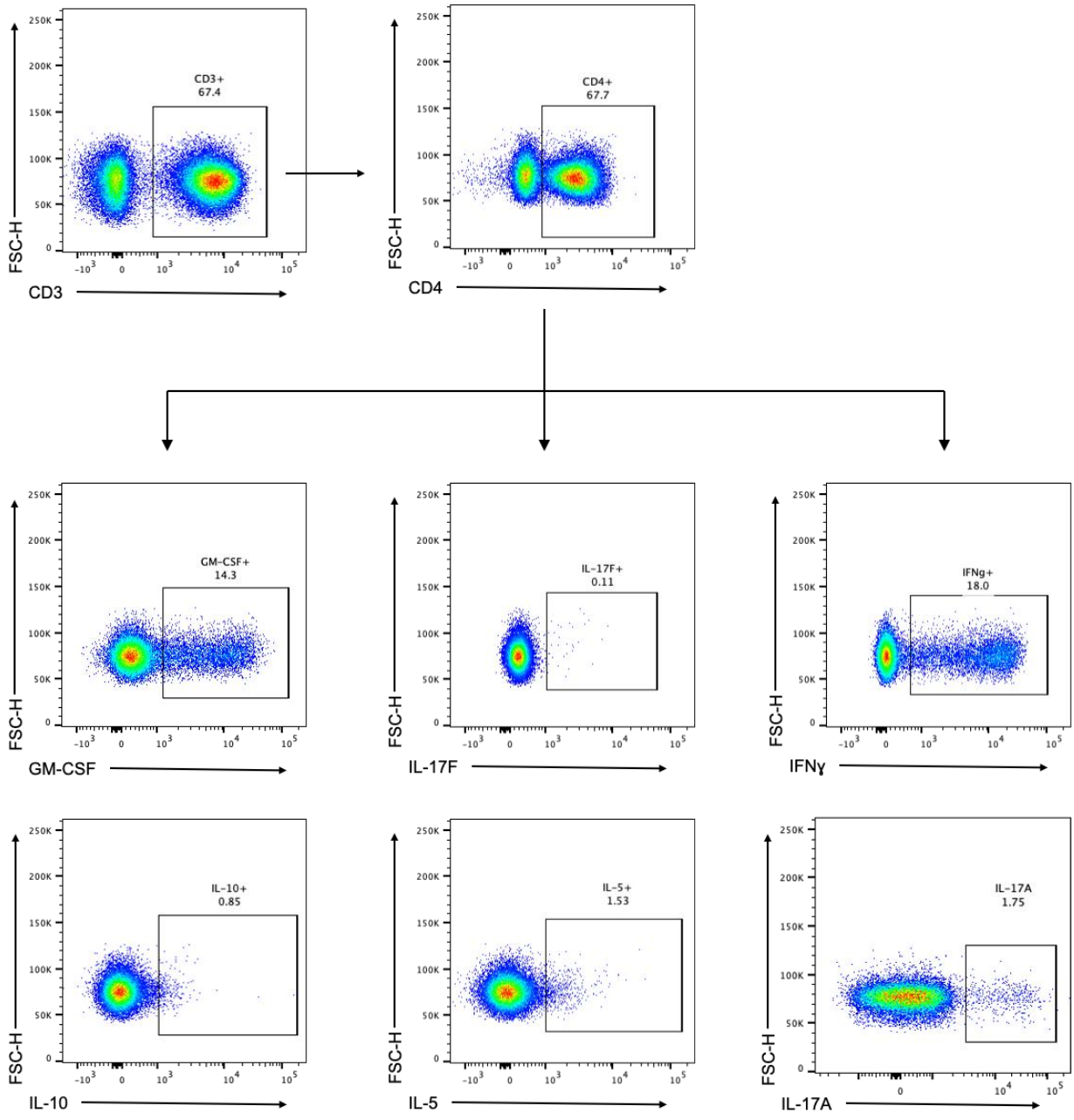


Appendix figure 4.3 Absolute numbers of Oligo-MM^{12} members from strain-specific qPCR. Strain-specific qPCR was completed on small intestine contents retrieved from Oligo-MM^{12} SKG mice injected with curdlan and naïve Oligo-MM^{12} SKG mice. A) I46, B) I48, C) I49, D) KB1, E) KB18, F) YL2, G) YL27, H) YL31, I) YL32, J) YL44, K) YL45, L) YL58. Number of bacteria are denoted as log(bacterial copies per gram of stool). *p<0.05. Student's t-test was completed for each member of the Oligo-MM^{12} with Benjamini-Hochberg correction for multiple testing. Boxplots denote median + interquartile range and individual data points are shown.



Appendix figure 4.4 Gating strategy for flow cytometry. Gating strategy for myeloid subsets; neutrophils, conventional DCs, CD206+ macrophages, CD206- macrophages, and CD103 DCs. Example plots are obtained from spleens of *B. animalis* colonised curdlan-injected mice.

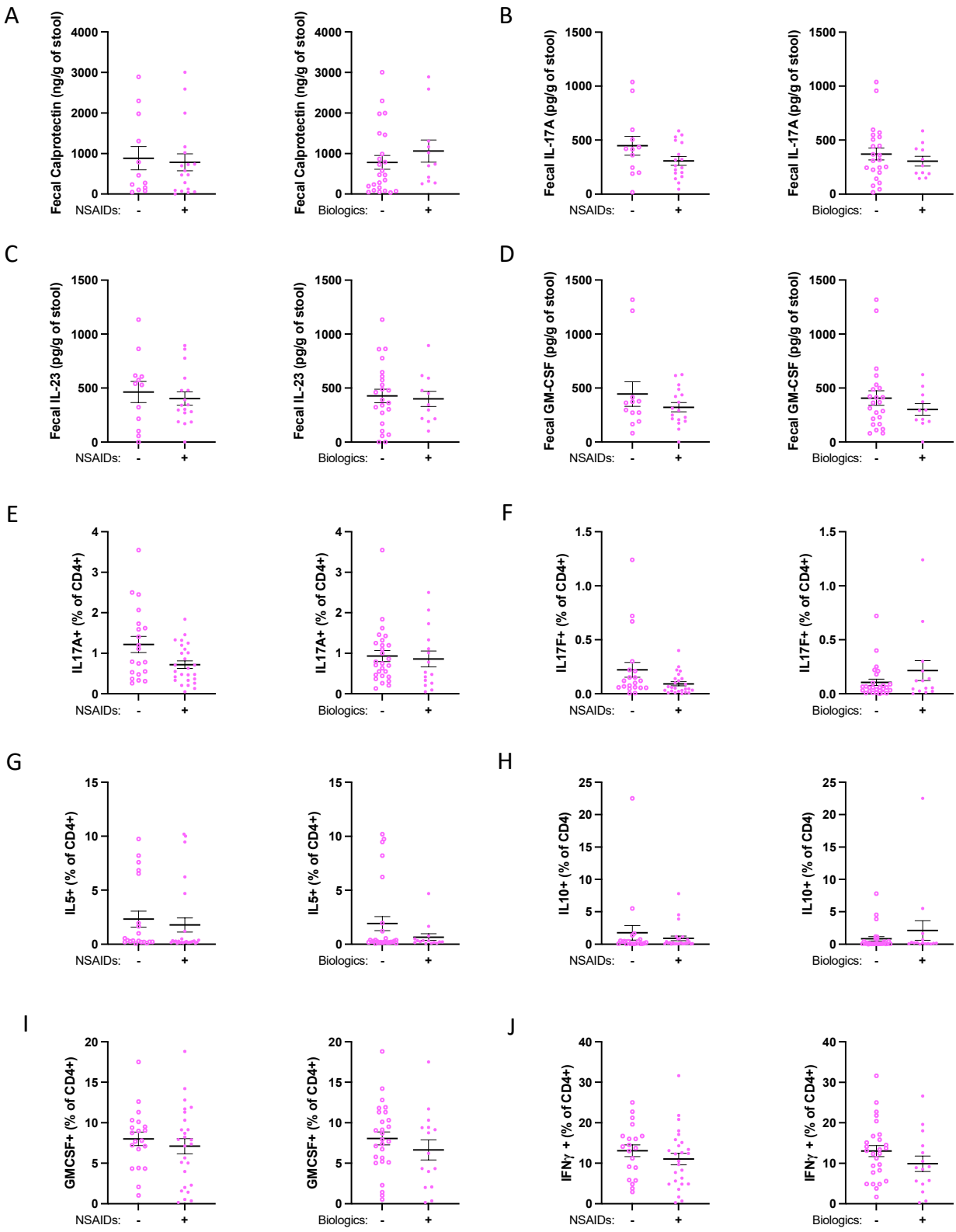
Chapter 5 Appendix:



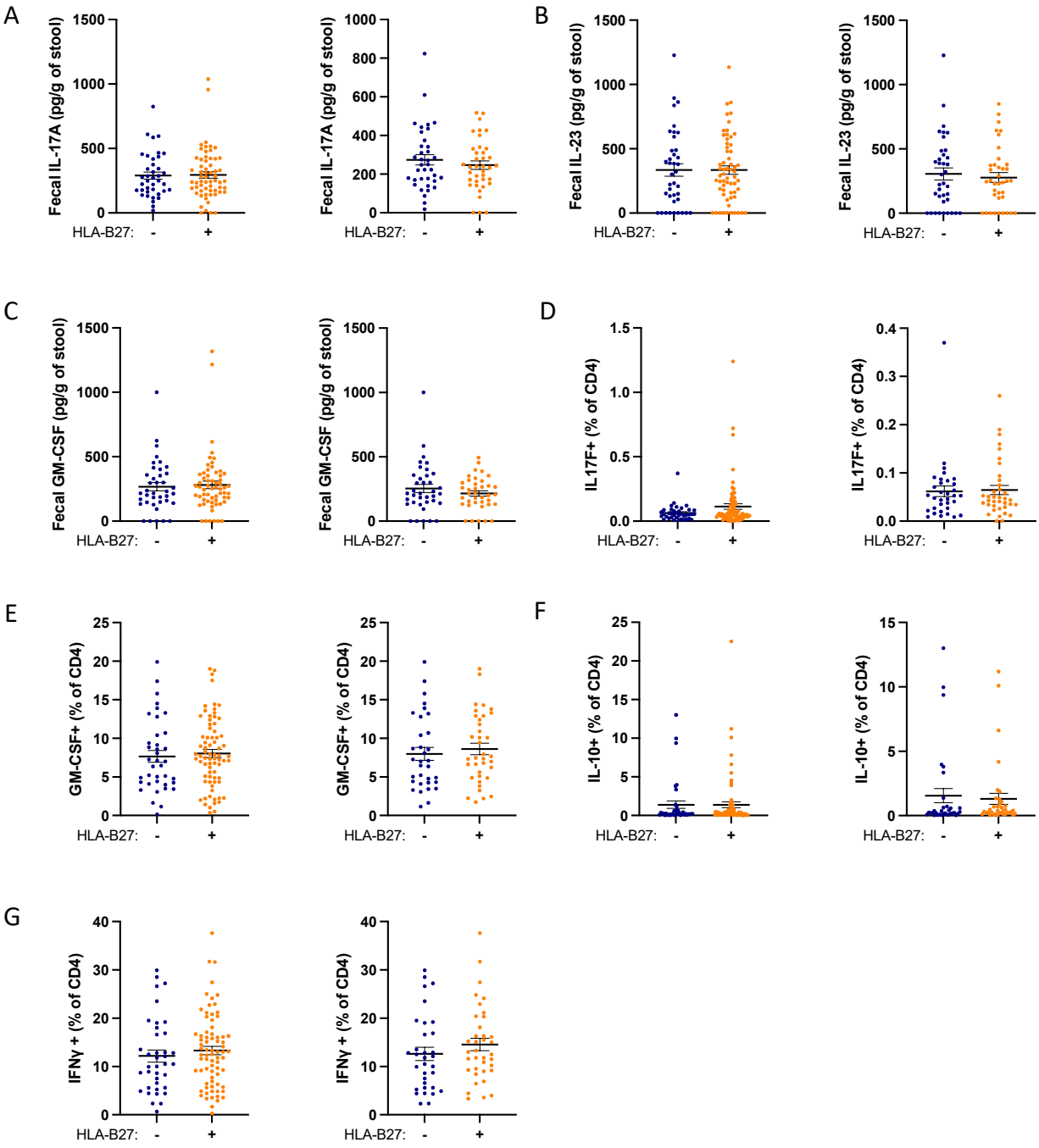
Appendix figure 5.1 Gating strategy for intracellular flow cytometry. Gating strategy for cytokine staining of GM-CSF, IL-17F, IFNγ, IL-10, IL-5, and IL-17A+ production from CD4+ T helper cells. Example plots are obtained from *ex vivo* peripheral blood mononuclear cells (PBMCs) of an AxSpA patient.

Protein	Levels (per gram of stool*)
Calprotectin (S100A8/9)	AxSpA (0-3004ng), HC (0-1500ng)
GM-CSF	AxSpA (0-1318pg), HC (0-1001pg)
IFNγ	Undetectable
IL-5	Undetectable
IL-6	Undetectable
IL-10	AxSpA (0-2102pg), HC (0-1419pg)
IL-17A	AxSpA (16-1039pg), HC (0-824pg)
IL-17F	Undetectable
IL-21	Undetectable
IL-22	Undetectable
IL-23	AxSpA (0-1134), HC (0-1227)
Myeloperoxidase (MPO)	AxSpA (0-3765pg), HC (0-464pg)
Oncostatin M (OSM)	Undetectable
TNFα	Undetectable

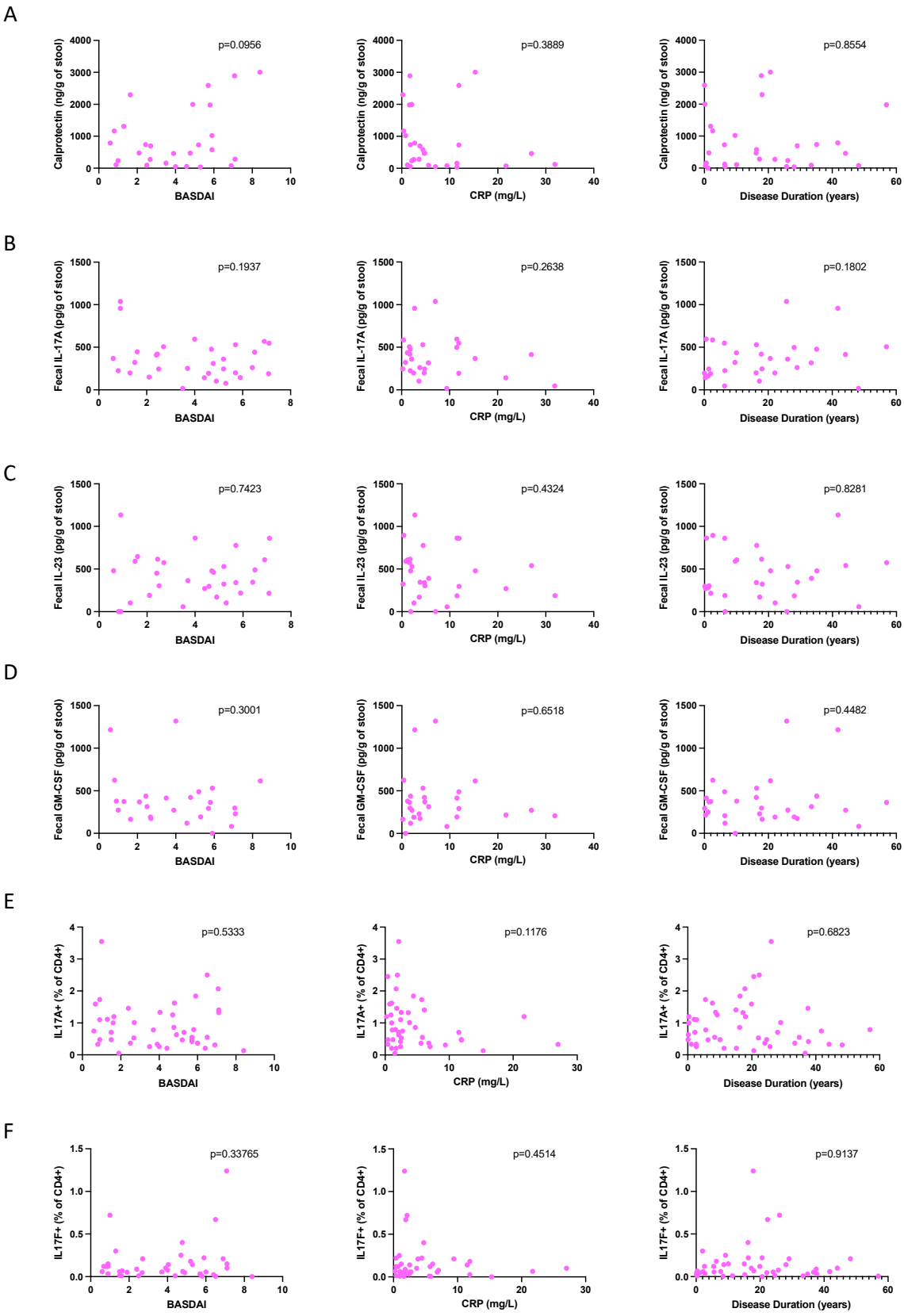
Appendix table 5.1 Proteins quantified by stool ELISA. *Fresh stool used; cytokines were not detected in ethanol-fixed stool.



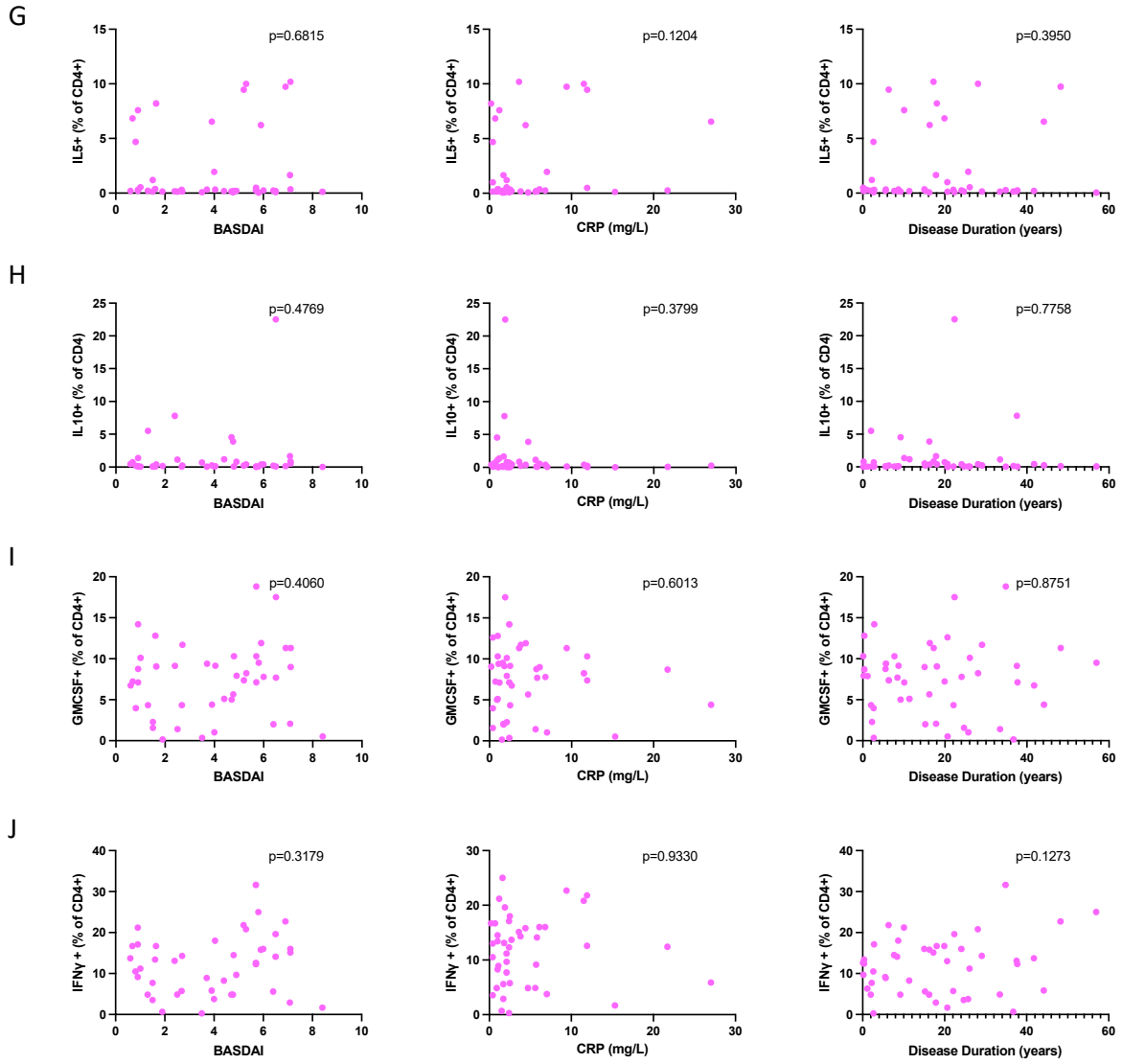
Appendix figure 5.2 NSAID and biologic usage associations with stool or circulating immune parameters. A) Stool calprotectin (ng/g of stool), B) stool IL-17A (pg/g of stool), C) stool IL-23 (pg/g of stool), D) stool GM-CSF (pg/g of stool), E) IL-17A+ (% of CD4+), F) IL-17F+ (% of CD4+), G) IL-5+ (% of CD4+), H) IL-10+ (% of CD4+), I) GM-CSF+ (% of CD4+), J) IFNγ+ (% of CD4+). Unpaired student's t-test with Welch's correction and Benjamini-Hochberg adjustment for multiple testing. Dotplots denote mean + standard error and individual data points are shown.



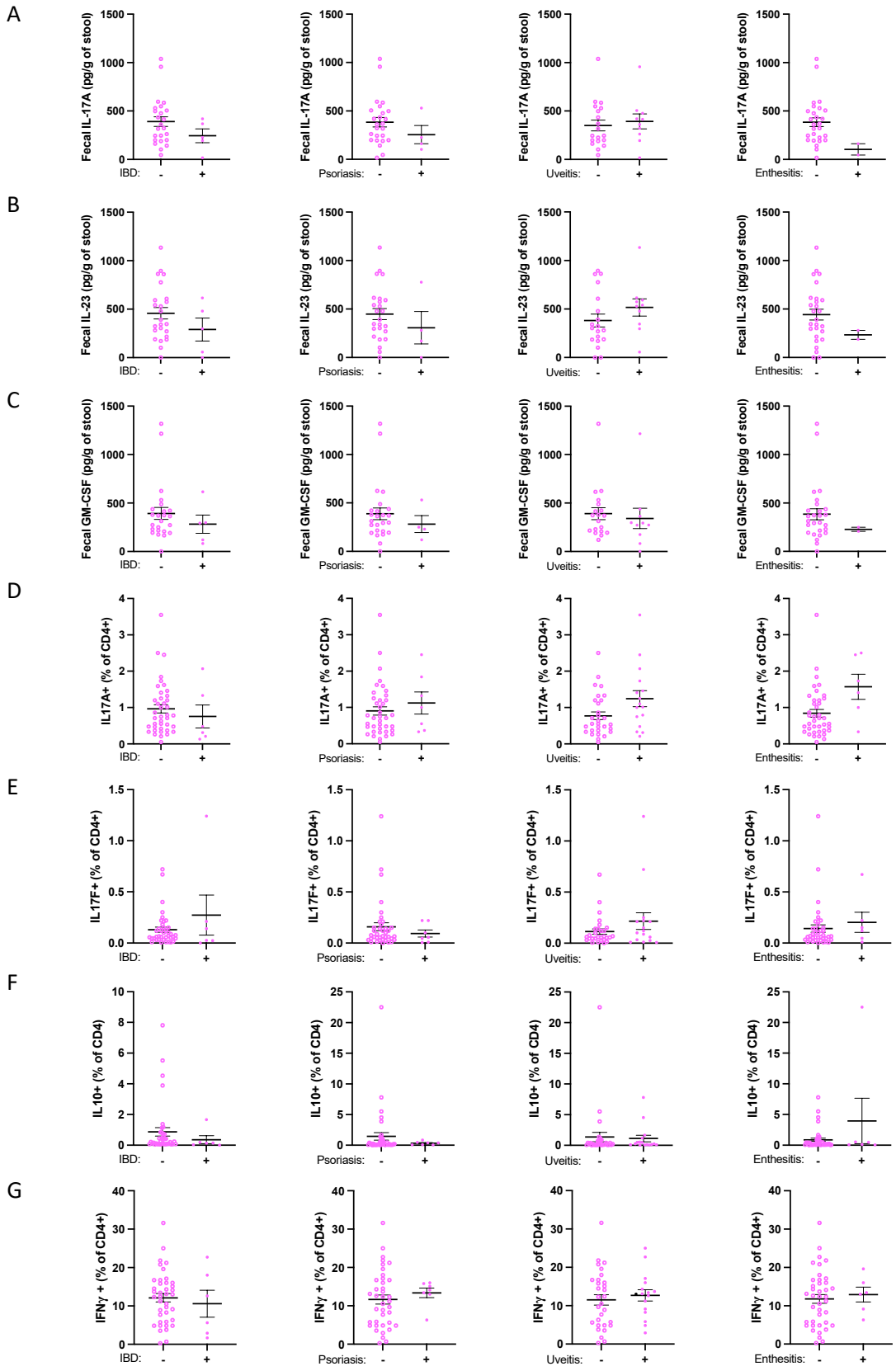
Appendix figure 5.3 HLA-B27 associations with immune parameters. A) Stool IL-17A (pg/g of stool), B) stool IL-23 (pg/g of stool), C) stool GM-CSF (pg/g of stool), D) IL-17F+ (% of CD4+), E) GM-CSF+ (% of CD4+), F) L-10+ (% of CD4+), G) IFNγ+ (% of CD4+). Unpaired student's t-test with Welch's correction and Benjamini-Hochberg adjustment for multiple testing. Dotplots denote mean + standard error and individual data points are shown.



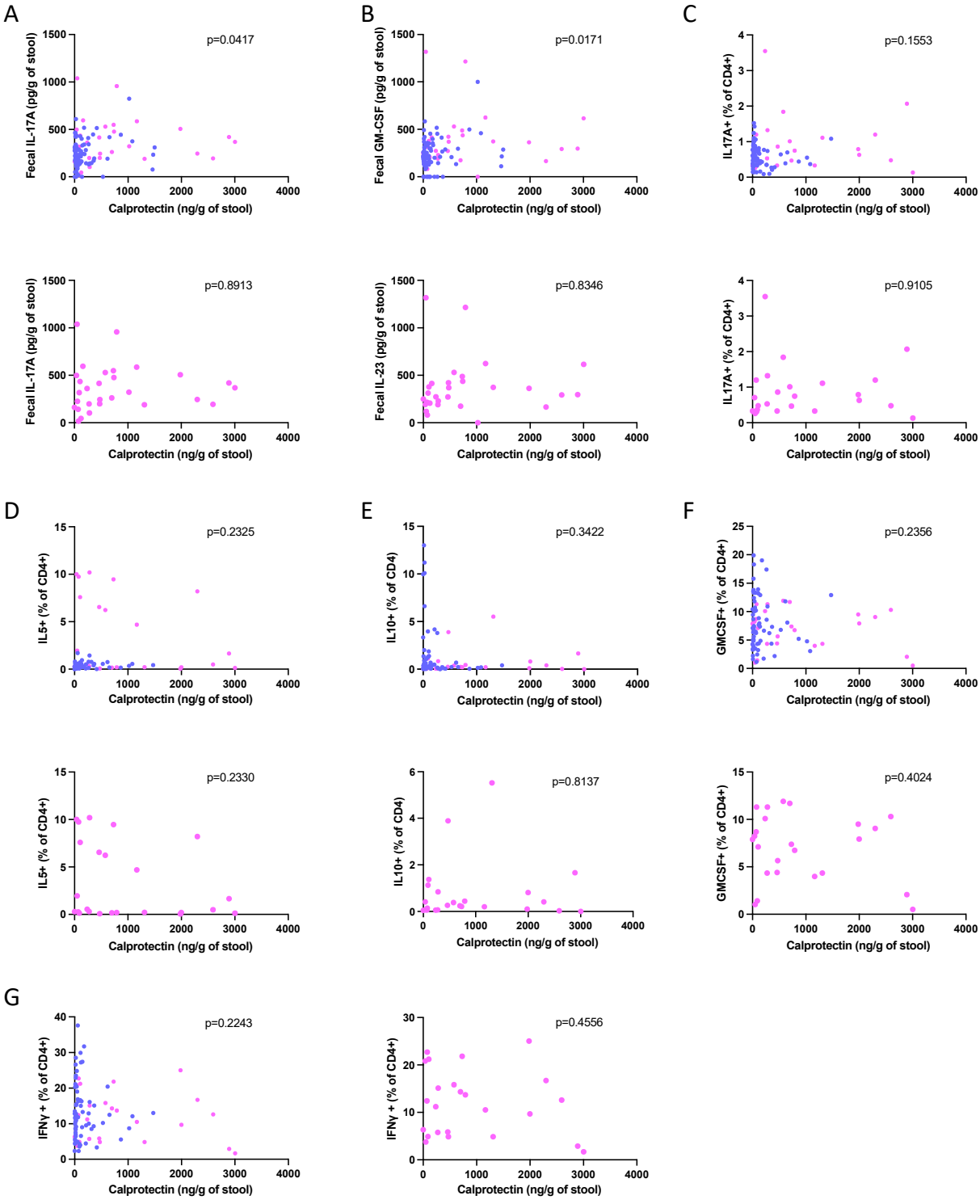
Appendix figure 5.4 Disease severity measures and disease duration associations with immune parameters in patients with AxSpA. A) Stool calprotectin (ng/g of stool), B) stool IL-17A (pg/g of stool), C) stool IL-23 (pg/g of stool), D) stool GM-CSF (pg/g of stool), E) IL-17A+ (% of CD4+), F) IL-17F+ (% of CD4+). Pearson's correlation was carried out with Benjamini-Hochberg adjustment for multiple testing. P value is denoted on each plot.



Appendix figure 5.4 (continued from previous page) Disease severity measures and disease duration associations with immune parameters in patients with AxSpA. G) IL-5+ (% of CD4+), H) IL-10+ (% of CD4+), I) GM-CSF+ (% of CD4+), J) IFNγ+ (% of CD4+). Pearson's correlation was carried out with Benjamini-Hochberg adjustment for multiple testing. P value is denoted on each plot.



Appendix figure 5.5 Extra-articular manifestations and associations with immune parameters (from left to right; IBD, psoriasis, uveitis, enthesitis). A) Stool IL-17A (pg/g of stool), B) stool IL-23 (pg/g of stool), C) stool GM-CSF (pg/g of stool), D) IL-17A+ (% of CD4+), E) IL-17F+ (% of CD4+), F) IL-10+ (% of CD4+), G) IFNγ+ (% of CD4+). Dotplots denote mean + standard error and individual data points are shown. Unpaired student's t test with Welch's correction and Benjamini-Hochberg adjustment for multiple testing.



Appendix figure 5.6 Stool calprotectin associations with immune parameters. A) Stool IL-17A (pg/g of stool), B) stool GM-CSF (pg/g of stool), C) IL-17A+ (% of CD4+), D) IL-5+ (% of CD4+), E) IL-10+ (% of CD4+), F) GM-CSF+ (% of CD4+), G) IFNγ+ (% of CD4+). Pink points refer to patients with AxSpA, and purple points refer to healthy controls. Pearson's correlation was carried out with Benjamini-Hochberg adjustment for multiple testing. P value is denoted on each plot.